MICROCOPY RESOLUTION TEST CHART
NATIONAL BUREAU OF STANDARDS 196

(1)

REPORT DOCUMENTATION PAGE

READ INSTRUCTION _
BEFORE COMPLETING FORM

1. REPORT NUMBER	2. GOVT ACCESSION NO.	3. RECIPIENT'S CATALOG NUMBER
AFIT/CI/NR 86- 131D		

4. TITLE *(and Subtitle)*	5. TYPE OF REPORT & PERIOD COVERED
Three-Dimensional Analytical Modeling Of Diffusion-Limited Solute Transport	THESIS/DISSERTATION
	6. PERFORMING ORG. REPORT NUMBER

7. AUTHOR(s)	8. CONTRACT OR GRANT NUMBER(s)
Mark Neil Goltz	

9. PERFORMING ORGANIZATION NAME AND ADDRESS	10. PROGRAM ELEMENT, PROJECT, TASK AREA & WORK UNIT NUMBERS
AFIT STUDENT AT: Stanford University	

11. CONTROLLING OFFICE NAME AND ADDRESS	12. REPORT DATE
AFIT/NR WPAFB OH 45433-6583	1986
	13. NUMBER OF PAGES
	172

14. MONITORING AGENCY NAME & ADDRESS*(if different from Controlling Office)*	15. SECURITY CLASS. *(of this report)*
	UNCLAS
	15a. DECLASSIFICATION/DOWNGRADING SCHEDULE

16. DISTRIBUTION STATEMENT *(of this Report)*

APPROVED FOR PUBLIC RELEASE; DISTRIBUTION UNLIMITED

DTIC
ELECTE
AUG 2 8 1986
S D
B

17. DISTRIBUTION STATEMENT *(of the abstract entered in Block 20, if different from Report)*

18. SUPPLEMENTARY NOTES

APPROVED FOR PUBLIC RELEASE: IAW AFR 190-1

LYNN E. WOLAVER
Dean for Research and
Professional Development
AFIT/NR

19. KEY WORDS *(Continue on reverse side if necessary and identify by block number)*

20. ABSTRACT *(Continue on reverse side if necessary and identify by block number)*

ATTACHED.

DD FORM _{1 JAN 73} **1473** EDITION OF 1 NOV 65 IS OBSOLETE

AD-A171 258

DTIC FILE COPY

THREE-DIMENSIONAL ANALYTICAL MODELING OF

DIFFUSION-LIMITED SOLUTE TRANSPORT

A DISSERTATION

SUBMITTED TO THE DEPARTMENT OF CIVIL ENGINEERING

AND THE COMMITTEE ON GRADUATE STUDIES

OF STANFORD UNIVERSITY

IN PARTIAL FULFILLMENT OF THE REQUIREMENTS

FOR THE DEGREE OF

DOCTOR OF PHILOSOPHY

By

Mark Neil Goltz

July 1986

I certify that I have read this thesis and that in my
opinion it is fully adequate, in scope and quality, as
a dissertation for the degree of Doctor of Philosophy.

(Principal Adviser)

I certify that I have read this thesis and that in my
opinion it is fully adequate, in scope and quality, as
a dissertation for the degree of Doctor of Philosophy.

I certify that I have read this thesis and that in my
opinion it is fully adequate, in scope and quality, as
a dissertation for the degree of Doctor of Philosophy.

I certify that I have read this thesis and that in my
opinion it is fully adequate, in scope and quality, as
a dissertation for the degree of Doctor of Philosophy.

Approved for the University Committee
on Graduate Studies:

_____
Dean of Graduate Studies

ii

ACKNOWLEDGMENTS

I would like to express my thanks to the "cast of thousands" who were involved with the Borden field experiment. The interesting results of that experiment provided the motivation for this research. Thanks to the Environmental Protection Agency, who funded the Borden experiment and provided logistical support for my research under Contract EPA-CR-808851. Much thanks to the U.S. Air Force, who sent me to Stanford for the best (and busiest) assignment I ever had. Also, sincere thanks to Ditter Peschcke-Koedt, who magically transformed my rough first draft into a clean, professional document.

Lastly, I'd like to thank my family. Mi Suk, my wife, bore the burden of caring for our boys, Hugh and Eric, while I worked on this dissertation. Mi Suk's love, support, and patience were instrumental in the successful completion of this work.

ABSTRACT

Previous experimental work conducted using laboratory soil columns has shown that diffusion into regions of immobile water can have a large effect on solute transport through porous media. This study focuses on the development, analysis, and application of an analytical model which incorporates the diffusion mechanism into the traditional three-dimensional advective/dispersive solute transport equation.

By consecutively applying the Laplace transform in time and the Fourier transform in space, analytical solutions are derived for the coupled partial differential equations which describe three-dimensional advective/dispersive transport through regions of mobile water and Fickian diffusion through immobile water regions of simple geometry (spherical, cylindrical, and layered).

To assist in the analysis of the models, a modified form of Aris' method of moments is presented, which permits the calculation of the spatial and temporal moments of the three-dimensional diffusion models, without having to invert the Laplace or Fourier transformed solutions. Using this method, the moments of the diffusion models are compared with one another, with the moments of a model that assumes equilibrium advective/dispersive transport, and with the moments of a model that assumes a first-order rate law governs mass transfer between the mobile and immobile regions. The method of moments is also used to analyze the differences in the spatial and temporal moment behavior of each transport model under discussion.

Finally, the results of a field experiment conducted to study sorbing solute transport are presented and interpreted using these models. It is shown that the first-order rate and diffusion models offer one plausible explanation of experimental observations which are unexplainable using the traditional advective/dispersive model approach.

TABLE OF CONTENTS

LIST OF ILLUSTRATIONS

LIST OF TABLES

a   Diffusion rate constant: $a = \dfrac{\nu(\nu + 2)D_e}{b^2}$, T^{-1}

where $\nu = 1$ for layered diffusion
$\nu = 2$ for cylindrical diffusion
$\nu = 3$ for spherical diffusion

b   Characteristic length of the immobile region geometry, L

Ber, Bei, Ber', Bei'   Kelvin functions

C Solute concentration, ML^{-3}

C_a Solute concentration at a point within the immobile region, ML^{-3}

C_m Solute concentration in the mobile region, ML^{-3}

C_{im} Volume averaged solute concentration in the immobile region, ML^{-3}

D_e' Diffusion coefficient within the immobile region: $D_e' = D_o/\chi$, L^2T^{-1}

D_e Modified immobile region diffusion coefficient: $D_e = D_e'/R_{im}$, L^2T^{-1}

$D_{effx}, D_{effy}, D_{effz}$ Effective dispersion coefficients in the x-, y-, and z-directions, respectively, L^2T^{-1}

D_o Liquid diffusion coefficient, L^2T^{-1}

D_{eff} Effective dispersion coefficient for use in the advection/dispersion equation, L^2T^{-1}

D_x', D_y', D_z' Dispersion coefficient in the x-, y-, and z-directions, respectively, L^2T^{-1}

D_{mx}, D_{my}, D_{mz} Mobile region dispersion coefficients in the x-, y-, and z-directions, respectively, L^2T^{-1}

D_x, D_y, D_z Modified dispersion coefficients in the x-, y-, and z-directions, respectively, L^2T^{-1}

For the equilibrium model: $D_x = \dfrac{D_x'}{R}$, $D_y = \dfrac{D_y'}{R}$, $D_z = \dfrac{D_z'}{R}$

For the nonequilibrium models: $D_x = \dfrac{D_{mx}}{R_m}$, $D_y = \dfrac{D_{my}}{R_m}$, $D_z = \dfrac{D_{mz}}{R_m}$

f   Fraction of sorption sites in direct contact with mobile water

$\mathcal{F}[f(x)]$ $\hat{f}(p)$ One-dimensional Fourier transform of the function $f(x)$

$\mathcal{F}[f(x,y,z)]$ $\bar{f}(p,q,u)$	Three-dimensional Fourier transform of the function $f(x,y,z)$
i	$\sqrt{-1}$
i_n	Modified spherical Bessel function of the first kind, order n: $$i_n(z) = \left(\frac{\pi}{2z}\right)^{1/2} I_{n+1/2}(z)$$
I_n	Modified Bessel function of the first kind, order n
k_f	External film transfer coefficient, LT^{-1}
K, K_{ads}, K_{des}	Freundlich isotherm coefficient
K_d	Distribution coefficient, $M^{-1}L^3$
K_n	Modified Bessel function of the second kind, order n
L, M, N	Half length, width, and depth of initial solute plume distribution, L
$L[f(t)]$ $\bar{f}(s)$	Laplace transform of the function $f(t)$
ℓ, m, n	x-, y-, and z-coordinates of location where concentration response is measured
M_T	Total mass associated with the mobile region, M
M'_1, M'_2, M'_3	Mass of solute injected into 1-, 2-, or 3-dimensional media, M
M_1, M_2, M_3	Modified injected mass, M For the equilibrium model: $M_i = M'_i/(\theta R)$ For the nonequilibrium models: $M_i = M'_i/(\theta_m R_m)$
m_j	One-dimensional j^{th} absolute spatial moment of the mobile concentration distribution
$m_{j,t}$	j^{th} absolute temporal moment of the mobile concentration response
$m_{jk\ell}$	Three-dimensional $(j+k+\ell)^{th}$ absolute spatial moment of the mobile concentration distribution
$n_{j,t}$	j^{th} absolute temporal moment of the immobile concentration response
$n_{jk\ell}$	Three-dimensional $(j+k+\ell)^{th}$ absolute spatial moment of the immobile concentration distribution
n, n_{ads}, n_{des}	Freundlich isotherm exponents
N_T	Total mass associated with the immobile region, M
p, q, u	Fourier transform variables in the x-, y-, and z-direction, respectively
Pe	Peclet number: $Pe = v_o \ell / D'_x$
Pe_{eff}	Effective Peclet number: $Pe_{eff} = \ell v_{eff}/D_{eff}$
Pe_m	Mobile region Peclet number: $Pe_m = v\ell/D_x = v_m \ell/D_{mx}$
r	Radial coordinate within the immobile region, L

R	Average retardation factor: $R = 1 + \dfrac{\rho K_d}{\theta}$
R_m	Mobile region retardation factor: $R_m = 1 + \dfrac{f \rho K_d}{\theta_m}$
R_{im}	Immobile region retardation factor: $R_{im} = 1 + \dfrac{(1-f)\rho K_d}{\theta_{im}}$
Re	Reynolds number: $Re = 2bv_m/\theta\nu$
S	Sorbed solute concentration
Sc	Schmidt number: $Sc = \nu/D_o$
St	Stanton number: $St = \alpha/(v/\ell)$
t	Time, T
$\hat{T}$	Dimensionless time: $\hat{T} = \theta_m V_m t/(\theta\ell R) = v_o t/(\ell R)$
v	Solute transport velocity in the x-direction, LT^{-1}
	For the equilibrium model: $v = v_o/R$
	For the nonequilibrium models: $v = v_m/R_m$
v_{eff}	Effective velocity for use in the advection/dispersion equation, LT^{-1}
v_{neff}	Effective velocity of immobile region concentration distribution, LT^{-1}
v_o	Average pore water velocity in the x-direction, LT^{-1}
v_m	Average mobile region pore water velocity in the x-direction, LT^{-1}
x,y,z	Spatial coordinates, L
x_c, y_c, z_c	Center of mass of the mobile region concentration distribution in the x-, y-, and z-directions, respectively, L
x_{nc}, y_{nc}, z_{nc}	Center of mass of the immobile region concentration distribution in the x-, y-, and z-directions, respectively, L

Greek

α'	First-order mass transfer rate constant, T^{-1}
α	Modified first-order mass transfer rate constant: $\alpha = \alpha'/(\theta_{im}R_{im})$, T^{-1}
β	Solute capacity ratio of the immobile to mobile regions: $\beta = (\theta_{im}R_{im})/(\theta_m R_m)$
γ	Ratio of diffusive to advective rates: for the first-order rate model, $\gamma = \alpha/(v/\ell)$; for the diffusion models, $\gamma = a/(v/\ell)$
$\delta(x)$	Dirac delta function
ϵ	Parameter used in spatial moment evaluation, T^{-1}
ϵ_a	Intragranular porosity
θ	Total water content: $\theta = \theta_m + \theta_{im}$

θ_m, θ_{im}	Mobile and immobile water contents, respectively
λ	Integration variable
$\mu_{2,t}$	Second central temporal moment, T^2
$\mu'_{j,t}$	j^{th} normalized absolute temporal moment
$\mu'_{jk\ell}$	Three-dimensional $(j+k+\ell)^{th}$ normalized absolute spatial moment of the mobile concentration distribution
ν	Kinematic viscosity, $L^2 T^{-1}$
$\nu'_{j,t}$	j^{th} normalized absolute temporal moment of the immobile region concentration response
$\nu'_{jk\ell}$	Three-dimensional $(j+k+\ell)^{th}$ normalized absolute spatial moment of the immobile concentration distribution
ρ	Bulk density of aquifer material, ML^{-3}
σ^2_{jk}	Component jk of the spatial covariance tensor, L^2
τ	Integration variable
ϕ	Ratio of mobile to total water content: $\phi = \theta_m/\theta$
χ	Tortuosity

CHAPTER 1

INTRODUCTION

BACKGROUND

In recent years, the problem of groundwater contamination has received widespread public attention. Hazardous chemical waste is being generated at the rate of 60 million tons annually (U.S. EPA, 1980). Whether intentionally disposed of or accidentally spilled, some of this waste can eventually reach the groundwater and contaminate it. Groundwater may transport the contaminants from the initial disposal site to an area where a threat to public health may be posed. Therefore, it is important to understand the processes affecting the transport of these contaminants in the subsurface environment. In a study of the problem, the Panel on Groundwater Contamination of the National Research Council remarked,

> Reliable and quantitative prediction of contaminant movement can be made only if we understand the processes controlling transport, hydrodynamic dispersion, and chemical, physical and biological reactions that affect soluble concentrations in the ground.
>
> (NRC, 1984).

Traditionally, the mathematical models used to describe solute transport in groundwater flow systems have been premised on the advection/dispersion equation. Advection refers to the average motion of solute due to the groundwater flow. Dispersion describes spreading of solute about the mean displacement position. Dispersion is usually attributed to molecular diffusion, so-called mechanical dispersion, and spatial variability. Mechanical dispersion is caused by local velocity variations along tortuous flow paths and the velocity distribution within each pore (Bear, 1979). Spatial variability produces velocity variations on a macroscopic scale. In the advection/dispersion model, the mechanical dispersion mechanism and spatial variability effects are often assumed to be diffusive (that is, the dispersive flux due to mechanical dispersion and spatial variability can be expressed by a Fickian type law). Usually, the effect of molecular diffusion is assumed negligible in comparison with the effect of mechanical dispersion (Gillham et al., 1984).

1

If the solute sorbs onto the aquifer material, it is often assumed that sorption is instantaneous, linear, and reversible. These assumptions permit modeling of sorbing solute transport using the advection/dispersion equation as well (Bear, 1979).

The advection/dispersion equation is usually implemented under the assumption that the dispersion coefficient is a constant property of the porous medium and the mean velocity. However, results of laboratory and field investigations have shown that the dispersion coefficient depends on the scale of the test or the size of the domain through which the solute travels, thereby invalidating the assumption underlying the advection/dispersion model in its simple form (Gillham et al., 1984). Stochastic models have been used to account for this scale effect. Stochastic models assume that the statistical structure of a conductivity field in a heterogeneous medium can be estimated. The models also assume that the heterogeneous medium is a single realization of an underlying stochastic process, and that the parameters of this process may be approximated using the statistics of the conductivity field. Also from these statistics, the dispersive capability of a single aquifer may be determined by ensemble averaging over the conceivable aquifer realizations (Gillham et al., 1984). These stochastic models have been used to show that ensemble solute spreading is generally not Fickian (Gelhar et al., 1979; Matheron and de Marsily, 1980; Smith and Schwartz, 1980; Gelhar and Axness, 1983). A disadvantage of the stochastic approach is that, since a real aquifer is conceived as a single realization, the solute plume must migrate a sufficient distance so that the ensemble averaging used in the stochastic model is interpretable (Gillham et al., 1984).

Many stochastic models that have been developed neglect the mechanisms of local mechanical dispersion and diffusion, so that spreading is strictly a consequence of heterogeneous advection (Warren and Skiba, 1964; Mercado, 1967; Schwartz, 1977; Smith and Schwartz, 1980). A heterogeneous advection model, when applied to a single aquifer realization, predicts local irregularities in the concentration distribution which will persist at a macroscopic scale (Sudicky, 1983). Sudicky (1983) noted that in a field experiment where detailed measurements of local concentration were obtained, this phenomenon was not observed, and in fact, local irregularities observed at early times were smoothed out

2

at later times. Sudicky (1983) proposed that the smoothness of the observed macroscopic concentration patterns was the result of transverse molecular diffusion, whereby solute which advects rapidly in the high permeability zones diffuses into the less permeable zones. Sudicky (1983) and Güven et al. (1984) discussed the impact of diffusion on solute transport in a layered system, and compared the so-called advection/diffusion model with stochastic models. It was shown that the deterministic advection/diffusion model provided results which were equivalent to results obtained from the stochastic theory developed by Gelhar et al. (1979). Sudicky's (1983) and Güven et al.'s (1984) studies were limited to the analysis of conservative solute transport in a stratified medium, where each stratum had a different hydraulic conductivity, and therefore a different, though steady, groundwater flow velocity.

The importance of diffusion into spehrical zones of low permeability was demonstrated in column experiments conducted by Rao et al. (1980) and Nkedi-Kizza et al. (1982). Goltz and Roberts (1984), using numerical simulations, demonstrated how a solute transport model which neglected the mechanism of diffusion could significantly underpredict long-time contaminant concentrations.

The effect on solute transport of diffusion into low permeability zones has been discussed in the chemical engineering literature over at least the past thirty years (Deisler and Wilhelm, 1953; Vermuelen, 1953; Rosen, 1954). More recently, these diffusion concepts have been applied to study contaminant transport by groundwater (van Genuchten and Wierenga, 1976; Rao et al., 1980; Nkedi-Kizza et al., 1982; Valocchi, 1985a; van Genuchten, 1985; Goltz and Roberts, 1986; Crittenden et al., 1986; Miller and Weber, 1986). These studies, however, have all presumed one-dimensional solute transport. Since the groundwater environment is three-dimensional, there is value in deriving three-dimensional formulations of transport models which incorporate the diffusion mechanism.

SCOPE OF THIS INVESTIGATION

This work was undertaken in response to the apparent importance of diffusion in affecting the groundwater transport of contaminants.

Previous models which have incorporated the diffusion mechanism have assumed one-dimensional transport, whereas this study will present a three-dimensional formulation. The specific objectives of this investigation can be summarized as follows:

1. Develop and test a transport model which incorporates the mechanisms of advection, dispersion, linear reversible sorption, and diffusion in a three-dimensional, infinite medium. This study will be limited to the special case where advection is due to a single, steady, groundwater flow velocity.

2. Compare how simulations of such a model differ from simulations of the advection/dispersion model, which traditionally has been used to describe contaminant transport. To facilitate this comparison, develop and apply methods for obtaining spatial and temporal moments of the concentration distributions simulated using the different models.

3. Compare and contrast simulations of the different diffusion model formulations.

4. Apply the model to the data set obtained in an extensive, high-resolution field experiment. Assess whether characteristics of the spatial and temporal data are explainable using models which incorporate diffusion. In addition, examine if alternate models which assume other mechanisms (e.g., nonlinear, hysteretic sorption) can explain experimental observations. This will require an analysis of the spatial moment behavior of these alternate models.

CHAPTER 2

MODEL FORMULATION

This chapter reviews the so-called two-region models, which couple an expression describing advective/dispersive solute transport in regions of mobile water with an expression describing mass transfer into regions of immobile water.

A three-dimensional formulation for such two-region models will be presented and an analytical solution derived. The solution technique involves consecutively applying the Laplace transform in time, and the Fourier transform in space to the coupled set of partial differential equations that mathematically describe the two-region models.

REVIEW OF EXISTING MODELS

Transport of hydrophobic organic chemicals in groundwater traditionally has been described using the homogeneous advective/dispersive transport equation with a sink term to account for sorption of the organic solute onto the soil matrix. This sorption term is often developed assuming local equilibrium and a linear, reversible equilibrium relationship between the quantity of the organic compound in the sorbed and solution phases. Several investigators have found, in laboratory column studies, that the nearly symmetric, sigmoid forms of breakthrough responses predicted using models making these simplifying assumptions, do not agree with experimental observations (van Genuchten and Wierenga, 1976; Rao et al., 1979; Reynolds et al., 1982; De Smedt and Wierenga, 1984). Frequently, experimental breakthrough responses exhibit highly asymmetric or nonsigmoid profiles, commonly termed tailing. Tailing may be attributable to the slow diffusion of solute into zones of immobile water. It has been hypothesized that these zones result from soil aggregation, slow flow, or unsaturated flow (van Genuchten and Wierenga, 1976; Rao et al., 1980; Nkedi-Kizza et al., 1982; De Smedt and Wierenga, 1984).

Various models have been proposed to describe the exchange of solute between mobile and immobile zones. The simplest of these, the first-order rate model, assumes completely mixed zones of immobile water, with a first-order rate expression describing diffusional

transfer of solute between the mobile and immobile regions (Coats and Smith, 1964; van Genuchten and Wierenga, 1976). These models couple the advection/dispersion equation with a first-order rate expression. First-order rate models have successfully simulated the observed tailing in laboratory column solute transport experiments (van Genuchten and Wierenga, 1977; van Genuchten et al., 1977; De Smedt and Wierenga, 1979a; Nkedi-Kizza et al., 1984). Analytical solutions for this type of model have been derived for different initial and boundary conditions applicable to finite and semi-infinite columns (Lindstrom and Narasimhan, 1973; van Genuchten and Wierenga, 1976; De Smedt and Wierenga, 1979b).

More complex models have been developed to describe the transfer of solute within immobile regions by Fick's second law of diffusion. These models, which couple the advection/dispersion equation with an expression to describe diffusion, will be referred to as diffusion models. Diffusion models have also been successfully used to simulate the observed tailing in laboratory column solute transport experiments (Rao et al., 1980; Nkedi-Kizza et al., 1982). These models assume a geometry for the immobile region. One-dimensional analytical solutions to diffusion models have been derived, for semi-infinite boundary conditions, assuming spherical (Pellett, 1966; Rasmuson and Neretnieks, 1980), rectangular (Sudicky and Frind, 1982), and cylindrical (Pellett, 1966; van Genuchten, 1985) immobile region geometries. Van Genuchten (1985) summarizes solutions for different immobile region geometries.

Recent research has begun to focus on solute transport in "semi-controlled" field settings (Leland and Hillel, 1982; Roberts et al., 1982; Sudicky et al., 1983; Mackay et al., 1986). Solute pulses have been introduced into groundwater under conditions corresponding to an infinite medium, in which the medium is effectively unbounded upgradient from the point of introduction as well as downgradient from the point(s) of observation. To permit proper analysis of the data from the perspective of dispersion and diffusion phenomena, solutions to the transport equation under the pertinent boundary conditions in a three-dimensional infinite medium are required. Although one-, two-, and three-dimensional solutions to the advection/dispersion equation in an infinite porous medium are available (Carslaw and Jaeger, 1959; Bear, 1972; Hunt, 1978), of the two-region models, only the first-order rate model has been solved analytically for infinite, multi-dimensional conditions

6

(Carnahan and Remer, 1984). Bibby (1979) combined a two-dimensional
finite element model with an analytical expression describing solute
diffusion into layers, to simulate chloride movement in a chalk aquifer.
However, to date, no multi-dimensional analytical solutions to diffusion
models have been presented. Such multi-dimensional solutions, with
infinite boundary conditions, are presented in this chapter.

ADVECTION/DISPERSION MODEL SOLUTION

Sorbing solute transport through a porous medium has often been
described using the advective/dispersive transport equation with a
sorption term (Bear, 1972):

$$\frac{\partial C(x,y,z,t)}{\partial t} = D_x' \frac{\partial^2 C}{\partial x^2} + D_y' \frac{\partial^2 C}{\partial y^2} + D_z' \frac{\partial^2 C}{\partial z^2} - v_o \frac{\partial C}{\partial x} - \frac{\rho}{\theta} \frac{\partial S}{\partial t} \qquad (2-1)$$

where $C(x,y,z,t)$ represents the aqueous solute concentration, $S(x,y,z,t)$
is the sorbed solute concentration, θ is the aquifer porosity, ρ the
bulk soil density, D_x', D_y', and D_z' are the principal components of the
dispersion tensor in the x-, y-, and z-directions, respectively, and v_o
is the average pore water velocity. Equation 2-1 implicitly assumes
steady, uniform flow in a homogeneous, isotropic porous medium. If
linear, reversible, equilibrium sorption is assumed, sorbed and aqueous
solute concentrations may be related using the concept of a partition or
distribution coefficient, K_d, such that:

$$S = K_d C$$

With these assumptions, a dimensionless retardation factor, R, can be
defined:

$$R = 1 + \frac{\rho}{\theta} K_d$$

so Eq. 2-1 can be rewritten as (Bear, 1972):

$$\frac{\partial C(x,y,z,t)}{\partial t} = \frac{D_x'}{R} \frac{\partial^2 C}{\partial x^2} + \frac{D_y'}{R} \frac{\partial^2 C}{\partial y^2} + \frac{D_z'}{R} \frac{\partial^2 C}{\partial z^2} - \frac{v_o}{R} \frac{\partial C}{\partial x} \qquad (2-2)$$

Equation 2-2 has been solved for the following initial/boundary condi-
tions, representing an instantaneous point source in an infinite medium:

7

$$C(x,y,z,0) = \frac{M_3'}{\theta R} \delta(x)\delta(y)\delta(z) \qquad (2-3a)$$

$$C(\pm\infty,y,z,t) = C(x,\pm\infty,z,t) = C(x,y,\pm\infty,t) = 0 \qquad (2-3b)$$

The solution is (Carslaw and Jaeger, 1959; Crank, 1975; Hunt, 1978):

$$C(x,y,z,t) = \frac{M_3'}{8\theta(\pi t)^{3/2}} \frac{R^{1/2}}{\sqrt{D_x' D_y' D_z'}} e^{-\frac{(Rx-v_o t)^2}{4D_x' Rt} - \frac{Ry^2}{4D_y' t} - \frac{Rz^2}{4D_z' t}} \qquad (2-4)$$

FIRST-ORDER RATE MODEL SOLUTION

We will begin our discussion of the two-region models by deriving the solution to the first-order rate model in a three-dimensional, infinite medium. This derivation will serve as a guide for the solution of the slightly more complex diffusion models.

In three dimensions, the first-order rate model for sorbing solute transport in a porous medium with immobile water zones may be written (van Genuchten and Wierenga, 1976):

$$\frac{\partial C_m(x,y,z,t)}{\partial t} = \frac{D_{mx}}{R_m}\frac{\partial^2 C_m}{\partial x^2} + \frac{D_{my}}{R_m}\frac{\partial^2 C_m}{\partial y^2} + \frac{D_{mz}}{R_m}\frac{\partial^2 C_m}{\partial z^2} - \frac{v_m}{R_m}\frac{\partial C_m}{\partial x} - \frac{\theta_{im}R_{im}}{\theta_m R_m}\frac{\partial C_{im}}{\partial t}$$

$$(2-5)$$

$$\frac{\partial C_{im}(x,y,z,t)}{\partial t} = \frac{\alpha'}{\theta_{im}R_{im}} (C_m - C_{im}) \qquad (2-6)$$

These equations assume groundwater flow in the positive x direction, and that D_{mx}, D_{my}, and D_{mz} represent the mobile zone dispersion coefficients in the x-, y-, and z-directions. C_m and C_{im} represent solute concentrations in the mobile and immobile regions, respectively, and θ_m and θ_{im} are mobile and immobile region water content, such that $\theta = \theta_m + \theta_{im}$. Equation 2-5 is the advection/dispersion equation with a sink term to describe the mass transfer of solute from the mobile to the immobile water region. Sorption onto the solids is assumed to be linear and reversible, with the effect of sorption incorporated into R_m and R_{im}, the retardation factors for the mobile and immobile regions. Following van Genuchten and Wierenga (1976), define:

$$R_m = 1 + \frac{f\rho K_d}{\theta_m}$$

and

$$R_{im} = 1 + \frac{(1-f)\rho K_d}{\theta_{im}}$$

where f is the fraction of sorption sites adjacent to regions of mobile water. Equation 2-6 is the first-order rate expression describing solute transfer between the mobile and immobile regions, where α' is the first-order rate constant.

For an instantaneous point source of solute in an infinite porous medium, the following initial/boundary conditions apply to 2-5 and 2-6:

$$C_m(x,y,z,0) = \frac{M_3'}{\theta_m R_m} \delta(x)\delta(y)\delta(z) \tag{2-7a}$$

$$C_{im}(x,y,z,0) = 0 \tag{2-7b}$$

$$C_m(\pm\infty,y,z,t) = C_m(x,\pm\infty,z,t) = C_m(x,y,\pm\infty,t) = 0 \tag{2-7c}$$

Equation 2-7a represents the initial solute distribution in the mobile zone, (2-7b) states that there is initially no solute in the immobile region, and (2-7c) gives the boundary conditions for an infinite medium.

The method to solve (2-5) and (2-6) simultaneously, subject to initial/boundary conditions (2-7), is given in Appendix A. The solution is

$$C_m(x,y,z,t) = \exp\left(\frac{-\alpha't}{\theta_m R_m}\right)G(x,y,z,t) + \frac{\alpha'}{\theta_m R_m} \int_0^t H(t,\tau)G(x,y,z,\tau)d\tau \tag{2-8}$$

where

$$H(t,\tau) = \exp\left[\frac{-\alpha'(t-\tau)}{\theta_{im}R_{im}} - \frac{\alpha'\tau}{\theta_m R_m}\right] \frac{(\theta_m R_m)^{1/2}\tau I_1\left\{\frac{2\alpha'}{\theta_{im}R_{im}}\left[\frac{\theta_{im}R_{im}(t-\tau)\tau}{\theta_m R_m}\right]^{1/2}\right\}}{[\theta_{im}R_{im}(t-\tau)\tau]^{1/2}}$$

$$G(x,y,z,t) = \frac{M_3'(R_m)^{1/2}}{8\theta_m(\pi t)^{3/2}(D_{mx}D_{my}D_{mz})^{1/2}} \exp\left[\frac{-(R_m x - v_m t)^2}{4D_{mx}R_m t} - \frac{R_m y^2}{4D_{my}t} - \frac{R_m z^2}{4D_{mz}t}\right]$$

and $I_1\{\ \}$ is a modified Bessel function. This solution is equivalent to the solution presented by Carnahan and Remer (1984).

The principle of superposition can now be used to integrate the point source response to obtain responses for other initial conditions. Carnahan and Remer (1984) provided solutions for various initial condition geometries.

DIFFUSION MODEL SOLUTION

For diffusion models, Eq. 2-5, the advection/dispersion equation, is still applicable. However, since these models allow for concentration gradients within the immobile regions, the dependent variable C_{im} in (2-5) now represents a volume-averaged solute concentration within the immobile zone. Of course, in the first-order rate model, where the immobile zone is assumed to be perfectly mixed, the solute concentration throughout the immobile zone equals the average concentration.

Spherical Geometry

Equation 2-5 makes no assumption regarding the immobile zone geometry. Assuming spherical immobile zones of radius b, the volume averaged concentration, C_{im}, can be defined as follows:

$$C_{im} = \frac{3}{b^3} \int_0^b r^2 C_a(r,x,y,z,t)dr \qquad (2-9)$$

Fick's law of diffusion within a sphere is written:

$$R_{im} \frac{\partial C_a}{\partial t} = \frac{D'_e}{r^2} \frac{\partial}{\partial r} \left(r^2 \frac{\partial C_a}{\partial r} \right) , \quad 0 \leq r \leq b \qquad (2-10)$$

with the boundary conditions:

$$C_a(0,x,y,z,t) \neq \infty \qquad (2-11a)$$

$$C_a(b,x,y,z,t) = C_m(x,y,z,t) \qquad (2-11b)$$

The method to solve (2-5), (2-9), and (2-10) simultaneously, for an instantaneous point source, subject to initial/boundary conditions (2-7) and (2-11), is presented in Appendix B. The solution is:

$$C_m(x,y,z,t) = \frac{M_3' D_e' \exp(v_m x/2D_{mx})}{\theta_m R_{im}(\pi b)^2 (D_{mx} D_{my} D_{mz})^{1/2} G}$$

$$\times \int_0^\infty [\lambda \, \exp(-R_m^{1/2} G Z_p) \, \text{Cos}(\frac{2D_e \lambda^2 t}{R_{im} b^2} - R_m^{1/2} G Z_m)] d\lambda \quad (2\text{-}12)$$

where:

$$G = (\frac{x^2}{D_{mx}} + \frac{y^2}{D_{my}} + \frac{z^2}{D_{mz}})^{1/2}$$

$$Z_p = (\frac{r_p + \Omega_1}{2})^{1/2} \, , \quad Z_m = (\frac{r_p - \Omega_1}{2})^{1/2}$$

$$r_p = (\Omega_1^2 + \Omega_2^2)^{1/2}$$

$$\Omega_1 = \frac{v_m^2}{4D_{mx} R_m} + \frac{3\theta_{im} D_e'}{R_m \theta_m b^2} \psi_1$$

$$\Omega_2 = \frac{2D_e' \lambda^2}{R_{im} b^2} + \frac{3\theta_{im} D_e'}{R_m \theta_m b^2} \psi_2$$

$$\psi_1 = \frac{\lambda(\text{Sinh } 2\lambda + \text{Sin } 2\lambda)}{\text{Cosh } 2\lambda - \text{Cos } 2\lambda} - 1$$

$$\psi_2 = \frac{\lambda(\text{Sinh } 2\lambda - \text{Sin } 2\lambda)}{\text{Cosh } 2\lambda - \text{Cos } 2\lambda}$$

Superposing this solution will provide responses for other initial conditions. It should be noted that solving for C_m in Eq. 2-12 requires the evaluation of an infinite integral. The integrand of this integral is the product of an exponentially decaying function and a sinusoidally oscillating function. The Gaussian quadrature methods described by Rasmuson and Neretnieks (1981) and van Genuchten et al. (1984) may be used to evaluate the integral numerically.

Cylindrical Geometry

For cylindrical immobile zones of radius b, the volume averaged concentration is:

11

$$C_{im} = \frac{2}{b^2} \int_0^b r C_a(r,x,y,z,t)dr \qquad (2\text{-}13)$$

and Fick's law of diffusion in a cylinder may be written:

$$R_{im} \frac{\partial C_a}{\partial t} = \frac{D'_e}{r} \frac{\partial}{\partial r} \left(r \frac{\partial C_a}{\partial r} \right) , \quad 0 \leq r \leq b \qquad (2\text{-}14)$$

with the boundary conditions (2-11a) and (2-11b). The analysis proceeds analogously to the spherical geometry case, with the three-dimensional point source response the same as (2-12), but in the case of cylindrical geometry:

$$\psi_1 = \frac{\frac{\sqrt{8}}{3} \lambda \left[\text{Ber}(\lambda\sqrt{2})\text{Ber}'(\lambda\sqrt{2}) + \text{Bei}(\lambda\sqrt{2})\text{Bei}'(\lambda\sqrt{2}) \right]}{\text{Ber}^2(\lambda\sqrt{2}) + \text{Bei}^2(\lambda\sqrt{2})}$$

$$\hspace{8cm} (2\text{-}15)$$

$$\psi_2 = \frac{\frac{\sqrt{8}}{3} \lambda \left[\text{Ber}(\lambda\sqrt{2})\text{Bei}'(\lambda\sqrt{2}) - \text{Bei}(\lambda\sqrt{2})\text{Ber}'(\lambda\sqrt{2}) \right]}{\text{Ber}^2(\lambda\sqrt{2}) + \text{Bei}^2(\lambda\sqrt{2})}$$

Rectangular Geometry

In the case of a rectangular immobile zone, it is physically more realistic to consider advective/dispersive transport in a two-dimensional mobile zone with diffusion into rectangular immobile zone layers of half-width b. The set of equations which describes such a system is:

$$\frac{\partial C_m(x,y,t)}{\partial t} = \frac{D_{mx}}{R_m} \frac{\partial^2 C_m}{\partial x^2} + \frac{D_{my}}{R_m} \frac{\partial^2 C_m}{\partial y^2} - \frac{v_m}{R_m} \frac{\partial C_m}{\partial x} - \frac{\theta_{im} R_{im}}{\theta_m R_m} \frac{\partial C_{im}}{\partial t} \qquad (2\text{-}16a)$$

$$R_{im} \frac{\partial C_a}{\partial t} = D'_e \frac{\partial^2 C_a}{\partial z^2} , \quad 0 \leq z \leq b \qquad (2\text{-}16b)$$

$$C_{im} = \frac{1}{b} \int_0^b C_a(x,y,z,t)dz \qquad (2\text{-}16c)$$

with the initial/boundary conditions:

$$C_m(x,y,0) = \frac{M'_2}{\theta_m R_m} \delta(x)\delta(y) \qquad (2\text{-}17a)$$

$$C_{im}(x,y,0) = 0 \qquad (2\text{-}17b)$$

12

$$C_m(\pm\infty, y, t) = C_m(x, \pm\infty, t) = 0 \qquad (2\text{-}17c)$$

$$C_a(x, y, 0, t) \neq \infty \qquad (2\text{-}17d)$$

$$C_a(x, y, b, t) = C_m(x, y, t) \qquad (2\text{-}17e)$$

Using the methods given in Appendix B, these equations can be solved to give the following result:

$$C_m(x, y, t) = \frac{2D_e' M_2' \exp(v_m x / 2D_{mx})}{\theta_m R_{im}(\pi b)^2 (D_{mx} D_{my})^{1/2}}$$

$$\times \int_0^\infty \text{Re}\left\{ \exp\left[\frac{12 D_e \lambda^2 t}{R_{im} b^2}\right] K_0 \left[R_m^{1/2} B Z_p + i R_m^{1/2} B Z_m\right]\right\} \lambda \, d\lambda \qquad (2\text{-}18)$$

where:

$$B = \left(\frac{x^2}{D_{mx}} + \frac{y^2}{D_{my}}\right)^{1/2}$$

K_0 is a modified Bessel function of the second kind, and Z_p and Z_m are as defined in Eq. 2-12, though for rectangular geometry:

$$\psi_1 = \frac{\lambda(\text{Sinh } 2\lambda - \text{Sin } 2\lambda)}{3(\text{Cosh } 2\lambda + \text{Cos } 2\lambda)}$$

$$\psi_2 = \frac{\lambda(\text{Sinh } 2\lambda + \text{Sin } 2\lambda)}{3(\text{Cosh } 2\lambda + \text{Cos } 2\lambda)}$$

MODEL TESTING

In the limiting case, as the volume of water in the immobile region becomes small, and the diffusion rate within the immobile region becomes large, the diffusion model solution should approach the solution of the advection/dispersion model. To verify this, a test situation, which is depicted in Figure 2.1, was devised. The concentration response to a rectangular prism initial solute distribution of half length, width, and depth L, M, N, respectively, may be calculated at a sampling well using the advection/dispersion and spherical diffusion models. The solution to the three-dimensional advection/dispersion model for a rectangular prism source is well known (Carslaw and Jaeger, 1959; Hunt, 1978). This
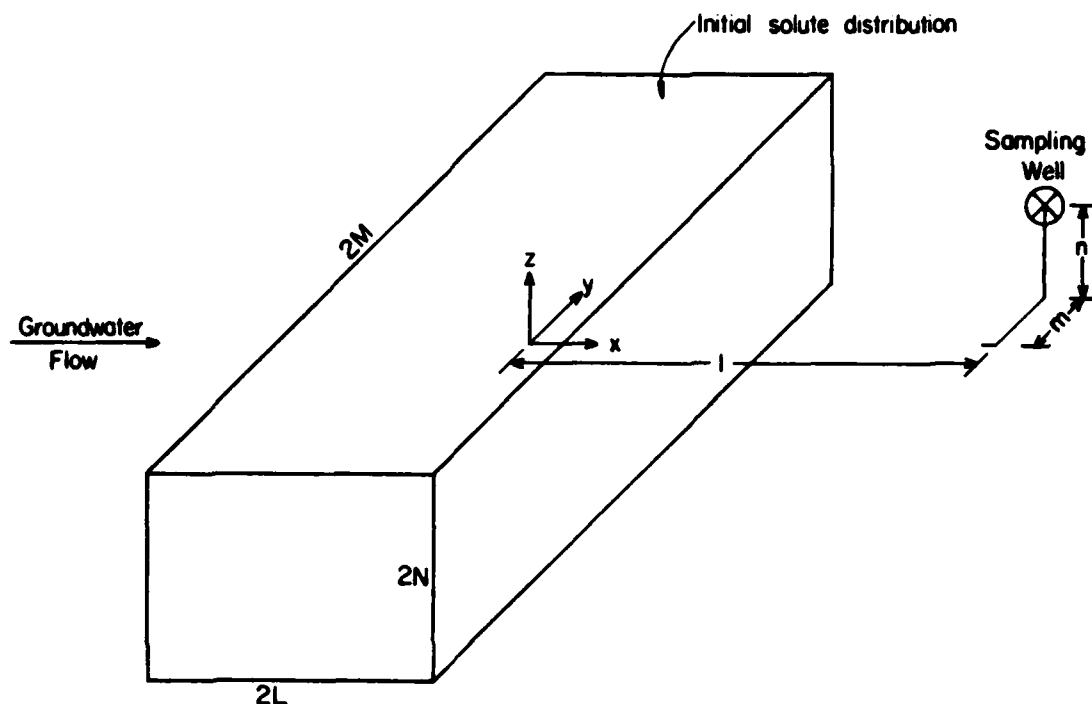
Figure 2.1. Initial condition for three-dimensional model testing.
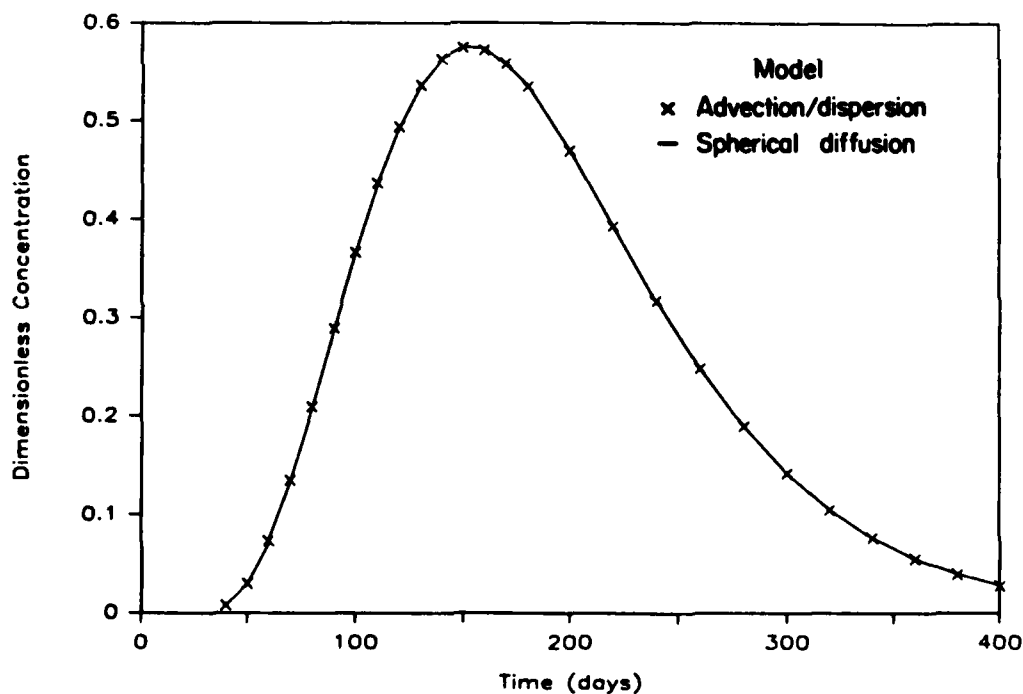
Figure 2.2. Comparison of the advection/dispersion model solution with the limiting case of the spherical diffusion model: $\phi = 0.999$, $v_m = 0.091$ m/d, $\theta = 0.38$, $D_{mx} = 0.0334$ m^2/d, $D_{my} = 0.0027$ m^2/d, $D_{mz} = 1.0 \times 10^{-5}$ m^2/d, $\ell = 5.0$ m, $m = 0.0$ m, $n = -0.40$ m, $L = 1.5$ m, $M = 3.0$ m, $N = 0.8$ m, $R_m = R_{im} = 3.0$, and $D_e'/b^2 = 0.715$ d^{-1}.

14

solution, for realistic parameter values, is plotted in Figure 2.2, as a breakthrough response curve at the sampling well. Also shown in Figure 2.2 is the solution to the spherical diffusion model with very low porosity in the immobile region [$\theta_{im} = 0.00038$] and relatively fast diffusion [$D'_e/(R_{im}b^2) = 0.238 \ d^{-1}$] within the immobile region. This solution was obtained, for a rectangular prism initial distribution, by numerically superposing the point source response (Eq. 2-12) over the length, width, and depth of the initial solute distribution. As expected, the solutions are identical, because the fraction of porosity in the immobile region was chosen to be so small as to be practically negligible.

Another means of testing the diffusion model solution makes use of the concept of approximate equivalence between the first-order rate model and the diffusion model. Van Genuchten (1985) showed that the concentration responses for the two models would be approximately the same if the first-order rate parameter and the spherical diffusion rate parameter were related by the expression:

$$\alpha' = 22.68 \ \frac{D'_e \theta_{im}}{b^2} \qquad (2\text{-}19)$$

The solution to the first-order rate model for a rectangular prism source may be obtained by superposing the point source response (Eq. 2-8) over the length, width, and depth of the initial solute distribution. This solution is Eq. 2-8 with:

$$G(x,y,z,t) = \frac{M'_3}{8R_m\theta_m} \left\{ erf\left[\frac{R_m(L+x) - v_m t}{2(D_{mx}R_m t)^{1/2}}\right] + erf\left[\frac{R_m(L-x) + v_m t}{2(D_{mx}R_m t)^{1/2}}\right]\right\}$$

$$\times \left\{ erf\left[\frac{R_m(M-y)}{2(D_{my}R_m t)^{1/2}}\right] + erf\left[\frac{R_m(M+y)}{2(D_{my}R_m t)^{1/2}}\right]\right\}$$

$$\times \left\{ erf\left[\frac{R_m(N-z)}{2(D_{mz}R_m t)^{1/2}}\right] + erf\left[\frac{R_m(N+z)}{2(D_{mz}R_m t)^{1/2}}\right]\right\} \qquad (2\text{-}20)$$

Figure 2.3 shows the first-order rate model solution (Eqs. 2-8 and 2-20) for some realistic parameter values.

15
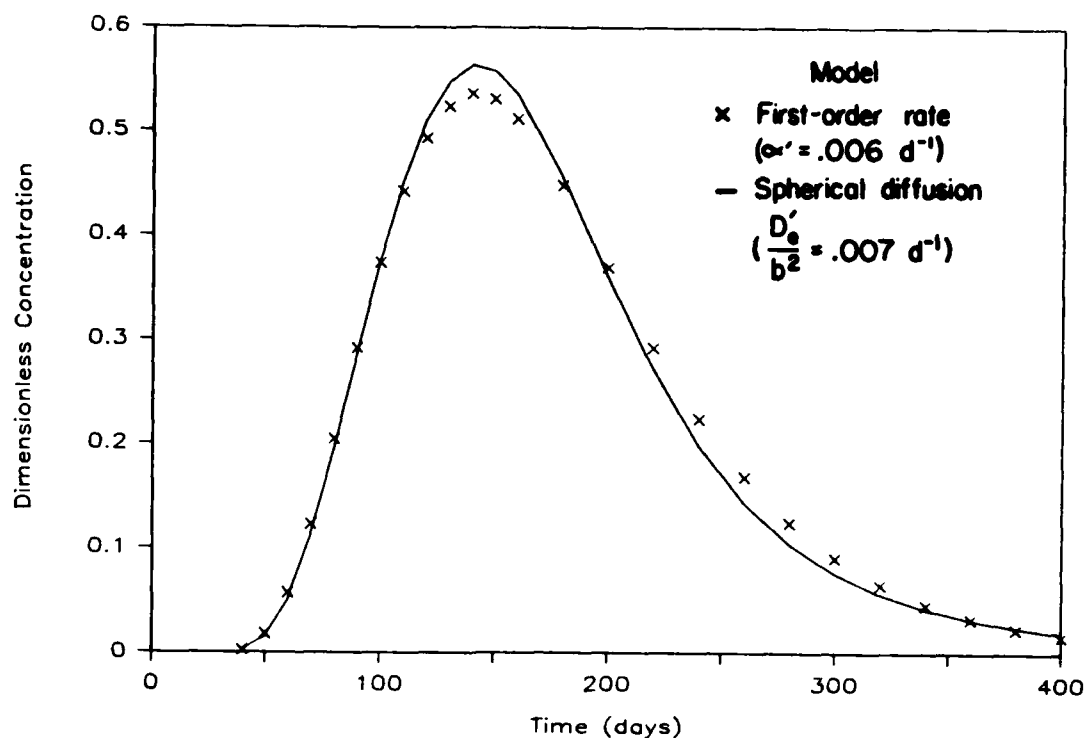
Figure 2.3. Comparison of the first-order rate and spherical diffusion model solutions: $\phi = 0.90$, $v_m = 0.091$ m/d, $\theta = 0.38$, $D_{mx} = 0.02$ m^2/d, $D_{my} = 0.0016$ m^2/d, $D_{mz} = 0.6 \times 10^{-5}$ m^2/d, $\ell = 5.0$ m, $m = 0.0$ m, $n = -0.40$ m, $L = 1.5$ m, $M = 3.0$ m, $N = 0.8$ m, $R_m = 2.78$, and $R_{im} = 5.00$.

Using Eq. 2-19, an equivalent spherical diffusion rate parameter may be obtained for use in the spherical diffusion model. As can be seen in Figure 2.3, the solutions of the first-order rate model and the spherical diffusion model are similar in form, but differ slightly in detailed shape. In Chapter 4, the concept of model equivalence will be discussed in more detail.

CHAPTER 3

MOMENT ANALYSIS

In the preceding chapter, models were presented that describe solute transport by integrating either a diffusion expression or first-order rate expression into the three-dimensional advective/dispersive equation. A convenient means of quantitatively studying the solute plume behavior predicted using such two-region or physical nonequilibrium models is to examine the moments in space and time of the models' simulated concentration distributions. In this chapter, a three-dimensional form of Aris' method of moments is presented, and then used to derive temporal moments associated with the mobile and immobile regions. In addition, a one- and three-dimensional spatial analog to Aris' method is developed, and used to examine spatial moment behavior in both the mobile and immobile regions. The moment analysis is extended to assess the effect of model dimensionality on the form of the moment expressions.

TEMPORAL MOMENT EQUATIONS

Mobile Region

Based on the definitions of the jth absolute temporal moment of a solute concentration distribution, $C_m(x,t)$:

$$m_{j,t} = \int_0^\infty t^j C_m(x,t) dt \qquad (3-1)$$

and the Laplace transform of the function $C_m(x,t)$:

$$L[C_m(x,t)] = \overline{C}_m(x,s) = \int_0^\infty e^{-st} C_m(x,t) dt \qquad (3-2)$$

where s is the Laplace transform variable, Aris (1958) showed that:

$$m_{j,t} = (-1)^j \lim_{s \to 0} \left[\frac{d^j \overline{C}_m(x,s)}{ds^j} \right] \qquad (3-3)$$

Equation 3-3, referred to as Aris' method of moments, is quite useful, since it allows the calculation of temporal moments without having to invert the Laplace transform. Aris' method has been widely used,

particularly in chemical engineering research, to analyze the temporal moments of concentration responses simulated by models which combine one-dimensional advective/dispersive transport with a diffusion expression (Kucera, 1965; Schneider and Smith, 1968; Wakao and Kaguei, 1982; Valocchi, 1985a).

Extension of Aris' method to two and three dimensions is straight-forward, though as far as can be ascertained, has not been utilized previously to describe solute transport. In three dimensions, Eq. 3-3 can be rewritten:

$$m_{j,t} = (-1)^j \lim_{s \to 0} \left[\frac{d^j \bar{C}_m(x,y,z,s)}{ds^j} \right] \qquad (3-4)$$

Table 3.1 presents one- and three-dimensional solutions, in the Laplace domain, for the mobile region concentration distributions of the local equilibrium, first-order rate, and diffusion models. These Laplace domain solutions are obtained from the derivations given in Appendices A and B.

Equation 3-3 can be applied to the one-dimensional expressions for mobile solute concentration listed in Table 3.1a. It is convenient to present the resulting moments in normalized form, where the jth normalized moment $\mu'_{j,t}$ is defined as:

$$\mu'_{j,t} = \frac{m_{j,t}}{m_{o,t}} \qquad (3-5)$$

Results for the zeroth, first, and second normalized absolute temporal moments are presented in Table 3.2. The moments for the local equilibrium and diffusion models have been reported previously by Kucera (1965), who used initial/boundary conditions identical to those used herein.

Similarly, Eq. 3-4 may be applied to the three-dimensional expressions in Table 3.1b. The temporal moments for the three-dimensional models are presented in Table 3.3.

An examination of Tables 3.2 and 3.3 reveals several important features of the moments. In one dimension, the zeroth absolute temporal moment, $m_{o,t}$, is constant for all three models, and is equal to M_1/v. The v term in the denominator is due to the model initial condition, which is expressed as a Dirac pulse of the solute in space (units of [M]),

18

TABLE 3.1

MOBILE REGION SOLUTE CONCENTRATION IN THE LAPLACE DOMAIN
FOR VARIOUS MODELS

a. One-Dimensional

$$\overline{C}_m(x,s) = \frac{M_1 \, e^{vx/2D_x}}{2\sqrt{D_x} \; \Omega(s)} \; e^{(-x/\sqrt{D_x})\Omega(s)}$$

where $\Omega(s) = \sqrt{\dfrac{v^2}{4D_x} + N^2}$

and

$N^2 = s$ for the local equilibrium model

$N^2 = \dfrac{\alpha\beta s}{s + \alpha} + s$ for the first-order rate model

$N^2 = \dfrac{\beta s \; \text{Sinh}(\omega b)}{\omega b \; \text{Cosh}(\omega b)} + s$ for the layered diffusion model

$N^2 = \dfrac{2\beta s I_1(\omega b)}{\omega b \; I_0(\omega b)} + s$ for the cylindrical diffusion model

$N^2 = \dfrac{3\beta s i_1(\omega b)}{\omega b \; i_0(\omega b)} + s$ for the spherical diffusion model

$\omega = \sqrt{\dfrac{s}{D_e}}$

b. Three-Dimensional

$$\overline{C}_m(x,y,z,s) = \frac{F}{G} \, e^{-G\Omega(s)}$$

where $F = \dfrac{M_3 \, e^{vx/2D_x}}{4\pi \sqrt{D_x D_y D_z}}$

and $G = \sqrt{\dfrac{x^2}{D_x} + \dfrac{y^2}{D_y} + \dfrac{z^2}{D_z}}$

$\Omega(s)$ is defined as above

TABLE 3.2

ABSOLUTE TEMPORAL MOMENTS FOR 1-D MOBILE SOLUTE CONCENTRATION RESPONSES

	Local Equilibrium Model*	First-Order Rate Model	Diffusion Model*
$m_{o,t}$	M_1/v	M_1/v	M_1/v
$\mu'_{1,t}$	$\dfrac{\ell}{v} + \dfrac{2D_x}{v^2}$	$\left(\dfrac{\ell}{v} + \dfrac{2D_x}{v^2}\right)(1+\beta)$	$\left(\dfrac{\ell}{v} + \dfrac{2D_x}{v^2}\right)(1+\beta)$
$\mu'_{2,t}$	$\dfrac{\ell^2}{v^2} + \dfrac{6D_x\ell}{v^3} + \dfrac{12D_x^2}{v^4}$	$\left[\dfrac{\ell^2}{v^2} + \dfrac{6D_x\ell}{v^3} + \dfrac{12D_x^2}{v^4}\right](1+\beta)^2$ $+ \left[\dfrac{2\ell}{v} + \dfrac{4D_x}{v^2}\right]\dfrac{\beta}{\alpha}$	$\left[\dfrac{\ell^2}{v^2} + \dfrac{6D_x\ell}{v^3} + \dfrac{12D_x^2}{v^4}\right](1+\beta)^2$ $+ \left[\dfrac{2\ell}{v} + \dfrac{4D_x}{v^2}\right]\dfrac{\beta}{a}$

where $a = \dfrac{\nu(\nu + 2)D_e}{b^2}$

and

$\nu = 1$ layered diffusion

$\nu = 2$ cylindrical diffusion

$\nu = 3$ spherical diffusion

*From Kucera (1965).

whereas the zeroth moment of a temporal distribution (one dimensional concentration versus time) has units of $[ML^{-1}T]$. Thus, to transform the zeroth moment of the initial condition in space [M] to the zeroth moment of a one-dimensional temporal distribution $[ML^{-1}T]$, it is necessary to multiply by a factor with units $[L^{-1}T]$. That factor is the constant $1/v$.

As expected, the zeroth moment for the one-dimensional models is independent of both the diffusion rate and model type, since all the mass which was initially put into the one-dimensional space must eventually flow past the sampling point. Perhaps less obvious is the fact that the zeroth moment is independent of the diffusion rate and model type for the three-dimensional models as well. However, considering a pathway connecting the initial solute distribution with any particular sampling location, it can be seen that, although diffusion would affect the speed with which solute "particles" reach the sampling point,

20

TABLE 3.3

ABSOLUTE TEMPORAL MOMENTS FOR 3-D MOBILE SOLUTE CONCENTRATION RESPONSES

	Local Equilibrium Model	First-Order Rate Model	Diffusion Model
$m_{0,t}$	$\dfrac{F}{G}\, e^{-G(v/2\sqrt{D_x})}$	$\dfrac{F}{G}\, e^{-G(v/2\sqrt{D_x})}$	$\dfrac{F}{G}\, e^{-G(v/2\sqrt{D_x})}$
$\mu'_{1,t}$	$\dfrac{G\sqrt{D_x}}{v}$	$\dfrac{G\sqrt{D_x}}{v}(1+\beta)$	$\dfrac{G\sqrt{D_x}}{v}(1+\beta)$
$\mu'_{2,t}$	$\dfrac{G^2 D_x}{v^2} + \dfrac{2GD_x^{3/2}}{v^3}$	$\dfrac{G^2 D_x}{v^2}(1+\beta)^2 + \dfrac{2GD_x^{3/2}}{v^3}(1+\beta)^2$ $+ \dfrac{2G\sqrt{D_x}}{v}\dfrac{\beta}{\alpha}$	$\dfrac{G^2 D_x}{v^2}(1+\beta)^2 + \dfrac{2GD_x^{3/2}}{v^3}(1+\beta)^2$ $+ \dfrac{2G\sqrt{D_x}}{v}\dfrac{\beta}{a}$

where $\quad a = \dfrac{v(v+2)D_e}{b^2}$

and $\quad v = 1 \quad$ layered diffusion

$\qquad\quad v = 2 \quad$ cylindrical diffusion

$\qquad\quad v = 3 \quad$ spherical diffusion

$$F = \frac{M_3\, e^{v\ell/2D_x}}{4\pi\,\sqrt{D_x D_y D_z}}$$

$$G = \sqrt{\frac{\ell^2}{D_x} + \frac{m^2}{D_y} + \frac{n^2}{D_z}}$$

the total amount of solute sampled would be dependent only on the total injected mass (M_3), the sampler location (ℓ,m,n), and the hydrodynamic parameters $(v,\ D_x,\ D_y,\ D_z)$.

It is interesting to compare the temporal first moments obtained from the one-dimensional and three-dimensional models. Considering the first moment of the three-dimensional models along the line of advective transport $(m = n = 0)$, it is found:

$$\mu'_{1,t} = \frac{\ell}{v} \tag{3-6}$$

for the local equilibrium model, and

$$\mu_{1,t}^{i} = \frac{\ell}{v}(1+\beta) \qquad\qquad (3-7)$$

for the first-order rate and diffusion models. These values are less than those of the one-dimensional models by a constant $2D_x/v^2$ for the local equilibrium model, and $2D_x(1+\beta)/v^2$ for the physical nonequilibrium models. This effect, of essentially delaying the arrival of the center of mass of the one-dimensional models, is due to the fact that with the three-dimensional models, solute which disperses in the negative x-direction may eventually disperse in the y- and z-directions as well, thereby never passing the sampling point on the $y = z = 0$ axis. However, with the one-dimensional models, the solute which has dispersed in the negative x-direction will nevertheless eventually pass the sampling point, thereby increasing the first temporal moment. For the same reason, the second temporal moments of the one-dimensional models are greater than those of the three-dimensional models along the line $y = z = 0$.

Immobile Region

The methods of the preceding section may be applied to determine the temporal moments of solute associated with the immobile regions. Before commencing the analysis, however, some explanation is required to define what is meant by the concentration distribution associated with the immobile region.

With regard to the temporal moments, the immobile region concentration response would be obtained by sampling the immobile region at a point in space. Conceptually, imagine a sampling point which yields volume-averaged solute concentrations from a region of immobile water. To insure mass balance, it is necessary to multiply moments obtained from the immobile region concentration distribution by a weighting factor. This weighting factor is required because solute is unevenly distributed between the mobile and immobile regions. To determine the value of this weighting factor, compare the total solute masses associated with the mobile and immobile regions of an incremental volume of aquifer (dV). The total mass associated with the mobile region (aqueous plus sorbed) is $C_m \theta_m R_m dV$, and the total mass associated with the immobile region (aqueous plus sorbed) is $C_{im} \theta_{im} R_{im} dV$. The ratio of immobile to mobile solute masses is therefore:

$$\frac{C_{1m} \theta_{1m} R_{1m}}{C_m \theta_m R_m} = \frac{\beta C_{1m}}{C_m}$$

Thus, to insure proper mass balance, moments obtained from the immobile region concentration distribution must be multiplied by the weighting factor β. Therefore, the jth temporal moment of the immobile region concentration distribution may be defined as:

$$n_{j,t} = \int_0^\infty t^j [\beta C_{1m}(x,t)] dt \qquad (3-8)$$

Of course, for the local equilibrium model, $\beta = 0$, and these moments are identically zero.

The immobile region analogs to Eqs. 3-3 and 3-4 are:

$$n_{j,t} = \beta(-1)^j \lim_{s \to 0} \left[\frac{d^j \overline{C}_{1m}(x,s)}{ds^j} \right] \qquad (3-9a)$$

$$n_{j,t} = \beta(-1)^j \lim_{s \to 0} \left[\frac{d^j \overline{C}_{1m}(x,y,z,s)}{ds^j} \right] \qquad (3-9b)$$

Equations 3-9a and 3-9b require solutions for the immobile concentrations in the Laplace domain, for the various models. Table 3.4 lists these solutions in one and three dimensions. The zeroth and first moments, obtained by applying Eqs. 3-9a and 3-9b to the immobile solute concentration expressions listed in Table 3.4, are presented in Table 3.5. As with the mobile concentration response moments, it is convenient to express moments greater than the zeroth in terms of normalized moments, defined as:

$$v'_{j,t} = \frac{n_{j,t}}{n_{o,t}} \qquad (3-10)$$

Compare Tables 3.2 and 3.5, to find that:

$$m_{o,t} + n_{o,t} = \frac{(1+\beta)}{v} M_1 \qquad (3-11)$$

for the one-dimensional physical nonequilibrium models. This is again due to the conversion of an initial condition in space to a zeroth moment in time. It should be noted, however, that the conversion factor

23

TABLE 3.4

IMMOBILE REGION SOLUTE CONCENTRATION IN THE LAPLACE DOMAIN
FOR VARIOUS MODELS

__One-Dimensional__

$$\overline{C}_{im}(x,s) = \frac{\alpha}{s + \alpha}\, \overline{C}_m(x,s)$$ for the first-order rate model

$$\overline{C}_{im}(x,s) = \frac{Sinh(\omega b)}{\omega b\ Cosh(\omega b)}\, \overline{C}_m(x,s)$$ for the layered diffusion model

$$\overline{C}_{im}(x,s) = \frac{2 I_1(\omega b)}{\omega b\ I_0(\omega b)}\, \overline{C}_m(x,s)$$ for the cylindrical diffusion model

$$\overline{C}_{im}(x,s) = \frac{3 i_1(\omega b)}{\omega b\ i_0(\omega b)}\, \overline{C}_m(x,s)$$ for the spherical diffusion model

where $\overline{C}_m(x,s)$ for each model is defined in Table 3.1.

__Three-Dimensional__

$$\overline{C}_{im}(x,y,z,s) = \frac{\alpha}{s + \alpha}\, \overline{C}_m(x,y,z,s)$$ for the first-order rate model

$$\overline{C}_{im}(x,y,z,s) = \frac{Sinh(\omega b)}{\omega b\ Cosh(\omega b)}\, \overline{C}_m(x,y,z,s)$$ for the layered diffusion model

$$\overline{C}_{im}(x,y,z,s) = \frac{2 I_1(\omega b)}{\omega b\ I_0(\omega b)}\, \overline{C}_m(x,y,z,s)$$ for the cylindrical diffusion model

$$\overline{C}_{im}(x,y,z,s) = \frac{3 i_1(\omega b)}{\omega b\ i_0(\omega b)}\, \overline{C}_m(x,y,z,s)$$ for the spherical diffusion model

where $\overline{C}_m(x,y,z,s)$ for each model is defined in Table 3.1.

for the total solute, mobile plus immobile, is $(1+\beta)/v$, whereas for the mobile solute alone, the conversion factor was $1/v$. This is because the total solute mass movement is slower than the mobile region mass movement due to the influence of the immobile region.

This effect can be seen more clearly by comparing the first temporal moments of the mobile and immobile solute concentration responses. The first moment of the immobile region response lags the first moment of the mobile by a constant: $1/\alpha$ for the first-order rate model, and $1/a$ for the diffusion models.

TABLE 3.5

ABSOLUTE TEMPORAL MOMENTS FOR IMMOBILE SOLUTE CONCENTRATION RESPONSES

	First-Order Rate Model	Diffusion Model
One-Dimensional		
$n_{o,t}$	$\dfrac{\beta M_1}{v}$	$\dfrac{\beta M_1}{v}$
$v'_{1,t}$	$\dfrac{\ell(1+\beta)}{v} + \dfrac{2D_x(1+\beta)}{v^2} + \dfrac{1}{\alpha}$	$\dfrac{\ell(1+\beta)}{v} + \dfrac{2D_x(1+\beta)}{v^2} + \dfrac{1}{a}$
Three-Dimensional		
$n_{o,t}$	$\beta\,\dfrac{F}{G}\,e^{-G(v/2\sqrt{D_x})}$	$\beta\,\dfrac{F}{G}\,e^{-G(v/2\sqrt{D_x})}$
$v'_{1,t}$	$\dfrac{G\sqrt{D_x}}{v}(1+\beta) + \dfrac{1}{\alpha}$	$\dfrac{G\sqrt{D_x}}{v}(1+\beta) + \dfrac{1}{a}$

$$\text{where} \quad a = \frac{v(v+2)D_e}{b^2}$$

$$\text{and} \quad v = 1 \quad \text{layered diffusion}$$
$$v = 2 \quad \text{cylindrical diffusion}$$
$$v = 3 \quad \text{spherical diffusion}$$

$$F = \frac{M_3\, e^{v\ell/2D_x}}{4\pi\,\sqrt{D_x D_y D_z}}\ , \quad G = \sqrt{\frac{\ell^2}{D_x} + \frac{m^2}{D_y} + \frac{n^2}{D_z}}$$

SPATIAL MOMENT EQUATIONS

Mobile Region

Analogous to definitions (3-1) and (3-2), the one-dimensional jth absolute spatial moment of the concentration distribution, $C_m(x,t)$, is:

$$m_j = \int_{-\infty}^{\infty} x^j C_m(x,t)dx \tag{3-12}$$

and the Fourier transform of the function, $C_m(x,t)$, is defined by:

$$F[C_m(x,t)] = \hat{C}_m(p,t) = \int_{-\infty}^{\infty} e^{-ipx}\, C_m(x,t)dx \tag{3-13}$$

where p is the Fourier transform variable. Using the following property of the Fourier transform (Spiegel, 1968):

$$F[x^j C_m(x,t)] = \int_{-\infty}^{\infty} e^{-ipx} x^j C_m(x,t)dx = i^j \frac{d^j \hat{C}_m(p,t)}{dp^j} \quad (3-14)$$

take the limit as $p \to 0$ to find:

$$\int_{-\infty}^{\infty} x^j C_m(x,t)dx = i^j \lim_{p \to 0} \frac{d^j \hat{C}_m(p,t)}{dp^j} \quad (3-15)$$

and then using Eq. 3-12 write:

$$m_j = i^j \lim_{p \to 0} \left[\frac{d^j \hat{C}_m(p,t)}{dp^j} \right] \quad (3-16)$$

This is the one-dimensional spatial analog to Aris' method of temporal moments. Although Eq. 3-16 is a well known property of Fourier transforms (Bremermann, 1963; Bracewell, 1978), it apparently has never been used previously to obtain moments of spatial concentration distributions for solute transport models.

The extension of Eq. 3-16 to two and three dimensions is straightforward. In three dimensions, the absolute spatial moment of the concentration distribution $C_m(x,y,z,t)$ is:

$$m_{jk\ell} = \int_{-\infty}^{\infty} \int_{-\infty}^{\infty} \int_{-\infty}^{\infty} x^j y^k z^\ell C_m(x,y,z,t)dxdydz \quad (3-17)$$

The Fourier transform in three dimensions is defined (Bracewell, 1978) by

$$F[C_m(x,y,z,t)] = \hat{C}_m(p,q,u,t) =$$
$$\int_{-\infty}^{\infty} \int_{-\infty}^{\infty} \int_{-\infty}^{\infty} e^{-i(px+qy+uz)} C_m(x,y,z,t)dxdydz \quad (3-18)$$

where p, q, and u are the Fourier transform variables in the x-, y-, and z-directions, respectively. With these definitions, follow the one-dimensional analysis directly to find:

$$m_{jk\ell} = i^{j+k+\ell} \lim_{\substack{p \to 0 \\ q \to 0 \\ u \to 0}} \frac{d^j}{dp^j} \left\{ \frac{d^k}{dq^k} \left[\frac{d^\ell \hat{C}_m(p,q,u,t)}{du^\ell} \right] \right\} \quad (3-19)$$

26

As with Aris' method for temporal moments, these spatial moment equations, (3-16) and (3-19), are quite useful, since they allow the calculation of moments in the Fourier domain, thereby eliminating the need for complicated inversions of the transforms.

Appendix C presents the details of deriving the absolute spatial moments for the local equilibrium, first-order rate, and diffusion models. The method followed for all three models is essentially the same. The model equations, with appropriate initial/boundary conditions for a solute pulse in an infinite medium, are Fourier transformed. The equations are then solved in the Fourier domain for $\hat{C}_m(p,q,u,t)$. Equation 3-19 is then applied to obtain the zeroth, first, and second absolute spatial moments. The derivations were done using the three-dimensional formulae. Conversion of the three-dimensional results to one dimension is trivial, using the relationships:

$$m_0 = m_{000} \tag{3-20a}$$

$$m_1 = m_{100} \tag{3-20b}$$

$$m_2 = m_{200} \tag{3-20c}$$

Thus, in space, model dimensionality has little effect on the moments. However, in time, model dimensionality plays an important role.

Table 3.6 presents the spatial moments for the three models, where

$$\mu'_{jk\ell} = \frac{m_{jk\ell}}{m_{000}} \tag{3-21}$$

defines the normalized absolute moment. The local equilibrium model results are well known (e.g., Freyberg, 1986). Valocchi (1985b), using a method different from that presented here, derived the moments in space for the first-order rate model. The diffusion model moments presented in Table 3.6 are new.

Immobile Region

The methods of the preceding section may be applied to determine the spatial moments of solute concentration associated with the immobile region. Analogous to Eq. 3-8, which defines the temporal moments of immobile region solute, we may define the spatial moments for the immobile region as:

27

TABLE 3.6

SPATIAL MOMENTS FOR THREE-DIMENSIONAL MOBILE SOLUTE DISTRIBUTIONS

Moment[a]	Local Equilibrium Model	First-Order Rate Model	Diffusion Models
m_{000}	M_3	$\dfrac{M_3(1+\beta A)}{1+\beta}$	$\lim_{c\to 0}\ \left[\dfrac{M_3}{2(1+\beta)} + \dfrac{4D_e M_3}{\pi b^2}B_1\right]$
μ'_{100}	vt	$\dfrac{vt(1+\beta^2 A)}{(1+\beta)(1+\beta A)} + \dfrac{2v\beta(1-A)}{a(1+\beta)^2(1+\beta A)}$	$\lim_{c\to 0}\ \dfrac{vt}{2(1+\beta)^2} + \dfrac{v}{\pi c(1+\beta)^2} + \dfrac{v\beta}{a(1+\beta)^3} + \dfrac{4vD_e}{\pi b^2}B_2$ $\left[\dfrac{1}{2(1+\beta)} + \dfrac{4D_e}{\pi b^2}B_1\right]$
μ'_{200}	$2D_z t + v^2 t^2$	$\dfrac{2D_x t(1+\beta^2 A)}{(1+\beta)(1+\beta A)} + \dfrac{4D_x\beta(1-A)}{a(1+\beta)^2(1+\beta A)}$ $+ \dfrac{v^2 t^2(1+\beta^3 A)}{(1+\beta)^2(1+\beta A)} + \dfrac{6v^2\beta(\beta-1)(1-A)}{a^2(1+\beta)^4(1+\beta A)}$ $+ \dfrac{6\beta v^2 t(1-\beta A)}{a(1+\beta)^3(1+\beta A)}$	$\lim_{c\to 0}\ \dfrac{2D_x}{\pi c(1+\beta)^2} + \dfrac{D_x t}{(1+\beta)^2} + \dfrac{2v^2 t}{\pi c(1+\beta)^3} + \dfrac{v^2 t^2}{2(1+\beta)^3} + \dfrac{6\beta^2 v^2}{a^2(1+\beta)^5}$ $+ \dfrac{-3v^2}{(1+\beta)^4 c} + \dfrac{6v^2\beta}{\pi c a(1+\beta)^4} + \dfrac{3v^2\beta t}{a(1+\beta)^4} + \dfrac{8D_x D_e}{\pi b^2}B_3 + \dfrac{8v^2 D_e}{\pi b^2}B_3$ $\left[\dfrac{1}{2(1+\beta)} + \dfrac{4D_e}{\pi b^2}B_1\right]$
μ'_{020}	$2D_y t$	$\dfrac{2D_y t(1+\beta^2 A)}{(1+\beta)(1+\beta A)} + \dfrac{4D_y\beta(1-A)}{a(1+\beta)^2(1+\beta A)}$	$\lim_{c\to 0}\ \dfrac{2D_y}{\pi c(1+\beta)^2} + \dfrac{D_y t}{(1+\beta)^2} + \dfrac{2D_y\beta}{a(1+\beta)^3} + \dfrac{8D_y D_e}{\pi b^2}B_2$ $\left[\dfrac{1}{2(1+\beta)} + \dfrac{4D_e}{\pi b^2}B_1\right]$
μ'_{002}	$2D_z t$	$\dfrac{2D_z t(1+\beta^2 A)}{(1+\beta)(1+\beta A)} + \dfrac{4D_z\beta(1-A)}{a(1+\beta)^2(1+\beta A)}$	$\lim_{c\to 0}\ \dfrac{2D_z}{\pi c(1+\beta)^2} + \dfrac{D_z t}{(1+\beta)^2} + \dfrac{2D_z\beta}{a(1+\beta)^3} + \dfrac{8D_z D_e}{\pi b^2}B_2$ $\left[\dfrac{1}{2(1+\beta)} + \dfrac{4D_e}{\pi b^2}B_1\right]$

where

$$A = e^{-at(1+\beta)}\ ;\quad B_1 = \int_{b\sqrt{\frac{c}{2D_e}}}^{\infty} \frac{e_1\ \text{Cos}\ \dfrac{2D_e\lambda^2 t}{b^2} + f_1\ \text{Sin}\ \dfrac{2D_e\lambda^2 t}{b^2}}{\left(\Omega_1^2 + \Omega_2^2\right)^i}\ \lambda d\lambda$$

$e_1 = \Omega_1\ ,\ e_2 = \Omega_1^2 - \Omega_2^2\ ,\ e_3 = \Omega_1^3 - 3\Omega_1\Omega_2^2\ ;\ f_1 = \Omega_2\ ,\ f_2 = 2\Omega_1\Omega_2\ ,\ f_3 = -\Omega_2^3 + 3\Omega_1^2\Omega_2$

and Ω_1, Ω_2, a, and c are as defined in Appendix C.

[a] $\mu'_{jk\ell} = 0$ for k or ℓ odd.

28

$$n_{jk\ell} = \int_{-\infty}^{\infty} \int_{-\infty}^{\infty} \int_{-\infty}^{\infty} x^j y^k z^\ell [\beta C_{im}(x,y,z,t)] dx\,dy\,dz \qquad (3\text{-}22)$$

and

$$\nu'_{jk\ell} = \frac{n_{jk\ell}}{n_{000}}$$

Again, for the local equilibrium model, $\beta = 0$, and the immobile region moments are identically zero. The immobile region analog to Eq. 3-19 is:

$$n_{jk\ell} = \beta\, i^{j+k+\ell} \lim_{\substack{p \to 0 \\ q \to 0 \\ u \to 0}} \frac{d^j}{dp^j} \left\{ \frac{d^k}{dq^k} \left[\frac{d^\ell \hat{C}_{im}(p,q,u,t)}{du^\ell} \right] \right\} \qquad (3\text{-}23)$$

Equation 3-23 may be applied to the Fourier transformed immobile region concentration, $\hat{C}_{im}(p,q,u,t)$, to obtain the immobile region moments. Details of deriving the immobile region spatial moments for the first-order rate and diffusion models are presented in Appendix D. Expressions for the zeroth and first immobile region moments are listed in Table 3.7. Valocchi (1985b) derived the first-order rate expressions shown in Table 3.7 by a different method.

Testing

Evaluation of the temporal moments for all three models, as well as evaluation of the spatial moments for the local equilibrium and first-order rate models, is straightforward; and in fact can easily be accomplished using a hand-held calculator. However, calculation of the diffusion model spatial moments requires numerical evaluation of an infinite integral using the Gaussian quadrature technique of Rasmuson and Neretnieks (1981) and van Genuchten et al. (1984); as well as evaluating a limit as the parameter ϵ approaches zero. Therefore, it is essential to assess the accuracy of the numerical evaluation, as well as to determine the appropriate values of ϵ to use.

One way to test the solution's accuracy is to compare the solution with the known solution of a limiting case. As β approaches zero, the diffusion model's spatial moments should approach the known spatial moments of the local equilibrium model. Figure 3.1 shows the relative error

TABLE 3.7

SPATIAL MOMENTS FOR THREE-DIMENSIONAL IMMOBILE SOLUTE DISTRIBUTIONS

Moment*	First-Order Rate Model	Diffusion Models
n_{000}	$\dfrac{M_3\beta(1-A)}{(1+\beta)}$	$M_3 - \dfrac{M_3}{2(1+\beta)} - \dfrac{4D_e M_3}{\pi b^2} B_1$
ν'_{100}	$\dfrac{vt(1-\beta A)}{(1+\beta)(1-A)} + \dfrac{v(\beta-1)}{\alpha(1+\beta)^2}$	$\lim_{\epsilon\to 0} \dfrac{\left[\dfrac{vt\beta}{2(1+\beta)^2} + \dfrac{v\beta}{\pi\epsilon(1+\beta)^2} + \dfrac{v(\beta-1)\beta}{2a(1+\beta)^3} - \dfrac{2v}{\pi} C_1 - \dfrac{4vD_e}{\pi b^2} B_2\right]}{\left[1 - \dfrac{1}{2(1+\beta)} - \dfrac{4D_e}{\pi b^2} B_1\right]}$

where

$$C_1 = \int_{b\sqrt{\frac{\epsilon}{2D_e}}}^{\infty} \frac{\Omega_2 \cos \dfrac{2D_e \lambda^2 t}{b^2} - \Omega_1 \sin \dfrac{2D_e \lambda^2 t}{b^2}}{\lambda(\Omega_1^2 + \Omega_2^2)} \, d\lambda$$

and Ω_1, Ω_2, and a are as defined in Appendix C. A and B_ℓ are as defined in Table 3.6.

*$\nu_{jk\ell} = 0$ for k or ℓ odd.
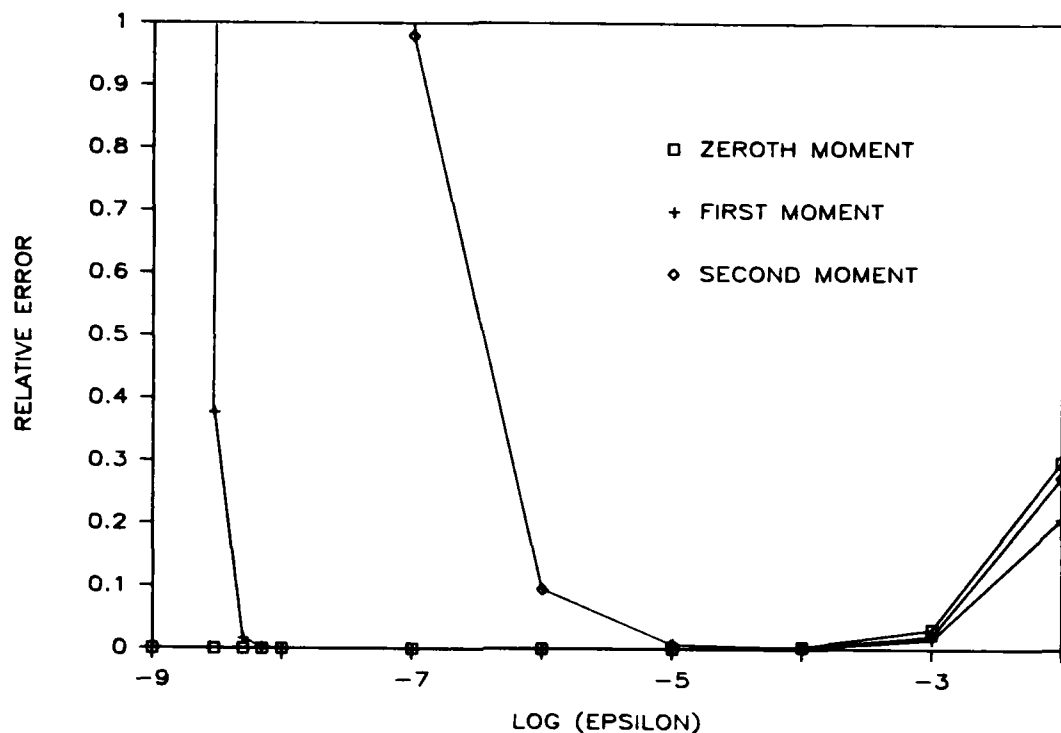
Figure 3.1. Relative error of the spherical diffusion model mobile region spatial moment calculation (comparison with limiting case of equilibrium transport): $v = 0.1$ m/d, $D_x = 0.04$ m^2/d, $D_e/b^2 = 0.006$ d^{-1}, $\beta = 0.0001$, and $t = 100$ d.

versus $\log(\epsilon)$ for the spherical diffusion model's zeroth, first, and second spatial moments in the mobile region, where relative error is defined as:

$$\text{Relative Error} = \frac{\left|\text{LE moment} - \text{Diffusion moment}\right|}{\text{LE moment}} \qquad (3-24)$$

Since the parameter, ϵ, has units of $[T^{-1}]$ (see Table 3.6), it is important that ϵ be small with respect to the other rate constants in the solution: a, a/β, and $1/t$. Thus, the constraint is imposed that:

$$\epsilon \ll \text{Min}(a, a/\beta, 1/t) \qquad (3-25)$$

For the parameters used in Figure 3.1,

$$\text{Min}(a, a/\beta, 1/t) = 0.01 \qquad (3-26)$$

From Figure 3.1, it is seen that the relative error of the zeroth moment solution approaches zero for $\log \epsilon < (-4)$. For the first moment, if

31

$(-8) < \log \epsilon < (-4)$ the relative error is small, and for the second moment solution, if $(-5) < \log \epsilon < (-4)$, the relative error is small. For the zeroth, first, and second moment solutions, an upper bound on ϵ may be defined by the expression:

$$\epsilon < 0.01[\text{Min}(a, a/\beta, 1/t)] \qquad (3-27)$$

However, to evaluate the first and second moments, there also is a lower bound on ϵ, as the definite integrals in the first and second moment formulae approach minus infinity as the lower limit of integration approaches zero. Thus, at very small values of ϵ, numerical errors in the quadrature technique used to evaluate the definite integrals become substantial. This is not the case for the zeroth moment integral; consequently, there is no lower bound on ϵ in the zeroth moment evaluation.

The lower bound of ϵ in the first and second moment solutions is dependent not only on the model parameters, but also on machine precision. In practice, to be confident of a first or second moment value obtained using the formulae in Table 3.6, it is necessary to calculate the solution over a range of values for ϵ, thus obtaining a plot similar to that shown in Figure 3.1. A flat region will usually be found, where the moment will not vary over a range of one or two orders of magnitude for ϵ. This value for the moment is correct within a few percent, as can be seen from Figure 3.1.

Another test is to compare the moments calculated using the formulae in Table 3.6 with the moments calculated by actually computing the spatial distribution of the solute, using formulae derived in Chapter 2, at repeated points in space, and then using a numerical quadrature technique to obtain the moments of the distribution. Figure 3.2 gives a plot of the relative error versus $\log(\epsilon)$ for the spherical diffusion model, where the relative error is now defined as:

$$\text{Relative error} = \frac{|\text{Moment from distribution} - \text{Moment from formula}|}{\text{Moment from distribution}} \qquad (3-28)$$

In comparing the errors of the moment estimator (Figures 3.1 and 3.2), it is apparent that, with the zeroth and first moments, an acceptable accuracy is assured over many orders of magnitude of ϵ. However, the window of acceptable accuracy is much narrower in the case of the second

32
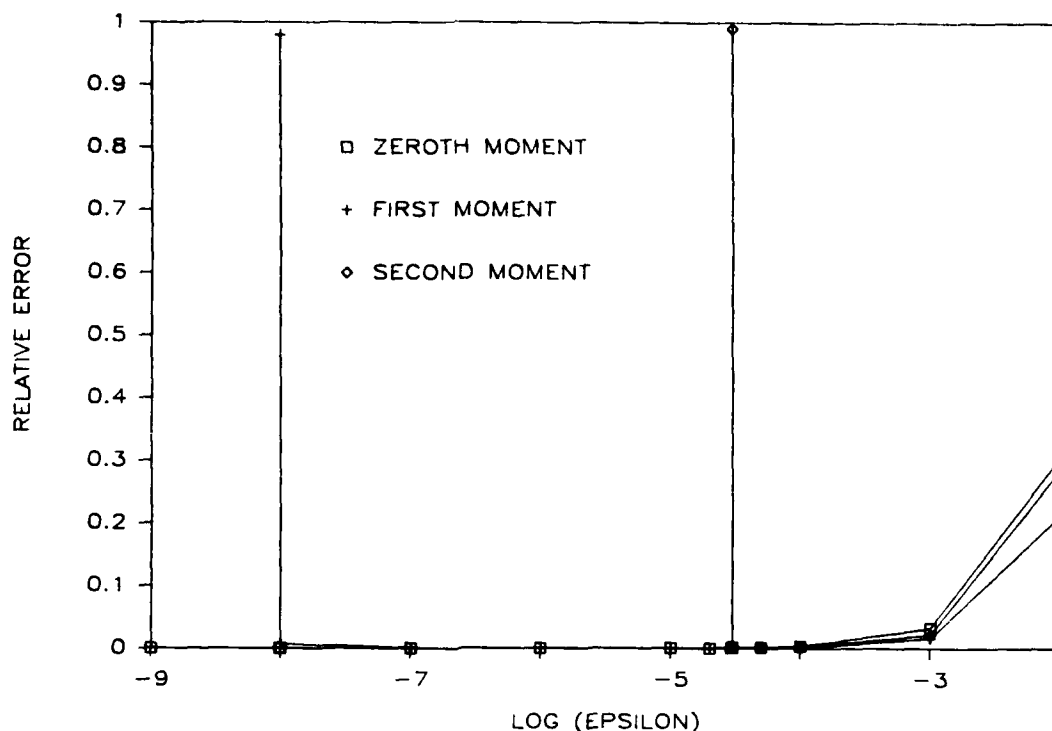
Figure 3.2. Relative error of the spherical diffusion model mobile region spatial moment calculation (comparison with numerically evaluated moments): $v = 0.1$ m/d, $D_x = 0.004$ m^2/d, $D_e/b^2 = 0.006$ d^{-1}, $\beta = 0.25$, and $t = 100$ d.

moment, being confined to 1 to 2 orders of magnitude in ε in the example shown.

A similar plot can be obtained for the zeroth and first immobile region moments, by comparing the formulae for the spherical diffusion model (Table 3.7) with results obtained by numerically integrating the immobile region concentration distribution. The immobile region concentration distribution was obtained by using the IMSL subroutine FLINV (IMSL, 1982) to numerically invert the Laplace domain solution for the immobile region concentration (Table 3.4), at repeated points in space. Figure 3.3 gives the relative error versus $\log(\varepsilon)$ for the zeroth and first immobile region moments of the spherical diffusion model.

For the parameter values used in Figures 3.2 and 3.3:

$$\text{Min}(a, a/\beta, 1/t) = 0.01 \qquad (3-29)$$

Again,

$$\varepsilon < 0.01[\text{Min}(a, a/\beta, 1/t)] \qquad (3-30)$$

33
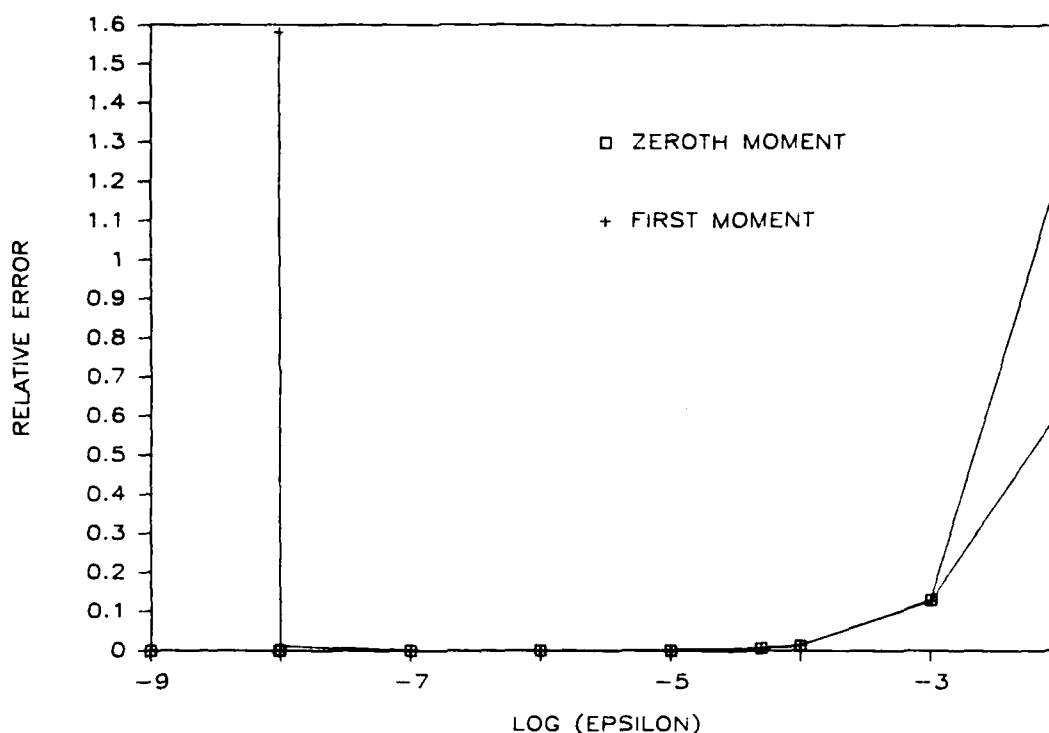
Figure 3.3. Relative error of the spherical diffusion model immobile region spatial moment calculation (comparison with numerically evaluated moments): $v = 0.1$ m/d, $D_x = 0.004$ m^2/d, $D_e/b^2 = 0.006$ d^{-1}, $\beta = 0.25$, and $t = 100$ d.

defines an upper bound on ϵ. Note, too, the sensitivity of the first and second moment solutions to excessively small values of ϵ.

In summary, the numerical evaluation of the zeroth moment formulae, shown in Tables 3.6 and 3.7 for the geometrical diffusion models, is straightforward, as long as ϵ is two orders of magnitude less than Min[a, a/β, 1/t]. Evaluation of the first and second moments is not as straightforward, since ϵ has a lower bound criterion which must also be satisfied, and which is not easily defined. When evaluating the first, and particularly the second moment formulae, it is necessary to determine how the result varies over a range of ϵ, before accepting a value for the moment. In some cases, there is a possibility that no value of ϵ can be found which meets both lower and upper bound criteria. This is especially true when evaluating the second moment, where, judging from Figures 3.1 and 3.2, the lower bound of ϵ can be orders of magnitude greater than the lower bound of the first moment formula.

TEMPORAL VERSUS SPATIAL DATA

Using the relationships derived above, which permit determination of temporal and spatial moments given parameters for the three models under discussion, it is possible to find how certain effective parameters behave with respect to model type, and with respect to type of measurement (in space or time). In particular, an effective velocity (v_{eff}) and an effective dispersion coefficient (D_{eff}) will be derived in terms of model parameters. These effective parameters are local equilibrium model equivalents which approximately duplicate the concentration responses of the physical nonequilibrium models. Use of these effective parameters will aid in understanding how the general behavior of the spatial and temporal concentration distributions differ.

Behavior of Mobile and Immobile Temporal Responses

Effective velocity and dispersion coefficients may be defined in terms of the temporal moments as follows (Valocchi, 1985a):

$$v_{eff} = \frac{\ell}{\mu'_{1,t}} \tag{3-31a}$$

and

$$D_{eff} = \frac{\mu_{2,t}}{2\mu'_{1,t}} v^2_{eff} \tag{3-31b}$$

where

$$\mu_{2,t} = \mu'_{2,t} - (\mu'_{1,t})^2$$

is the central second moment.

Thus, using the expressions for the mobile region temporal moments in Tables 3.2 and 3.3, it is straightforward to determine v_{eff} and D_{eff} in terms of the parameters of the one- and three-dimensional local equilibrium, first-order rate, and diffusion models.

Table 3.8a lists the effective parameters in one dimension for the three models, making the assumption of large Peclet number (Pe $= v\ell/D_x$ $\gg$ 1). Table 3.8b lists the effective parameters in three dimensions, along the line $y = z = 0$. Due to the assumption of large Peclet number in the one-dimensional case, the effect of dispersion in the negative x-direction (which was discussed earlier) becomes negligible, so that the one- and three-dimensional solutions are identical. Of course, since

TABLE 3.8

EFFECTIVE VELOCITY AND DISPERSION COEFFICIENTS FROM TEMPORAL MOMENTS

	Local Equilibrium Model	First-Order Rate Model	Diffusion Model

a. One Dimension (at high values of Pe)

$$v_{eff} \qquad v \qquad \frac{v}{1+\beta} \qquad \frac{v}{1+\beta}$$

$$D_{eff} \qquad D_x \qquad \frac{D_x}{1+\beta} + \frac{v^2\beta}{\alpha(1+\beta)^3} \qquad \frac{D_x}{1+\beta} + \frac{v^2\beta}{a(1+\beta)^3}$$

$$\text{where} \quad a = \frac{\nu(\nu+2)D_e}{b^2}$$

and ν is as defined in Table 3.3.

b. Three Dimensions (along the line y = z = 0)

$$v_{eff} \qquad v \qquad \frac{v}{1+\beta} \qquad \frac{v}{1+\beta}$$

$$D_{eff} \qquad D_x \qquad \frac{D_x}{1+\beta} + \frac{v^2\beta}{\alpha(1+\beta)^3} \qquad \frac{D_x}{1+\beta} + \frac{v^2\beta}{a(1+\beta)^3}$$

the effective parameters represent local equilibrium model equivalents, v_{eff} and D_{eff} for the local equilibrium model are v and D_x, respectively. The high Peclet number expressions for v_{eff} and D_{eff} for the first-order rate and diffusion models, which are presented in Table 3.8a, are well known in one dimension (Baker, 1977; De Smedt and Wierenga, 1984; Valocchi, 1985a). The application to three dimensions is new. By applying Eq. 3-31 to the moment formulae of Table 3.3, values for effective velocity and dispersion coefficients can be obtained at any point in space, for a given model.

The effective velocity of the immobile region response (v_{neff}) may be obtained by applying

$$v_{neff} = \frac{\ell}{v'_{1,t}} \qquad\qquad (3-32)$$

36

to the immobile region moment formulae shown in Table 3.5. Again considering high Peclet numbers in the one-dimensional case, and along the line $y = z = 0$ in the three-dimensional case, yields:

$$v_{neff} = \frac{\ell}{\frac{\ell(1+\beta)}{v} + \frac{1}{\alpha}}$$

(3-33a)

for the first-order rate model, and

$$v_{neff} = \frac{\ell}{\frac{\ell(1+\beta)}{v} + \frac{1}{a}}$$

(3-33b)

for the diffusion models. Of course, the concept of an immobile region solute distribution velocity is not applicable to the local equilibrium model. As expected, the effective velocity in the immobile region is less than that in the mobile region.

In a forthcoming section, the equations derived in this section will be used to compare temporal and spatial behavior.

Behavior of Mobile and Immobile Spatial Distributions

The following relationships between the spatial moments and the total mass associated with the mobile region (M_T), the center of mobile mass location (x_c, y_c, z_c) and the elements of the spatial covariance tensor may be written (Freyberg, 1986):

$$M_T = \theta_m R_m m_{000}$$

$$x_c = \mu'_{100} \quad , \quad y_c = \mu'_{010} = 0 \quad , \quad z_c = \mu'_{001} = 0$$

$$\sigma^2_{xx} = \mu'_{200} - x^2_c$$

(3-34)

$$\sigma^2_{yy} = \mu'_{020}$$

$$\sigma^2_{zz} = \mu'_{002}$$

$$\sigma^2_{xy} = \sigma^2_{yx} = \sigma^2_{xz} = \sigma^2_{zx} = \sigma^2_{yz} = \sigma^2_{zy} = 0$$

As with the temporal moment discussion, effective velocity and dispersion coefficients may also be defined as:

37

$$v_{eff} = \frac{dx_c}{dt} \qquad (3\text{-}35)$$

$$D_{effx} = \frac{1}{2}\frac{d\sigma_{xx}^2}{dt} \quad , \quad D_{effy} = \frac{1}{2}\frac{d\sigma_{yy}^2}{dt} \quad , \quad D_{effz} = \frac{1}{2}\frac{d\sigma_{zz}^2}{dt} \qquad (3\text{-}36)$$

Thus, starting with the spatial moment relationships of Table 3.6, it is possible to derive expressions for the effective velocity and dispersion coefficients for the three models under consideration. In practice, evaluating the effective velocity and dispersion coefficients for the diffusion models requires the numerical evaluation of the derivatives in (3-35) and (3-36).

Figure 3.4 shows how M_T, v_{eff}, and D_{effx} behave as a function of time for each of the three model types. Model parameters for the example were arbitrarily chosen, except that the first-order (α) and the diffusion model (a) rate parameters were selected so that

$$\alpha = a \qquad (3\text{-}37)$$

The use of this equality to obtain the first-order rate parameter will be discussed further in the next chapter.

Figure 3.4a compares the total solute mass associated with the mobile region (M_T) versus time for each of the models. In the local equilibrium model, the total mass is constant over time. The physical nonequilibrium models show a loss of mass with time. Initially, all the mass is associated with the mobile region. With time, more and more solute diffuses into the immobile region, so that eventually, the mass in the mobile region equals $1/(1+\beta)$ times the original mass. The differences between the first-order rate and diffusion models do not appear to be significant.

The behavior of v_{eff} shown in Figure 3.4b is similar to the total mass behavior. The local equilibrium model predicts constant velocity ($v_{eff} = v$), whereas the physical nonequilibrium models predict a deceleration with time, going from $v_{eff} = v$ at $t = 0$ to $v_{eff} = v/(1+\beta)$ at large times.

It is important to realize that the simulated decline in mass and deceleration of the mobile region plume are due to the initial condition, which assumes no mass associated with the immobile region at $t = 0$.
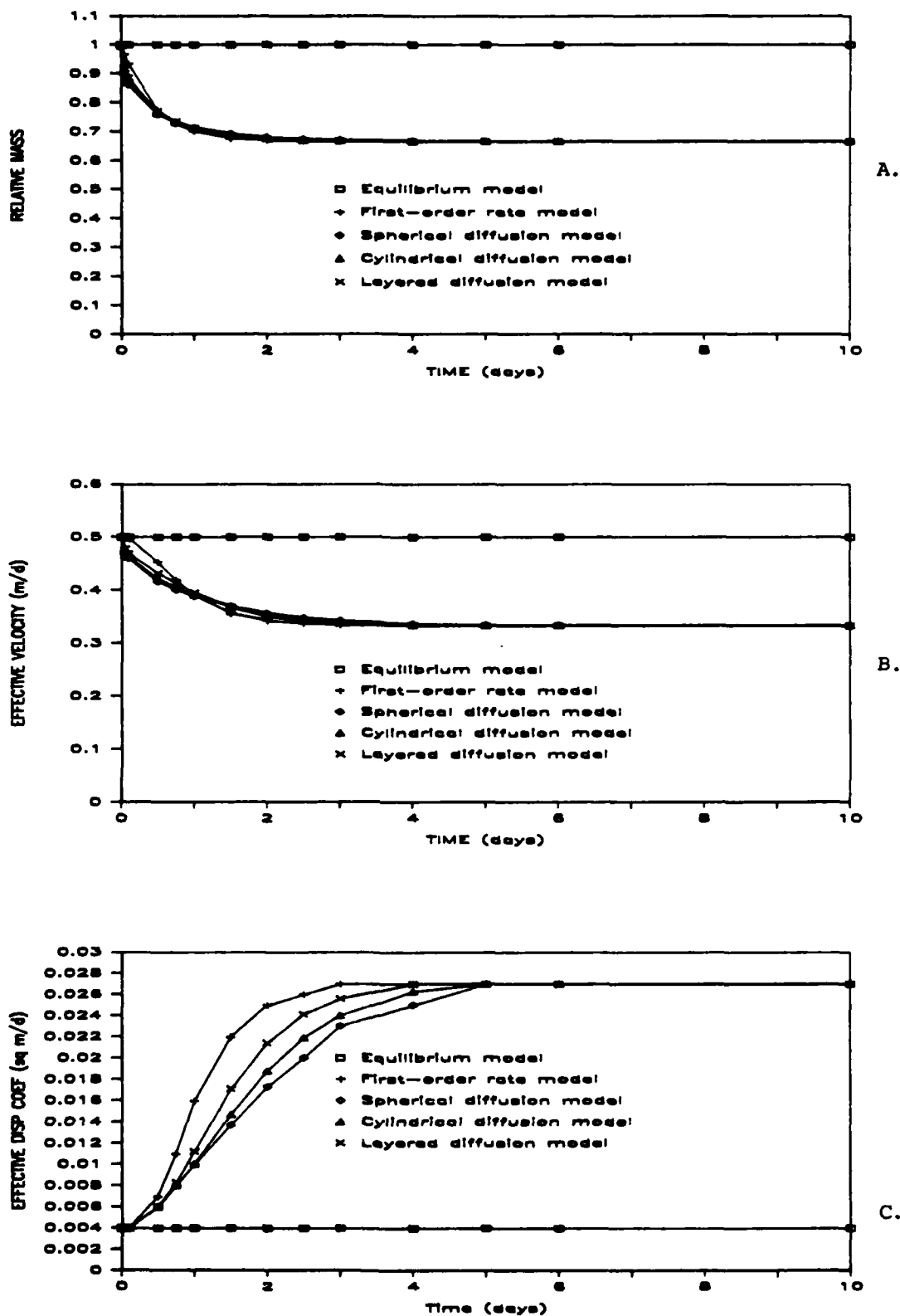
Figure 3.4. Behavior with time of the mobile region plume concentration distribution for equilibrium, first-order rate, and diffusion models: $v = 0.5$ m/d, $D_x = 0.004$ m^2/d, $\alpha = 1.5$ d^{-1}, and $\beta = 0.5$. a) Relative mass, b) Effective velocity, and c) Effective dispersion coefficient.

If this assumption is inappropriate, the mobile region plume mass and velocity behavior would differ from the Figure 3.4 simulations. The validity of this initial condition assumption, for a field experiment, will be discussed in Chapter 5.

The behavior of D_{effx} with time is shown in Figure 3.4c. The effective dispersion coefficient in the x-direction is constant for the local equilibrium model ($D_{effx} = D_x$), while the values of D_{effx} calculated using the physical nonequilibrium models increase from $D_{effx} = D_x$ at $t = 0$ to

$$D_{effx} = \frac{D_x}{1+\beta} + \frac{v^2\beta}{\alpha(1+\beta)^3} \qquad (3\text{-}38)$$

for the first-order rate model and

$$D_{effx} = \frac{D_x}{1+\beta} + \frac{v^2\beta}{a(1+\beta)^3} \qquad (3\text{-}39)$$

for the diffusion models, at large times.

Expressions similar to Eqs. 3-34 and 3-35 may be written relating the total mass associated with the immobile region (N_T), ᴛᴀe center of immobile mass location (x_{nc}, y_{nc}, z_{nc}), and the effective velocity for the immobile distribution (v_{neff}), to the immobile region moments:

$$N_T = \theta_m R_m n_{000}$$

$$x_{nc} = v'_{100}$$

$$y_{nc} = v'_{010} = 0 \quad , \quad z_{nc} = v'_{001} = 0 \qquad (3\text{-}40)$$

$$v_{neff} = \frac{dx_{nc}}{dt}$$

Figure 3.5a shows the total mobile and immobile masses over time for the first-order rate model. Since total mass must be conserved, the sum of the mobile and immobile masses remains constant.

Figure 3.5b plots the effective velocity of the solute plumes in the mobile and immobile regions. The figure illustrates the deceleration of the mobile solute distribution from $v_{eff} = v$ at early times to $v_{eff} = v/(1+\beta)$ at later times. The immobile solute distribution has an effective velocity (v_{neff}) of $v/2$ initially. This initial value is a consequence of the first-order rate expression, which controls the amount of
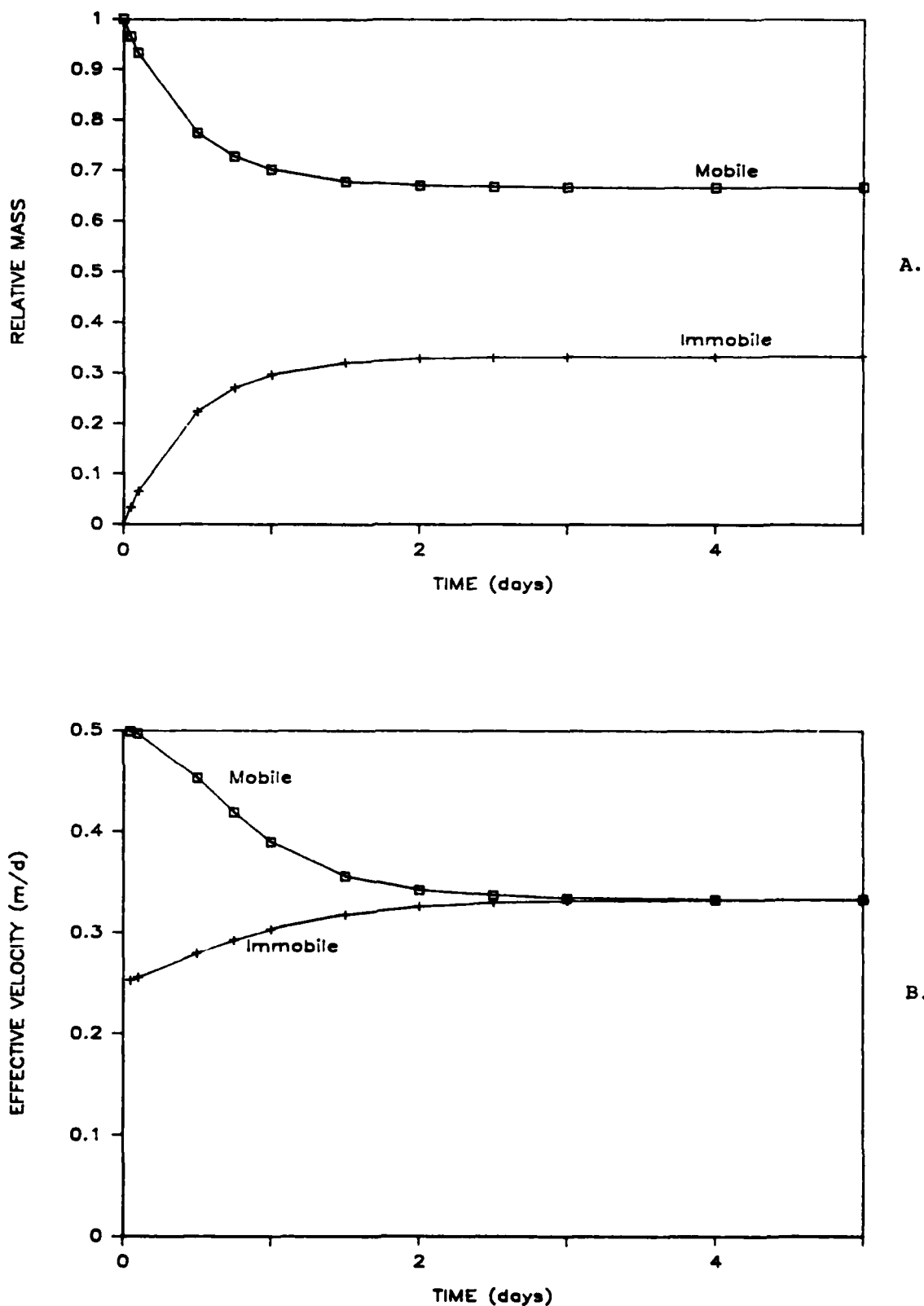
Figure 3.5. Comparison of the mobile and immobile region plume behavior
with time simulated by the first-order rate model: $v = 0.5$
m/d, $D_x = 0.004$ m^2/d, $\alpha = 1.5$ d^{-1}, and $\beta = 0.5$. a) Relative
mass, and b) Effective velocity.

solute entering and leaving the immobile region. At early times, there is a large concentration gradient driving the solute into the immobile region, but no gradient in the reverse direction, since the initial immobile region concentration is assumed equal to 0. Since only times very close to $t = 0$ are being considered, the concentration of the mobile plume may be assumed approximately constant (i.e., very little solute is transferred into the immobile region). Thus, based on the first-order rate expression which controls the transfer of solute, the (small) amount of solute which is transferred into the immobile region between time $t = 0$ and $t = \Delta t$ (as the mobile plume moves from $x = 0$ to $x = \Delta x$) is approximately the same as the (small) amount of solute which is transferred between $t = \Delta t$ and $t = 2\Delta t$ (as the mobile plume moves from $x = \Delta x$ to $x = 2\Delta x$). Therefore, in the time it takes the mobile plume to move a distance $2\Delta x$, the center of mass of the immobile plume moves from $x = 0$ (at $t = 0$) to $x = \Delta x$ (at $t = 2\Delta t$), leading to the result, indicated in Figure 3.5b, that as $t \to 0$, $v_{neff} \to v/2$. In a mathematical analysis of two-layer flow incorporating first-order mass transfer between the layers, Christodoulou (1986) obtained this same result.

Eventually, at long times, the mobile and immobile region plumes must move with the same velocity:

$$v_{eff} = v_{neff} = \frac{v}{1+\beta} \qquad (3-41)$$

Depending on the values of v and β, the immobile region plume will either accelerate or decelerate from its initial value of $v/2$ to attain this final velocity. It should be noted that if

$$\frac{v}{2} = \frac{v}{1+\beta} \qquad (3-42)$$

(i.e., $\beta = 1$), the immobile region plume moves at a constant velocity for all time. Figure 3.6 illustrates this behavior for the special case of Eq. 3-42.

Figure 3.7 is the spherical diffusion model analog of Figure 3.5. The total mobile and immobile solute masses of the diffusion model (Figure 3.7a) qualitatively behave as did the masses simulated using the first-order rate model in Figure 3.5a. The effective velocities of the mobile and immobile region plumes (Figure 3.7b) also behave similarly,

42
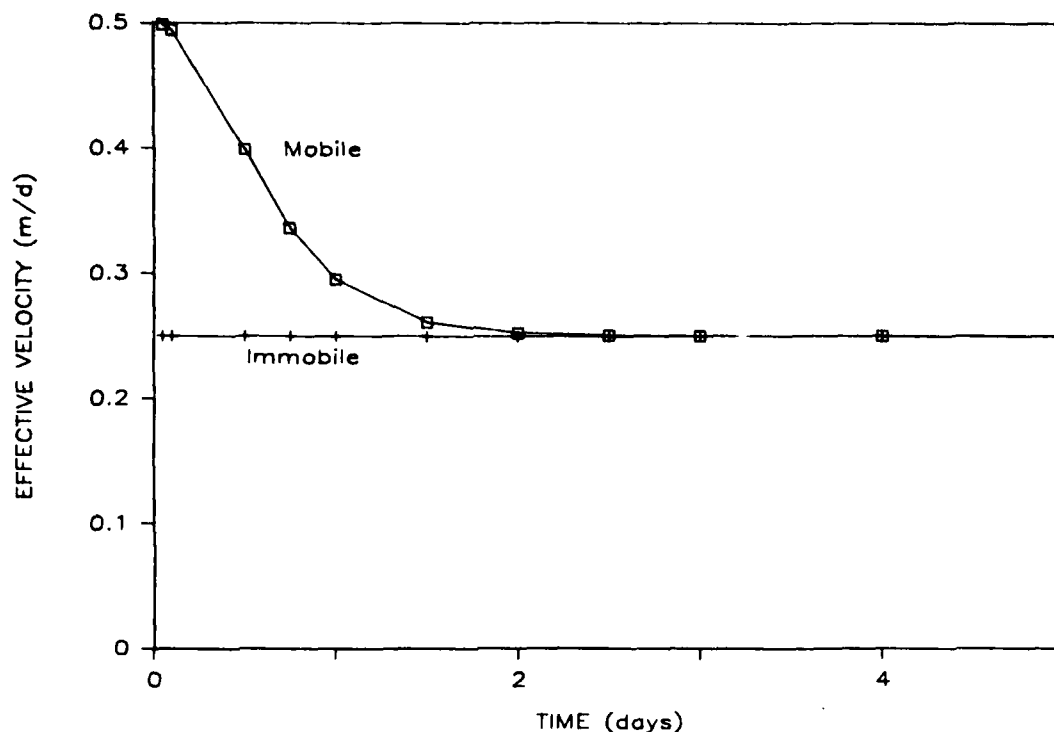
Figure 3.6. Comparison of the mobile and immobile region plume effec-
tive velocity behavior with time simulated by the first-
order rate model with $\beta = 1.0$.

except that the initial immobile plume velocity is $2v/3$ in the case of
the diffusion model. This difference is due to the different model
structure describing solute transfer into and within the immobile
region. Again, at large times, both the mobile and immobile region
plumes attain an effective velocity of $v/(1+\beta)$. If

$$\frac{2v}{3} = \frac{v}{1+\beta} \tag{3-43}$$

(i.e., $\beta = 0.50$), then the immobile plume center of mass moves at the
same velocity at short and long times. Figure 3.7b illustrates that for
$\beta = 0.50$ the short- and long-time velocities are equal, while at inter-
mediate times the velocity-time relationship exhibits a shallow minimum.
This minimum is due to the mathematical formulation of the diffusion
model.
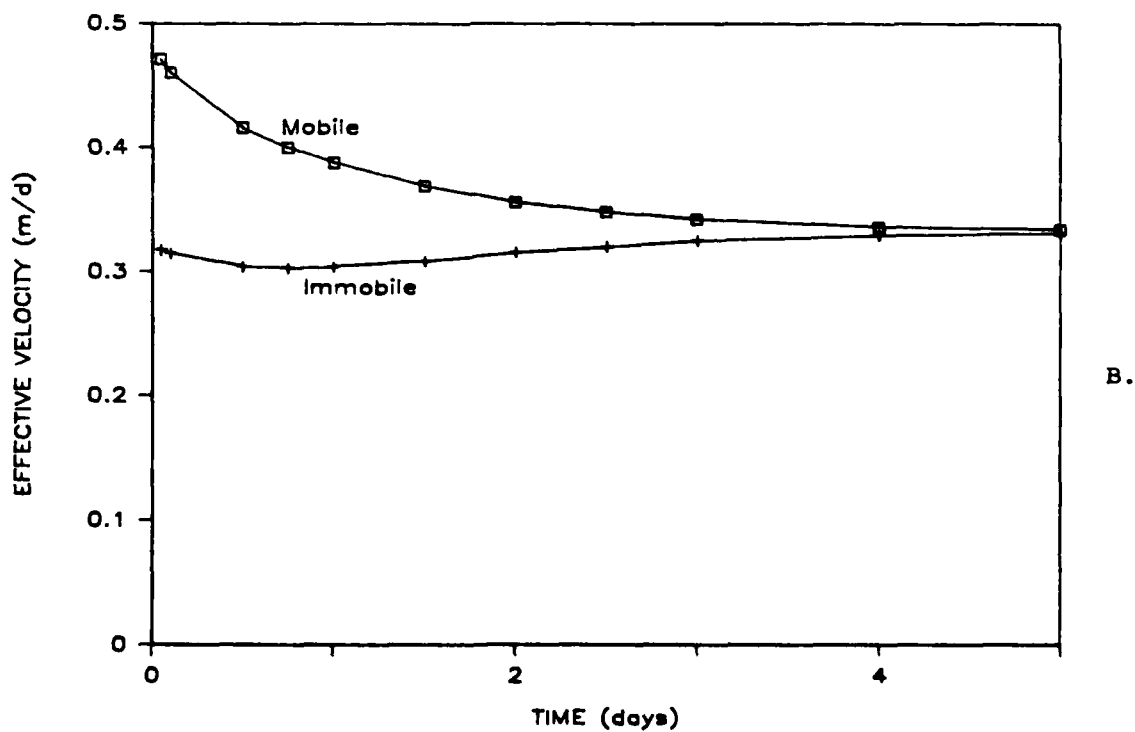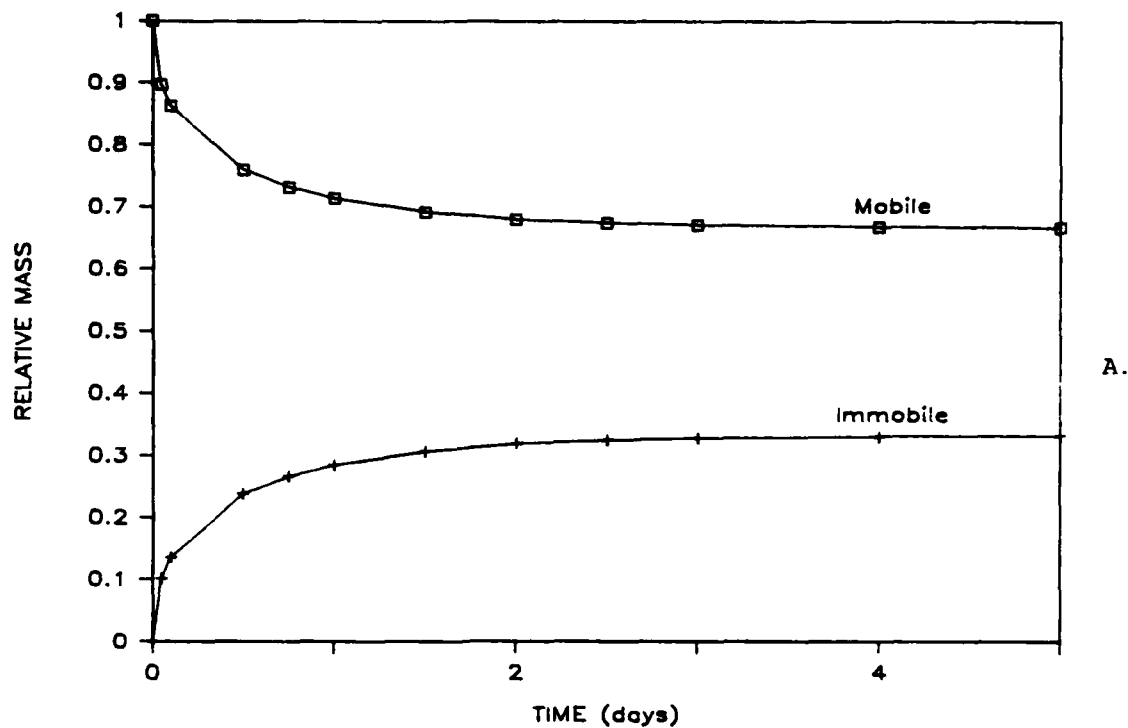
Figure 3.7. Comparison of the mobile and immobile region plume behavior with time simulated by the spherical diffusion model: $v = 0.5$ m/d, $D_x = 0.004$ m^2/d, $D_e/b^2 = 0.1$ m^2/d, and $\beta = 0.5$. a) Relative mass, and b) Effective velocity.

Comparison of Temporal versus Spatial Behavior

The expressions for M_T, v_{eff}, D_{eff}, N_T, and v_{neff} derived in the preceding sections provide a convenient tool for comparing the temporal and spatial behavior of the concentration distributions. The three-dimensional models can be assessed by comparing their spatial behavior over the entire distribution with the temporal behavior along the line $y = z = 0$. This is equivalent to comparing the result of sampling the entire concentration distribution at points in time, with the break-through responses obtained from sampling wells along the centerline of the solute trajectory.

Zeroth moment

Mobile region. Examining the zeroth temporal moment of the mobile distributions, it is seen that

$$M_T = \frac{M_3'}{4\pi \sqrt{D_y D_z}\ \ell} \tag{3-44}$$

whereas the zeroth spatial moment is model dependent. The zeroth spatial moment for the local equilibrium model remains constant at

$$M_T = M_3' \tag{3-45}$$

while the zeroth spatial moments of the physical nonequilibrium models decline from

$$M_T = M_3' \tag{3-46}$$

at early times to

$$M_T = \frac{M_3'}{1+\beta} \tag{3-47}$$

at later times.

Immobile region. For the physical nonequilibrium models, the temporal zeroth moments are

$$N_T = \frac{\beta M_3'}{4\pi \sqrt{D_y D_z}\ \ell} \tag{3-48}$$

while the spatial moments increase from

45

$$N_T = 0 \tag{3-49}$$

at early times to

$$N_T = \frac{\beta M_3'}{1+\beta} \tag{3-50}$$

at later times. Another significant difference is that the sum of the mobile and immobile zeroth spatial moments remains constant over time, whereas the sum of the temporal moments is inversely proportional to the sampling distance, ℓ.

First moment

Mobile region. Before comparing effective velocities, which are derived from the spatial or temporal first moments of a distribution, it is useful to recall the definition of the effective velocity (v_{eff}). The effective velocity is defined as the velocity parameter which would be used in an equilibrium model to obtain the same spatial or temporal first moment that would be calculated using an equivalent nonequilibrium model. Effective velocity does not represent a physical quantity, and as this section will emphasize, the effective velocity obtained from an analysis of the spatial distribution is both quantitatively and qualitatively different from the effective velocity calculated from a temporal moment analysis.

Comparing effective velocities, it is seen that for the physical nonequilibrium models, the effective velocity obtained using the temporal moments remains constant at

$$v_{eff} = \frac{v}{1+\beta} \tag{3-51}$$

at all sampling distances, while the effective velocity obtained using spatial moments declines from

$$v_{eff} = v \tag{3-52}$$

at early times to

$$v_{eff} = \frac{v}{1+\beta} \tag{3-53}$$

at later times. This difference can be understood qualitatively in the following way: since the temporal first moment reflects behavior averaged over all time, it provides an equilibrium value for the effective

velocity, whereas the spatial first moment estimate provides a "snapshot" of the instantaneous velocity with which the solute distribution is moving, at particular points in time.

This difference in spatial and temporal behavior has interesting repercussions in light of the concept of a retardation factor. The basic premise for using retardation factors is that local equilibrium is a valid assumption. Under equilibrium conditions, a retarded solute will move through an aquifer at a speed equal to the speed with which a conservative solute moves, divided by the retardation factor. The retardation factor (R) may be determined by any of the following equations:

$$R = \frac{\mu'_{1,t} \text{ (retarded)}}{\mu'_{1,t} \text{ (conservative)}} \qquad (3\text{-}54a)$$

$$R = \frac{v_{eff} \text{ (conservative)}}{v_{eff} \text{ (retarded)}} \qquad (3\text{-}54b)$$

using either spatial or temporal definitions for v_{eff}, and

$$R = \frac{\mu'_{100} \text{ (conservative)}}{\mu'_{100} \text{ (retarded)}} \qquad (3\text{-}54c)$$

For the local equilibrium model, all of the above equations will yield identical values. However, if the assumption of local equilibrium is invalid (physical nonequilibrium, for example), although the temporal moments will yield the same retardation factor, independent of sampling location, the spatial moments will yield different retardation factors, depending on the time at which the spatial data were obtained. The "nonequilibrium" retardation factors obtained from the spatial data will be an increasing function of time, eventually approaching the equilibrium retardation factor value at long times.

Another consequence of the "equilibrium" behavior of the temporal distribution first moment will now be discussed. Van Genuchten and Wierenga (1976) showed that, for small values of α, the first-order rate constant, a temporal breakthrough response could be simulated using a local equilibrium model with

$$v_{eff} = v \qquad (3\text{-}55)$$

and for large values of α, the response could be simulated by a local equilibrium model with

$$v_{eff} = \frac{v}{1+\beta} \qquad (3-56)$$

Goltz and Roberts (1986) presented similar results, and further defined small and large values of α relative to an advective rate constant (v/ℓ) such that if $\alpha \ll v/\ell$, Eq. 3-55 would apply, and if $\alpha \gg v/\ell$, Eq. 3-56 would apply. In chemical engineering research, the ratio of a mass transfer rate (α) to an advective rate (v/ℓ) is defined as a Stanton number (Cussler, 1984), where:

$$St = \frac{\alpha}{(v/\ell)} \qquad (3-57)$$

Thus, for $St \ll 1$, Eq. 3-55 would apply, and for $St \gg 1$, Eq. 3-56 would apply. The validity of (3-55) and (3-56) is illustrated in Figure 3.8a. For the simulation at a low mass transfer rate, $\alpha = 0.0003$ d^{-1} and $v/\ell = 0.10$ d^{-1} (St = 0.003). Thus, $St \ll 1$, and the local equilibrium model with $v_{eff} = v$ approximates the first-order rate response quite adequately. For the simulation at a high mass transfer rate, $\alpha = 0.75$ d^{-1} and $v/\ell = 0.10$ d^{-1} (St = 7.5). The local equilibrium model with

$$v_{eff} = \frac{v}{1+\beta}$$

approximates the first-order rate response. Interestingly, an examination of the temporal moments does not reveal this equivalence, as it was found that the first temporal moments are independent of the mass transfer rate. This is due to the existence of a very small, long tail in the temporal response, which causes the first temporal moment to remain constant even as $\alpha \to 0$. Thus, in Figure 3.8a, the first-order rate model breakthrough responses for the high and low mass transfer rates have the same first moment, contrary to the visual impression given by the figure. Figure 3.8b, which depicts the tailing of the high and low mass transfer rate simulations, indicates how the long tail of the low rate simulation could cause the two simulations shown in Figure 3.8a to have the same first moment. Although mathematically real, the tail which leads to this equality may be below detection limits (visual and analytical), and it is reasonable to approximate the first-order model response at small α using the local equilibrium model with v_{eff} as defined in Eq. 3-55. The equations for the first spatial moment provide

48
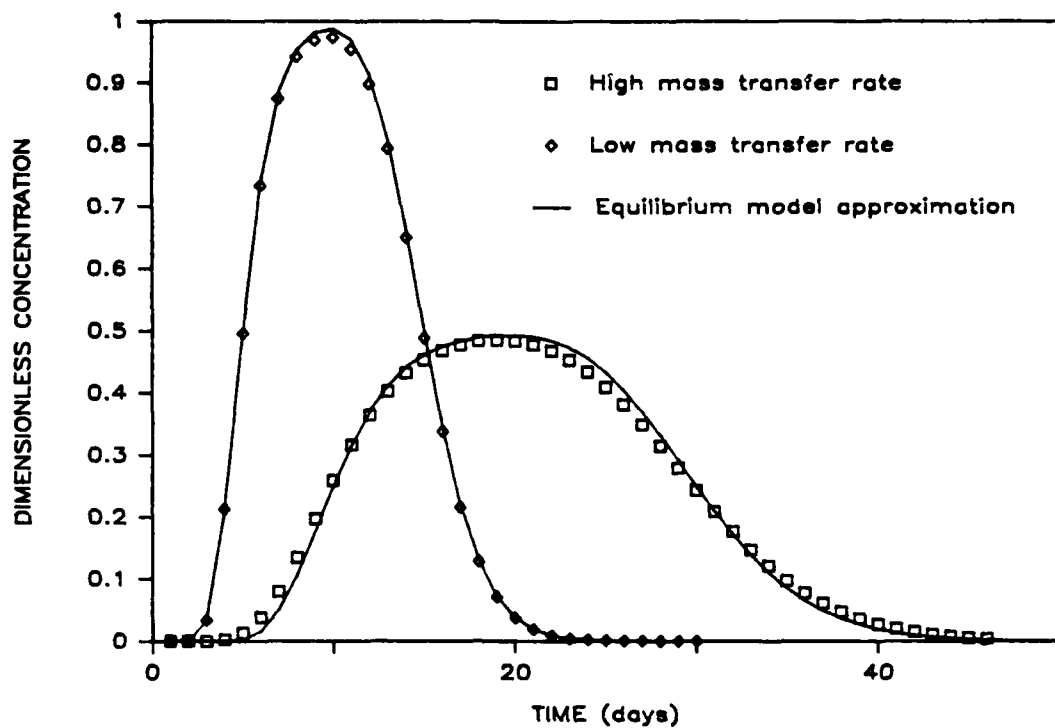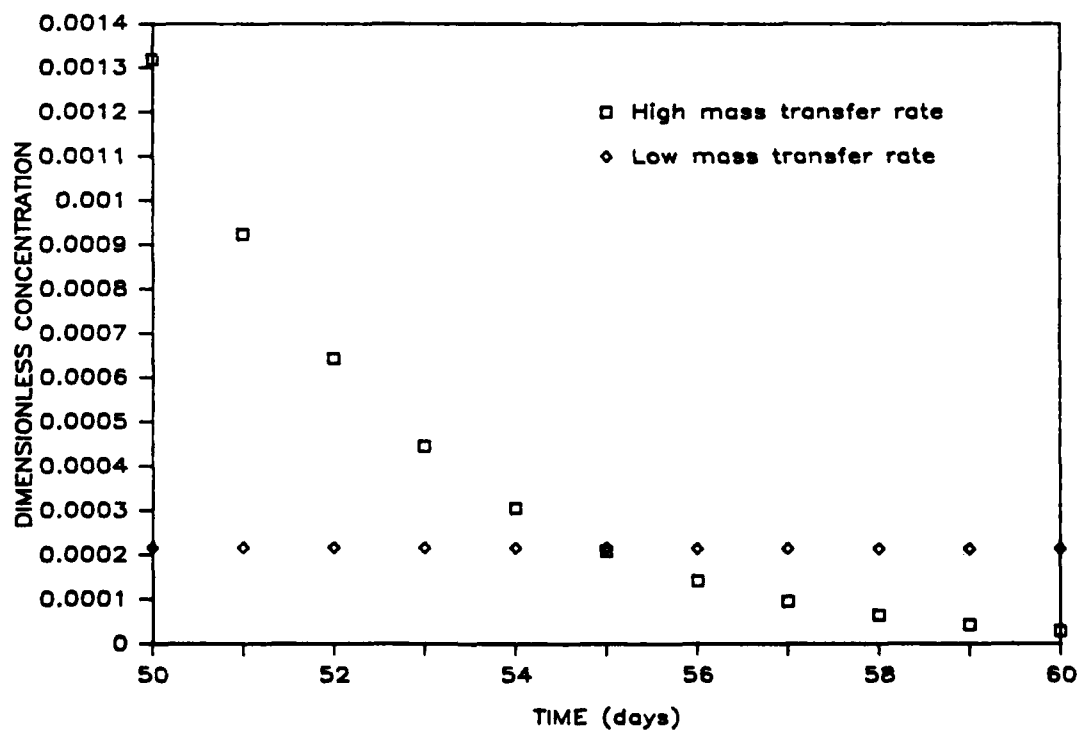
Figure 3.8. First-order rate model simulations for high (St = 7.5) and low (St = 0.003) values of the first-order mass transfer rate constant. a) Equilibrium model approximations, and b) Comparison of tailing at high and low rates.

49

a mathematical justification for this approximation. Differentiate the first spatial moment expression in Table 3.6 to find

$$v_{eff} = \frac{d\mu'_{100}}{dt} = \frac{v(1 + \beta^2 A)}{(1 + \beta)(1 + \beta A)} + \frac{v\beta A(2 + \alpha t - \alpha t \beta)}{(1 + \beta A)^2} \quad (3\text{-}58)$$

where

$$A = e^{-\alpha t(1+\beta)}$$

The synoptic sampling time, t, in Eq. 3-58 may be replaced by the term ℓ/v, to obtain

$$v_{eff} = \frac{v(1 + \beta^2 A)}{(1 + \beta)(1 + \beta A)} + \frac{v\beta A(2 + \frac{\alpha \ell}{v} - \frac{\alpha \ell \beta}{v})}{(1 + \beta A)^2} \quad (3\text{-}59)$$

where

$$A = e^{(-\alpha \ell/v)(1+\beta)}$$

From Eq. 3-59, it is seen that indeed for $\alpha \ll v/\ell$ (St $\ll$ 1)

$$A \to 1 \quad \text{and} \quad v_{eff} \to v$$

whereas for $\alpha \gg v/\ell$ (St $\gg$ 1)

$$A \to 0 \quad \text{and} \quad v_{eff} \to \frac{v}{1+\beta}$$

These approximations could not be obtained by an examination of the first temporal moment.

Immobile region. The effective velocity of the immobile solute distributions based on temporal moments behaves in accordance with Eq. 3-33. At small distances ($\ell \ll v/[\alpha(1+\beta)]$ or $\ell \ll v/[a(1+\beta)]$),

$$v_{neff} = \alpha \ell \quad \text{or} \quad v_{neff} = a\ell \quad (3\text{-}60)$$

while at large distances, v_{neff} changes (it either increases or decreases, depending on parameter values) to

$$v_{neff} = \frac{v}{1+\beta} \quad (3\text{-}61)$$

As discussed above, the effective velocity of the immobile region plume calculated from the spatial moments changes from the small time value of

$$v_{neff} = \frac{v}{2} \qquad (3\text{-}62)$$

for the first-order rate model, and

$$v_{neff} = \frac{2v}{3} \qquad (3\text{-}63)$$

for the diffusion models, to the large time value of

$$v_{neff} = \frac{v}{1+\beta} \qquad (3\text{-}64)$$

Second moment

The value of D_{eff} calculated from the temporal moments remains constant over the sampling distance, with values of

$$D_{eff} = D_x \qquad (3\text{-}65)$$

for the local equilibrium model and

$$D_{eff} = \frac{D_x}{1 + \beta} + \frac{v^2 \beta}{\alpha(1 + \beta)^3}$$
$$D_{eff} = \frac{D_x}{1 + \beta} + \frac{v^2 \beta}{a(1 + \beta)^3} \qquad (3\text{-}66)$$

for the physical nonequilibrium models.

For the physical nonequilibrium models, the effective dispersion coefficient calculated from the spatial moments increases from

$$D_{effx} = D_x \qquad (3\text{-}67)$$

at small times, to

$$D_{effx} = \frac{D_x}{1 + \beta} + \frac{v^2 \beta}{\alpha(1 + \beta)^3}$$
$$D_{effx} = \frac{D_x}{1 + \beta} + \frac{v^2 \beta}{a(1 + \beta)^3} \qquad (3\text{-}68)$$

at large times. D_{effx} for the local equilibrium models remains constant at $D_{effx} = D_x$.

Notice that all the large time parameter values obtained using the first and second spatial moments are equivalent to the values obtained using the temporal moments.

Table 3.9 summarizes the parameter values obtained at small and large values of sampling distance and time, based on the temporal and spatial moments respectively.

SUMMARY

One- and three-dimensional forms of Aris' method of moments were developed and used to analyze the temporal and spatial moment behavior of concentration distributions obtained using both equilibrium and physical nonequilibrium solute transport models.

It was shown that although the zeroth and first temporal moments are independent of the rate of mass transfer between the mobile and immobile regions, all the spatial moments are dependent on the mass transfer rate. One implication of this is that the retardation factors calculated from breakthrough responses should, at least mathematically, be independent of the distance to the sampling well and the rate of mass transfer. On the other hand, the retardation factors calculated from spatial data can be expected to increase with time under conditions of physical nonequilibrium, with the rate of increase a function of the mass transfer rate.

The temporal and spatial moment behavior of the solute within the immobile region was also examined. It was demonstrated that the zeroth spatial moment increases from zero, indicating no solute mass within the immobile region at $t = 0$, to a constant value at long time. The effective velocity of the immobile region plume, calculated from the spatial moment, changes (it may increase or decrease) from a fraction of the initial mobile plume velocity at $t = 0$, to a constant value at long times, with the large-time value equal to the large-time value of the mobile plume velocity.

Finally, it was shown that for infinite boundary conditions, the first temporal moment simulated using a one-dimensional model would be greater than the first temporal moment using a three-dimensional model with the same velocity, owing to the effect of one-dimensional versus three-dimensional dispersion.

TABLE 3.9

COMPARISON OF EFFECTIVE PARAMETER VALUES CALCULATED FROM TEMPORAL* AND SPATIAL MOMENTS

MOBILE DISTRIBUTION

Local Equilibrium Model

	Temporal		Spatial	
	Small x	Large x	Small t	Large t
M_T	M_3'	$\dfrac{M_3'}{4\pi\ell\sqrt{D_yD_z}}$	M_3'	M_3'
v_{eff}	v	v	v	v
D_{eff}†	D_x	D_x	D_x	D_x

First-Order Rate Model

	Temporal		Spatial	
	Small x	Large x	Small t	Large t
M_T	$\dfrac{M_3'}{4\pi\ell\sqrt{D_yD_z}}$	$\dfrac{M_3'}{4\pi\ell\sqrt{D_yD_z}}$	M_3'	$\dfrac{M_3'}{1+\beta}$
v_{eff}	$\dfrac{v}{1+\beta}$	$\dfrac{v}{1+\beta}$	v	$\dfrac{v}{1+\beta}$
D_{eff}†	$\dfrac{D_x}{1+\beta} + \dfrac{v^2\beta}{\alpha(1+\beta)^3}$	$\dfrac{D_x}{1+\beta} + \dfrac{v^2\beta}{\alpha(1+\beta)^3}$	D_x	$\dfrac{D_x}{1+\beta} + \dfrac{v^2\beta}{\alpha(1+\beta)^3}$

Diffusion Models

	Temporal		Spatial	
	Small x	Large x	Small t	Large t
M_T	$\dfrac{M_3'}{4\pi\ell\sqrt{D_yD_z}}$	$\dfrac{M_3'}{4\pi\ell\sqrt{D_yD_z}}$	M_3'	$\dfrac{M_3'}{1+\beta}$
v_{eff}	$\dfrac{v}{1+\beta}$	$\dfrac{v}{1+\beta}$	v	$\dfrac{v}{1+\beta}$
D_{eff}†	$\dfrac{D_x}{1+\beta} + \dfrac{v^2\beta}{\alpha(1+\beta)^3}$	$\dfrac{D_x}{1+\beta} + \dfrac{v^2\beta}{\alpha(1+\beta)^3}$	D_x	$\dfrac{D_x}{1+\beta} + \dfrac{v^2\beta}{\alpha(1+\beta)^3}$

IMMOBILE DISTRIBUTION

Local Equilibrium Model

	Temporal		Spatial	
	Small x	Large x	Small t	Large t
N_T				
v_{neff}		Intrinsically inapplicable		

First-Order Rate Model

	Temporal		Spatial	
	Small x	Large x	Small t	Large t
N_T	$\dfrac{\beta M_3'}{4\pi\ell\sqrt{D_yD_z}}$	$\dfrac{\beta M_3'}{4\pi\ell\sqrt{D_yD_z}}$	0	$\dfrac{\beta M_3'}{1+\beta}$
v_{neff}	$\alpha\ell$	$\dfrac{v}{1+\beta}$	$\dfrac{v}{2}$	$\dfrac{v}{1+\beta}$

Diffusion Models

	Temporal		Spatial	
	Small x	Large x	Small t	Large t
N_T	$\dfrac{\beta M_3'}{4\pi\ell\sqrt{D_yD_z}}$	$\dfrac{\beta M_3'}{4\pi\ell\sqrt{D_yD_z}}$	0	$\dfrac{\beta M_3'}{1+\beta}$
v_{neff}	$\alpha\ell$	$\dfrac{v}{1+\beta}$	$\dfrac{2v}{3}$	$\dfrac{v}{1+\beta}$

*Calculated along the line of advective transport: $y = z = 0$. †D_{eff_x} calculated for the spatial distribution.

CHAPTER 4

MODEL COMPARISONS

In the preceding chapter, the spatial and temporal moments obtained using different transport models were compared. These moment formulations will now be used to define equivalent parameters for the different transport models, and to examine the similarities and differences of breakthrough responses (which typically would be measured in a field situation) simulated using these equivalent parameters. In contrast to earlier studies, which concentrated on equivalence among one-dimensional models, this work will deal with the three-dimensional models discussed in the previous chapters. The reason for this analysis of model equivalence is to determine if differentiation among different models, based on breakthrough data, is feasible. A related question, which will also be addressed in this chapter, concerns the differences in breakthrough responses owing to different assumptions regarding boundary conditions.

MODEL EQUIVALENCE

The concept of equivalence between local equilibrium and physical nonequilibrium models has been discussed in the literature. Baker (1977), De Smedt and Wierenga (1984), and Valocchi (1985a) showed that in one dimension, for $Pe_m = v\ell/D_x > 1000$, the first-order rate model could be approximated by a local equilibrium model, with an effective dispersion coefficient of:

$$D_{eff} = \frac{D_x}{1 + \beta} + \frac{\beta v^2}{\alpha(1 + \beta)^3} \qquad (4-1)$$

Rao et al. (1980), and Valocchi (1985a) showed for diffusion into spheres, and Passioura (1971) showed for diffusion into cylinders as well as into spheres, that at large Pe_m the diffusion models could be approximated by a local equilibrium model with an effective dispersion coefficient of:

$$D_{eff} = \frac{D_x}{1 + \beta} + \frac{\beta v^2}{a(1 + \beta)^3} \qquad (4-2)$$

In the subsequent discussion, it will be shown that Eq. 4-2 can be used to approximate diffusion into layers also. Valocchi (1985a) showed that

an effective velocity for a local equilibrium model equivalent to the physical nonequilibrium models is:

$$v_{eff} = \frac{v}{1 + \beta} \qquad (4\text{-}3)$$

Equations 4-1 through 4-3 may also be obtained using the concept of temporal moment equivalence. From Table 3.2 of the previous chapter, it is seen that the effective parameter values expressed in Eqs. 4-1 through 4-3 are the same as the parameter values obtained by considering the breakthrough responses of the one-dimensional models at high Peclet numbers, and by setting the first and second temporal moments of the equilibrium and nonequilibrium models equal to each other. Inspecting the first moment expressions in Table 3.2, it is seen that at high Peclet numbers, Eq. 4-3 can be used in equating an equilibrium model effective velocity to all of the physical nonequilibrium models, regardless of whether a geometrical diffusion or first-order rate model is formulated.

Comparing the second moment expressions in Table 3.2, and setting the equilibrium and diffusion model expressions equal to each other, at high Peclet numbers, shows Eq. 4-2 applicable to spherical, cylindrical, and layered diffusion models. In the same way, Eq. 4-1 is obtained by setting the equilibrium model expression for the second temporal moment equal to the first-order rate model expression for the same moment. To define equivalence between first-order rate and diffusion model parameters, it is necessary merely to set the second temporal moment formulations of the two models, shown in Table 3.2, equal to each other, to find:

$$\alpha = a \qquad (4\text{-}4)$$

Note that the validity of Eq. 4-4 does not depend on the Peclet number.

Parker and Valocchi (1986) used the moment analysis approach described above to define equivalent equilibrium, first-order rate, and spherical diffusion model parameters. Here, their analysis is extended to include cylindrical and layered diffusion models.

Van Genuchten (1985) used an empirical method to obtain shape factors which could be used to define equivalent rate constants for the various physical nonequilibrium models. Similar factors can be obtained using Eq. 4-4. Table 4.1 compares equivalent rate constants obtained using

TABLE 4.1

EQUIVALENT RATE CONSTANTS FOR NONEQUILIBRIUM MODELS

	First-Order Rate Model	Diffusion Models		
		Spherical	Cylindrical	Layered
Empirical[*]	α	$\dfrac{22.7\ D_e}{b^2}$	$\dfrac{11\ D_e}{b^2}$	$\dfrac{3.5\ D_e}{b^2}$
Moment Analysis (Eq. 4-4)	α	$\dfrac{15\ D_e}{b^2}$	$\dfrac{8\ D_e}{b^2}$	$\dfrac{3\ D_e}{b^2}$

[*]Van Genuchten (1985).

van Genuchten's (1985) empirical formulae with rate constants derived using the moment analysis described above.

Van Genuchten (1985) and Parker and Valocchi (1986) provide comparisons of the one-dimensional breakthrough responses of the equilibrium and nonequilibrium models. In this work, it is shown that their findings are also applicable in three dimensions.

With regard to the physical nonequilibrium models, Parker and Valocchi (1986) considered only the first-order rate and spherical diffusion models. However, as was shown by van Genuchten (1985) and is apparent from Figure 3.4c, these two model types bracket the range of behavior of the other geometrical diffusion models. Therefore, the following three-dimensional analysis will follow Parker and Valocchi (1986) and be limited to discussing the first-order rate and spherical diffusion models. Parker and Valocchi (1986) also found that the deviations between models are greater for an instantaneous source than for continuous or pulse injections. Hence, the following discussion will focus on the breakthrough responses to an instantaneous point source.

The instantaneous point source analysis which will be discussed in this work is applicable to sampling wells far from a finite source, in the line of advective transport. Parameter values used for the analysis are listed in Table 4.2. The parameter γ is a measure of the ratio of diffusive to advective rate constants. For the first-order rate model:

$$\gamma = \frac{\alpha}{(v/\ell)} \qquad (4-5)$$

TABLE 4.2

PARAMETER VALUES USED IN FIGURES 4.1 THROUGH 4.3

	γ	β	R	Pe_{eff}	Pe_m
Figure 4.1	30.0	1	1	27.3	50
	0.3	1	1	0.593	50
Figure 4.2	0.3	1	1	0.593	50
	0.3	0.0526	1	18.3	50
Figure 4.3	0.3	1	1	0.593	50
	0.3	1	50	18.7	50

and for the diffusion models:

$$\gamma = \frac{a}{(v/\ell)} \tag{4-6}$$

Note that in the case of the first-order rate model (Eq. 4-5), γ is equivalent to the Stanton number defined in Chapter 3. In the case of the diffusion models (Eq. 4-6), γ is the ratio of a diffusion rate to an advection rate. This ratio has been defined as an intra-aggregate diffusion

Figure 4.1. Effect of γ on simulated breakthrough responses of the equilibrium, first-order rate, and spherical diffusion models.
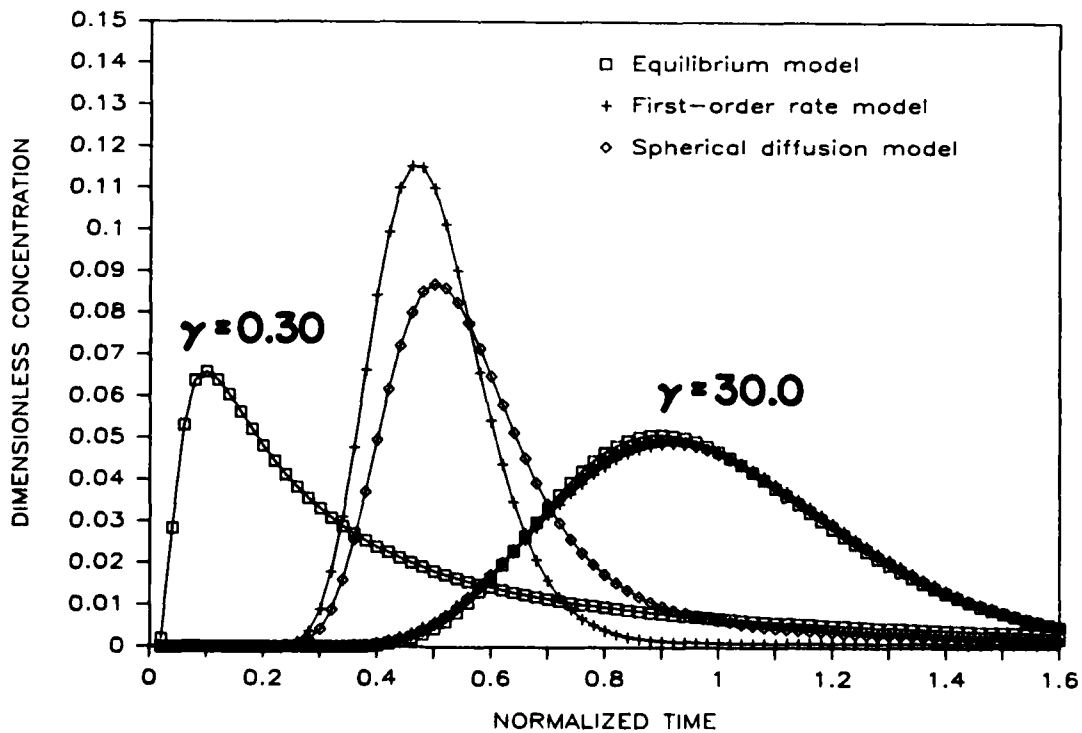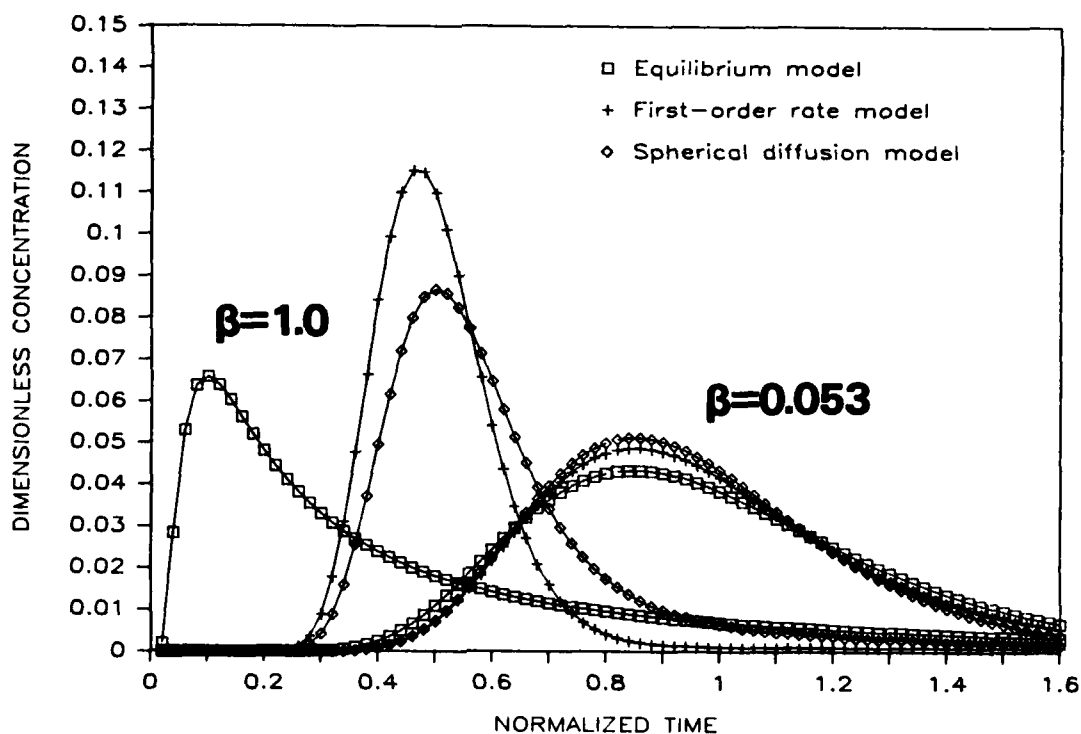
Figure 4.2. Effect of β on simulated breakthrough responses of the equilibrium, first-order rate, and spherical diffusion models.
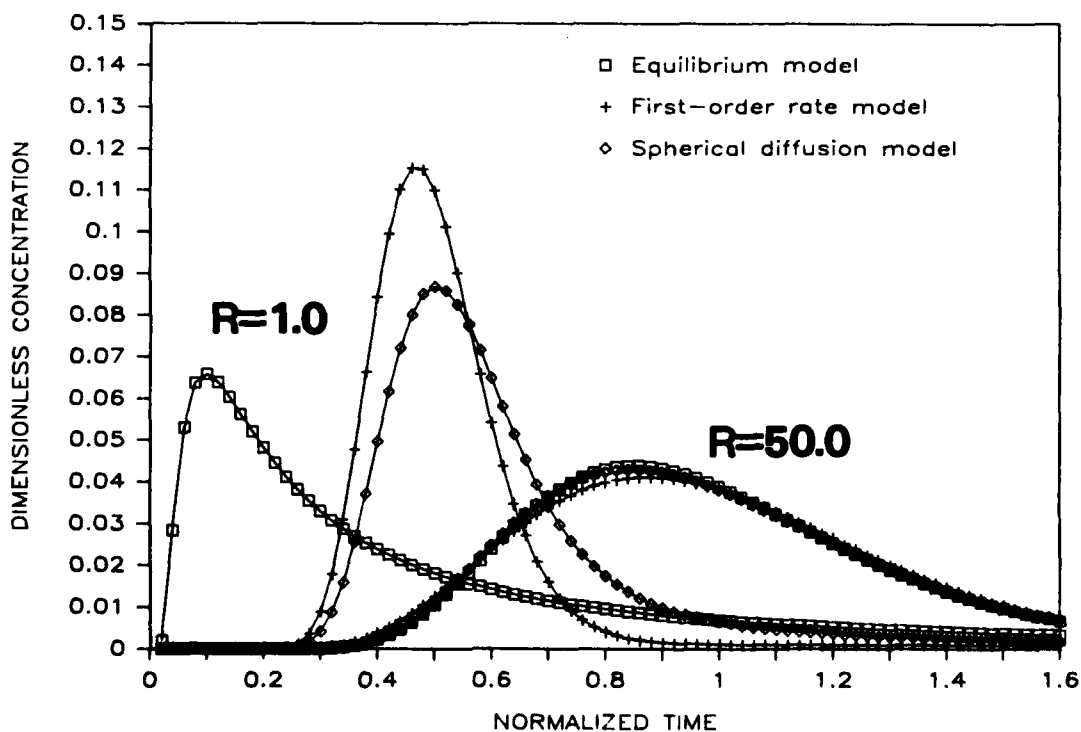
Figure 4.3. Effect of R on simulated breakthrough responses of the equilibrium, first-order rate, and spherical diffusion models.

modulus (Crittenden et al., 1986). Nonequilibrium model parameters were chosen to provide a range of behavior. The equivalent equilibrium model parameter values were calculated using Eqs. 4-1 through 4-3. The equivalent equilibrium model parameter values are contained in the effective Peclet number, $P_{eff} = v_{eff}\ell/D_{eff}$.

Both van Genuchten (1985) and Parker and Valocchi (1986) found that for large values of γ, the ratio of the diffusive rate constant to the advective rate constant (i.e., approach to equilibrium), the simulations of the local equilibrium, first-order rate, and diffusion models converged upon each other. Figure 4.1, which plots normalized concentration versus normalized time ($\hat{T}$), where

$$\hat{T} = \frac{\theta_m v_m t}{\theta \ell R} = \frac{v_o t}{\ell R} \tag{4-7}$$

demonstrates this for a three-dimensional simulation. For high values of γ, the equilibrium and nonequilibrium models produce similar breakthrough reponses, whereas for low values of γ, the equilibrium and nonequilibrium responses diverge.

Figure 4.2 shows the effect of β, the solute capacity ratio of immobile to mobile regions, upon simulated breakthrough responses. As β approaches zero (i.e., where very little solute is associated with the immobile region), the nonequilibrium responses approach the equilibrium responses. For higher values of β, which implies more solute associated with the immobile region, the deviation from equilibrium increases. Parker and Valocchi (1986) showed a similar effect in one dimension.

The effect of increasing the retardation factor, R, upon the simulated responses is shown in Figure 4.3. As can be seen, increasing R decreases the deviation from equilibrium.

Figures 4.1 through 4.3 show that for certain parameter values, even if Pe_m < 1000, Eqs. 4-1 through 4-3 are applicable. This was also shown by Parker and Valocchi (1986). The figures also indicate that for other parameter values, the differences between the geometrical diffusion models and the equivalent first-order rate model may be significant. This observation was also made, for one-dimensional formulations, by van Genuchten (1985) and Parker and Valocchi (1986). Van Genuchten (1985) noted, however, that considering the uncertainty in the many parameters needed in the two-region models, the first-order rate model acceptably

approximated the responses of the more complex diffusion models. In the above analysis, the differences in model responses were maximized by choosing an instantaneous point source and comparing the two most dissimilar models. Nevertheless, the differences between the responses were not very great. This observation supports van Genuchten's (1985) conclusion that, owing to parameter uncertainty, attempts to differentiate between the two types of models based on field data would be difficult.

Figure 4.4 offers further evidence in support of this conclusion. As Figures 4.1 through 4.3 showed, for certain parameter values, the differences between the first-order rate and spherical diffusion models could be significant. However, with relatively minor changes in the first-order rate model parameter values, the responses of the two models can be made to be almost identical. In Figure 4.4, v and D_x were changed by 10% from the Figure 4.1 through 4.3 values, and the first-order rate constant, α, was calculated using van Genuchten's (1985) empirical formula (see Table 4.1) instead of using Eq. 4-4. As the figure shows, the responses of the two models are quite similar.
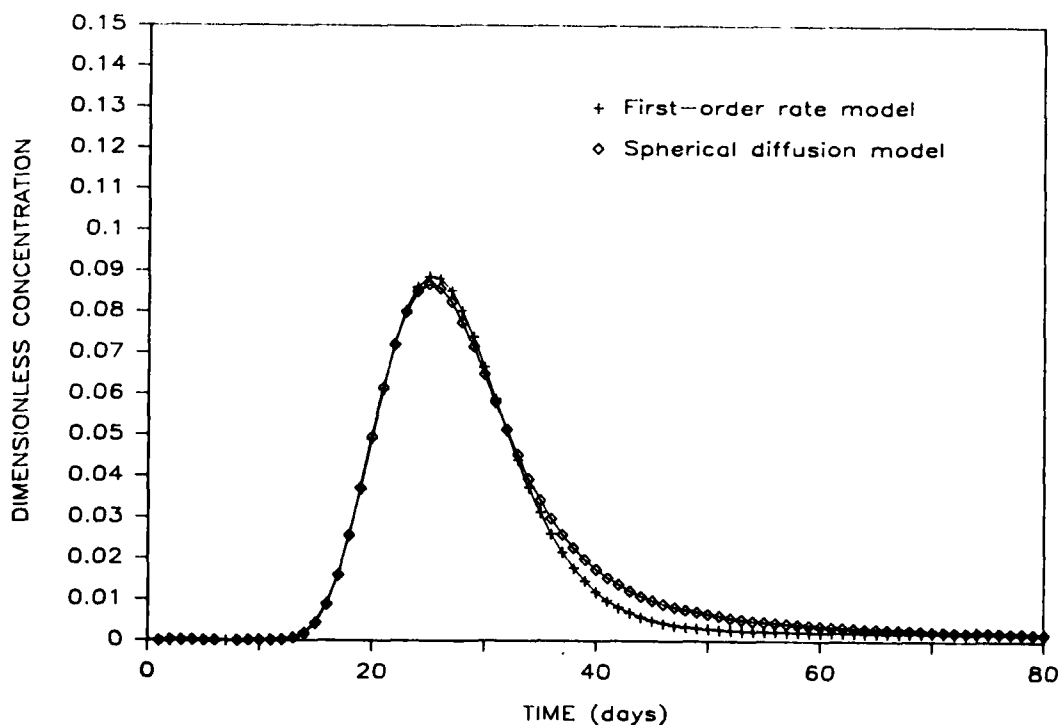
Figure 4.4. Comparison of simulated breakthrough responses of the first-order rate and spherical diffusion models.

Parker and Valocchi (1986) showed that for certain parameter values, it is possible for a local equilibrium model simulation to deviate even less than a first-order rate model from a diffusion model simulated breakthrough response. Thus, the likelihood of successfully differentiating among the three types of models based on field break-through response data appears to be small.

Recall, however, from the discussion in the previous chapter that there is a qualitative difference between the spatial moment predictions of the equilibrium and nonequilibrium models. Thus, from spatial data, it may be possible to differentiate between equilibrium and nonequilibrium models, although as can be seen from Figure 3.4, differentiating between the different nonequilibrium model formulations remains difficult.

INFINITE AND SEMI-INFINITE BOUNDARY CONDITIONS

To examine the effect of infinite versus semi-infinite boundary conditions on the breakthrough responses, one-dimensional breakthrough simulations of semi-infinite and infinite versions of the first-order rate and spherical diffusion models will be compared in this section.

Lindstrom and Narasimhan (1973) derived the first-order rate model solution for an initially distributed solute slug in a one-dimensional semi-infinite medium. The analogous solution, for the following initial and boundary conditions corresponding to an infinitesimal point source:

$$(-D_{mx} \frac{\partial C_m}{\partial x} + v_m C_m)_{x=0} = 0 \tag{4-8a}$$

$$\frac{\partial C_m}{\partial x} \bigg|_{x \to \infty} = 0 \tag{4-8b}$$

$$C_m(x,0) = \frac{M_1'}{\theta_m R_m} \delta(x) \tag{4-8c}$$

$$C_{im}(x,0) = 0 \tag{4-8d}$$

is:

$$C_m(x,t) = \exp\left[-\frac{\alpha' t}{\theta_m R_m}\right] G(x,t) + \frac{\alpha'}{\theta_m R_m} \int_0^t H(t,\tau) G(x,\tau) d\tau \tag{4-9}$$

where:

$$G(x,t) = \frac{M_1'}{\theta_m (\pi D_{mx} R_m t)^{1/2}} \exp\left[- \frac{(R_m x - v_m t)^2}{4 D_{mx} R_m t}\right]$$

$$- \frac{v_m M_1'}{2\theta_m D_{mx} R_m} \exp\left(\frac{v_m x}{D_{mx}}\right) \text{erfc}\left[\frac{R_m x + v_m t}{2(D_{mx} R_m t)^{1/2}}\right]$$

and $H(t,\tau)$ is as defined in Eq. 2-8.

Using Appendix A, the one-dimensional version of Eq. 2-8 may be written

$$C_m(x,t) = \exp\left[- \frac{\alpha' t}{\theta_m R_m}\right] G(x,t) + \frac{\alpha'}{\theta_m R_m} \int_0^t H(t,\tau) G(x,\tau) d\tau \qquad (4\text{-}10)$$

where

$$G(x,t) = \frac{M_1'}{2\theta_m (\pi D_{mx} R_m t)^{1/2}} \exp\left[- \frac{(R_m x - v_m t)^2}{4 D_{mx} R_m t}\right]$$

Equation 4-10 represents the response to an instantaneous point source in a one-dimensional infinite medium.

Wakao and Kaguei (1982) examined the differences in using either semi-infinite or infinite boundary conditions in a model which included both advective/dispersive transport and diffusion into zones of immobile water. They found that deviations between the two solutions were dependent on the dimensionless group, $Pe_m = (v_m \ell / D_{mx})$. Figure 4.5 shows dimensionless concentration versus time solutions of the first-order rate model in both a semi-infinite (4-9) and an infinite (4-10) medium, for various values of Pe_m. For low values of Pe_m, differences between the two solutions become significant. At low values of Pe_m, the dispersive term in the advection/dispersion equation is large enough to cause differences between the semi-infinite solution, which does not allow for dispersive solute flux into the region $x < 0$, and the infinite solution, which does permit upgradient dispersion. As expected, Figure 4.5 shows that at low values of Pe_m, the infinite solution exhibits more spreading than does the semi-infinite solution. At high values of Pe_m, however (i.e., $Pe_m > 50$), the differences between the semi-infinite and infinite solutions are insignificant.
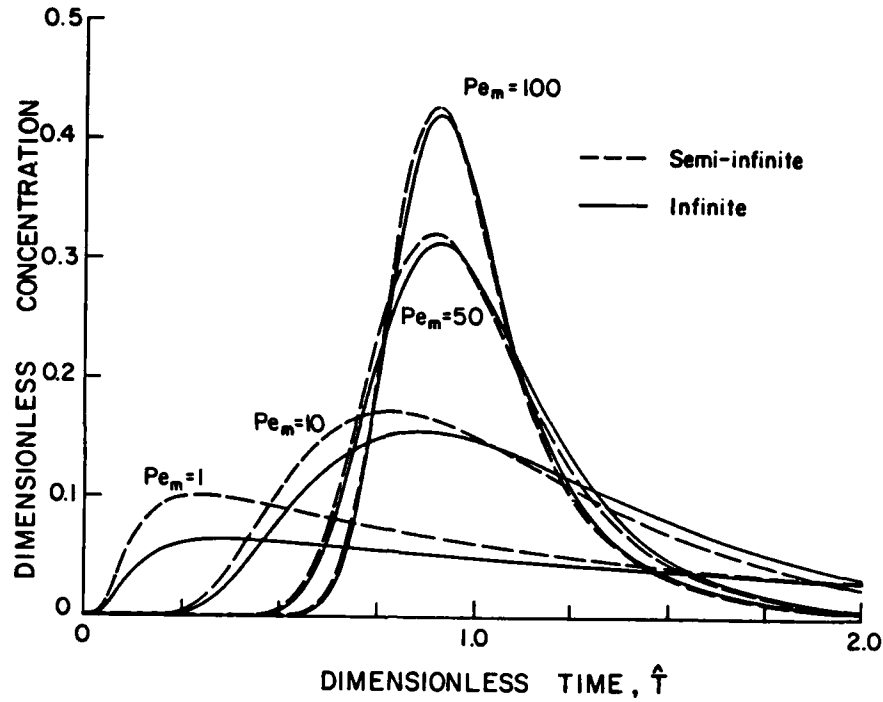
Figure 4.5. Comparison of semi-infinite and infinite solutions to the first-order rate model: $\phi = 0.90$, $\alpha = 0.004$ d^{-1}, v/ℓ = 0.02 d^{-1}, and $R_m = R_{im} = 1.0$.

The solution of the spherical diffusion model in a one-dimensional semi-infinite medium is found by a straightforward application of the methods of Rasmuson and Neretnieks (1980) and van Genuchten et al. (1984). The solution, for an instantaneous point source, is:

$$C_m(x,t) = \frac{4M_1'D_e'\exp(v_m x/2D_{mx})}{\theta_m R_{im}\pi b^2 D_{mx}} \int_0^\infty \left\{ \frac{\exp\left[-\left(\frac{R_m}{D_{mx}}\right)^{1/2} xZ_p\right]}{\left[\frac{v_m}{2D_{mx}} + \left(\frac{R_m}{D_{mx}}\right)^{1/2} Z_p\right]^2 + \frac{R_m}{D_{mx}} Z_m^2} \right.$$

$$\times \left[\left(\frac{v_m}{2D_{mx}} + \left(\frac{R_m}{D_{mx}}\right)^{1/2} Z_p\right) \cos\left(\frac{2D_e'\lambda^2 t}{R_{im}b^2} - \left(\frac{R_m}{D_{mx}}\right)^{1/2} xZ_m\right) \right.$$

$$\left. \left. + \left(\frac{R_m}{D_{mx}}\right)^{1/2} Z_m \sin\left(\frac{2D_e'\lambda^2 t}{R_{im}b^2} - \left(\frac{R_m}{D_{mx}}\right)^{1/2} xZ_m\right) \right] \lambda \right\} d\lambda \qquad (4-11)$$

where Z_p and Z_m are defined in Eq. 2-12.

Using the methods of Appendix B, the one-dimensional version of Eq. 2-12 may be written:

$$C_m(x,t) = \frac{2M_1' D_e' \exp(v_m x/2D_{mx})}{\theta_m R_{1m} \pi b^2 (D_{mx} R_m)^{1/2}}$$

$$\times \int_0^\infty \left\{ \frac{\exp\left[-\left(\frac{R_m}{D_{mx}}\right)^{1/2} |x| Z_p \right]}{z_p^2 + z_m^2} \left[Z_p \cos\left(\frac{2D_e' \lambda^2 t}{R_{1m} b^2} - \left(\frac{R_m}{D_{mx}}\right)^{1/2} |x| Z_m \right) \right. \right.$$

$$\left. \left. + Z_m \sin\left(\frac{2D_e' \lambda^2 t}{R_{1m} b^2} - \left(\frac{R_m}{D_{mx}}\right)^{1/2} |x| Z_m \right) \right] \lambda \right\} d\lambda \qquad (4\text{-}12)$$

where, again, Z_p and Z_m are defined in Eq. 2-12. Equation 4-12 represents the response to an instantaneous point source in a one-dimensional infinite medium.

Figure 4.6 compares dimensionless concentration versus time solutions of the spherical diffusion model in both a semi-infinite (4-11) and an infinite (4-12) medium, for various values of Pe_m. The results are quite similar to the results obtained using the first-order rate model. At high values of Pe_m, the difference between the semi-infinite and infinite solutions decreases.

CONCLUSIONS

In this chapter, the equivalence between the local equilibrium, first-order rate, and geometrical diffusion models was evaluated. It was shown that the equivalence relationships derived using one-dimensional model formulations of the various models are also applicable in three dimensions, and that breakthrough responses simulated using the one- and three-dimensional models show a similar dependence on input parameter values.

Use of field breakthrough (temporal) data to differentiate between the three types of models does not seem feasible, though spatial moment data may be useful in differentiating between the equilibrium and non-equilibrium model formulations.
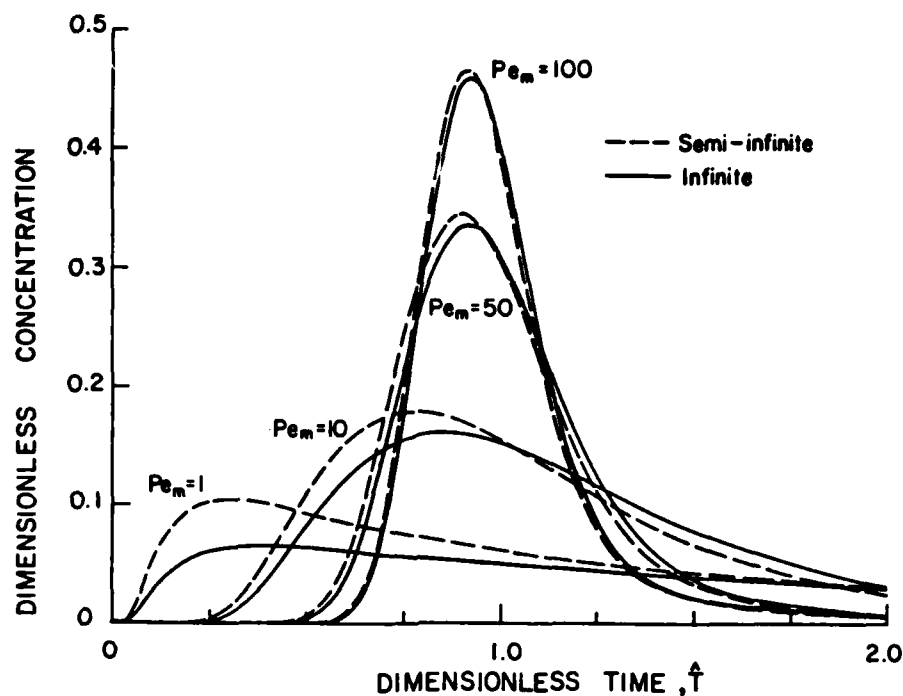
Figure 4.6. Comparison of semi-infinite and infinite solutions to the spherical diffusion model: $\phi = 0.90$, $D_e/b^2 = 0.004$ d^{-1}, $v/\ell = 0.02$ d^{-1}, and $R_m = R_{im} = 1.0$.

It was also demonstrated that the solutions for semi-infinite and infinite boundary conditions are similar at large values of the Peclet number. This is convenient, since the infinite solution is simpler and obtained in a more straightforward manner than the semi-infinite solution.

CHAPTER 5

APPLICATION TO THE INTERPRETATION OF DATA FROM A
LARGE-SCALE TRANSPORT EXPERIMENT UNDER NATURAL CONDITIONS

The discussion thus far has concentrated on the development and analysis of three-dimensional physical nonequilibrium models. In this chapter, spatial and temporal data obtained from a large-scale transport experiment will be interpreted using such models. The physical nonequilibrium models, with parameters obtained from direct measurement, literature correlations, and laboratory experiments, will be used in an attempt to simulate the spatial and temporal behavior of the solute distributions which were observed over the course of the experiment. In addition, the complementarity of the results from spatial and temporal sampling will be assessed in two ways. First, a direct comparison will be made of spatial and temporal results obtained at comparable time/distance scales. Second, equilibrium and physical nonequilibrium model parameters obtained from spatial sampling will be used to simulate temporal response data. Finally, a brief review will be made of various alternative models which may be used in interpreting the field results. This review will include an examination of the spatial moment behavior predicted by some of the alternative models, a subject that previously has not been evaluated systematically.

PROJECT BACKGROUND

A large-scale, long-term field experiment to study natural gradient transport of solutes in groundwater was conducted by a group of investigators from Stanford University and the University of Waterloo, at a site in Borden, Ontario (Mackay et al., 1986; Freyberg, 1986; Roberts et al., 1986). Well-defined initial conditions were achieved by injecting approximately 12 m^3 of a solution containing known masses of two inorganic tracers (chloride and bromide) and five halogenated organic compounds (bromoform, carbon tetrachloride, tetrachloroethylene, 1,2-dichlorobenzene, and hexachloroethane). The transport of the organic solutes was monitored over a two-year period with a dense, three-dimensional array of more than 4000 sampling points. Figure 5.1 depicts the sampling network.
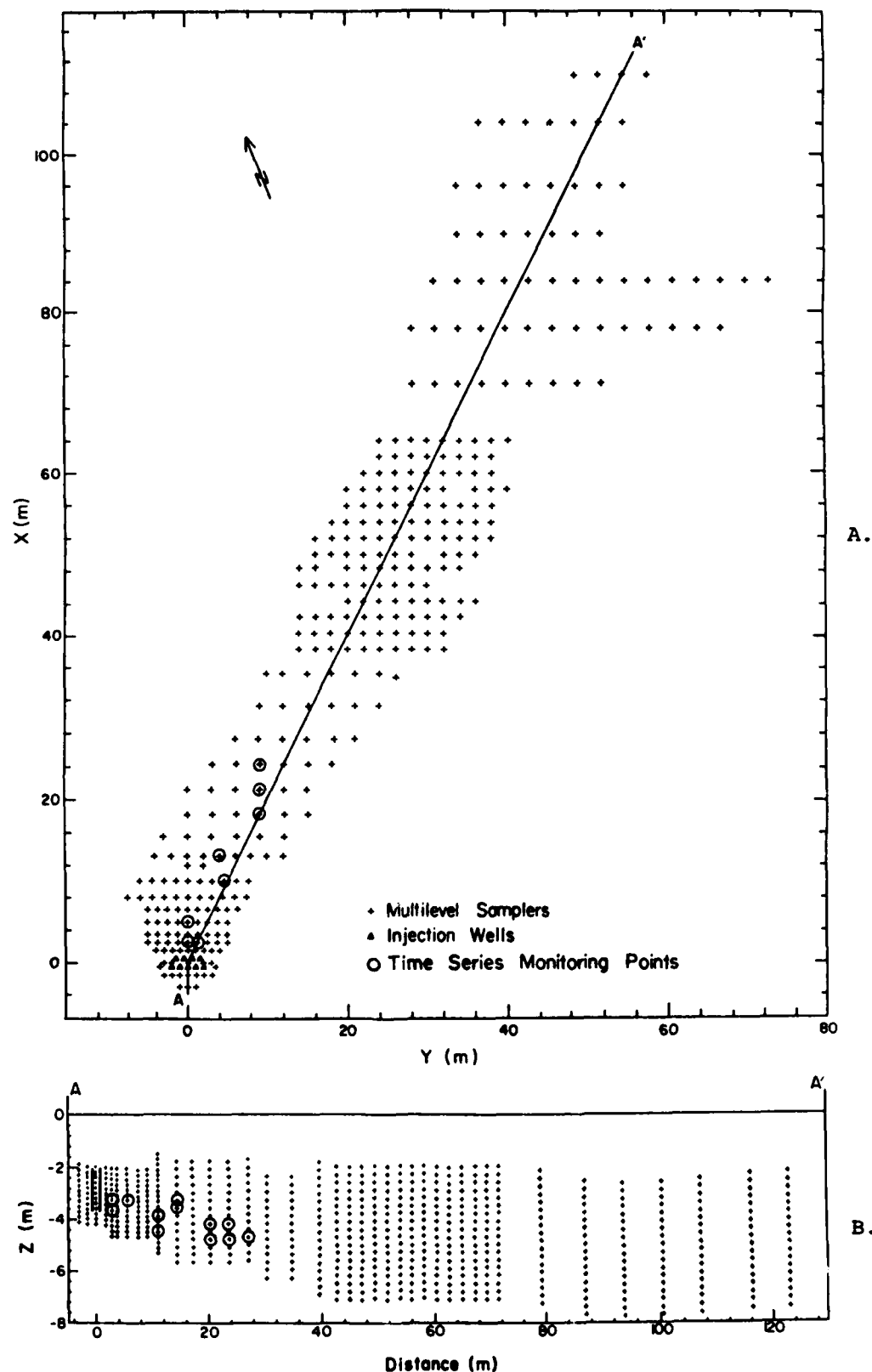
A.

B.

Figure 5.1. Locations of multilevel sampling and injection wells as of
January 1986:   a) Plan view, and b) Approximate vertical
distribution of sampling points (+) projected onto cross
section AA' (vertical exaggeration = 4.6).

Two types of sampling were conducted. Spatial data were obtained from synoptic or "snapshot" sampling sessions, each of which measured the three-dimensional spatial distribution of solute concentration at a particular point in time. Temporal data were obtained by measuring the solute concentration at a relatively high sampling frequency (i.e., daily in the early stages, biweekly or weekly later on) at a few pre-selected sampling points. Tables 5.1 and 5.2 summarize the synoptic and time series monitoring programs. Details of the experimental design and implementation may be found in Mackay et al. (1986).

The aquifer in which the experiment was conducted is unconfined, consisting of horizontally bedded fine- to medium-grained sand (Sudicky et al., 1983). The hydrogeology and geochemistry of the study area have been described by MacFarlane et al. (1983) and Dance (1980).

TABLE 5.1

SUMMARY OF SYNOPTIC MONITORING PROGRAM

Date	Days Since Injection	Tracers	Organics	Number of Samples Analyzed
		Solutes		
08/24/82	1	X	X	392
09/01/82	9	X	X	419
09/08/82	16	X	X	408
09/21-22/82	29	X	X	629
10/05-06/82	43	X	X	671
10/25-26/82	63	X	X	700
11/16-17/82	85	X	X	712
05/09-11/83	259	X		1219
06/22/83	303		X	233
07/19-20/83	330		X	1150
07/21/83	332	X		362
09/07-08/83	380		X	839
09/08-09/83	381	X		496
10/04/83	407		X	949
10/26-28/83	429	X		1883
11/28/83	462	X		1343
05/17/84	633		X	1122
05/31-06/02/84	647	X		958
08/01-02/84	709		X	1119
06/26-28/85	1038	X		1205

TABLE 5.2

SUMMARY OF TIME SERIES MONITORING PROGRAM

	Sample Point (x,y,z) (m)	Duration	Number of Samples Collected as of 1/1/86
Near-Field	2.5, 0.0, -3.20	Aug. 82 - Dec. 83	188
	2.5, 1.25, -3.62	Aug. 82 - Dec. 83	188
	5.0, 0.0, -3.26	Aug. 82 - Dec. 83	183
Mid-Field	10.0, 4.6, -3.88	Nov. 83 - Jun. 85	45
	10.0, 4.6, -4.48	Nov. 83 - Jun. 85	27
	13.1, 4.05, -3.42	Jul. 84 - Jun. 85	32
	13.1, 4.05, -3.72	Jul. 84 - Jun. 85	31
Far-Field	18.0, 9.0, -4.13	Mar. 83 - Jun. 85	119
	18.0, 9.0, -4.73	Mar. 83 - Jun. 85	121
	21.0, 9.0, -4.17	Mar. 83 - Jun. 85	117
	21.0, 9.0, -4.77	Mar. 83 - Jun. 85	117
	24.0, 9.0, -4.76	Mar. 83 - Nov. 83	78

Time Series Data

Concentration responses at each of the twelve high frequency sampling points are shown in Appendix E. Chloride data are not depicted, in the interest of clarity, since the chloride and bromide observations are nearly indistinguishable (Freyberg, 1986). For the purpose of this study, 1,2-dichlorobenzene and hexachloroethane data have also been omitted. As discussed in Roberts et al. (1986), both of these compounds behaved anomalously. Hexachloroethane concentrations declined to non-quantifiable levels by the end of the first three months of the experiment, and the concentration of 1,2-dichlorobenzene declined precipitously at one of the three near-field sampling wells and was never found in significant levels thereafter. Significant concentration levels of 1,2-dichlorobenzene were not seen at either of the other two near-field wells. A full discussion of the near-field, early-time behavior of these two compounds may be found in Roberts et al. (1986). This study will focus on those compounds that remained at significant concentration levels after the first three months of monitoring.

Appendix E also shows that of the four solutes being considered, every solute is not seen at every sampling point. The four mid-field wells were sampled specifically for tetrachloroethylene. Bromide and the two faster moving organics, carbon tetrachloride and bromoform, had largely passed by these wells before sampling commenced. At the five

69

far-field wells, tetrachloroethylene had yet to arrive upon conclusion of the experiment. At the most distant well, only bromide was seen, since sampling at this well was terminated prior to the arrival of the organic solutes.

Synoptic Data

Freyberg (1986) described how the synoptic concentration data were used to obtain estimates of the spatial moments of the solute plume distributions. Freyberg (1986) and Roberts et al. (1986) present estimates of the zeroth and first moments for the inorganic and organic plumes, respectively. Freyberg (1986) also presents estimates of the second moment for the inorganic plumes. Following his methods, the organic plumes' second moment estimates were calculated as well (Freyberg, 1985). In this work, estimates of the second moment are presented as σ_{xx}^2 and σ_{yy}^2, the principal values of the spatial covariance tensor. Freyberg (1986) noted that the vertical components of the spatial covariance tensor could not be distinguished from sampling noise, and that the vertical thickness of the tracer plumes remained essentially constant over the course of the experiment. Therefore, the principal vertical component of the covariance tensor, σ_{zz}^2, has not been considered and will be assumed to be negligible.

Comparison of Time Series and Synoptic Results

Roberts et al. (1986) demonstrated that the results of time series sampling of the near-field wells (x $\leq$ 5 m) were qualitatively consistent with synoptic sampling results. In this section, far-field (x > 15 m) time series sampling results for bromoform and carbon tetrachloride are presented, and compared with synoptic sampling results, to further demonstrate the complementarity of spatial and temporal transport behavior. The comparison is made in terms of the retardation factor, which is calculated using temporal or spatial first moment estimates, and the relative mass ratio, which is obtained from temporal or spatial zeroth moment estimates. The following definitions are used:

1. Retardation factors are defined by Eqs. 3-55a and 3-55c, based on temporal and spatial first moment estimates, respectively.

2. Relative mass is defined as the total solute mass calcu-
lated from the temporal or spatial zeroth moment estimate,
normalized by the total solute mass initially injected
into the aquifer. The relative mass ratio is the rela-
tive mass of a retarded solute divided by the relative
mass of the conservative tracer. The relative mass cal-
culated from the temporal zeroth moment is proportional
to the area under the breakthrough response curve. The
relative mass calculated from the spatial zeroth moment
is proportional to the product of the zeroth moment and
the retardation factor. As noted above, for this analy-
sis, the retardation factor at a particular synoptic
sampling time is obtained from Eq. 3-55c. The reason the
mass calculated from the spatial moment is proportional
to the retardation factor while the mass calculated from
the temporal moment is not, goes back to the discussion
in Chapter 3. When determining the spatial moment at an
instant in time, only the aqueous solute concentration is
measured. The sorbed solute must be accounted for, in
this instance, by use of the retardation factor. On the
other hand, when determining the temporal zeroth moment,
all the solute passing by a particular sampling point is
accounted for in the breakthrough response curve.

In order to graphically compare spatial and temporal behavior, it
is useful to plot the two types of results on the same scale. Spatial
data are obtained at particular sampling times. The sampling distances
at which temporal data are obtained may be converted to equivalent time
values. For this analysis, the first moment of the breakthrough re-
sponse curve of the solute of interest at a sampling point is defined as
the equivalent time for that point.

Figures 5.2 and 5.3 depict the relative mass ratios and the retar-
dation factors for bromoform and carbon tetrachloride calculated from
temporal and spatial moment estimates. For bromoform, the decrease in
mass and the increase in the retardation factor which was found by an
examination of the spatial data (Roberts et al., 1986) is also clearly
seen by comparing near- and far-field temporal results. The obvious
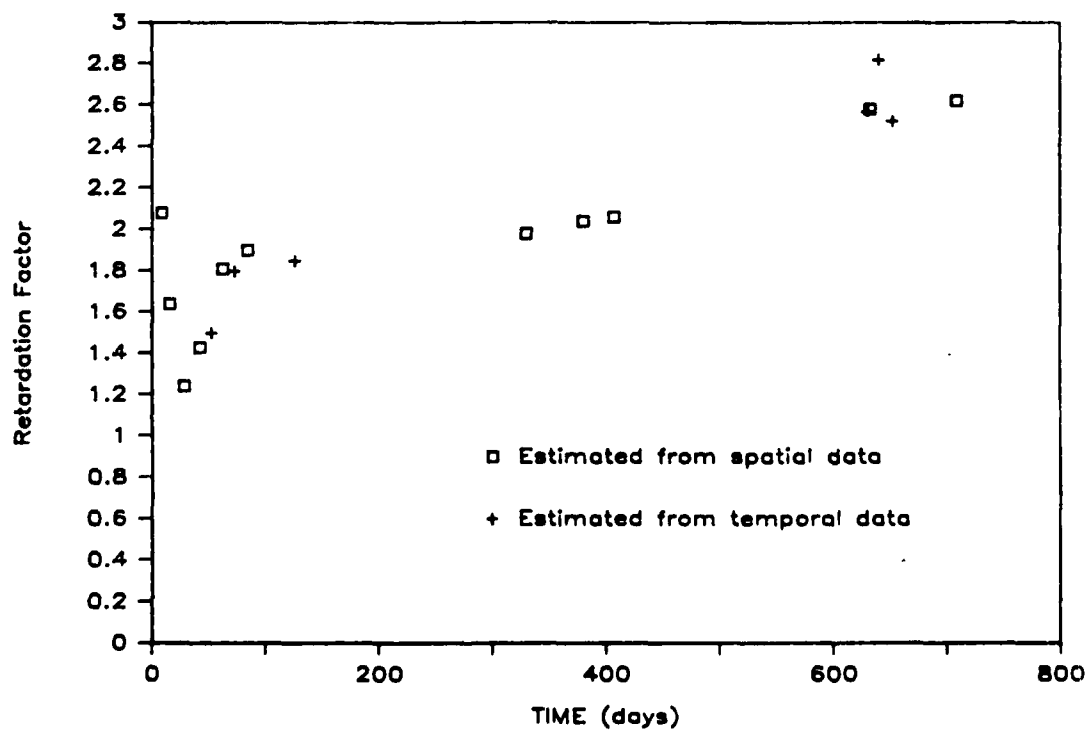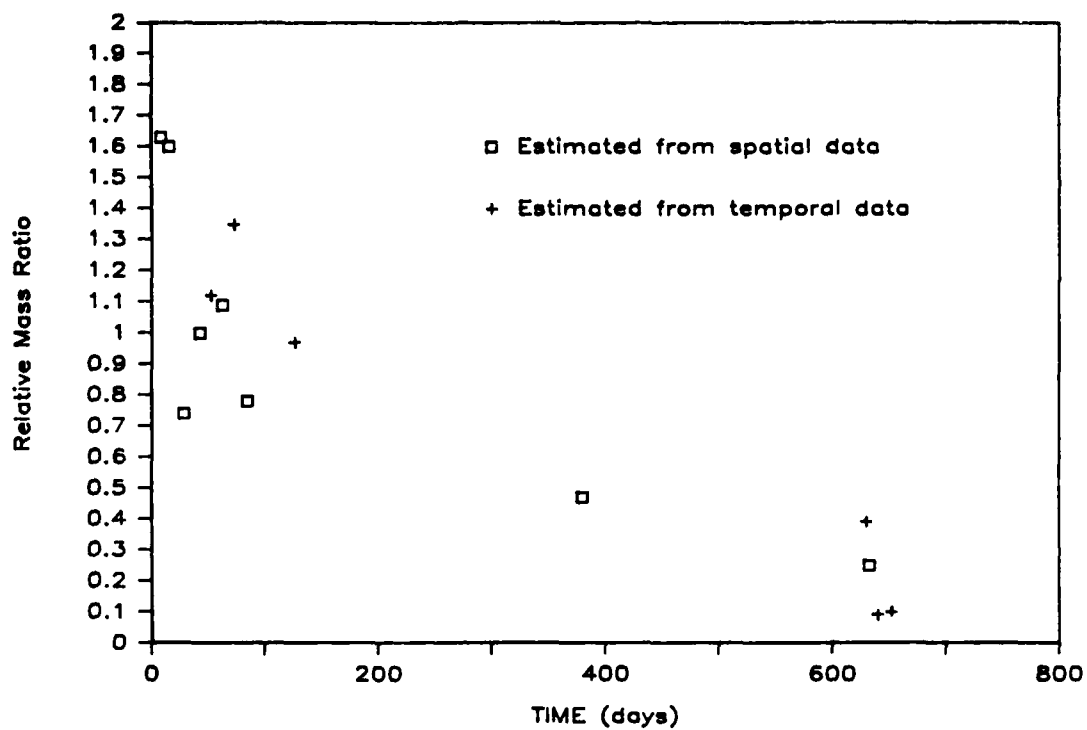disappearance of bromoform (Figure 5.2) was attributed to transformation

Figure 5.2. Comparison of the bromoform plume behavior determined from spatial and temporal data: a) Relative mass ratio, and b) Retardation factor versus time.
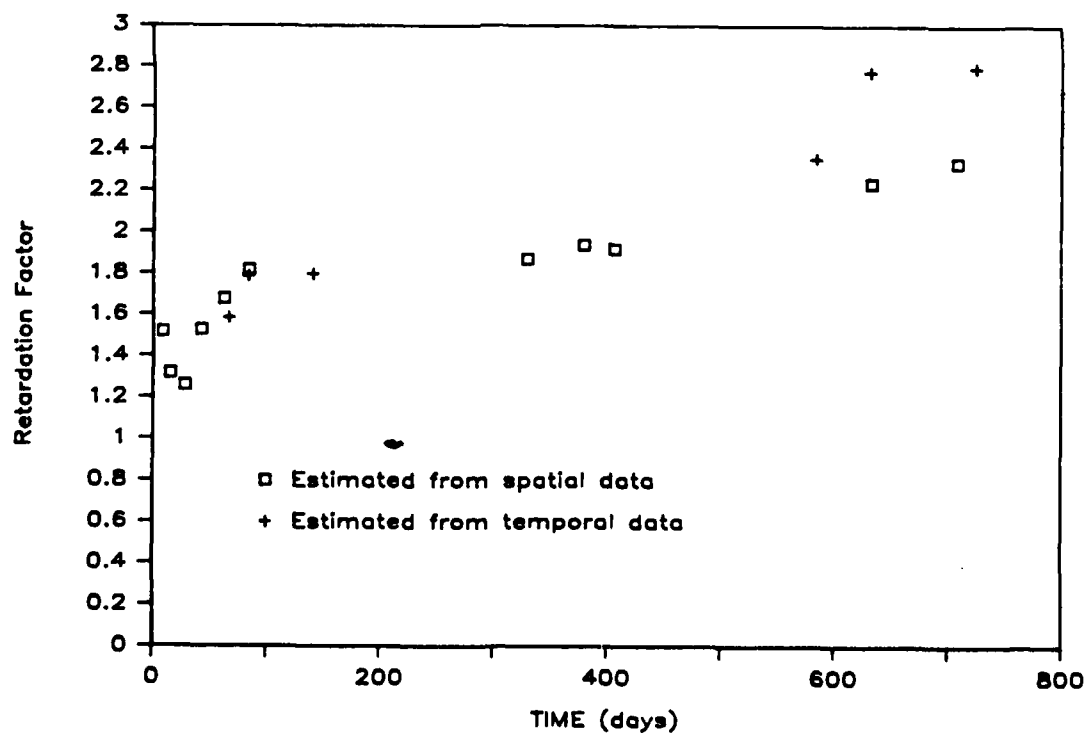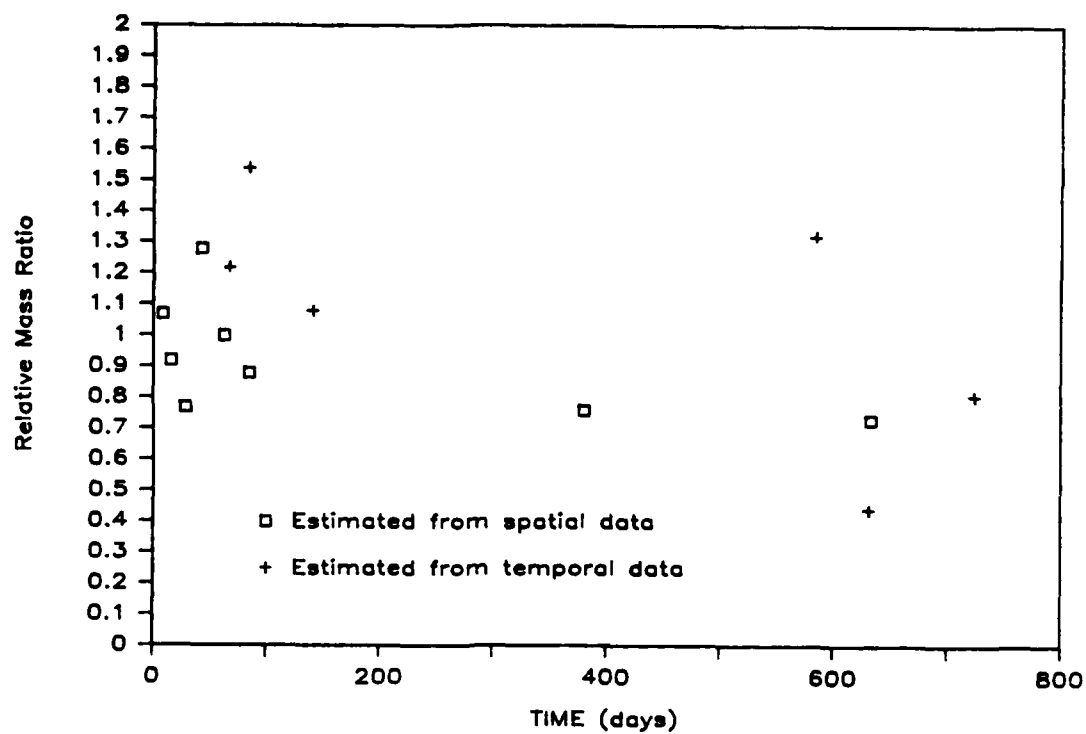
72

Figure 5.3. Comparison of the carbon tetrachloride plume behavior determined from spatial and temporal data: a) Relative mass ratio, and b) Retardation factor versus time.

73

by Roberts et al. (1986). More variability is evident in the calculations of the relative mass for carbon tetrachloride, though again, the increase in the retardation factor over the course of the experiment is evident. The variability of the relative mass ratios obtained from the temporal data may reflect local variations in aquifer properties along the flow paths to the individual sampling points (Roberts et al., 1986). Nevertheless, there is good general agreement between the results of the spatial and temporal analyses.

MODEL APPLICATION

One goal of modeling is to predict real behavior using independently obtained parameter values. In this section, an attempt is made to predict zeroth and first spatial moment behavior using first-order rate model parameters equivalent to the spherical and layered diffusion model parameters. Model parameter values are estimated based on direct measurement, literature correlations, and soil adsorption isotherms measured in the laboratory.

Spherical Diffusion Model

Based on the approximately spherical shape of the aquifer material, it is reasonable to assume solute diffusion into spherical grains may be influencing transport. Table 5.3 lists parameter values for use in a spherical diffusion model. The parameters in Table 5.3 were obtained independently of the experimental data. The mass of each solute initially injected into the aquifer (M_j^i) was known (Mackay et al., 1986). Values for bulk density (ρ), and total porosity (θ) were obtained by direct measurement (Mackay et al., 1986) as was the range of median grain sizes (b) (O'Hannesin, 1981). The value for the pore water velocity (v_0) was based on estimates of hydraulic conductivity and hydraulic gradient (Mackay et al., 1986). The ratio of mobile to total water content (ϕ) was calculated using the following expression:

$$\phi = \frac{\theta - \varepsilon_a}{\theta(1 - \varepsilon_a)} \tag{5-1}$$

where ε_a is the intragranular porosity. Intragranular porosity was measured by mercury porosimetry (Demond, 1984). The distribution coefficients (K_d) for the various organic compounds and Borden aquifer material

74

TABLE 5.3

PARAMETER VALUES FOR USE IN A SPHERICAL DIFFUSION MODEL

Bulk soil density (ρ)	1.81 g/cm^3
Total porosity (θ)	0.33
Intraparticle porosity (ϵ_a)	0.01
Ratio of mobile to total water content (ϕ)	0.979
Pore water velocity (v_o)	0.079 m/d
Fraction of "mobile" sorption sites (f)	0.0
Median grain radius (b)	0.035-0.35 mm

	Bromide	Bromo-form	Carbon Tetra-chloride	Tetra-chloro-ethylene
Distribution coeff. (K_d), cm^3/g	0.0	0.17	0.17	0.48
Mass of injected solute (M_3'), g	3,870	0.38	0.37	0.36
Liquid diffusion coeff. (D_o), m^2/d	1.74×10^{-4}	7.17×10^{-5}	7.34×10^{-5}	6.83×10^{-5}
Effective intraparticle diffusion coeff. (D_e'), m^2/d	1.74×10^{-6}	7.17×10^{-7}	7.34×10^{-7}	6.83×10^{-7}
Equivalent first-order rate constant (α'), d^{-1}	1.44-144	0.594-59.4	0.608-60.8	0.566-56.6

were measured by Curtis et al. (1986) in a series of batch sorption experiments. Bromide, the inorganic tracer, is assumed to be nonsorbing. The liquid diffusion coefficients (D_o) for the organic compounds were estimated using the Wilke and Chang (1955) correlation. The liquid diffusion coefficient for bromide was calculated using a method described by Cussler (1984) for estimating the diffusion coefficient of electrolytes. Since intraparticle diffusion is likely to be hindered by the interaction of the solute and the sorbent grain, the effective intraparticle diffusion coefficient (D_e') is some fraction of the liquid diffusion coefficient. Defining tortuosity (χ) such that:

$$D_e' = \frac{D_o}{\chi} \tag{5-2}$$

Wakao and Smith (1962) proposed:

$$\chi = \frac{1}{\epsilon_a}$$

Given the measured value of ε_a of 0.01, $\chi = 100$. Equation 5-2 was used to calculate the effective intraparticle diffusion coefficients for the compounds being considered. Finally, a value for f, the fraction of sorption sites adjacent to regions of mobile water is required for model input. Nkedi-Kizza et al. (1982) assumed that for an aggregated soil, virtually all the sorption occurs within the aggregate, so that there are no sorption sites in direct contact with mobile water. Following Nkedi-Kizza et al. (1982), it will be assumed that sorption occurs either within the aquifer material grains or within aggregates, so that f = 0.0 for this model.

It is now possible to apply the moment analysis formulae of Table 4.1 to obtain first-order rate constants (α') equivalent to the spherical diffusion rates which can be calculated using the values of D'_e, b, ϕ, and θ in Table 5.3. This conversion to a first-order rate model is chosen because of the convenience and computational efficiency of the first-order rate model as compared to the diffusion models. In Chapter 4, it was shown that simulations obtained from each of the two model types are quite similar, and probably indistinguishable considering the accuracy of the experimental data and the accuracy with which the input parameters are estimated. The range in values for α' is due to the range in median grain sizes.

Before using the parameter values estimated above in the first-order rate model, and comparing simulations with experimental data, it is useful to discuss the relevance of the boundary and initial conditions assumed in the model to the experimental conditions. The assumption of infinite boundary conditions would seem applicable in describing the experimental conditions at Borden, in which the medium is unbounded upgradient from the point of introduction, as well as downgradient from the observation points. In any event, as was discussed in Chapter 4, except for observation points close to the point of solute introduction, the impact of boundary conditions on model predictions is small.

As was noted in Chapter 3, the assumption that no mass is initially associated with the immobile region has a large effect on the mobile region plume mass and velocity behavior. A related assumption is that water which is obtained from the sampling wells is mobile water. The former assumption implies, and the latter states, that water which is injected into the aquifer by the injection system, or withdrawn from the

76

aquifer by the sampling system, is mobile water. Conceptually, these assumptions seem reasonable. If it is assumed that regions of immobile water do indeed exist in the Borden aquifer (within dead-end pores or zones of low permeability, for example), it follows that during injection or extraction, mobile water will be preferentially displaced. In light of this preferential displacement, the initial condition assumption and the assumption regarding the sampling water appear reasonable. Therefore, in the following discussion, the moments calculated from the spatial data will be assumed to be mobile region plume moments.

Figures 5.4 through 5.7 compare the mass in solution and first spatial moments of the four mobile region solute plumes (Freyberg, 1986; Roberts et al., 1986) with the moments simulated using the first-order rate model. The Table 5.3 parameter values were used in the model. Also shown in Figures 5.4 through 5.7 are the moments simulated using the local equilibrium model. The local equilibrium model simulations use the values of v_o, M_3^1, ρ, θ, and K_d from Table 5.3, and implicitly assume $\phi = f = 1$ (i.e., all water is mobile water). As these figures show, the local equilibrium model and the physical nonequilibrium model produce virtually identical results for the parameters used. These results indicate that, based on the assumed diffusion coefficients and grain sizes, for the time scale considered, local equilibrium is a valid assumption. In particular, notice that varying the first-order rate constant over two orders of magnitude has no effect on the results. The reason for this insensitivity to the rate constant is that even for the minimum value of the rate constant, local equilibrium is valid. Therefore, increasing the rate constant has no effect on the simulations. Note, though, that the qualitative fit of the models to the data is poor. The mass loss and the deceleration of the solute plumes which was observed experimentally is not simulated by the models. One way to simulate the observed spatial moment behavior is to adjust the diffusion rate constant. Either a tenfold increase in the maximum median grain size (from $b = 0.35$ mm to $b = 3.5$ mm, while holding D_e^1 constant) or a one-hundredfold decrease in the effective intraparticle diffusion coefficient (while holding $b = 0.35$ mm constant) will lead to a one-hundredfold decrease in the minimum rate constant. Figures 5.8 through 5.11 compare the simulations of the first-order rate model using this decreased rate constant with the experimental observations. As the

77

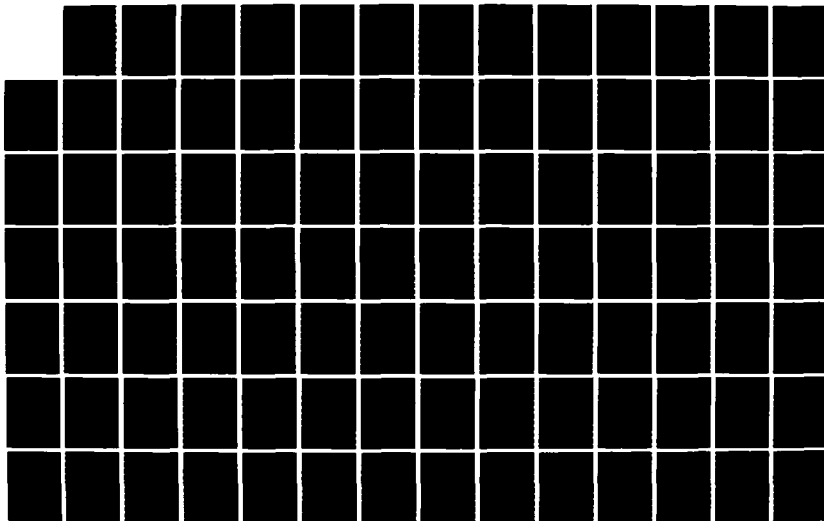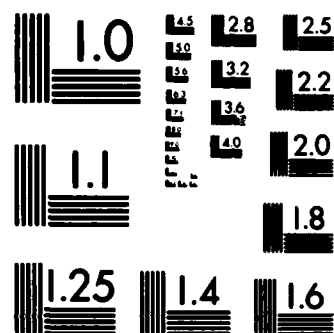MICROCOPY RESOLUTION TEST CHART
NATIONAL BUREAU OF STANDARDS-1963-A

Figure 5.4. Comparison of the bromide mobile region plume: a) Mass in solution, and b) First spatial moment, estimated from synoptic data and simulated using an equilibrium and a first-order rate model equivalent to a spherical diffusion model.
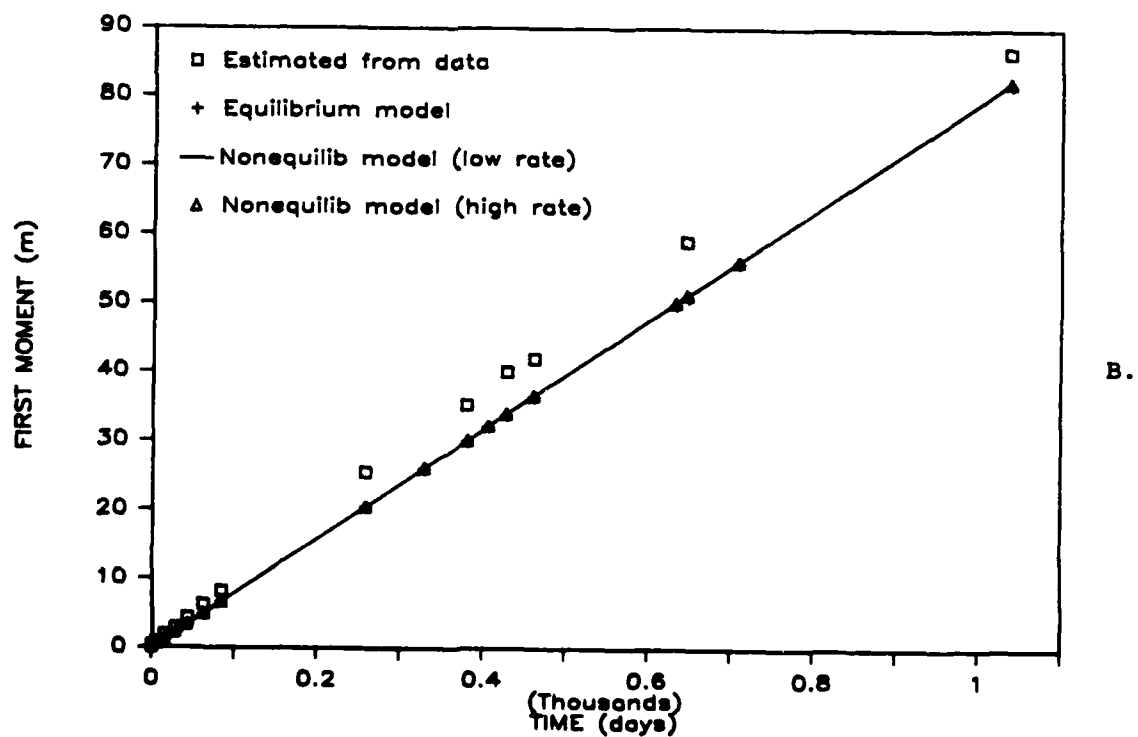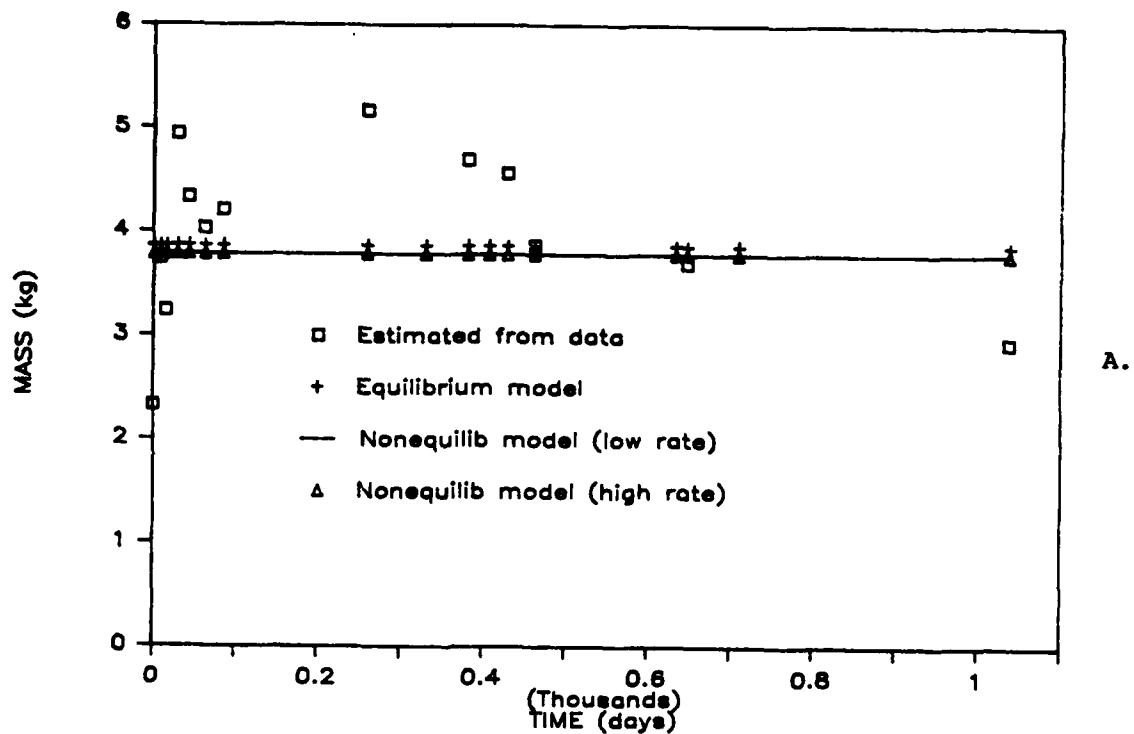
Figure 5.5. Comparison of the bromoform mobile region plume: a) Mass in solution, and b) First spatial moment, estimated from synoptic data and simulated using an equilibrium and a first-order rate model equivalent to a spherical diffusion model.

79

A.

B.

Figure 5.6. Comparison of the carbon tetrachloride mobile region plume:
a) Mass in solution, and b) First spatial moment, estimated
from synoptic data and simulated using an equilibrium and a
first-order rate model equivalent to a spherical diffusion
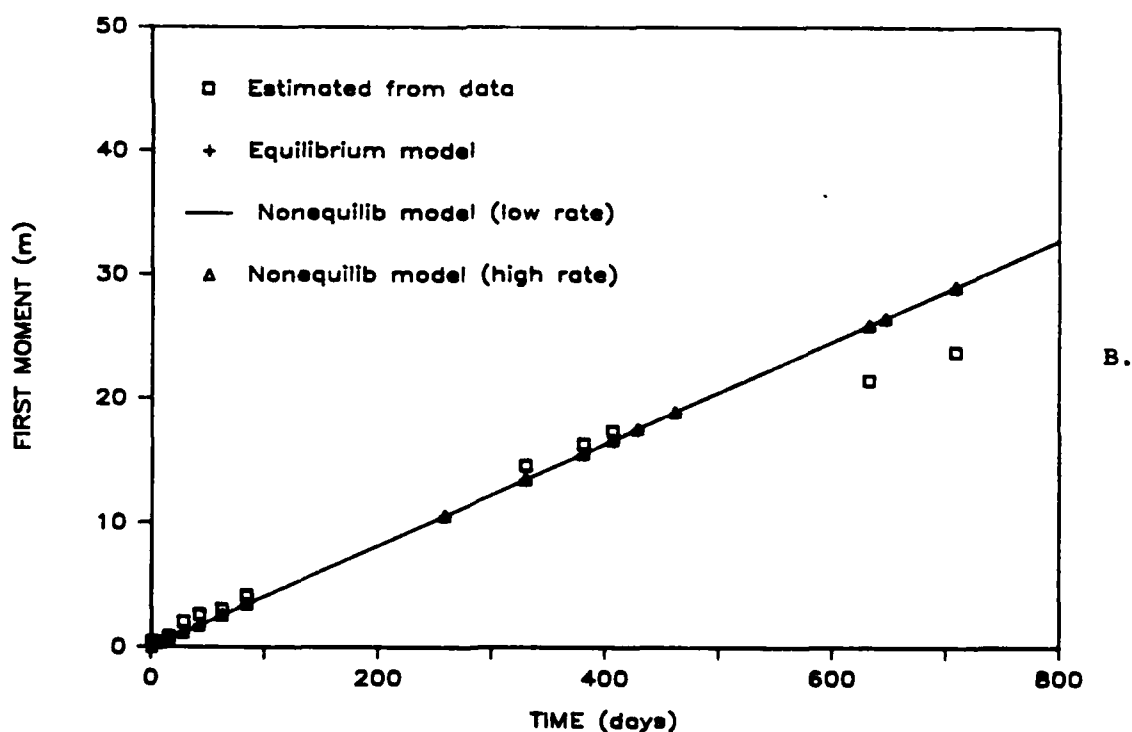model.

80

Figure 5.7. Comparison of the tetrachloroethylene mobile region plume: a) Mass in solution and b) First spatial moment, estimated from synoptic data and simulated using an equilibrium and a first-order rate model equivalent to a spherical diffusion model.
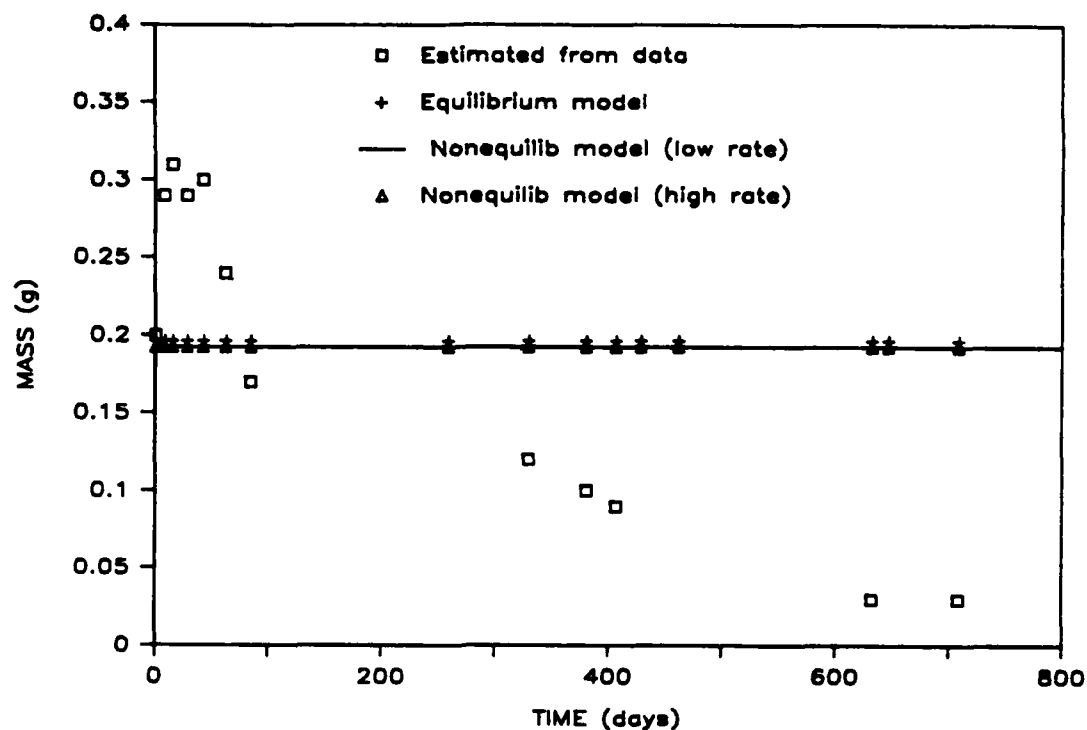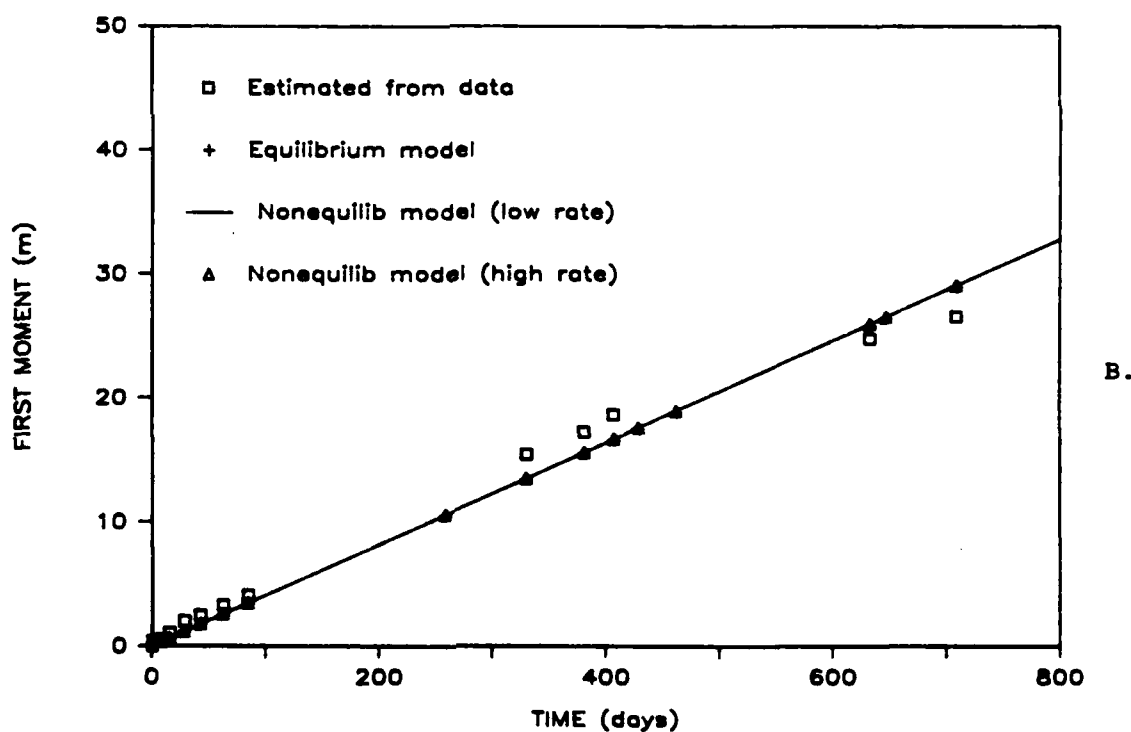
A.

B.
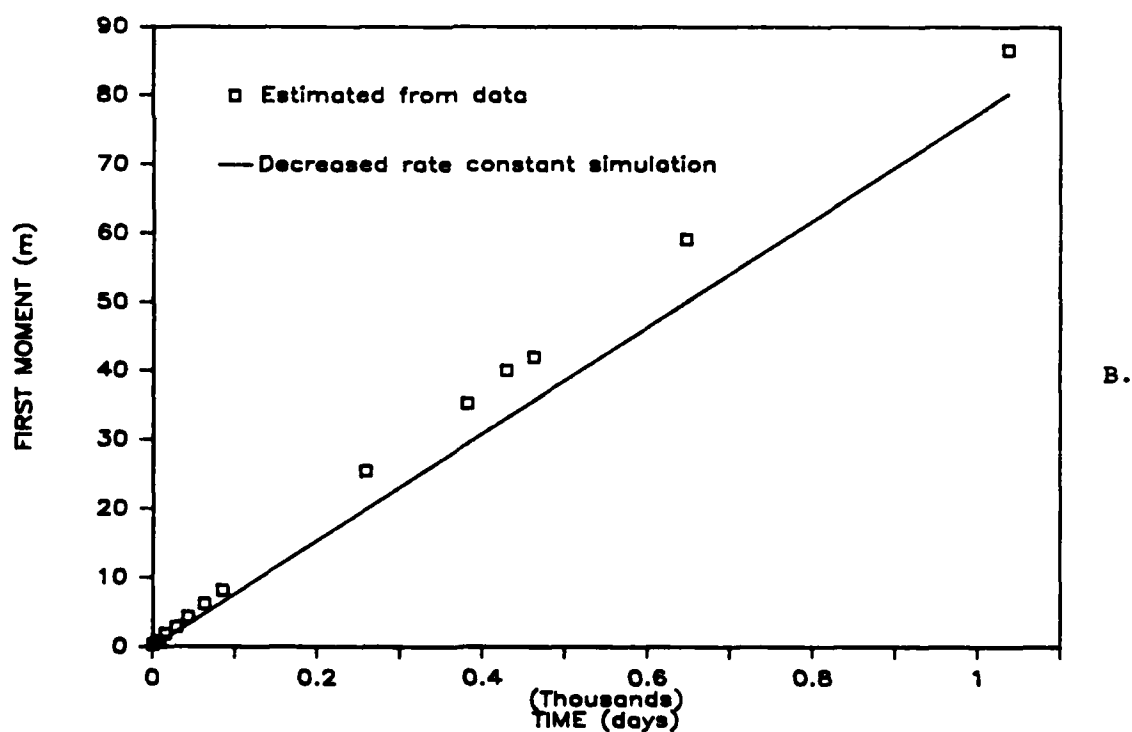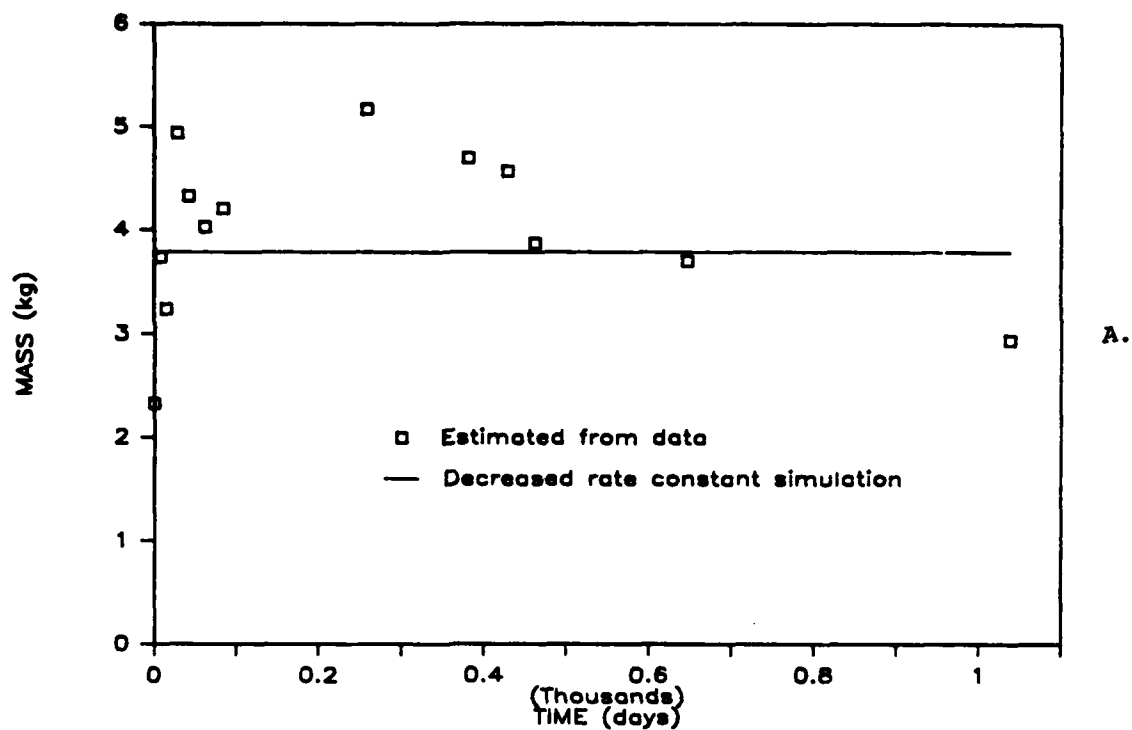
Figure 5.8. Comparison of the bromide mobile region plume: a) Mass in solution, and b) First spatial moment, estimated from synoptic data and simulated using a first-order rate model equivalent to a spherical diffusion model, with a very low rate constant ($\alpha' = 0.0144$ d^{-1}).

82
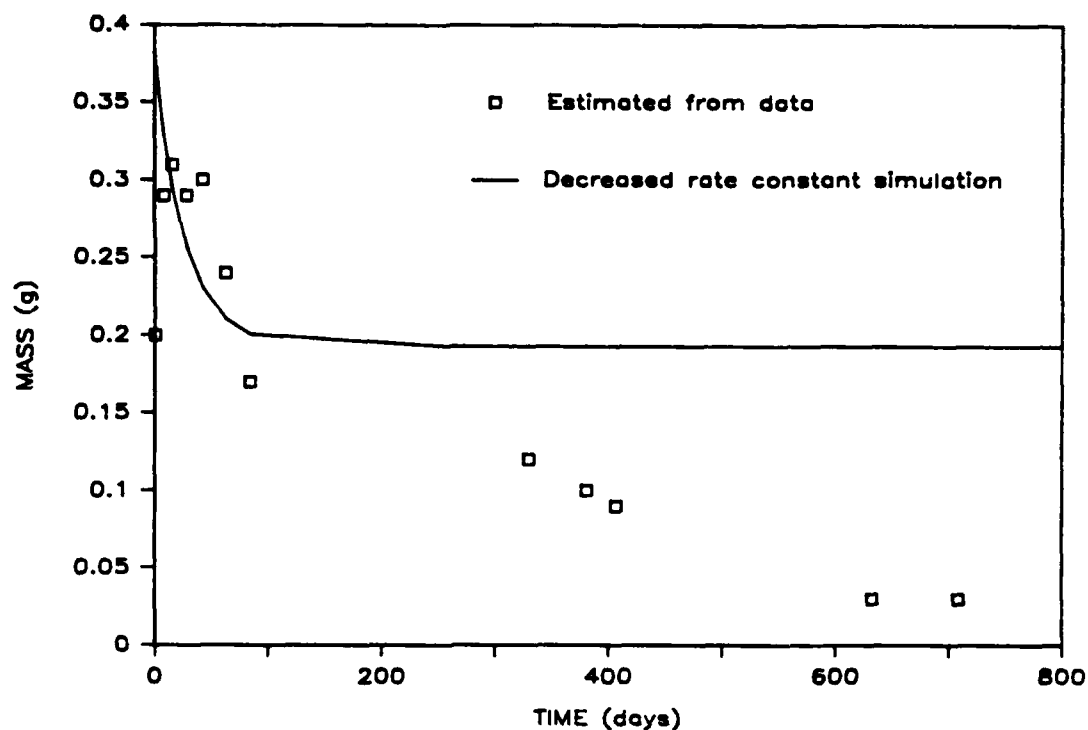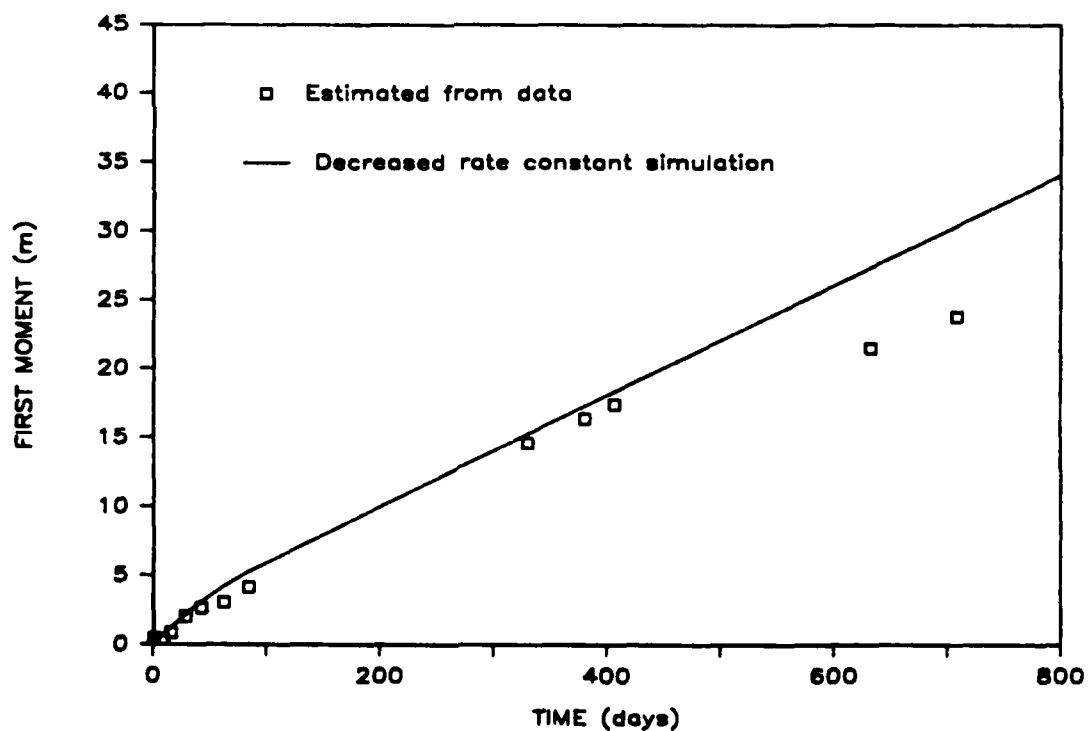
Figure 5.9. Comparison of the bromoform mobile region plume: a) Mass in solution, and b) First spatial moment, estimated from synoptic data and simulated using a first-order rate model equivalent to a spherical diffusion model, with a very low rate constant ($a' = 0.00594$ d^{-1}).
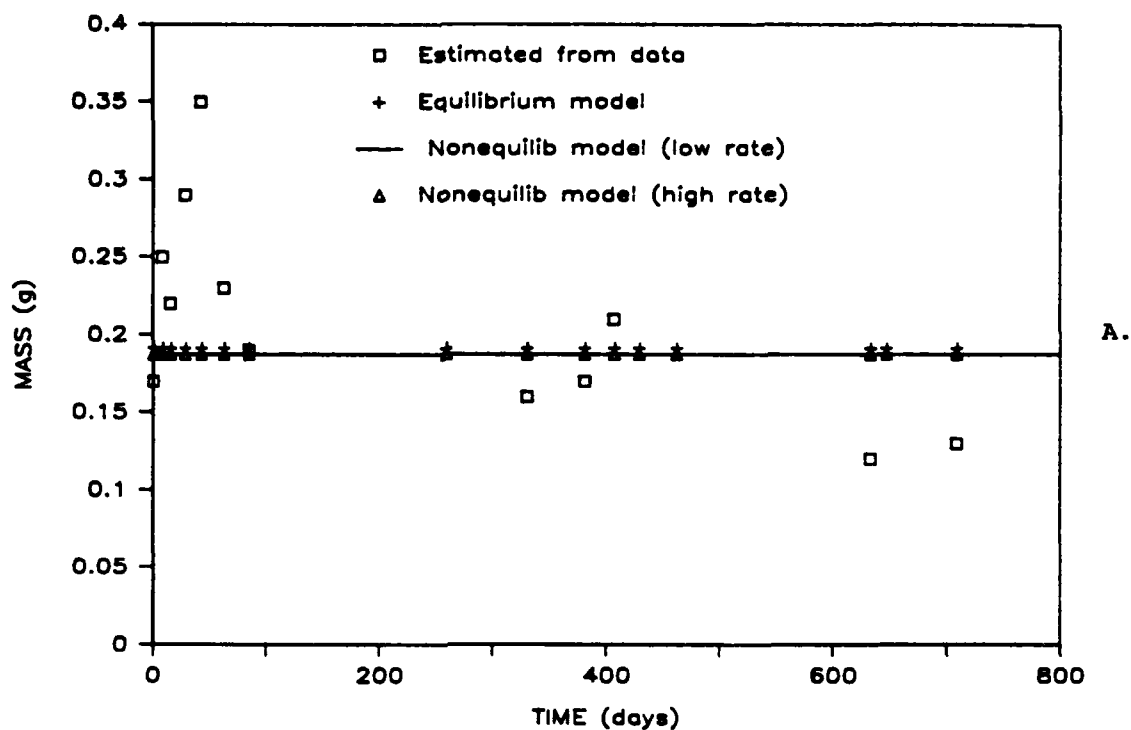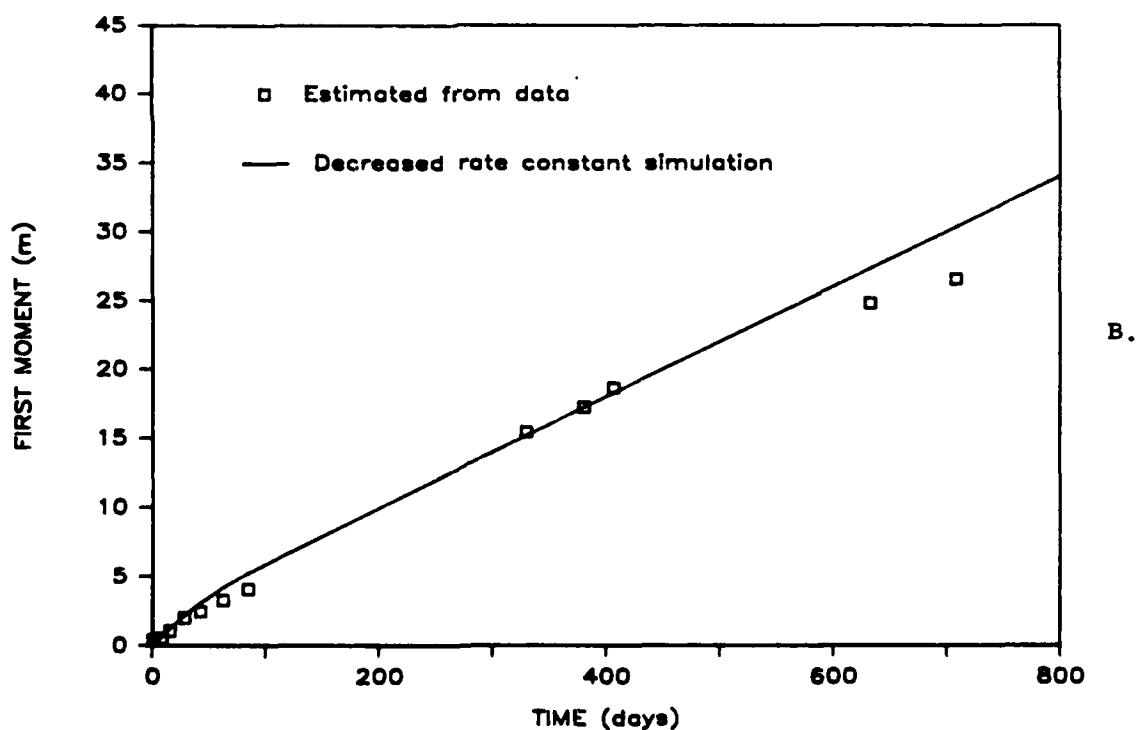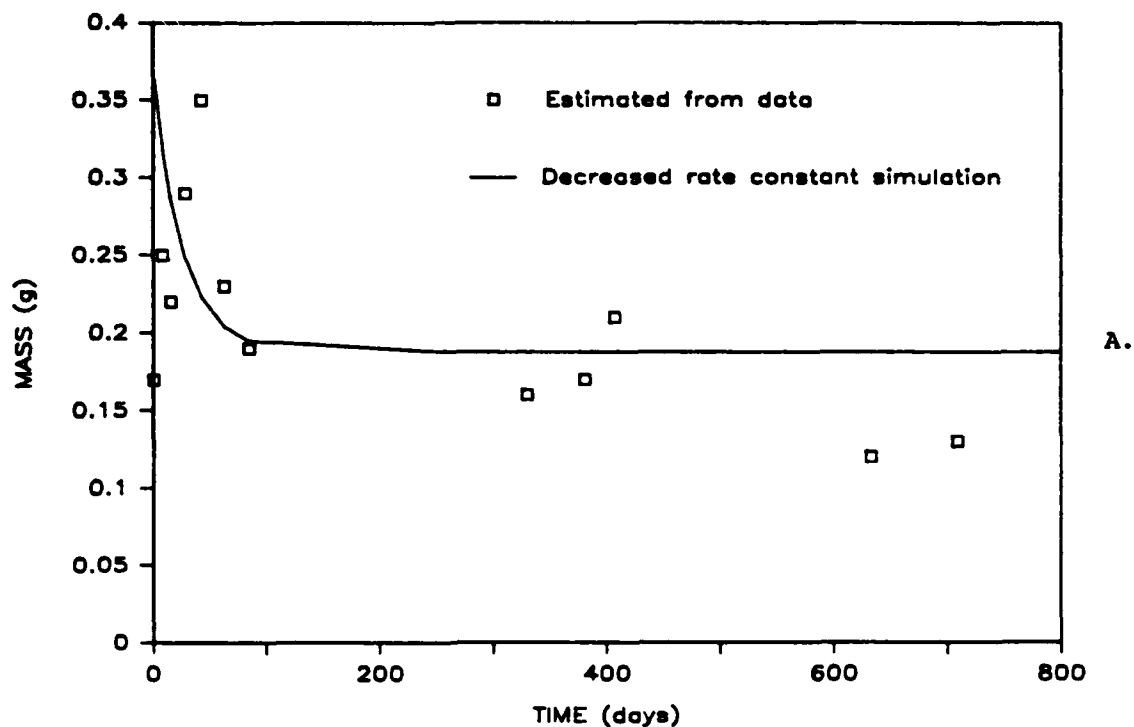
Figure 5.10. Comparison of the carbon tetrachloride mobile region plume:
a) Mass in solution, and b) First spatial moment, esti-
mated from synoptic data and simulated using a first-order
rate model equivalent to a spherical diffusion model, with
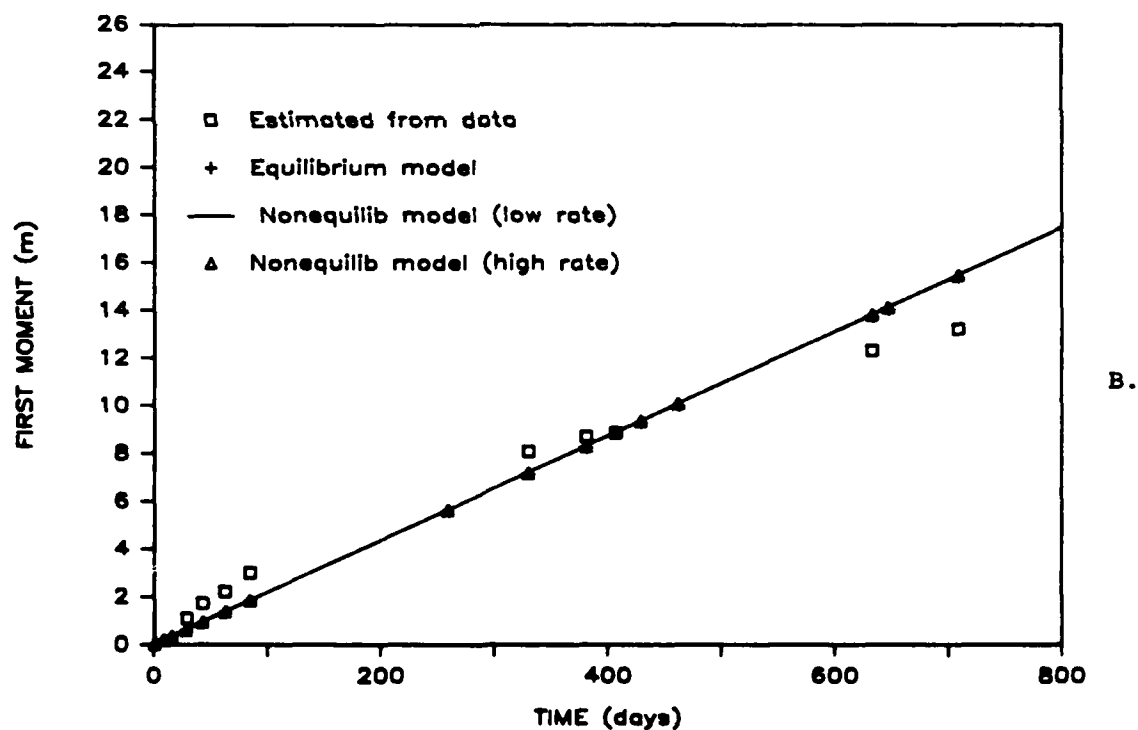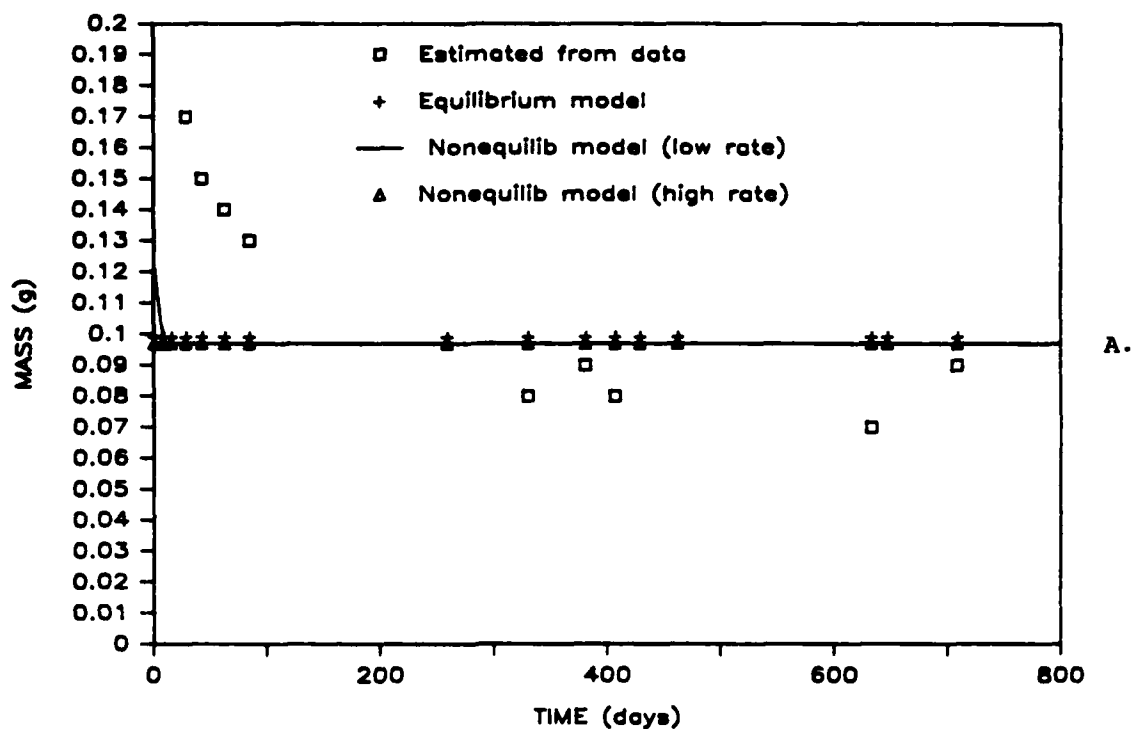a very low rate constant ($\alpha' = 0.00608$ d^{-1}).

Figure 5.11. Comparison of the tetrachloroethylene mobile region plume: a) Mass in solution, and b) First spatial moment, estimated from synoptic data and simulated using a first-order rate model equivalent to a spherical diffusion model, with a very low rate constant ($a' = 0.00566$ d^{-1}).
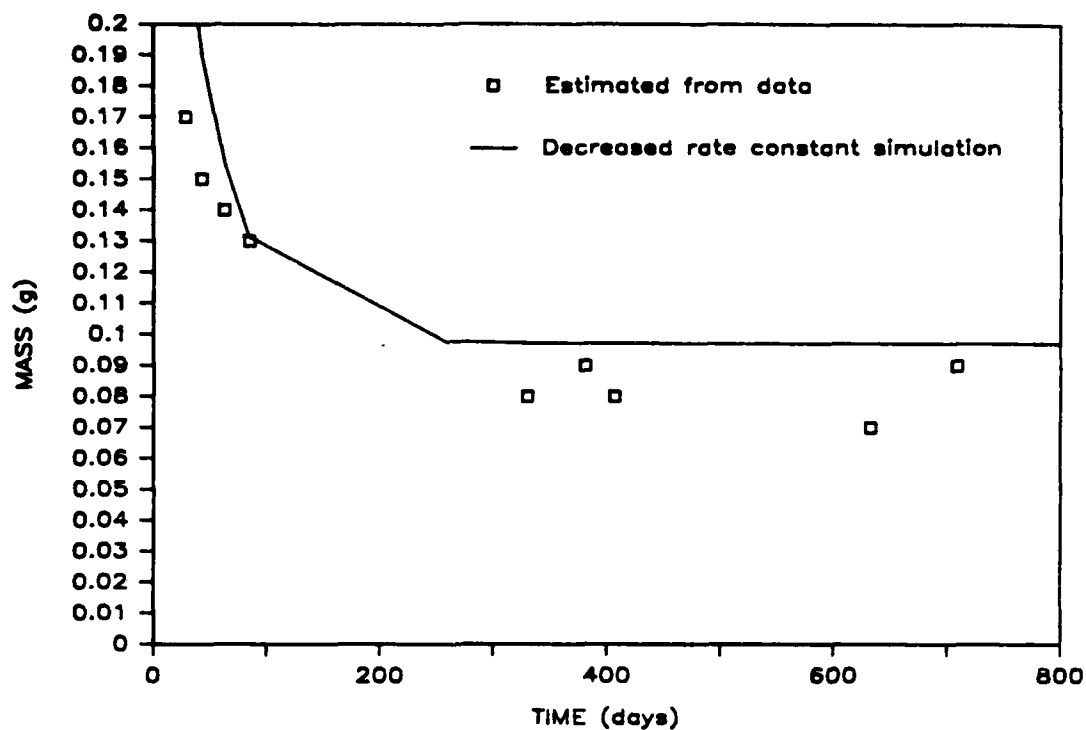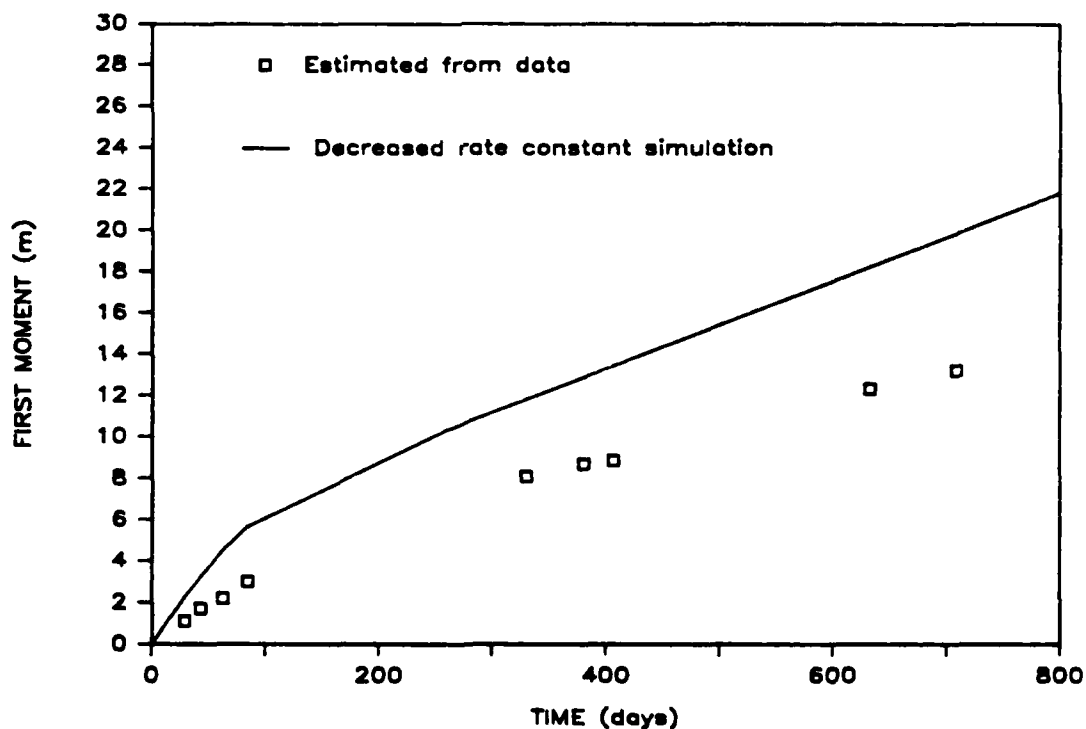
figures show, the salient characteristics of the data are simulated by the model. The mass in mobile solution moment simulations demonstrate good fits to the data, except in the case of bromoform. The model, which predicts no mass loss of bromide over the course of the experiment, is consistent with the data. The mass loss of carbon tetrachloride and tetrachloroethylene is simulated by the model. The observed mass loss of bromoform, however, is significantly greater than model predictions. This discrepancy may be due to the biotransformation of bromoform, a possibility which was discussed by Roberts et al. (1986). The observed deceleration of the organic plumes, and the constant velocity of the bromide plume are qualitatively simulated.

The only parameter which was adjusted to fit the model to the data in Figures 5.8 through 5.11 was the rate constant describing solute transfer into the regions of immobile water. The fitted value of this rate constant is 100x less than was calculated using literature correlations and the maximum median grain size. However, this hundredfold discrepancy is not entirely unrealistic. Hutzler et al. (1986), using a similar spherical diffusion model to simulate soil column breakthrough responses, found that grain sizes on the order of 7-20x greater than the mean particle grain size were required to get a good fit of the model simulations to the experimental data. This increase in grain size is equivalent to a 49- to 400-fold decrease in the rate constants calculated using literature correlations. An alternate explanation is that strongly hindered diffusion is occurring. Such hindered diffusion has been reported in the literature. Roberts (1966) estimated that hexane diffusivity in zeolite crystals was seven orders of magnitude less than bulk diffusivity. Satterfield et al. (1973) found that, for solute molecular diameters on the same order as sorbent pore diameters, liquid-phase diffusivities of hydrocarbons were less than bulk diffusivity values by several orders of magnitude. Prasher and Ma (1977) cited other studies where the reported diffusivity values for organic solutes in zeolites were several orders of magnitude less than bulk diffusivity values. In addition, Ball and Roberts' (1985) finding that the attainment of equilibrium in batch sorption studies measuring tetrachloroethylene uptake by Borden aquifer material required at least several months also supports the hypothesis of strongly hindered diffusion within Borden aquifer material.

Layered Diffusion Model

Based on Sudicky's (1986) finding of low permeability horizontal lenses within the Borden aquifer, it is also reasonable to suppose that solute diffusion into these layers may influence transport. Table 5.4 lists parameter values for use in a layered diffusion model. The ratio of mobile to total water content (ϕ) was obtained from a semi-independent measurement. Freyberg (1986) showed that the velocity of the conservative tracers averaged 0.091 m/d. The value of v_o calculated based on hydraulic conductivity and hydraulic gradient estimates, and assuming a porosity of 0.33, was 0.079 m/d (Mackay et al., 1986). If it is assumed that the difference between the two velocity estimates is caused by zones of immobile water which do not contribute to transport, the value of ϕ can be calculated as follows:

$$\phi = \frac{0.079 \text{ m/d}}{0.091 \text{ m/d}} = 0.86$$

TABLE 5.4

PARAMETER VALUES FOR USE IN A LAYERED DIFFUSION MODEL

Bulk soil density (ρ)	1.81 g/cm^3
Total porosity (θ)	0.33
Ratio of mobile to total water content (ϕ)	0.86
Pore water velocity (v_o)	0.079 m/d
Fraction of "mobile" sorption sites (f)	0.86
Layer half-width (b)	0.01-0.05 m

	Bromide	Bromo-form	Carbon Tetra-chloride	Tetra-chloro-ethylene
Distribution coeff. (K_d), cm^3/g	0.0	0.17	0.17	0.48
Mass of injected solute ($M_3^!$), g	3,870	0.38	0.37	0.36
Liquid diffusion coeff. (D_o), m^2/d	1.74×10^{-4}	7.17×10^{-5}	7.34×10^{-5}	6.83×10^{-5}
Effective diffusion coeff. ($D_e^!$), m^2/d	$2.9-8.7 \times 10^{-5}$	$1.2-3.6 \times 10^{-5}$	$1.2-3.7 \times 10^{-5}$	$1.1-3.4 \times 10^{-5}$
Equivalent first-order rate constant (α'), d^{-1}	$1.57 \times 10^{-3} - 1.18 \times 10^{-1}$	$6.51 \times 10^{-4} - 4.86 \times 10^{-2}$	$6.63 \times 10^{-4} - 4.98 \times 10^{-2}$	$6.18 \times 10^{-4} - 4.65 \times 10^{-2}$

Of course, it must be realized that the value of v_o represents a rough estimate, so that the value of ϕ calculated above should be viewed as a gross approximation. However, for this exercise, which is meant to compare qualitative characteristics of model simulations with the data, such an approximation is adequate.

In the case of the layered model, diffusion is not assumed to be intraparticle as it was for the spherical model, but rather interparticle. For interparticle diffusion, values of χ of 2-6 have been reported (Cussler, 1984). Thus, a range of D'_e may be calculated by dividing D_o for the various compounds by a factor of 2 to 6. The range of immobile layer half-widths (b) was estimated based on the approximate dimensions of the low permeability layers noted in Freyberg (1986). The fraction of sorption sites adjacent to zones of mobile water (f) was approximated assuming an equal distribution of sorption sites within the mobile and immobile region volumes. Other parameter values are the same as those used with the spherical diffusion model.

As with the spherical diffusion model, it is now possible to calculate first-order rate constants (α') equivalent to the diffusion model rate constants which can be obtained from the Table 5.4 parameter values. The range in the values of α' is due to the range in the values of D'_e and b, with the maximum α' calculated using the maximum value of D'_e and the minimum value of b, and the minimum α' obtained using the minimum D'_e and the maximum b.

Figures 5.12 through 5.15 compare the mass in solution and first spatial moments calculated from the data of the four mobile region solute plumes with the mass in solution and first moments simulated using the first-order rate model equivalent to the layered diffusion model. Also shown are simulations using the local equilibrium model. As in Figures 5.4 through 5.7 depicting the spherical diffusion model, the differences between the nonequilibrium and the equilibrium simulations do not appear significant, though at least for the low rate constant simulations, the salient aspects of the solute behavior (mass loss and deceleration) are seen. The magnitude of the simulated behavior, however, is considerably less than that exhibited by the actual plumes. The insignificance of the effect of the immobile region is largely due to the assumption of the equal distribution of sorption sites between the mobile and immobile water regions. Due to this assumption, the effect of

88

Figure 5.12. Comparison of the bromide mobile region plume: a) Mass in
solution, and b) First spatial moment, estimated from syn-
optic data and simulated using an equilibrium and a first-
order rate model equivalent to a layered diffusion model.

Figure 5.13. Comparison of the bromoform mobile region plume: a) Mass in solution, and b) First spatial moment, estimated from synoptic data and simulated using an equilibrium and a first-order rate model equivalent to a layered diffusion model.

Figure 5.14. Comparison of the carbon tetrachloride mobile region plume:
a) Mass in solution and b) First spatial moment, estimated
from synoptic data and simulated using an equilibrium and
a first-order rate model equivalent to a layered diffusion
model.

91

Figure 5.15. Comparison of the tetrachloroethylene mobile region plume:
a) Mass in solution and b) First spatial moment, estimated
from synoptic data and simulated using an equilibrium and
a first-order rate model equivalent to a layered diffusion
model.

the immobile region on solute transport is limited, since relatively little solute is associated with the immobile regions. Figures 5.16 through 5.19 demonstrate the impact of decreasing the value of f, thus implying that more sorption sites are within regions of low permeability. The assumption that low permeability regions, perhaps made up of silty material, have a higher sorption capacity is not unreasonable, though at the Borden site, there is no evidence correlating low hydraulic conductivity with high distribution coefficients (Durant, 1986).

As Figures 5.16 through 5.19 show (using a value of f = 0.4 and a value of the rate constant based on average values of D_e' and b), the main characteristics of the data can be simulated, again with the exception of the decrease in bromoform mass (Figure 5.17), which is attributed to transformation.

If diffusion into low permeability lenses is occurring, and if advective transport through the lenses is faster than diffusive transport into and out of the lenses, then advective transport would dominate and the effect of diffusion into the lenses would be minor.

The concept of comparing advective and diffusive rates, introduced in Chapter 3, may be used to determine the relative importance of advective and diffusive transport into low permeability lenses. Assume lenses that are 0.06 m thick (b = 0.03 m), with hydraulic conductivity two orders of magnitude less than the hydraulic conductivity of the "mobile" regions. Therefore:

$$v_{lens} = \frac{v_m}{100} = 9.1 \times 10^{-4} \text{ m/d}$$

and the advective rate constant for tetrachloroethylene transport in the lenses would be:

$$\frac{v_{lens}}{2b\,R_{im}} = \frac{(9.1 \times 10^{-4} \text{ m/d})}{2(0.03 \text{ m})(12.5)} = 1.21 \times 10^{-3} \text{ d}^{-1}$$

The diffusive rate constant would be:

$$a = \frac{3D_e'}{R_{im}b^2} = \frac{3(1.71 \times 10^{-5} \text{ m}^2/\text{d})}{(12.5)(0.03 \text{ m})^2} = 4.56 \times 10^{-3} \text{ d}^{-1}$$

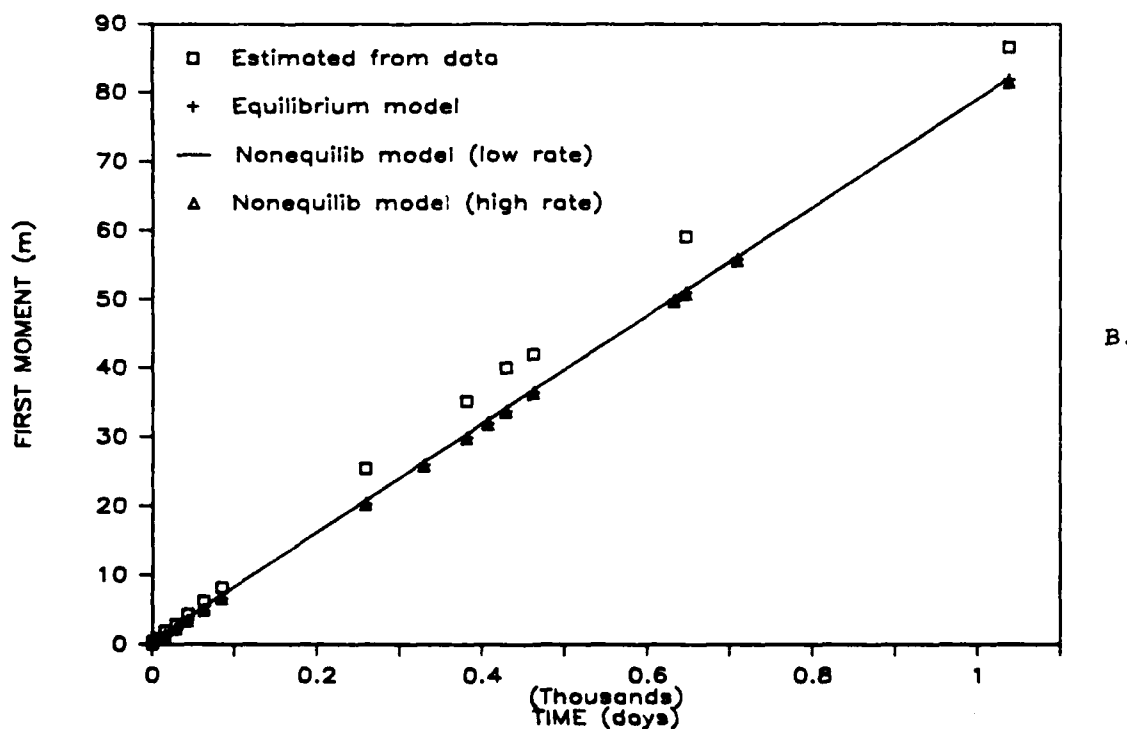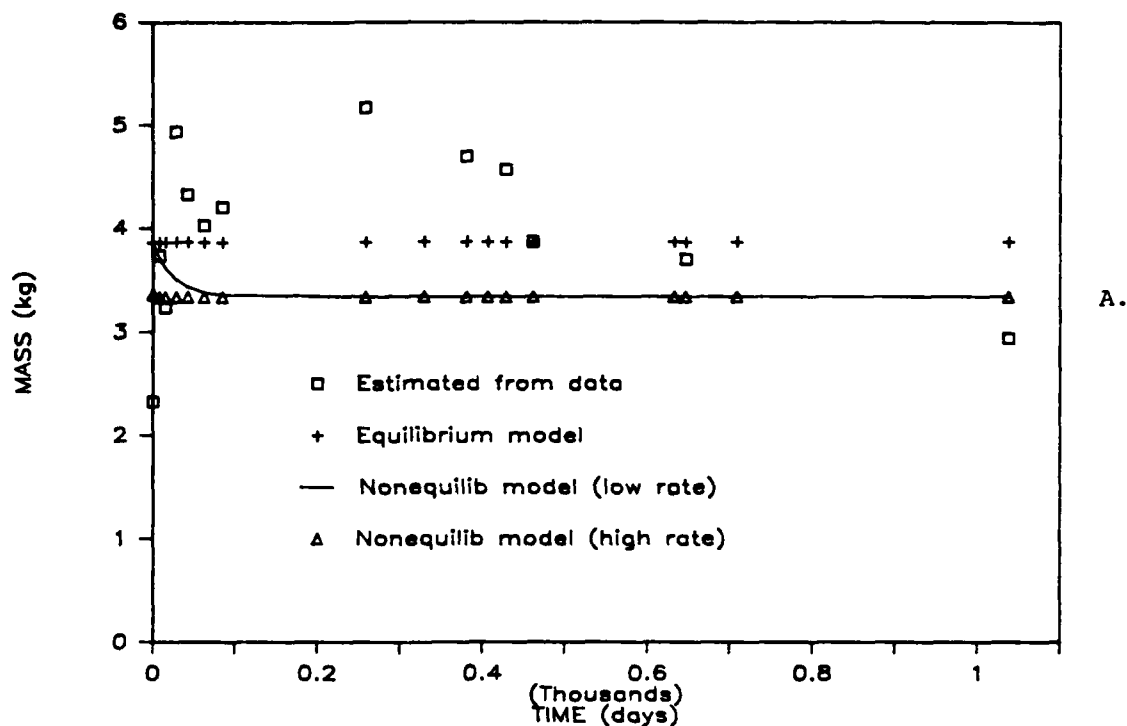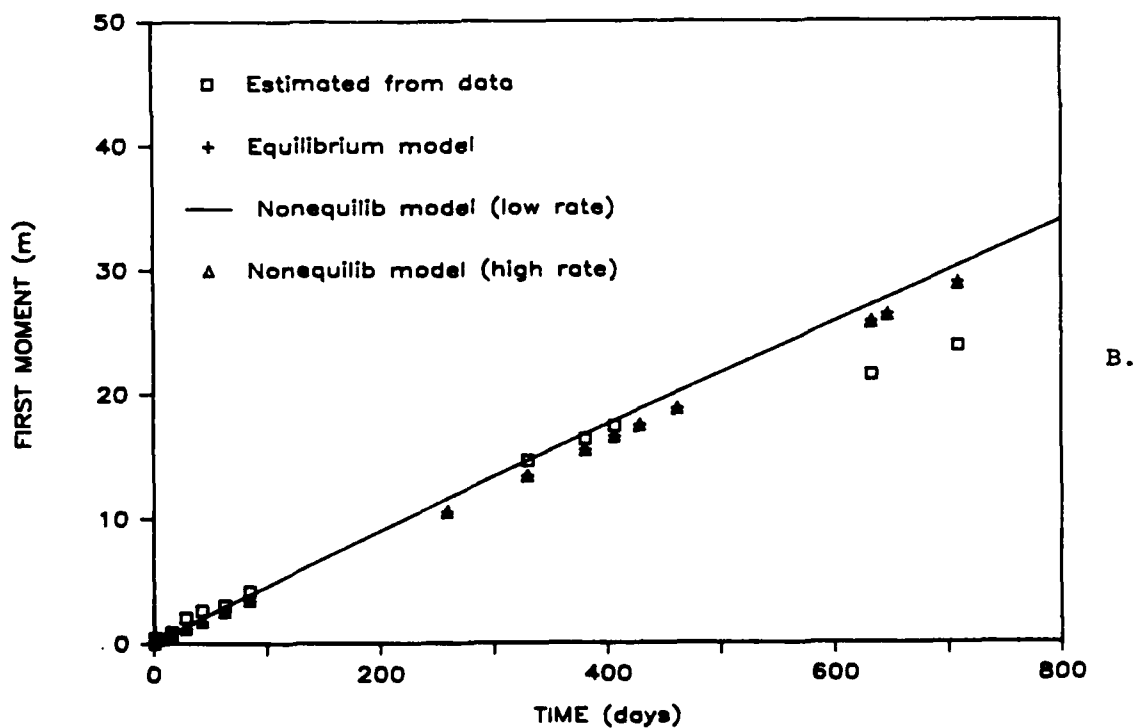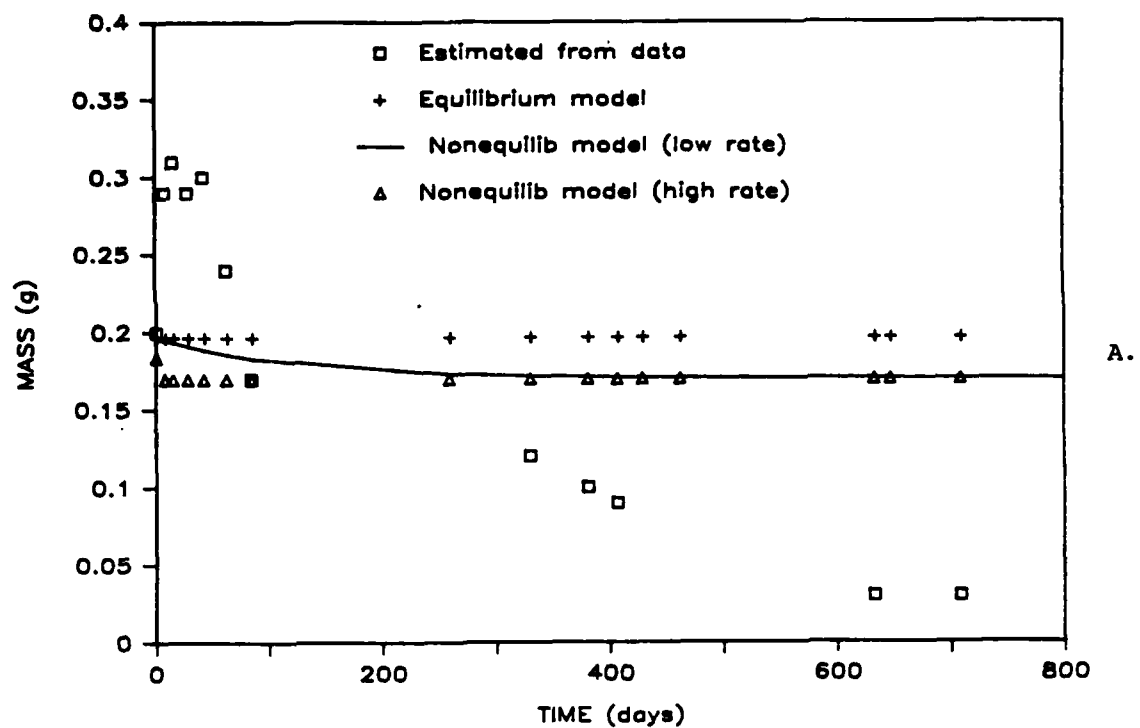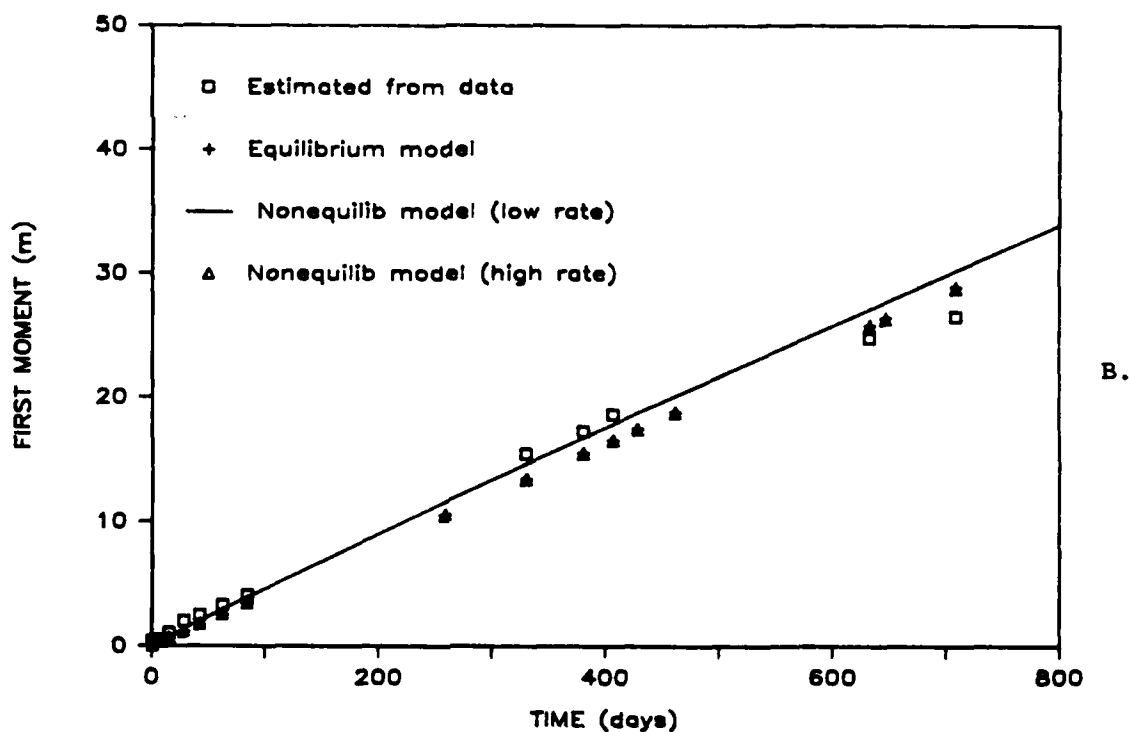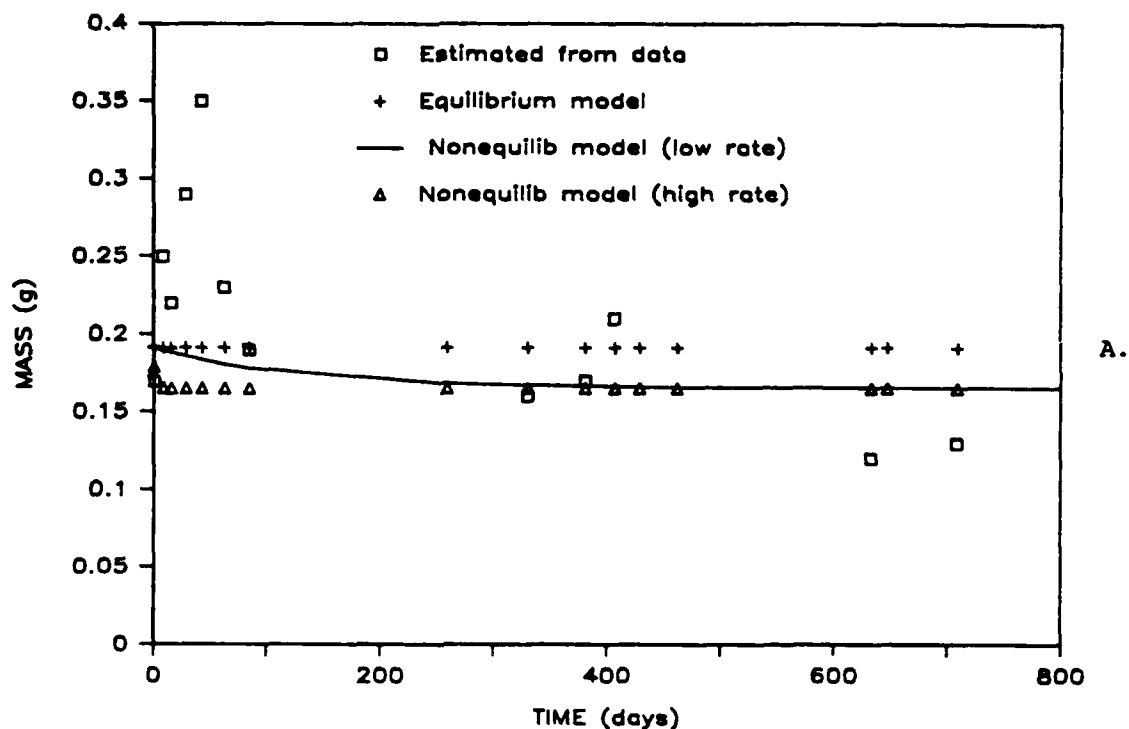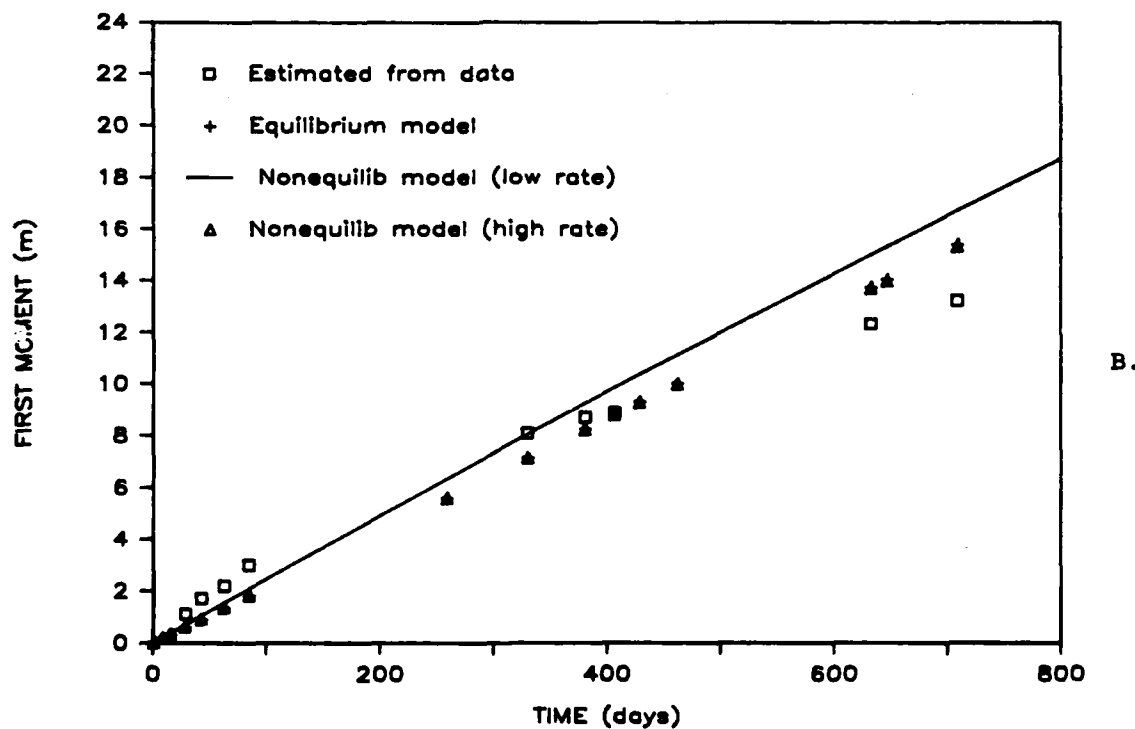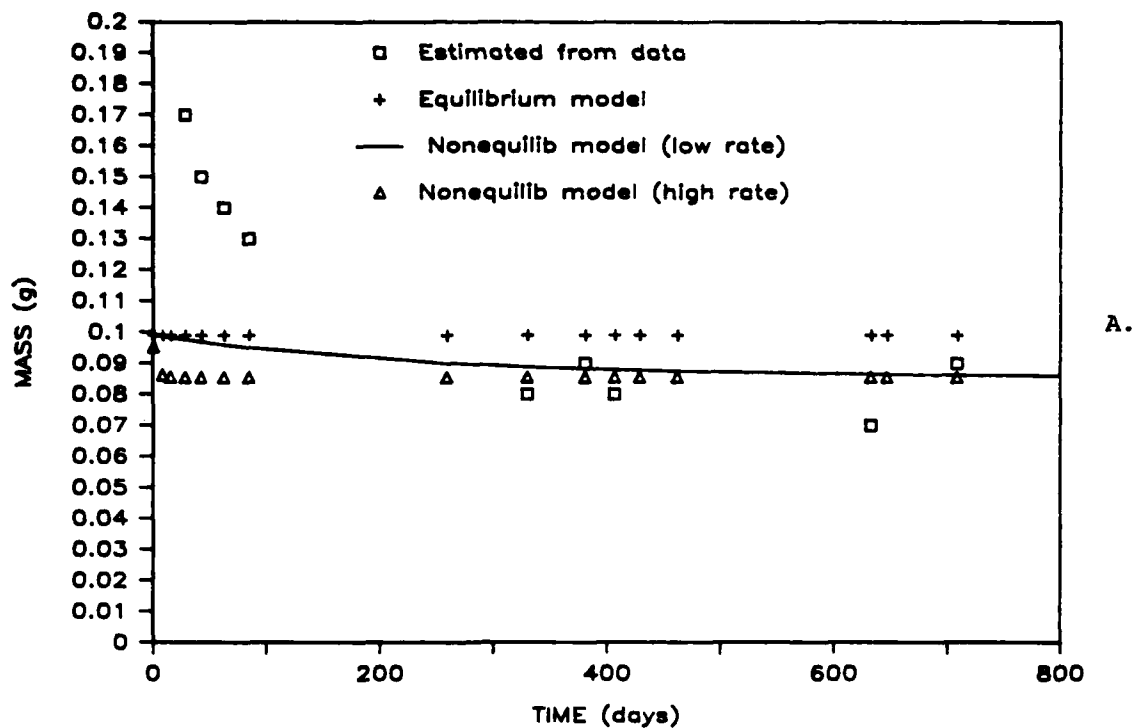using $\chi = 4$ to calculate D_e' from D_o.

93

Figure 5.16. Comparison of the bromide mobile region plume: a) Mass in solution, and b) First spatial moment, estimated from synoptic data and simulated using a first-order rate model equivalent to a layered diffusion model, with high sorption capacity within the immobile regions (f = 0.4).

94

A.

B.
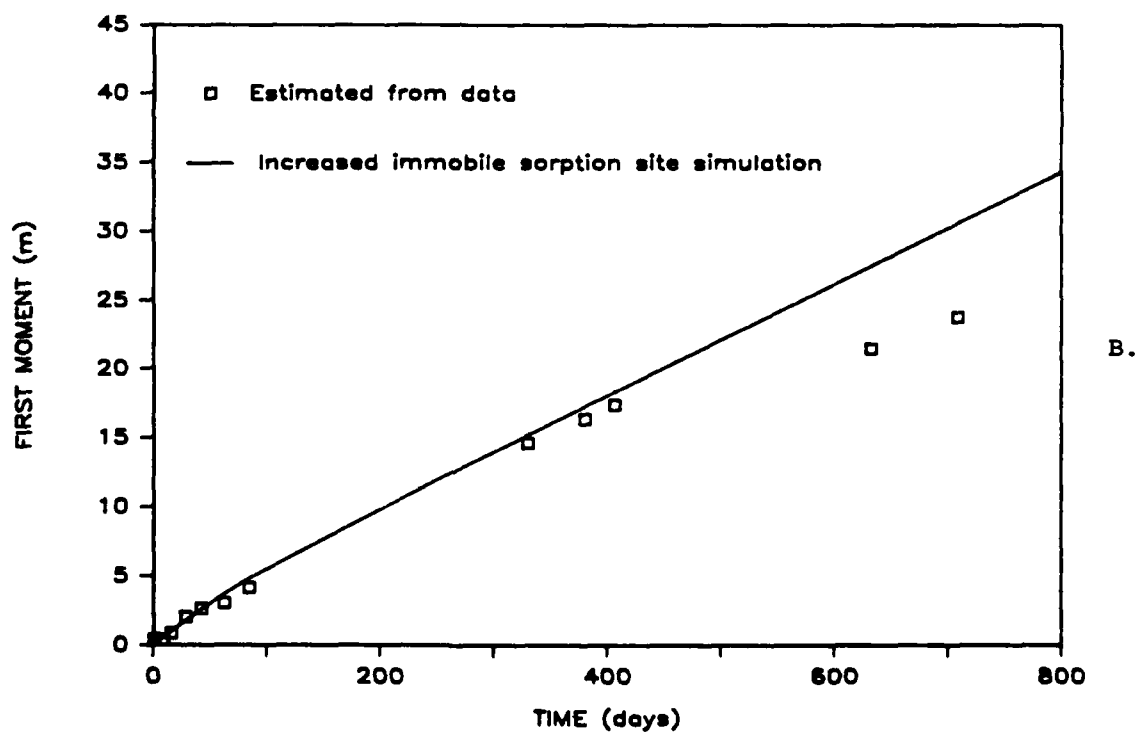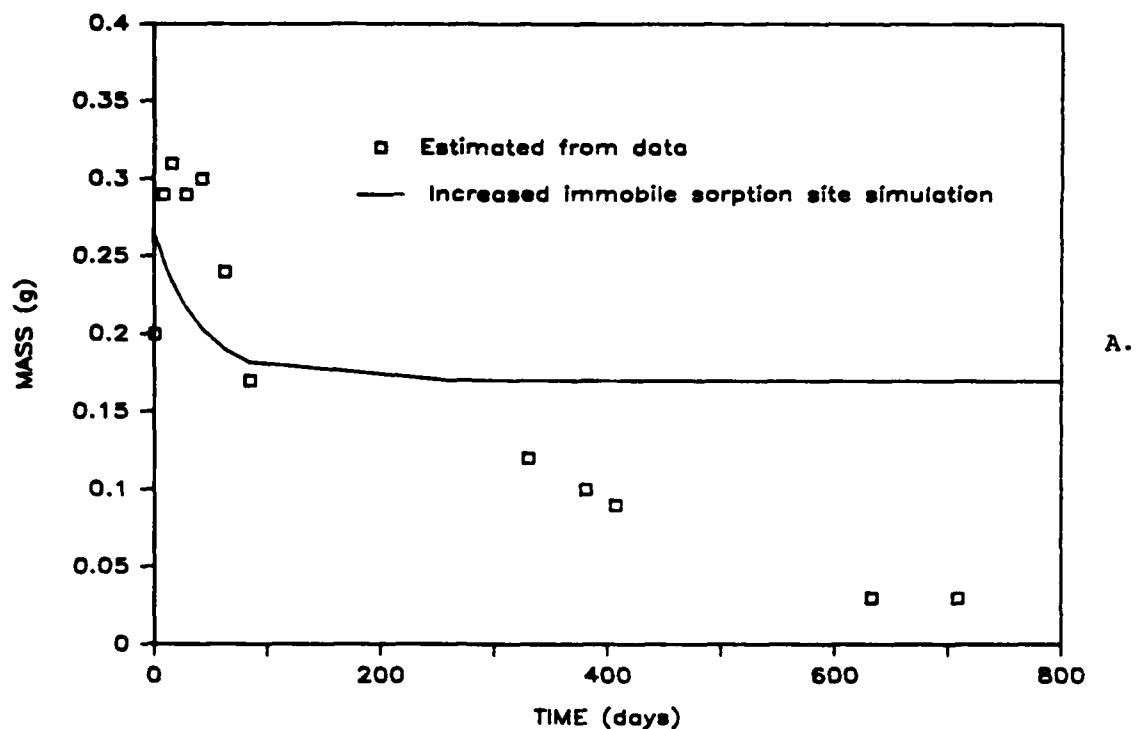
Figure 5.17. Comparison of the bromoform mobile region plume: a) Mass
            in solution, and b) First spatial moment, estimated from
            synoptic data and simulated using a first-order rate model
            equivalent to a layered diffusion model, with high sorp-
            tion capacity within the immobile regions (f = 0.4).

95

Figure 5.18. Comparison of the carbon tetrachloride mobile region plume:
a) Mass in solution, and b) First spatial moment, estimated
from synoptic data and simulated using a first-order rate
model equivalent to a layered diffusion model, with high
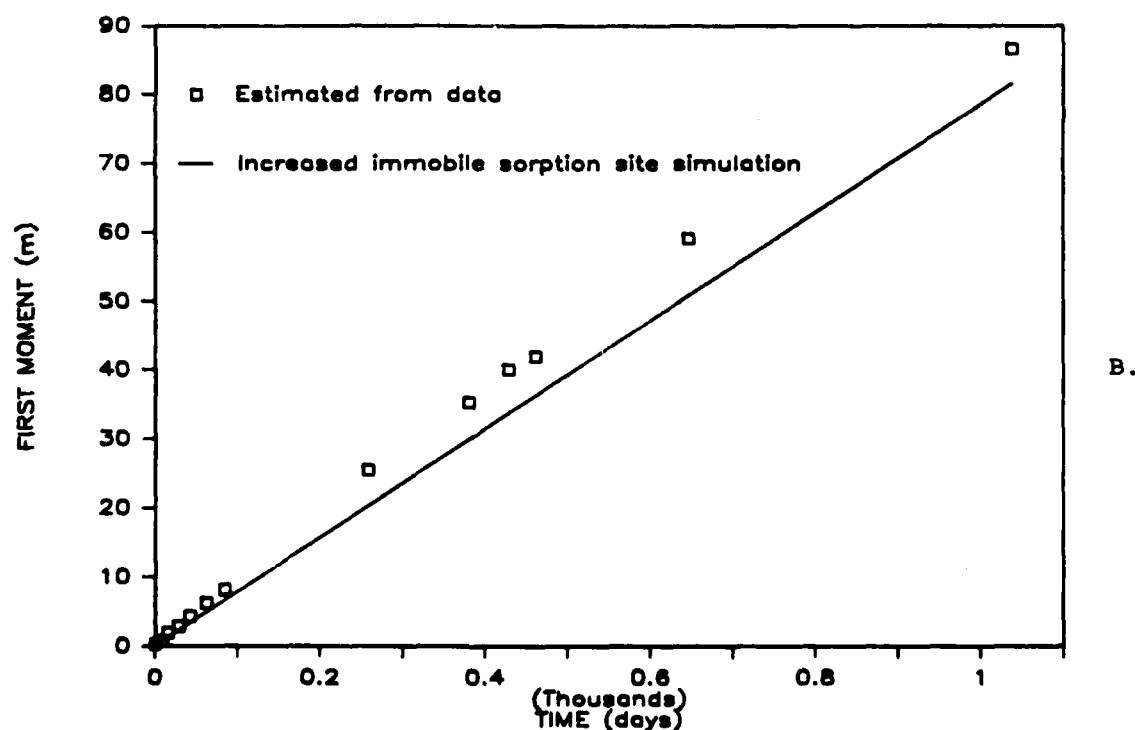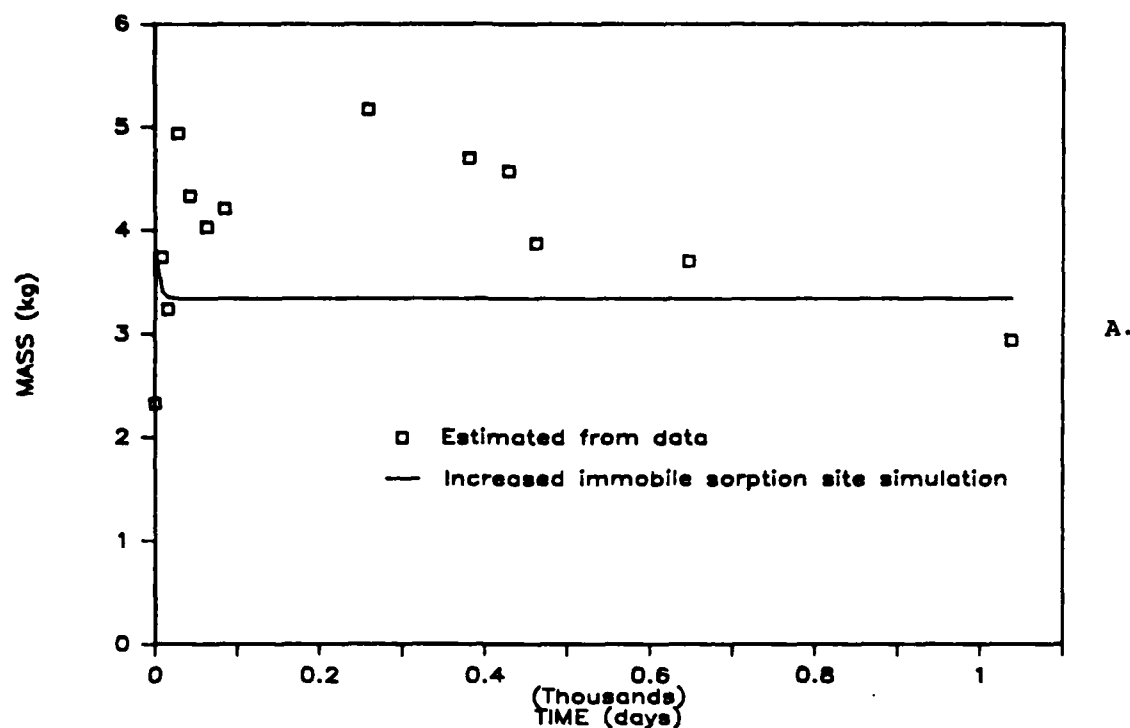sorption capacity within the immobile regions (f = 0.4).

96

Figure 5.19. Comparison of the tetrachloroethylene mobile region plume:
a) Mass in solution, and b) First spatial moment, estimated
from synoptic data and simulated using a first-order rate
model equivalent to a layered diffusion model, with high
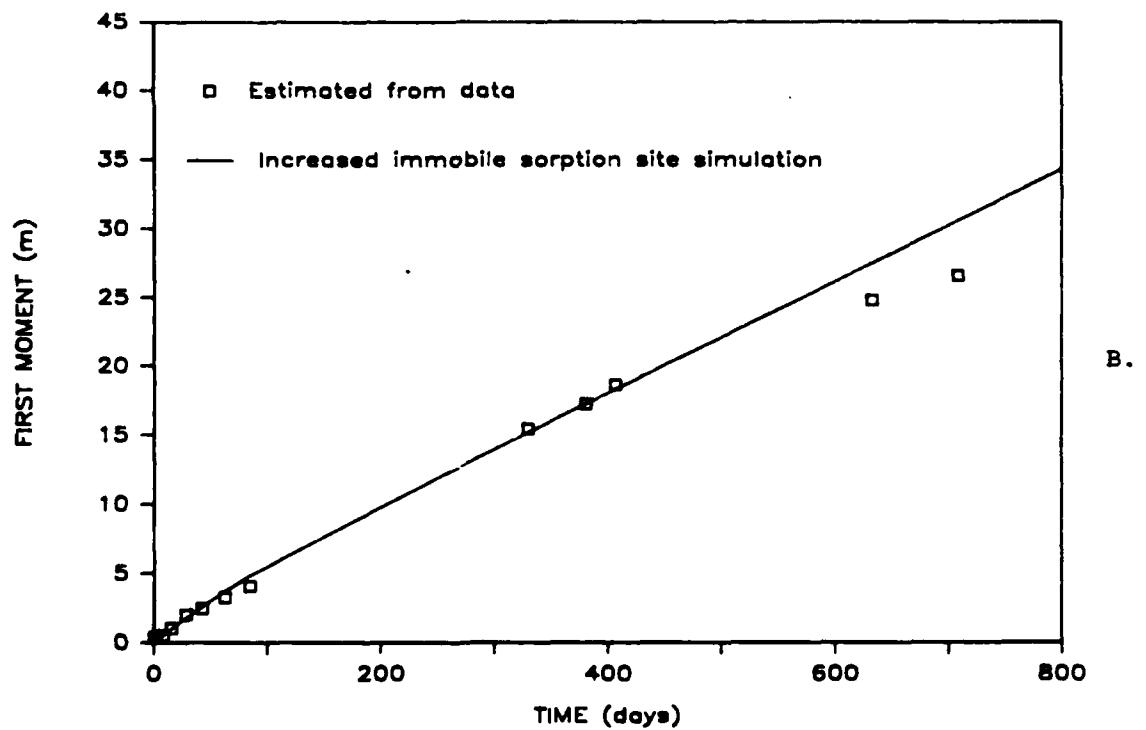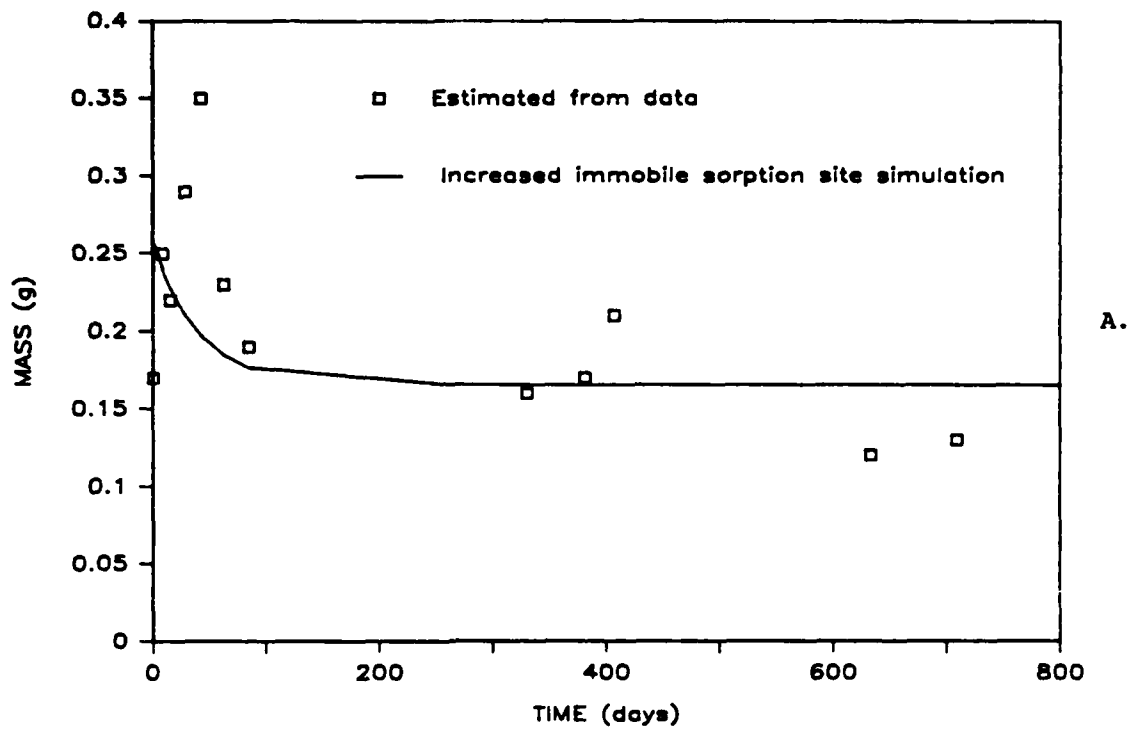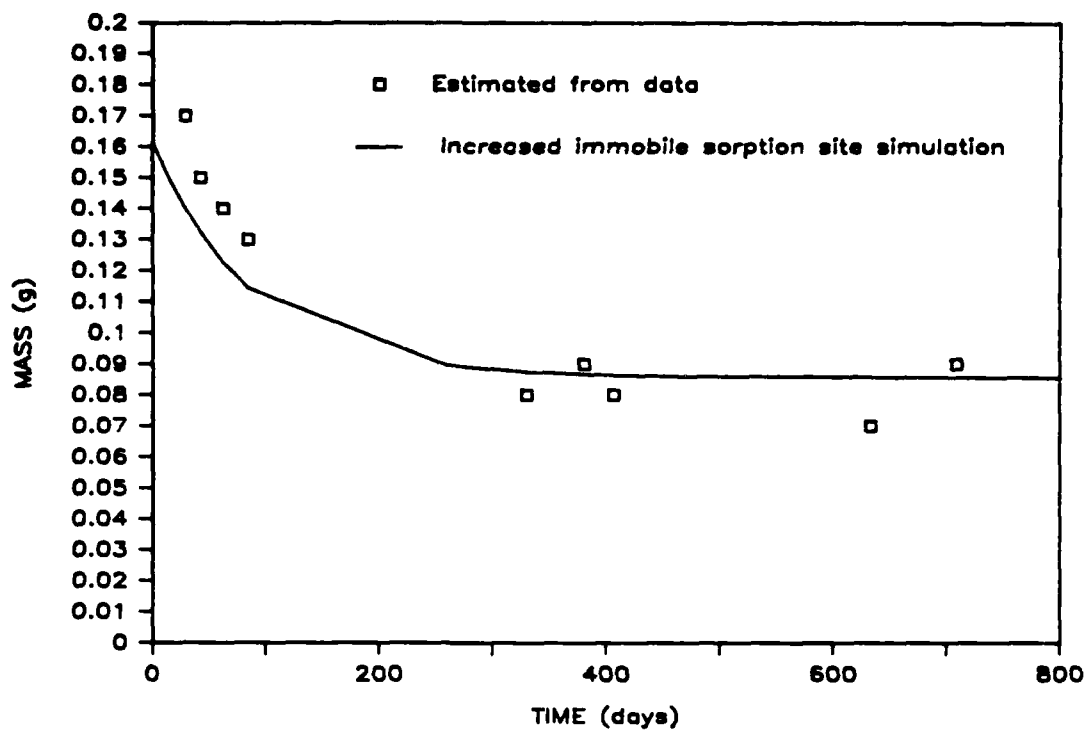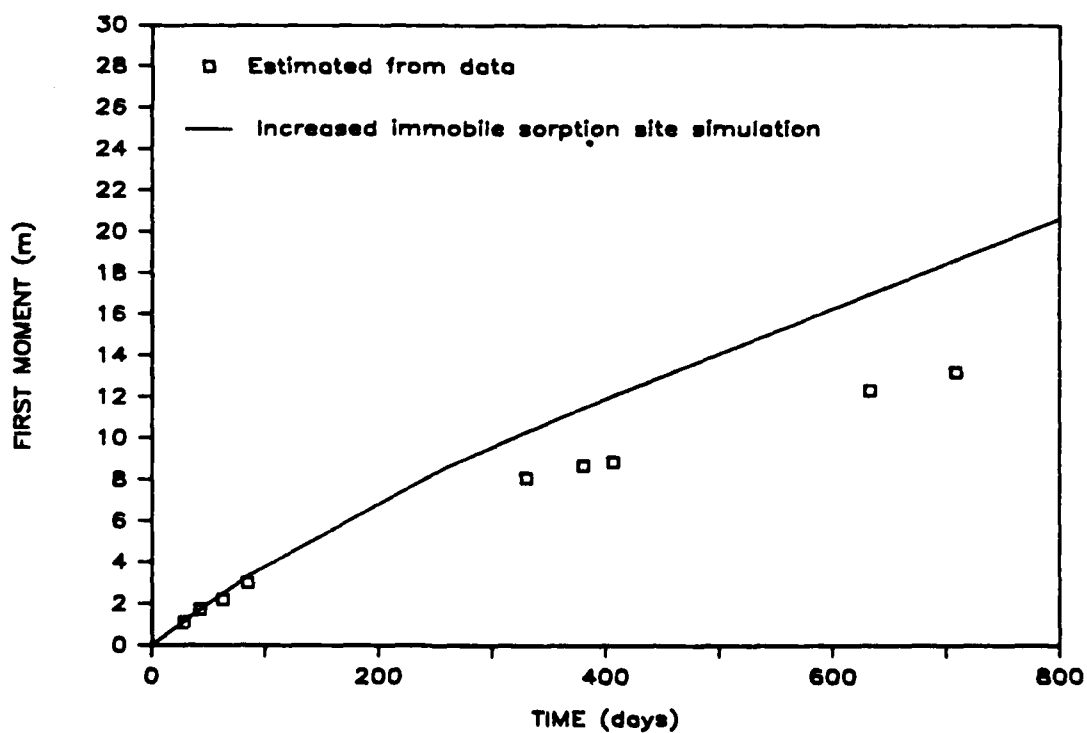sorption capacity within the immobile regions (f = 0.4).

Comparing the two rate constants, it is seen that for the assumed parameter values, the diffusive rate constant is nearly four times greater than the advective rate constant. This indicates that for reasonable assumptions regarding lens characteristics (b $\geq$ 0.03 m; lens hydraulic conductivity $\leq$ 0.01 mobile region hydraulic conductivity), the effect of diffusive transport would dominate the effect of advective transport within the lenses. As the ratio of advective to diffusive rate constants is independent of R_{im}, the dominance of diffusive transport applies for all the compounds, since of all the solutes, tetrachloroethylene has the lowest estimated value of D_e'.

Temporal Data Simulation

Another way of demonstrating the complementarity of spatial and temporal transport behavior is to use the model parameters obtained in the preceding analysis of the zeroth and first spatial moments to simulate temporal responses. The following discussion will use parameters obtained assuming that layered diffusion dominates transport (Table 5.4 with f = 0.40), although either the layered or spherical diffusion model assumptions could have been used for this exercise.

Values for longitudinal and transverse dispersion coefficients and initial plume dimensions must be determined for use as model input parameters. These parameters may be estimated from the second spatial moment data. Figures 5.20 through 5.27 show σ_{xx}^2 and σ_{yy}^2, the principal values of the spatial covariance tensor, calculated for the four solutes at each synoptic sampling time. Figures 5.20a through 5.27a compare simulations of the local equilibrium model with principal values of the covariance tensor. The values of the longitudinal and transverse dispersion coefficients (D_x' and D_y') and the initial plume length and width (2L and 2M) were chosen to provide simultaneously a visual best fit to the eight data sets. The other parameter values used in the equilibrium model (v_o, K_d, ρ and θ) were obtained in the preceding section. Similarly, Figures 5.20b through 5.27b compare the second spatial moment data with simulations of the first-order rate model. Recall that the first-order rate constant used in the model was calculated to be equivalent to the layered diffusion model rate parameter. As with the local equilibrium model, the longitudinal and transverse dispersion coefficients in the mobile region (D_{mx} and D_{my}) and the initial plume dimensions (2L and

98
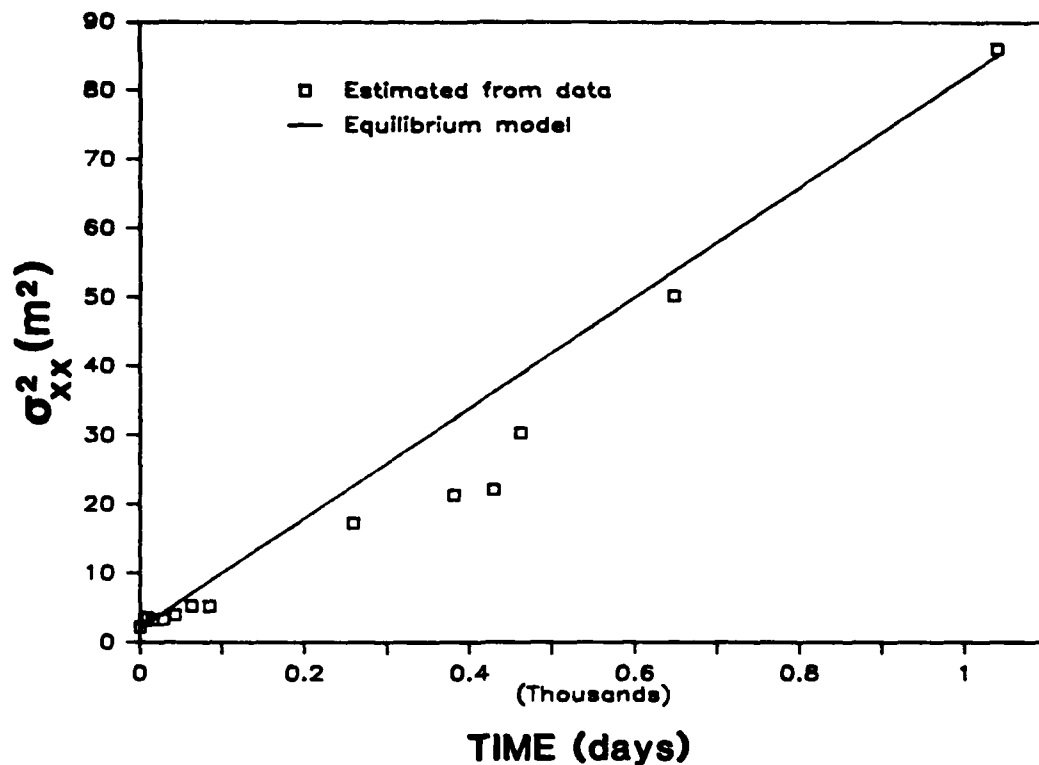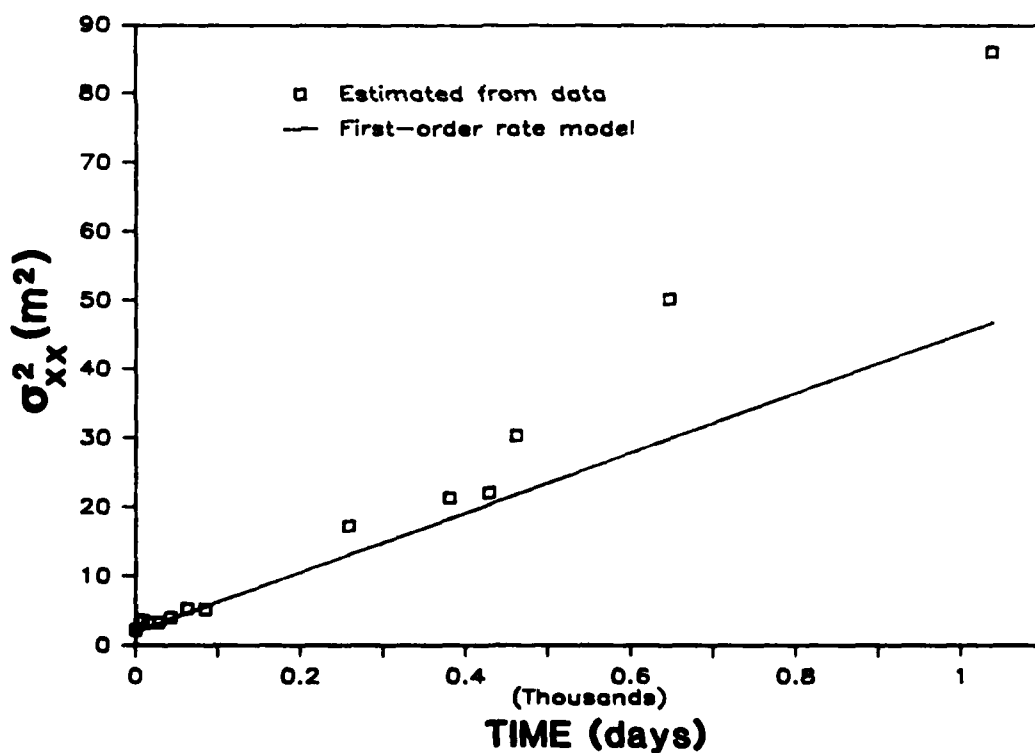
Figure 5.20. Comparison of the bromide mobile region plume principal component of the spatial covariance tensor in the longitudinal direction (σ_{xx}^2) estimated from the synoptic data and simulated by fitting the a) Equilibrium model, and b) First-order rate model to the estimates.
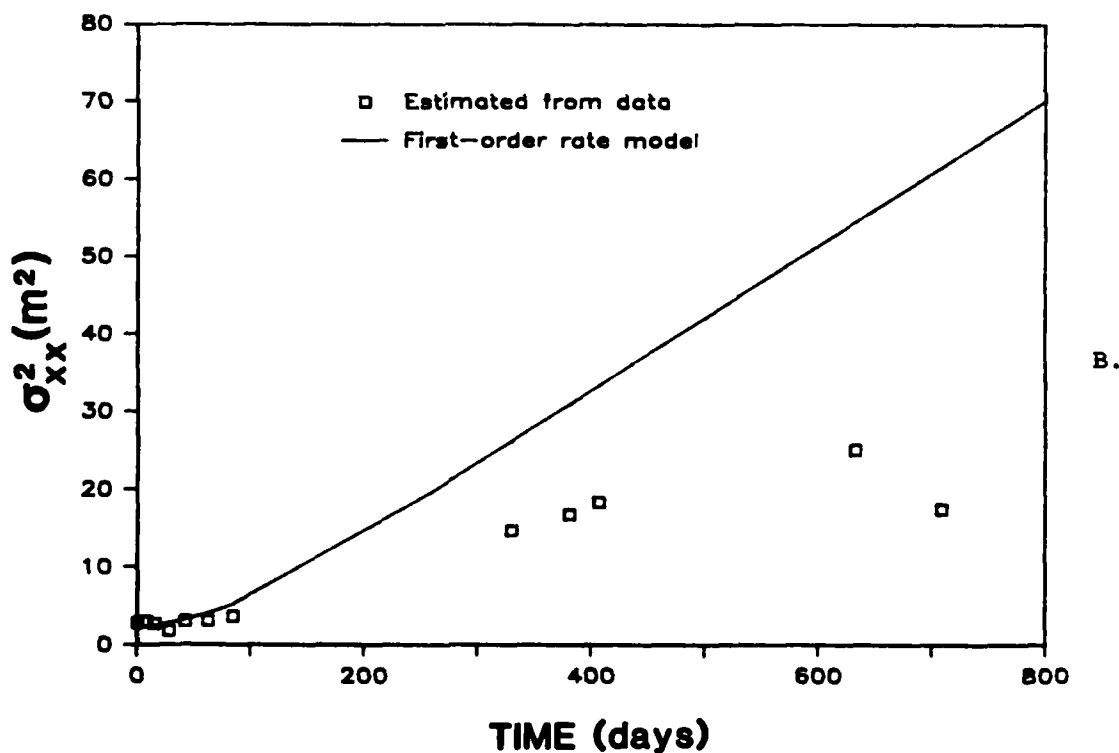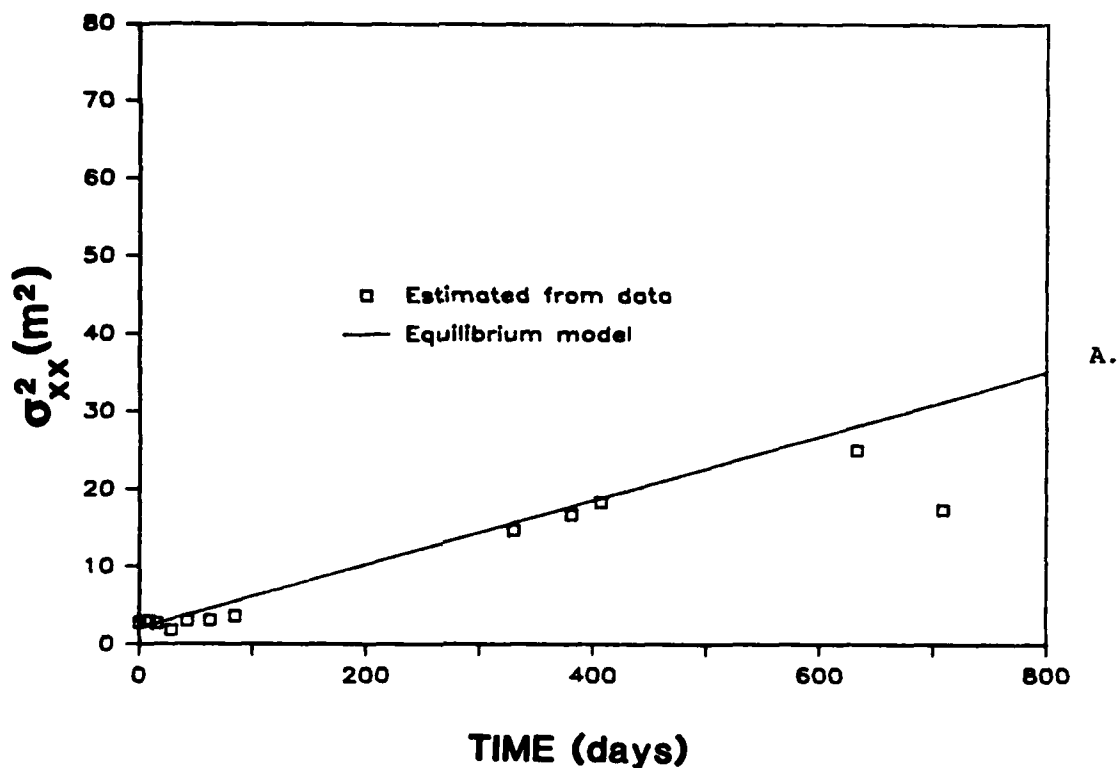
Figure 5.21. Comparison of the bromoform mobile region plume principal component of the spatial covariance tensor in the longitudinal direction (σ^2_{xx}) estimated from the synoptic data and simulated by fitting the a) Equilibrium model, and b) First-order rate model to the estimates.
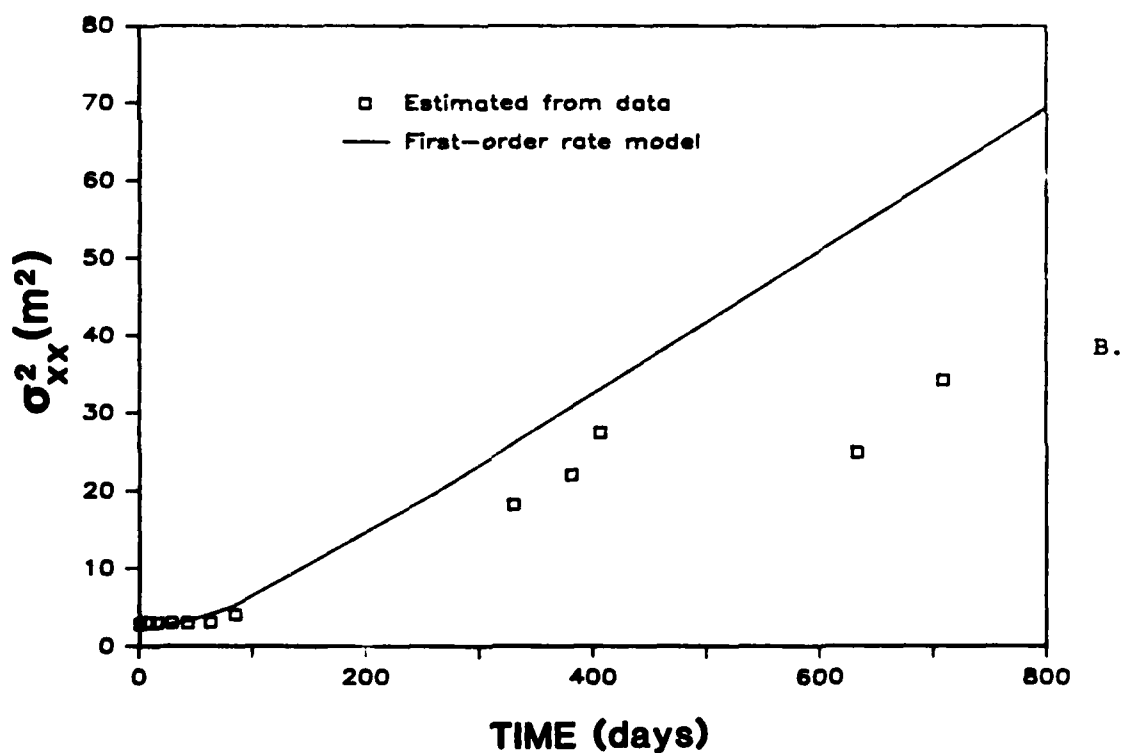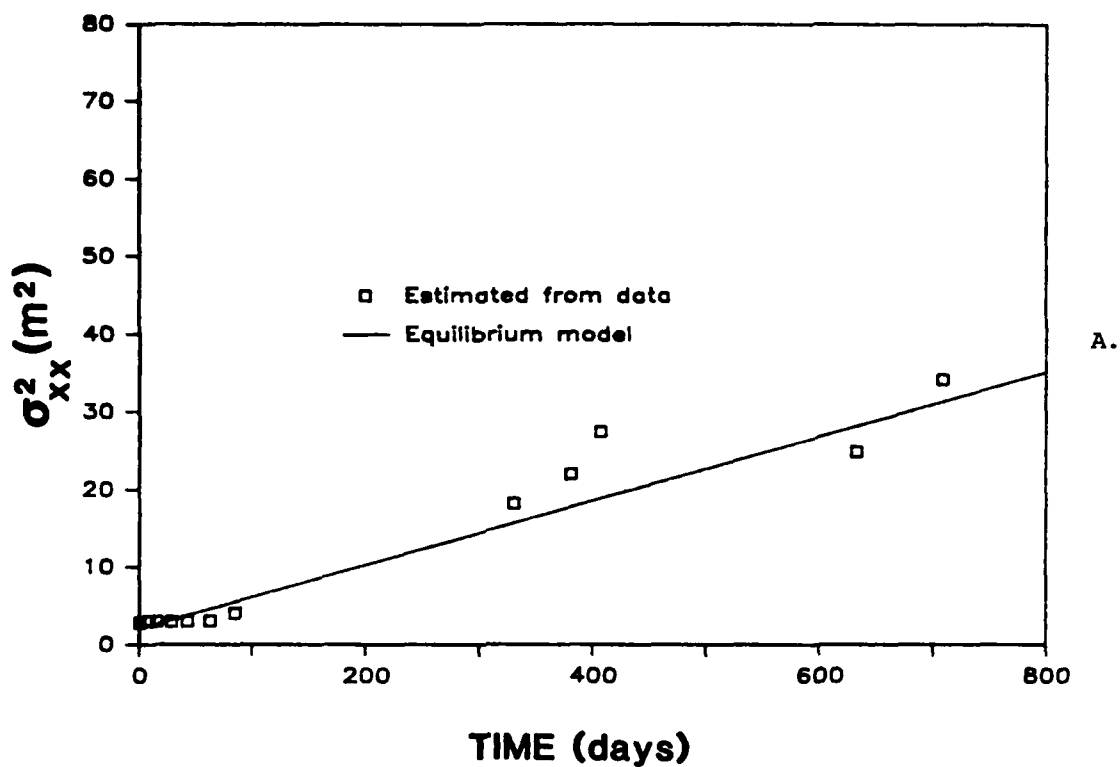
Figure 5.22. Comparison of the carbon tetrachloride mobile region plume principal component of the spatial covariance tensor in the longitudinal direction (σ^2_{xx}) estimated from the synoptic data and simulated by fitting the a) Equilibrium model, and b) First-order rate model to the estimates.
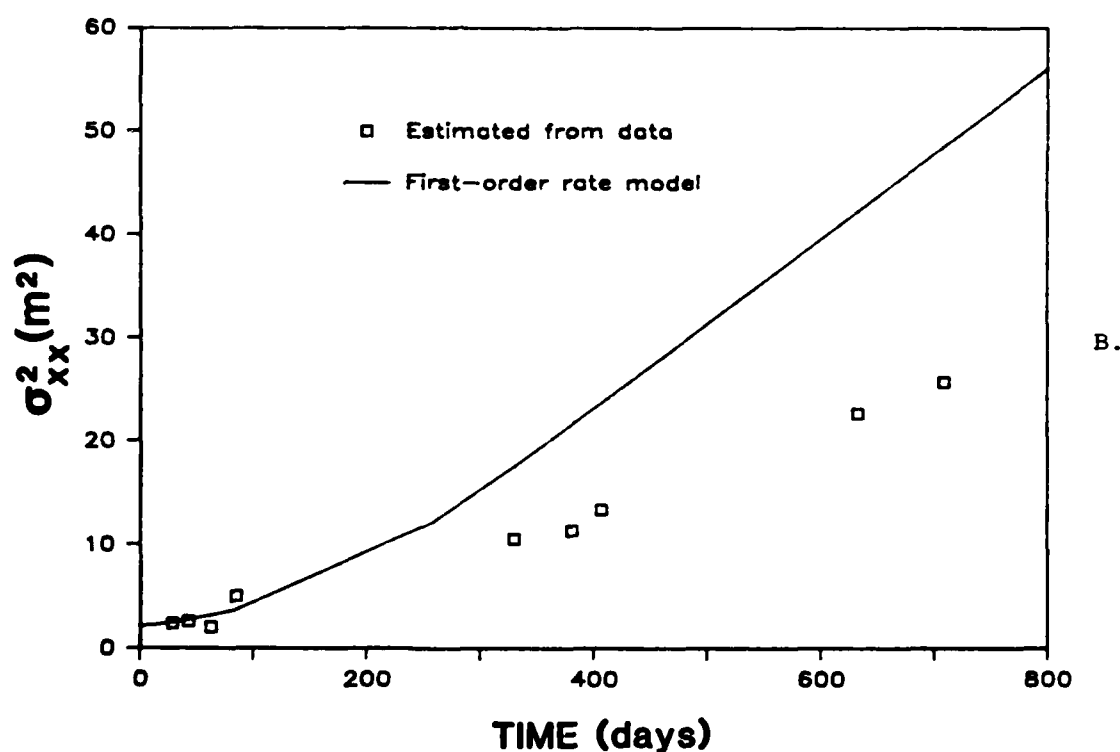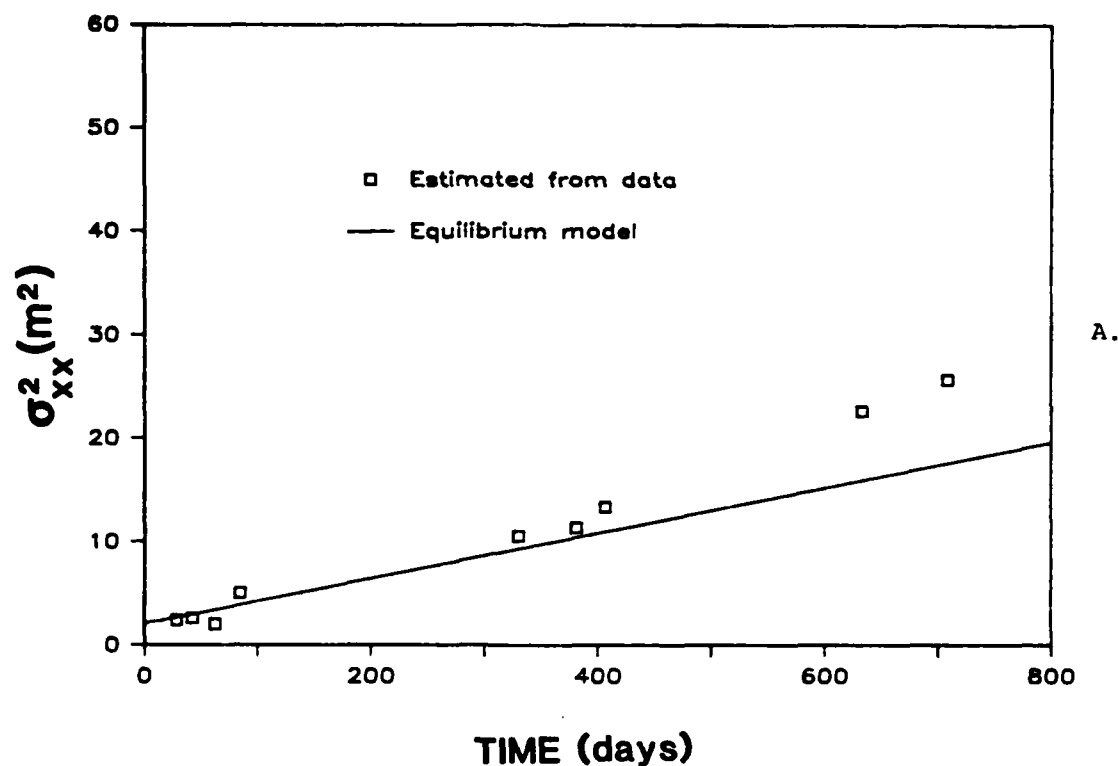
Figure 5.23. Comparison of the tetrachloroethylene mobile region plume principal component of the spatial covariance tensor in the longitudinal direction (σ^2_{xx}) estimated from the synoptic data and simulated by fitting the a) Equilibrium model, and b) First-order rate model to the estimates.
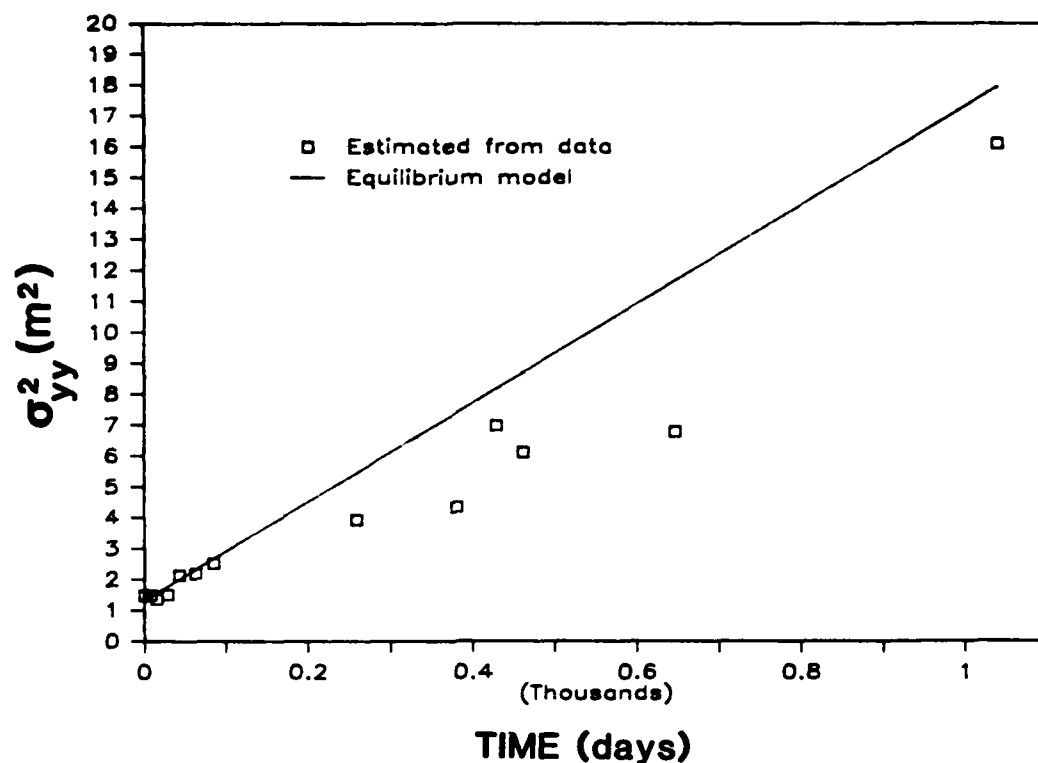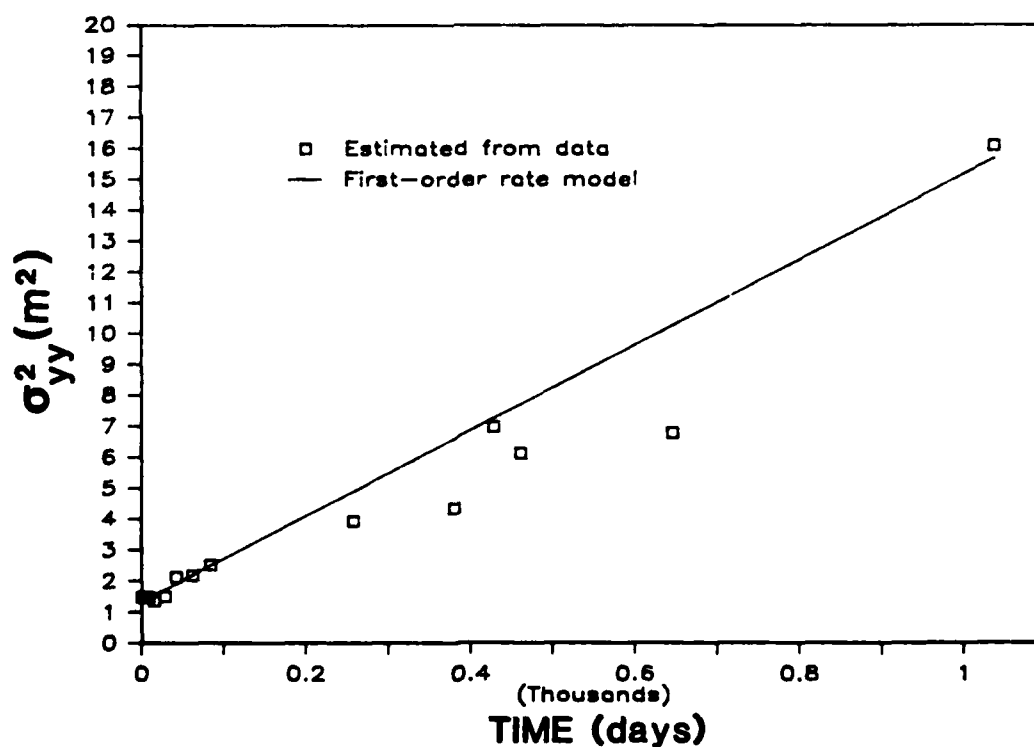
Figure 5.24. Comparison of the bromide mobile region plume principal component of the spatial covariance tensor in the transverse direction (σ_{yy}^2) estimated from the synoptic data and simulated by fitting the a) Equilibrium model, and b) First-order rate model to the estimates.
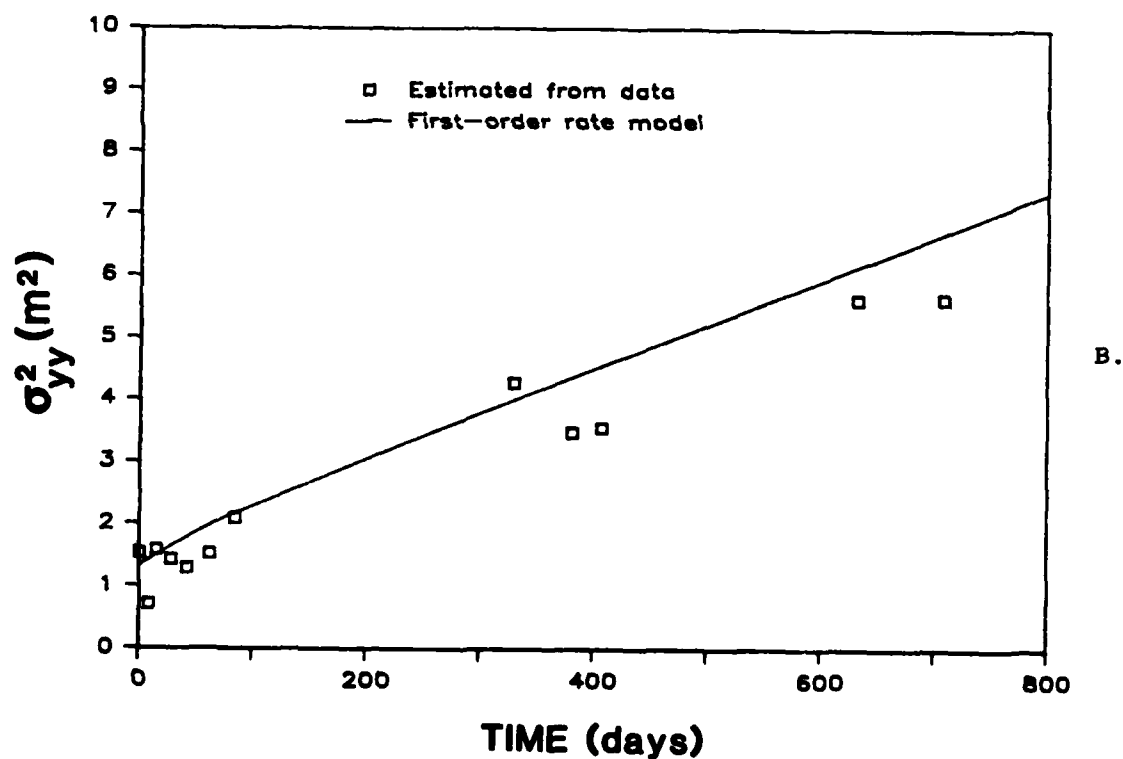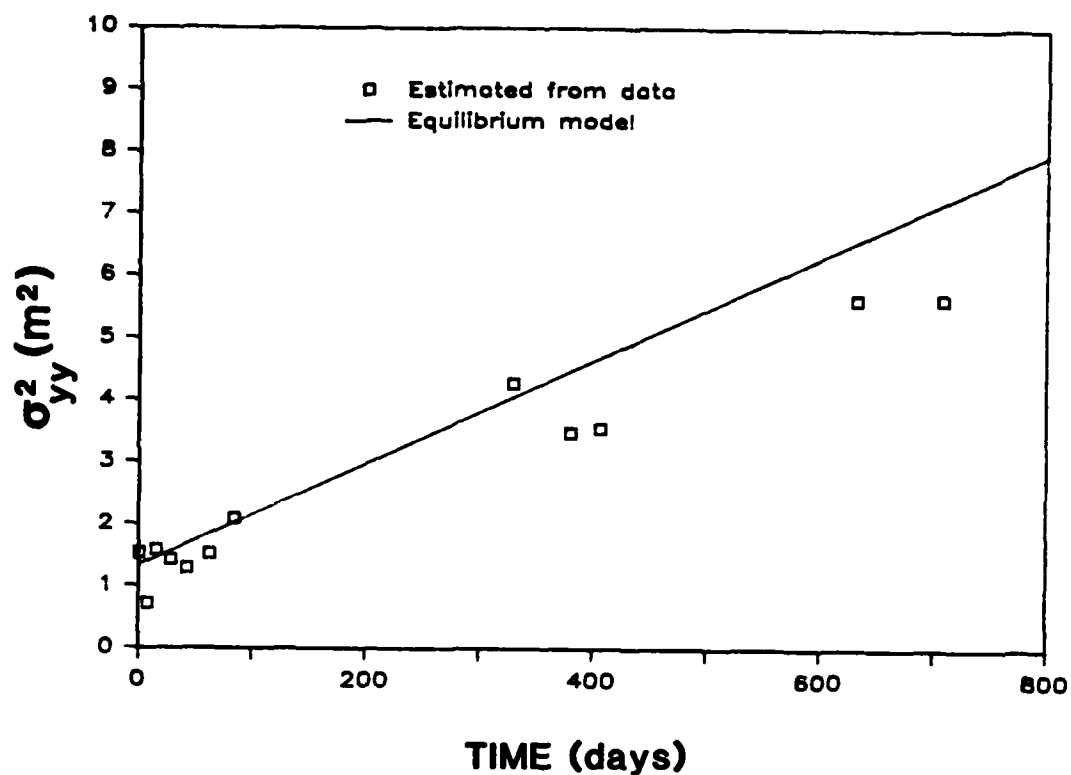
Figure 5.25. Comparison of the bromoform mobile region plume principal component of the spatial covariance tensor in the transverse direction (σ^2_{yy}) estimated from the synoptic data and simulated by fitting the a) Equilibrium model, and b) First-order rate model to the estimates.
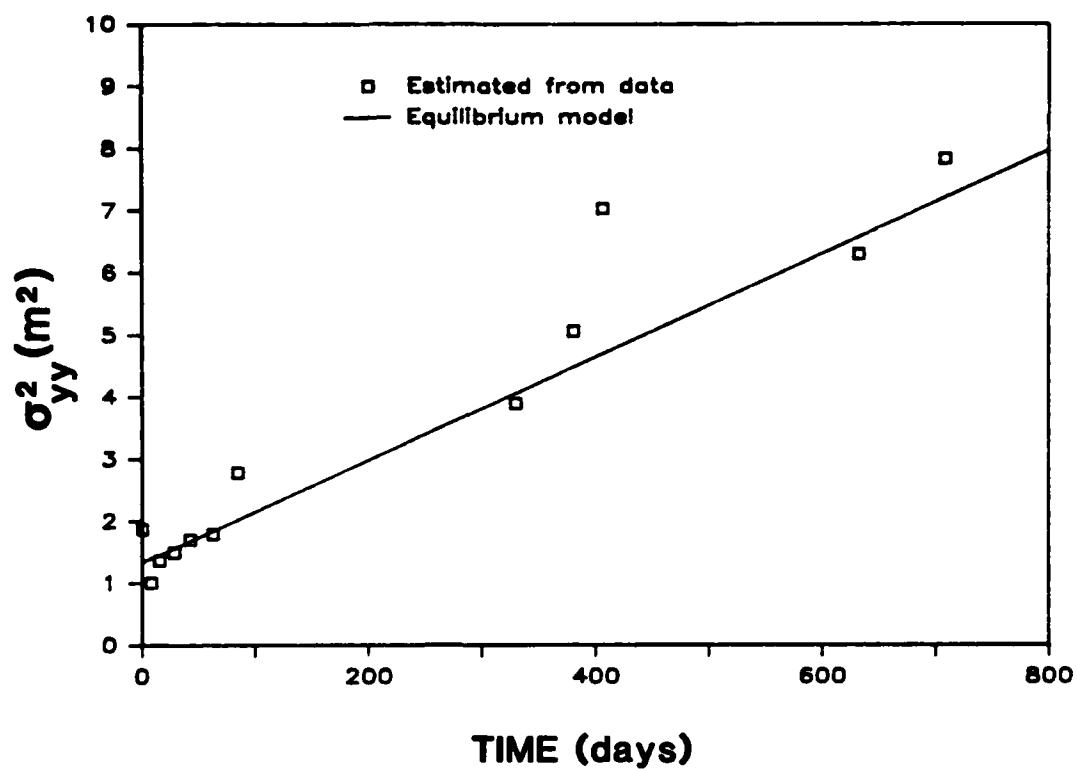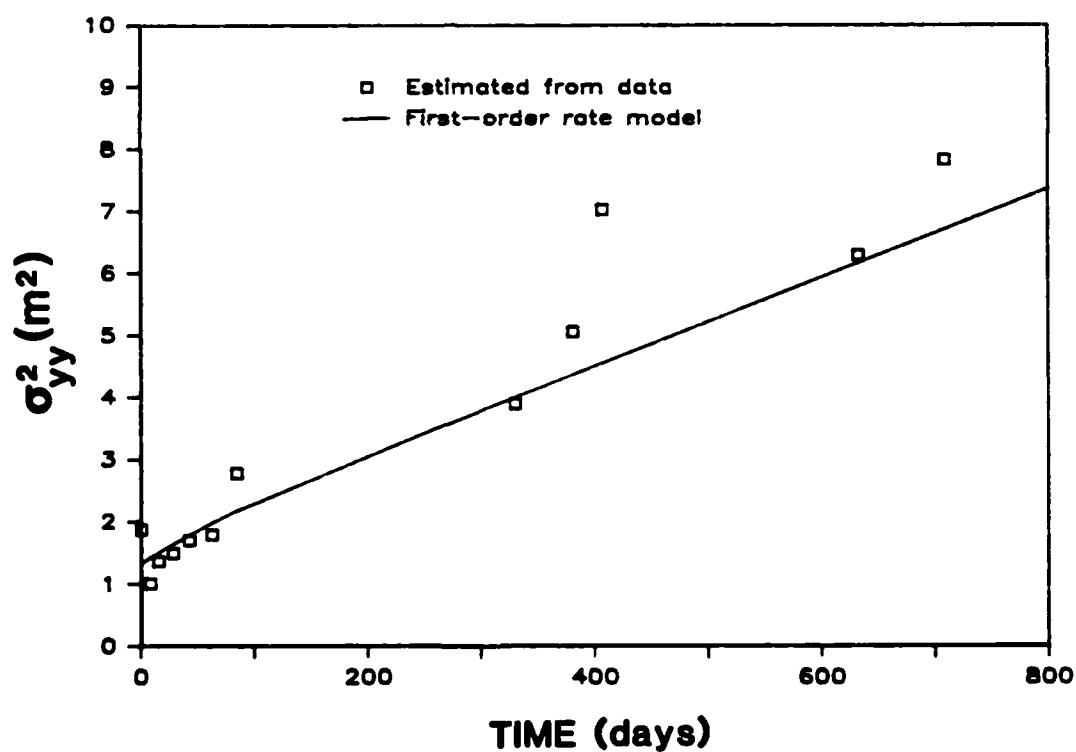
Figure 5.26. Comparison of the carbon tetrachloride mobile region plume principal component of the spatial covariance tensor in the transverse direction (σ_{yy}^2) estimated from the synoptic data and simulated by fitting the a) Equilibrium model, and b) First-order rate model to the estimates.

105
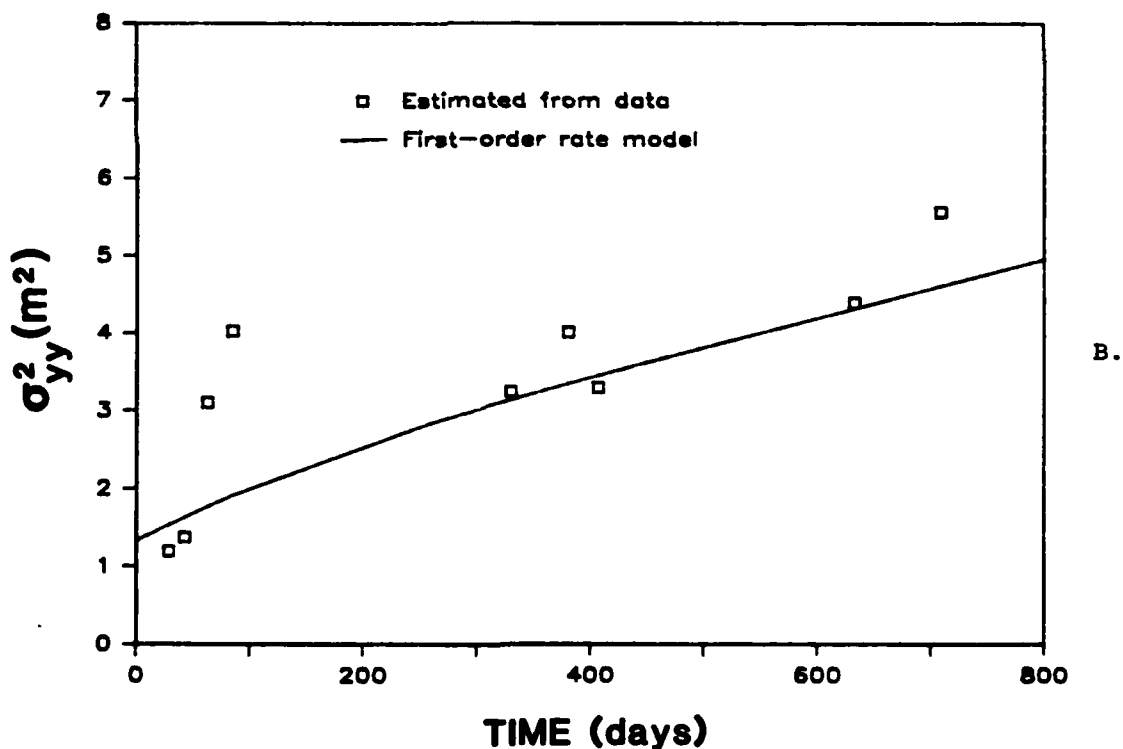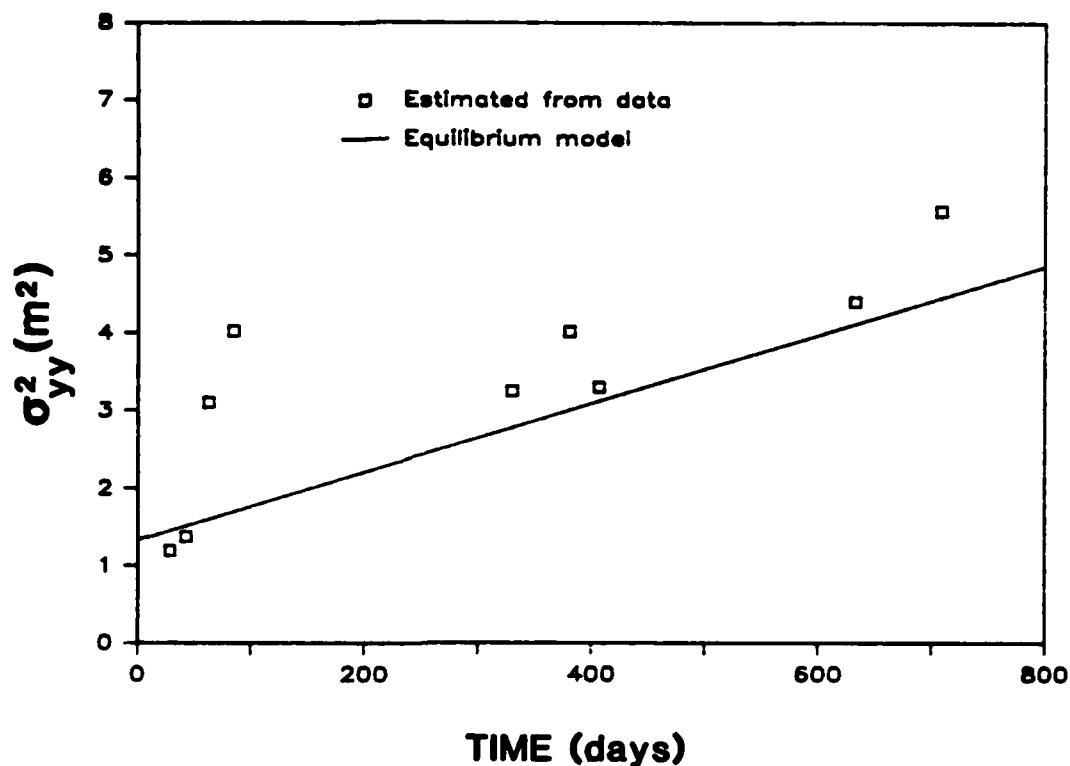
Figure 5.27. Comparison of the tetrachloroethylene mobile region plume principal component of the spatial covariance tensor in the transverse direction (σ^2_{yy}) estimated from the synoptic data and simulated by fitting the a) Equilibrium model, and b) First-order rate model to the estimates.

2M) were adjusted to obtain simultaneously a visual best fit to the eight data sets being considered. Other parameters used in the model were obtained in the previous section (Table 5.4). A value of f = 0.4 was used to test whether parameters which have been shown to simulate the spatial behavior can also simulate the temporal behavior. Table 5.5 lists the values for the dispersion coefficients and the initial plume dimensions which will be used in the following analysis of the temporal behavior.

TABLE 5.5

VALUES FOR DISPERSION COEFFICIENTS AND INITIAL PLUME
DIMENSIONS OBTAINED FROM SPATIAL SECOND MOMENT DATA

Local Equilibrium Model	$D'_x = 0.04$ m^2/d
	$D'_y = 0.008$ m^2/d
	L = 2.5 m
	M = 2.0 m
First-Order Rate Model[*]	
	$D_{mx} = 0.02$ m^2/d
	$D_{my} = 0.008$ m^2/d
	L = 2.5 m
	M = 2.0 m

[*]Equivalent to layered diffusion model.

Using the parameter values in Tables 5.4 and 5.5, it is possible to simulate both the temporal moments and the measured temporal responses at particular sampling wells. Figures 5.28 through 5.31 compare zeroth and first temporal moments estimated from the data with predictions of equilibrium and nonequilibrium models. Moment estimates were obtained by numerically evaluating the breakthrough response data at the various sampling wells, depicted in Appendix E, using the formulae:

$$m_{o,t} = \sum_{j=1}^{n} C_j (t_j - t_{j-1})$$

$$\mu'_{1,t} = \frac{\sum_{j=1}^{n} C_j t_j (t_j - t_{j-1})}{m_{o,t}}$$

(5-3)

where C_j = the normalized concentration measured at time t_j.
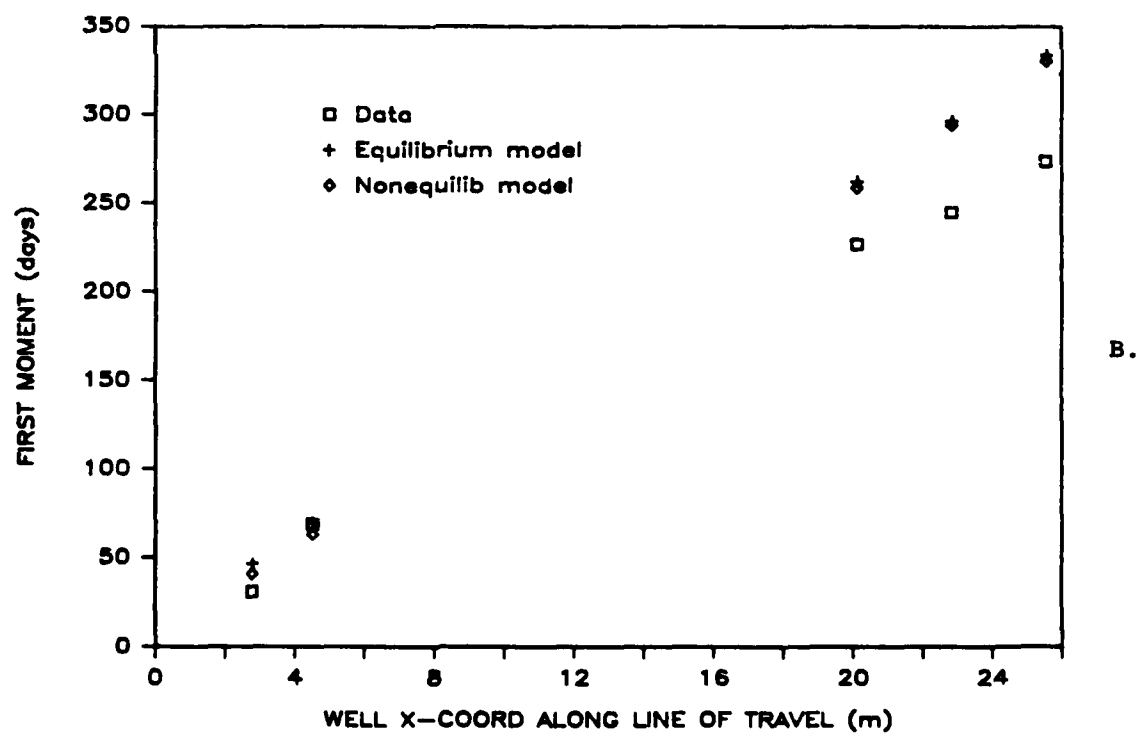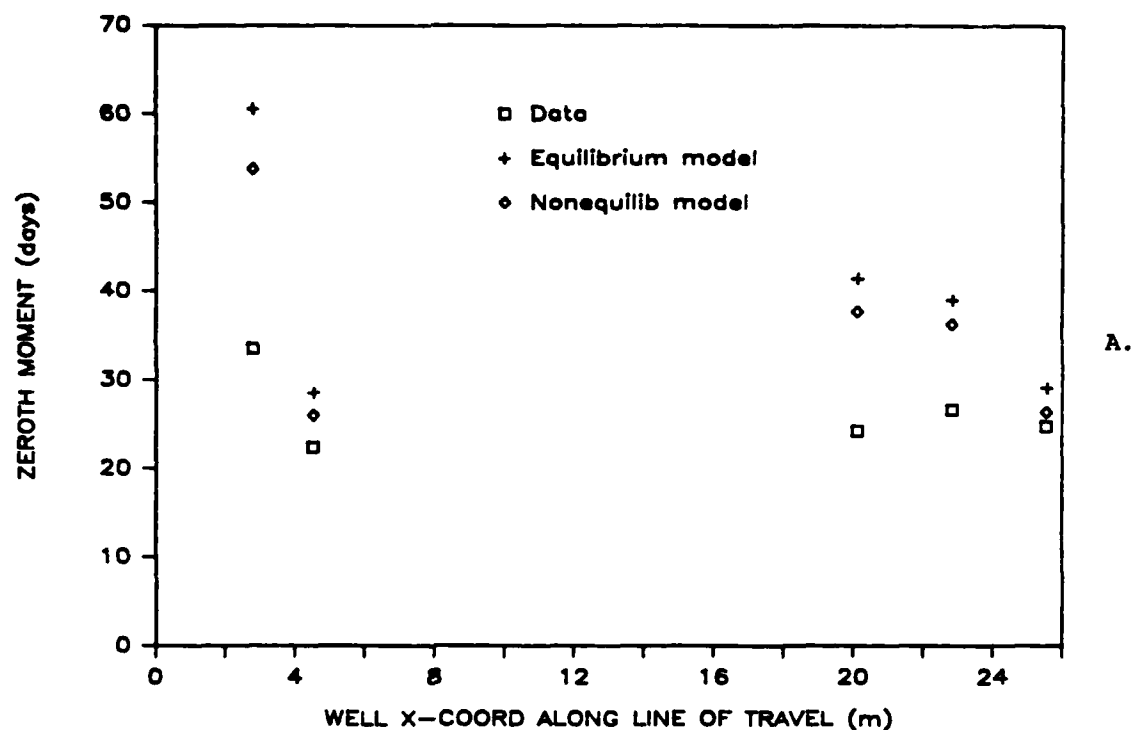
Figure 5.28. Comparison of bromide temporal moments estimated from the data and predicted by equilibrium and nonequilibrium models: a) Zeroth, and b) First moments.

108
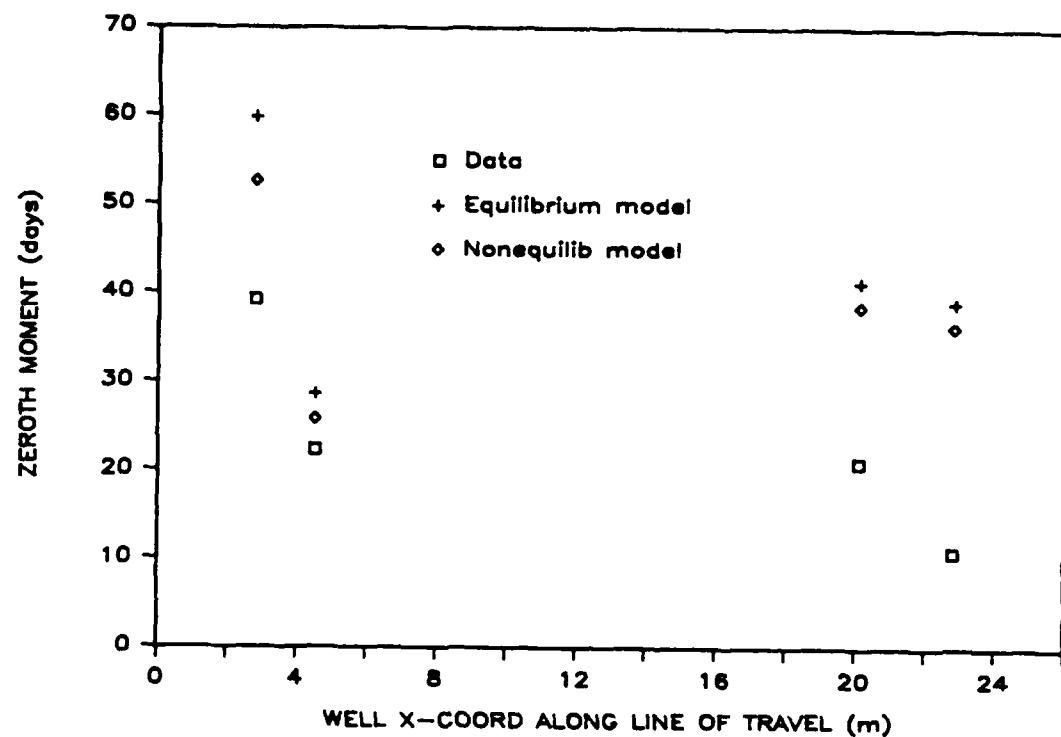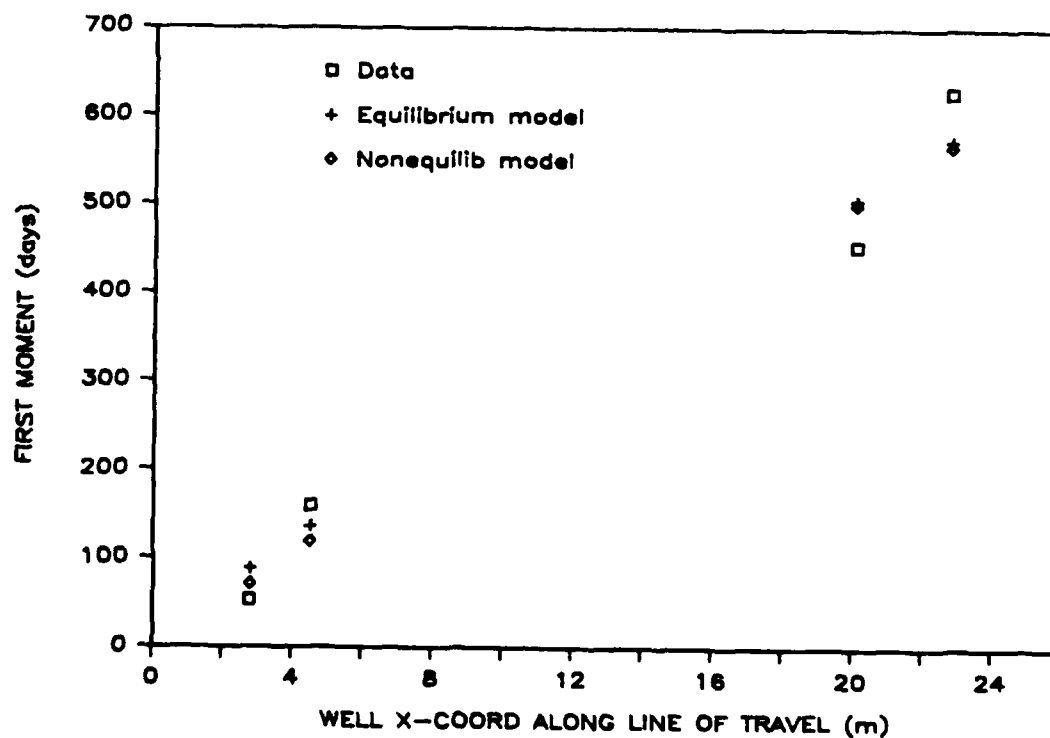
Figure 5.29. Comparison of bromoform temporal moments estimated from the data and predicted by equilibrium and nonequilibrium models: a) Zeroth, and b) First moments.

109
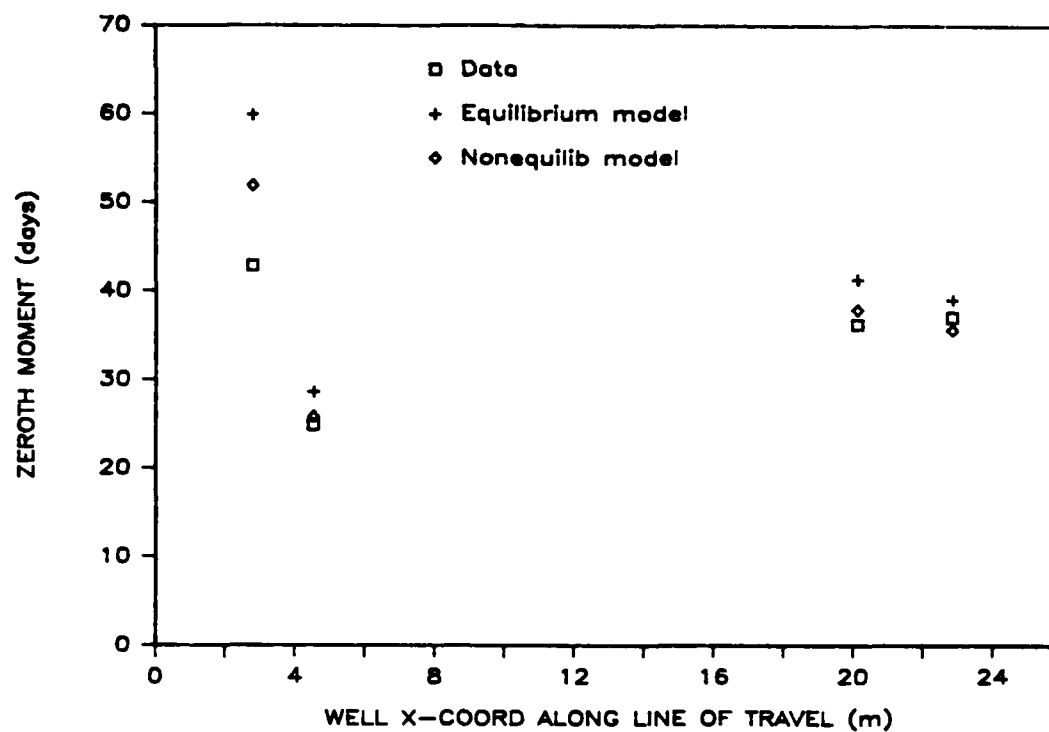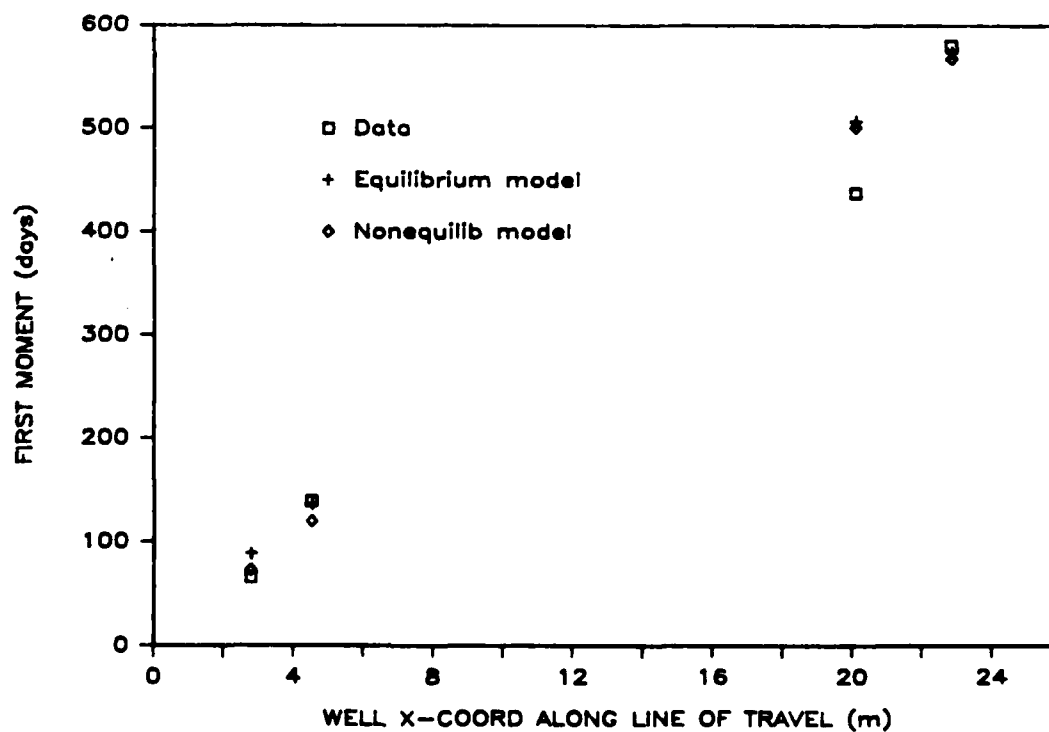
Figure 5.30. Comparison of carbon tetrachloride temporal moments esti-
mated from the data and predicted by equilibrium and non-
equilibrium models: a) Zeroth, and b) First moments.

110
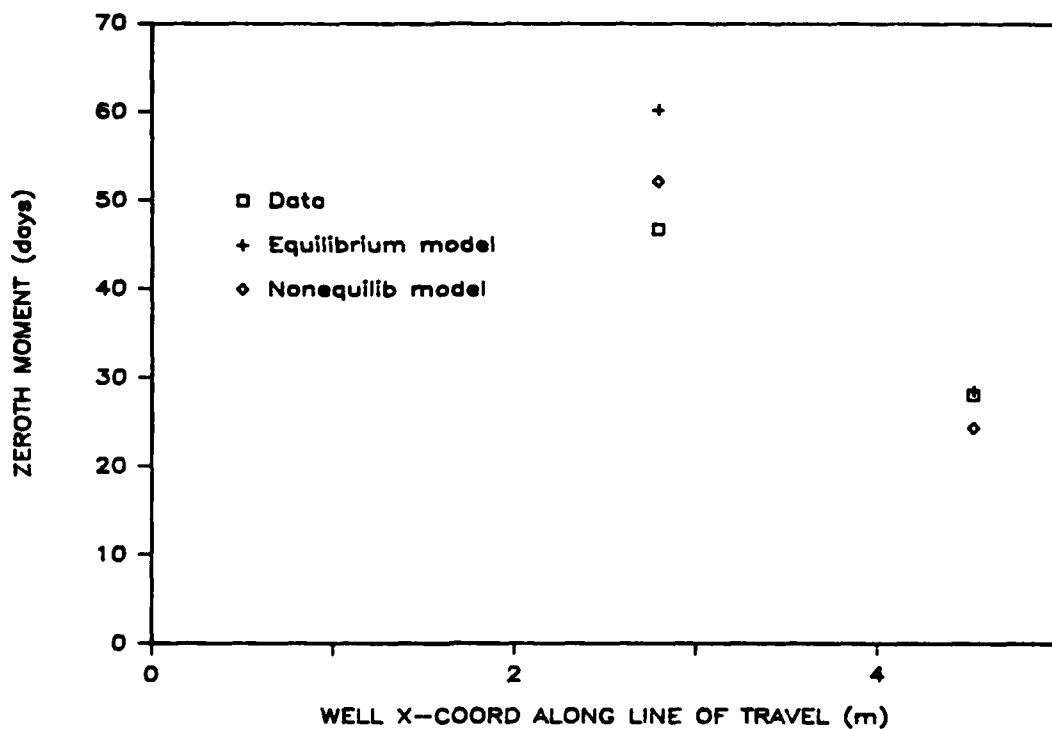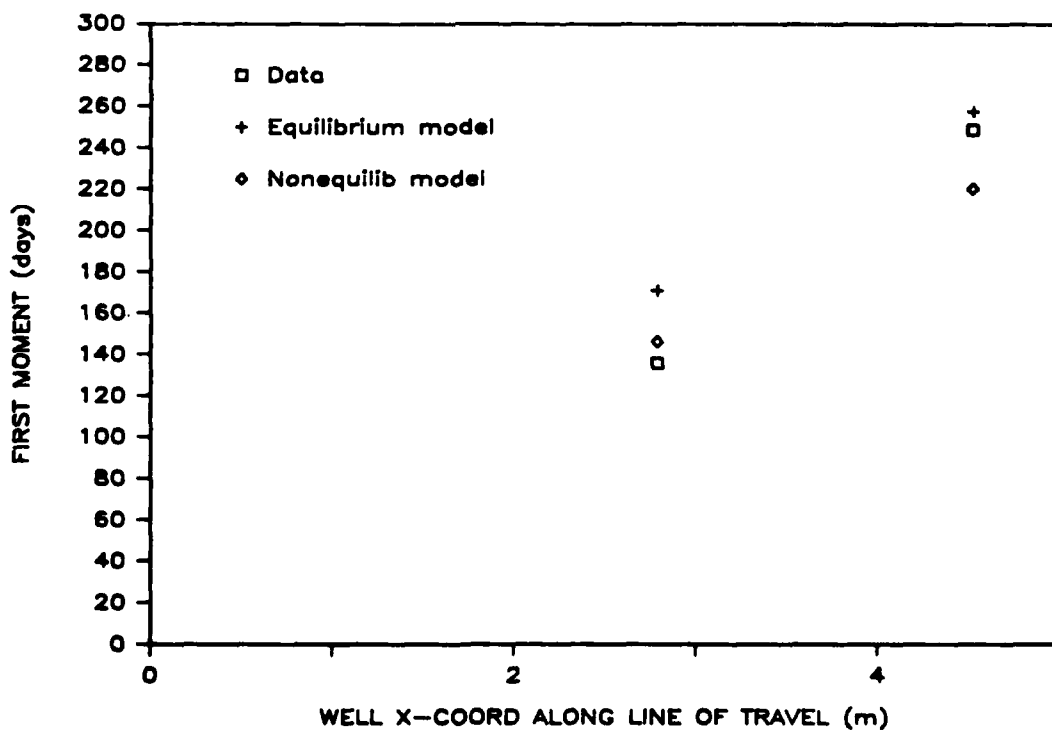
Figure 5.31. Comparison of tetrachloroethylene temporal moments esti-
mated from the data and predicted by equilibrium and non-
equilibrium models: a) Zeroth, and b) First moments.

111

Model predictions were made using the equilibrium and nonequilibrium models to simulate breakthrough responses. The moments of these responses were then evaluated using the same numerical technique that had been applied to the data. In Chapter 3, Table 3.3, it was shown that both equilibrium and nonequilibrium models have the same expression for the zeroth temporal moment in terms of the model's parameters. Thus, differences in the zeroth moment simulations of the two model types are due to parameter differences, and not to model structure. Although certain trends are evident, the zeroth moment data and simulations show a fair amount of scatter. Both models simulate the low values of the zeroth moment found at the sampling well located at $x = 4.79$ m. This low value is observed because the sampling well is offset a considerable distance from the center line of the plume. It is also apparent that the zeroth moment data values for bromoform at the far-field wells are considerably lower than the simulated values. This discrepancy may be due to the possible biotransformation of bromoform, which was discussed earlier in connection with the zeroth spatial moment results.

From Table 3.3 in Chapter 3, it was also found that the first temporal moment calculated using the nonequilibrium models is equal to the first temporal moment of the equilibrium model multiplied by a constant. Again, therefore, any differences in the first temporal moment simulations are due to parameter differences, rather than to differences in model structure. Figures 5.28b through 5.31b show the first temporal moment as a function of distance in the x direction. Reasonably good agreement is found between simulated moments and moments calculated from the data.

Judging from the zeroth and first temporal moment simulations, there is little evidence for saying one model or the other is better at describing the data, largely because both type models can be considered "pseudo-equilibrium models" with respect to temporal moments. That is, since the zeroth and first temporal moments calculated using the nonequilibrium models are independent of the rate parameter, the zeroth and first moments can be reproduced by an equivalent equilibrium model. Figures 5.28 through 5.31 do indicate, however, that the parameter values obtained from fitting the spatial moment data can be used to predict the temporal moment data fairly well, for both equilibrium and nonequilibrium models.

112

Another way of examining the temporal data is to inspect the break-
through responses themselves, at various wells. Using one-dimensional
models, Goltz and Roberts (1986) showed that the sharp breakthrough and
tailing exhibited by the near-field well breakthrough response data was
better simulated using nonequilibrium than equilibrium models. Figures
5.32 through 5.39 compare simulations of three-dimensional equilibrium
and first-order rate models with the data. For each solute, two wells
were chosen for comparison, one near-field well and one far-field well.
Figure 5.37, which compares simulations of the equilibrium and first-
order rate models with the near-field well response data for bromoform,
also includes a layered diffusion model simulation. The similarity of
the first-order rate and layered diffusion model simulations provides
further evidence justifying the use of the first-order rate model to
approximate the more complex diffusion models.

As the temporal moments have already been discussed, the following
analysis will concentrate on the general characteristics and form of the
breakthrough responses. The breakthrough responses simulated for the
four solutes at the far-field wells are fairly symmetric, with the non-
equilibrium model response exhibiting a bit more asymmetry than that of
the equilibrium model. It is interesting to note that for the bromide
simulated responses, the equilibrium model curve exhibits more spreading
and a lower peak value than that of the nonequilibrium model, whereas
for the organic simulations, the situation is reversed. The reason for
this behavior may be found by applying Eq. 3-66 to the nonequilibrium
model parameter values for the different solutes. Applying Eq. 3-66,
which calculates an equivalent dispersion coefficient (D_{eff}), reveals
D_{eff} for the bromide at the sampling well to be less than D_{eff} for the
organics. The value of D_{eff} which is calculated using Eq. 3-66 is an
equilibrium model equivalent parameter which combines the effect of
dispersion in the mobile region with the effect of so-called "holdup
dispersion" (Koch and Brady, 1986). (Holdup dispersion describes a
spreading mechanism caused by solute diffusion into immobile regions.)
Owing to the sorption of the organic solutes within the immobile region,
the impact of holdup dispersion on the organic compounds' behavior is
more pronounced than the impact on the conservative tracer's behavior,
so the organic simulations exhibit relatively more spreading at the far-
field sampling points.

113
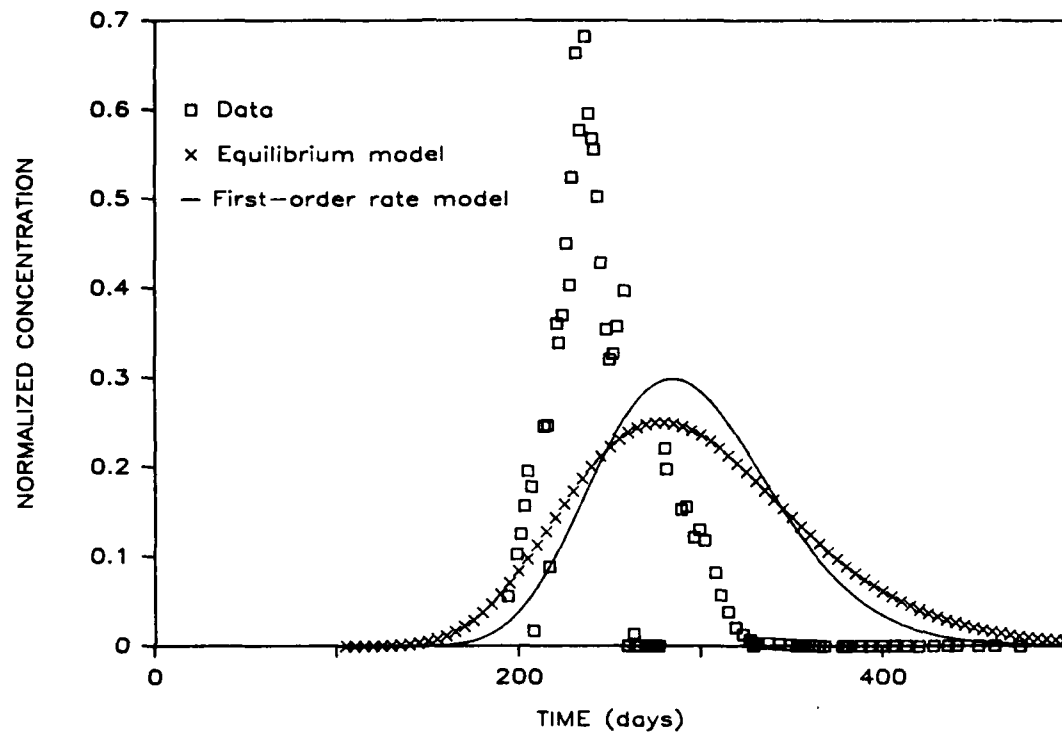
Figure 5.32. Breakthrough response data and model predictions for bromide at a far-field well (x = 21.0 m, y = 9.0 m, z = -4.17 m).
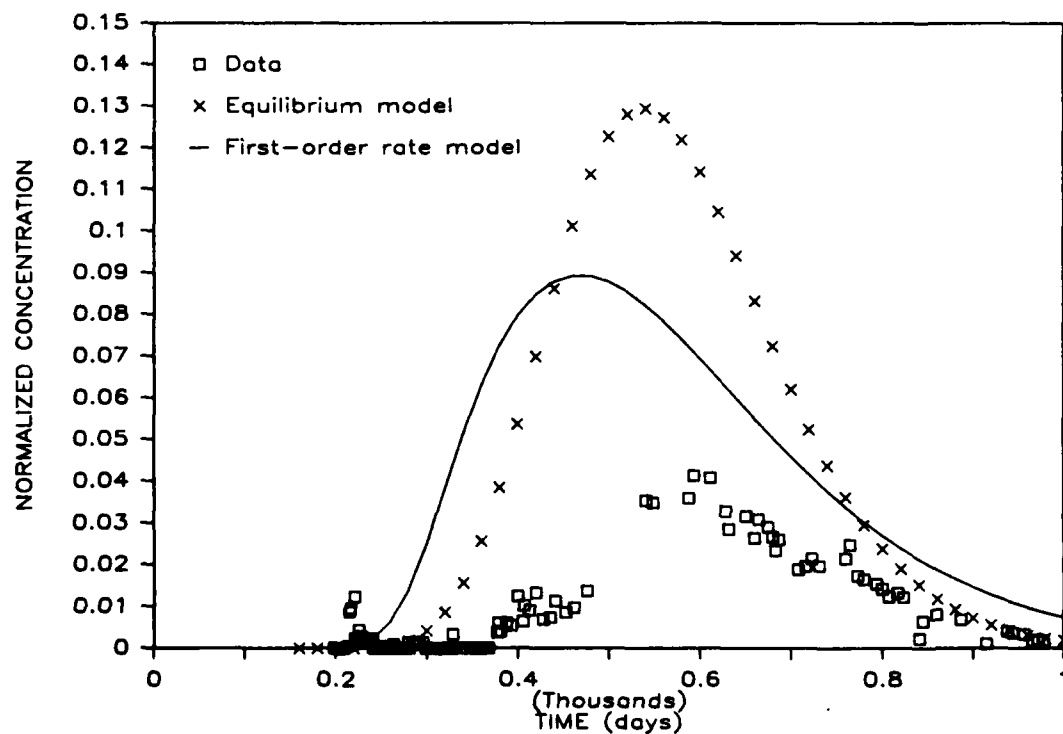
Figure 5.33. Breakthrough response data and model predictions for bromoform at a far-field well (x = 21.0 m, y = 9.0 m, z = -4.17 m).

114
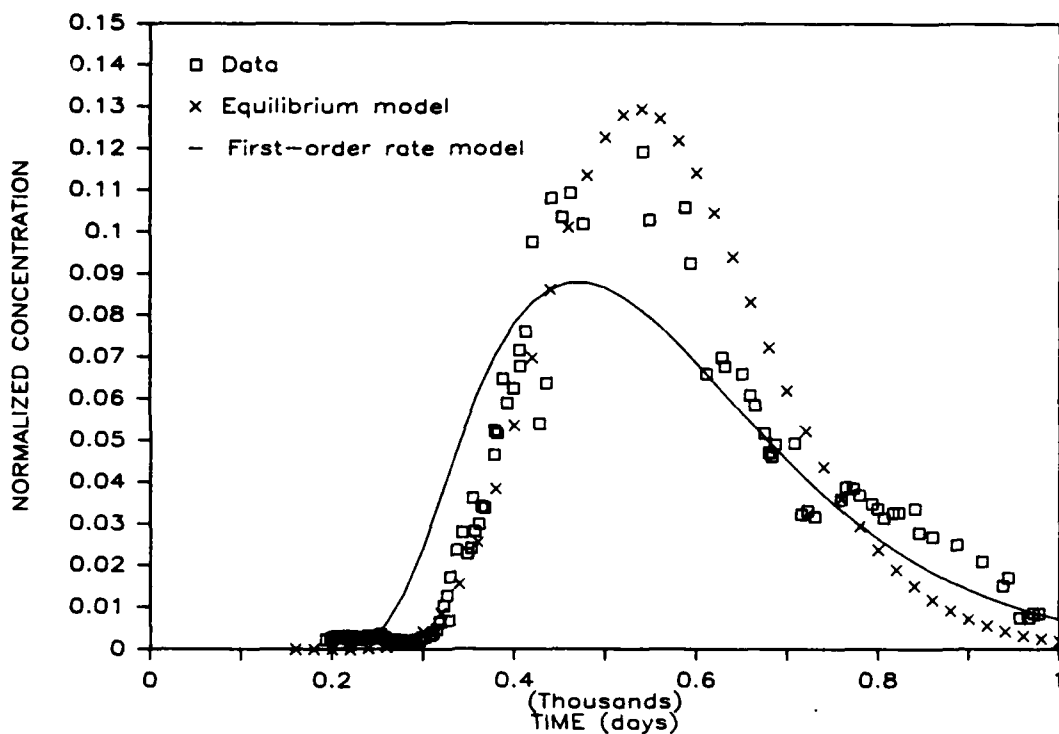
Figure 5.34. Breakthrough response data and model predictions for carbon tetrachloride at a far-field well (x = 21.0 m, y = 9.0 m, z = -4.17 m).
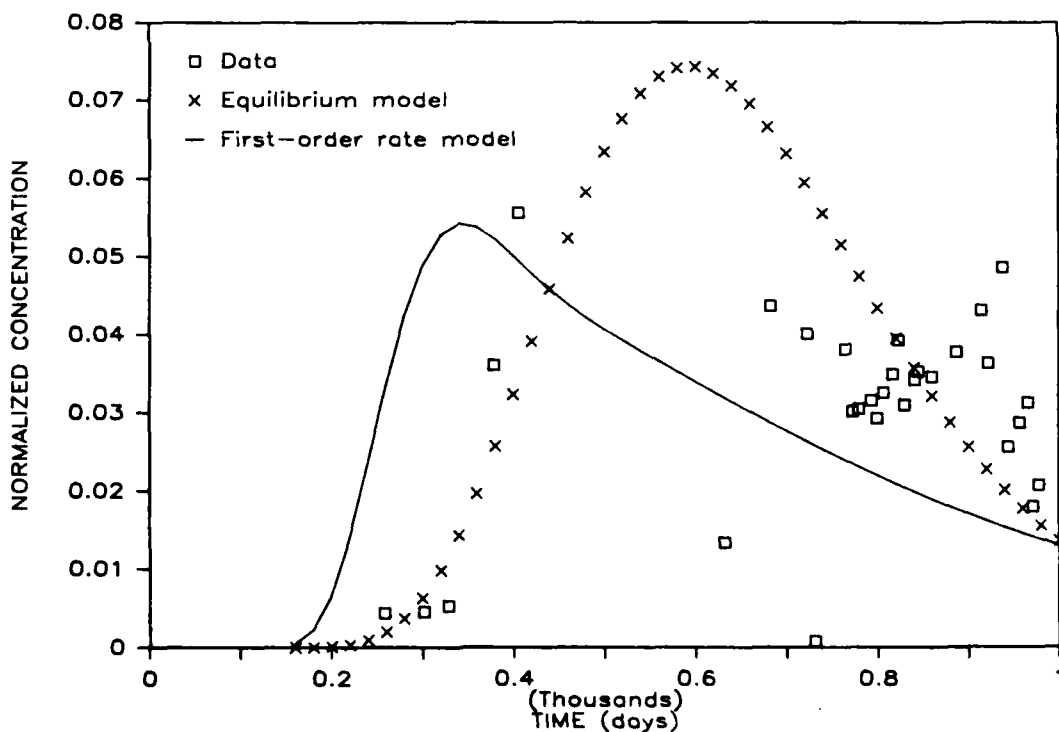
Figure 5.35. Breakthrough response data and model predictions for tetrachloroethylene at a mid-field well (x = 13.1 m, 4.05 m, -3.72 m).
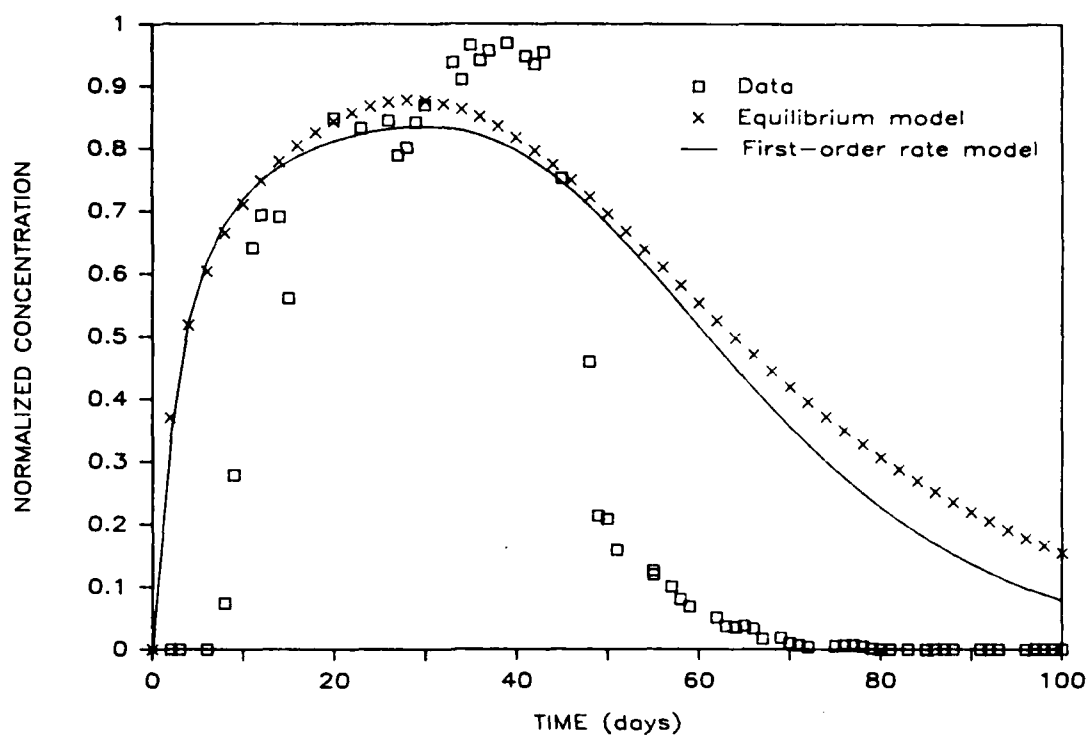
Figure 5.36. Breakthrough response data and model predictions for bromide at a near-field well (x = 2.5 m, y = 1.25 m, z = -3.62 m).
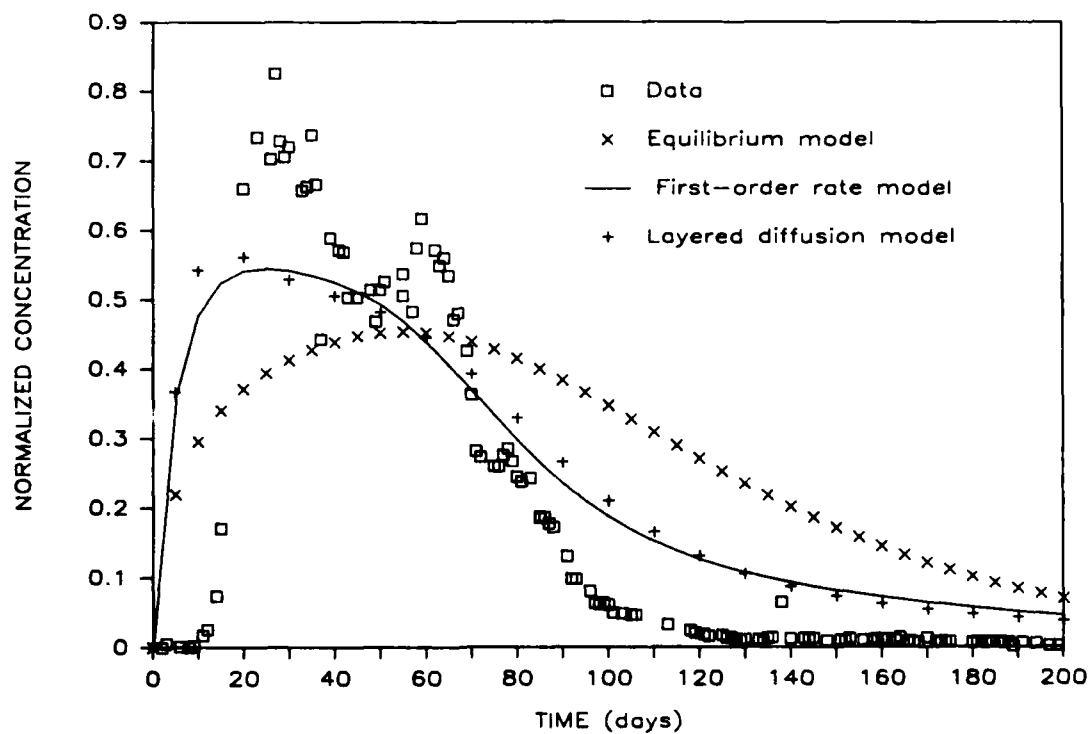
Figure 5.37. Breakthrough response data and model predictions for bromoform at a near-field well (x = 2.5 m, y = 1.25 m, z = -3.62 m).

116
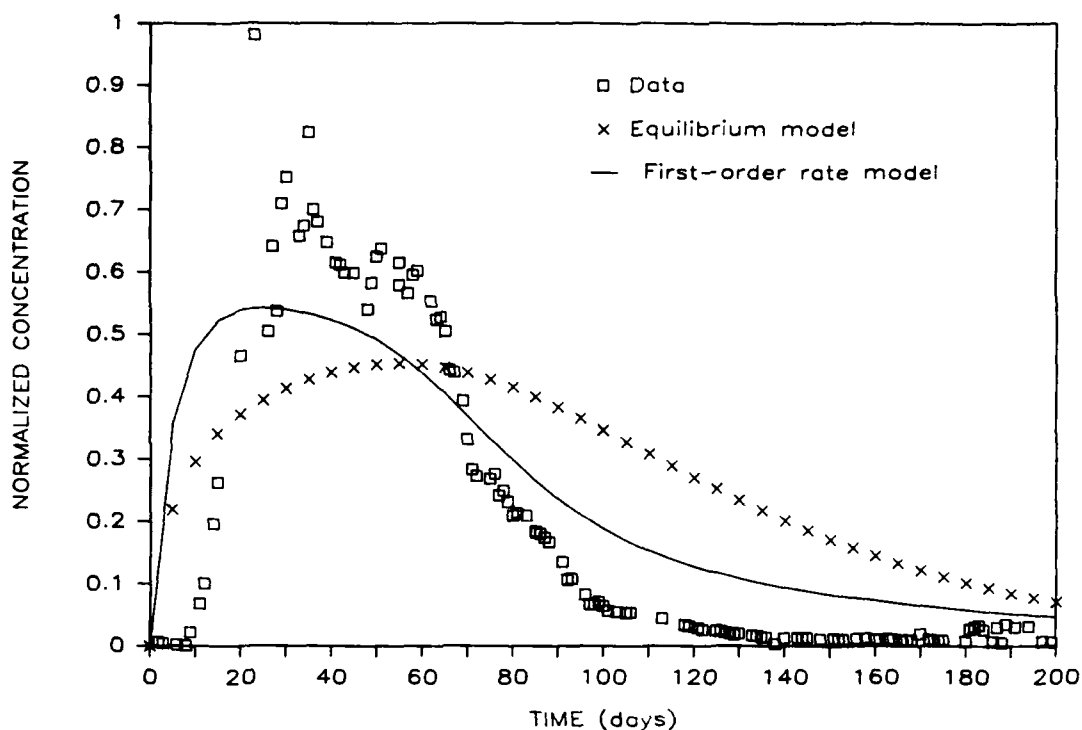
Figure 5.38.   Breakthrough response data and model predictions for carbon tetrachloride at a near-field well (x = 2.5 m, y = 1.25 m, z = -3.62 m).
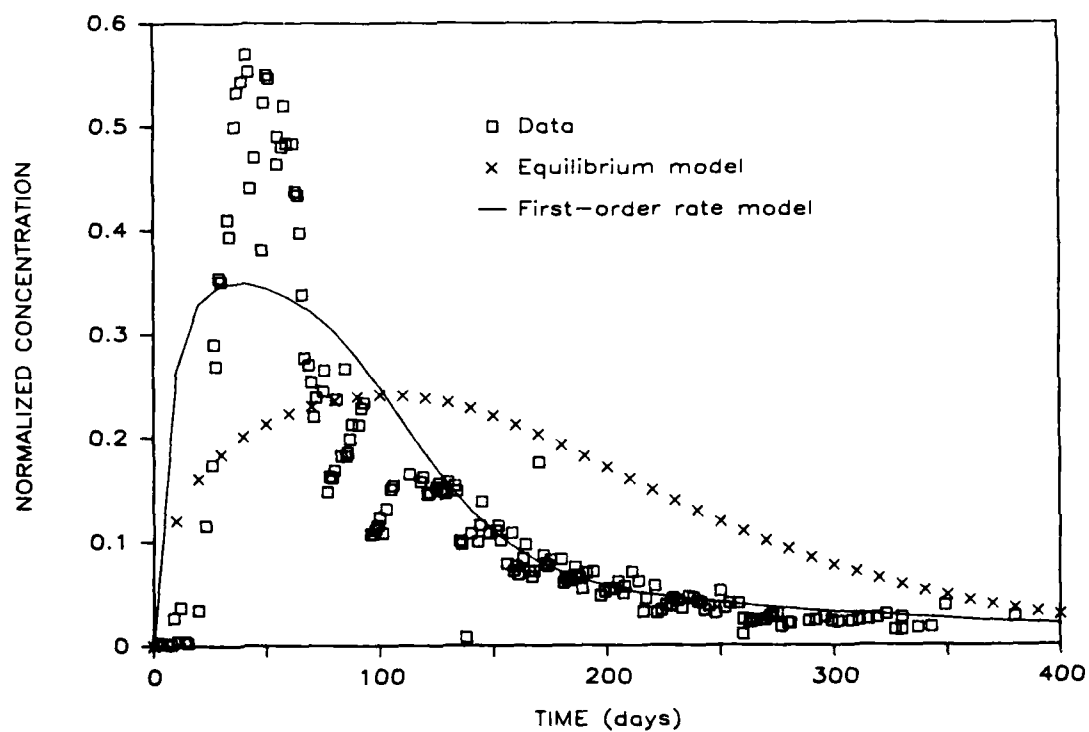
Figure 5.39.   Breakthrough response data and model predictions for tetrachloroethylene at a near-field well (x = 2.5 m, y = 1.25 m, z = -3.62 m).

117

Examination of the near-field responses seems to confirm Goltz and Roberts' (1986) conclusion that the characteristically sharp breakthrough and tailing of the breakthrough response data are better simulated with the nonequilibrium models. On the other hand, in the far field neither model type offers a significant advantage over the other for simulating the data. This is to be expected, since at long distances, the nonequilibrium models can be approximated by equivalent equilibrium models.

Overall, considering the fact that input parameters were not fitted to the temporal data, both type models quite adequately simulate the observed data. However, especially in the case of tetrachloroethylene, the solute expected to be most impacted by nonequilibrium effects due to its high distribution coefficient, the salient characteristics of the near-field data seem to be better captured by the nonequilibrium model simulations. Also Figure 5.37 shows little difference between first-order rate and diffusion model breakthrough simulations, certainly not enough difference to choose one model over the other based solely on the goodness of fit.

ALTERNATE HYPOTHESES

Although the hypothesis of physical nonequilibrium appears to explain the observed temporal and spatial behavior of the sorbing and nonsorbing solutes, there are other hypotheses which also may adequately explain the observations. This section examines some of these alternative hypotheses, in light of what is known about the Borden situation.

Nonlinear Sorption

If solute transport is assumed to be governed by the advective/dispersive equation, with sorption described by a Freundlich isotherm (van Genuchten and Cleary, 1982), the following equations, written for one-dimensional transport, apply:

$$\frac{\partial C}{\partial t} = D'_x \frac{\partial^2 C}{\partial x^2} - v_o \frac{\partial C}{\partial x} - \frac{\rho}{\theta} \frac{\partial S}{\partial t} \tag{5-4a}$$

$$S = KC^n \tag{5-4b}$$

For n < 1, sharp breakthrough and tailing are characteristic of the breakthrough responses, making them similar to those seen at Borden (van Genuchten and Cleary, 1982). These breakthrough response characteristics are due to the fact that at high aqueous concentrations, the sorption partition coefficient is smaller than at low concentrations, so that the main body of the solute pulse overtakes the leading edge. On the other hand, the low concentrations in the trailing edge of the pulse are sorbed more strongly than the main body of the pulse, creating a long tail.

Qualitatively, at least, this explanation accounts for the relative symmetry of the nonsorbing bromide tracer breakthrough responses, as well as the sharp breakthrough and tailing of the organic solutes' breakthrough responses. It may also explain the loss in mass and the deceleration of the organic solutes; as the solute plume disperses over time, the aqueous concentrations decline, and the overall sorption increases. To examine these qualitative statements in more detail, a numerical analysis was performed.

A Crank-Nicolson finite difference representation of Eq. 5-4 was developed. Parameters for the model were obtained from Curtis et al. (1986). By performing batch equilibrium sorption studies using the Borden aquifer material, Curtis et al. (1986) found that at the low concentrations seen in the Borden experiment, the sorption of the organic compounds could be modeled by a linear isotherm. However, Curtis et al. (1986) fit their isotherm data with a Freundlich model as well. They found that of all the solutes, tetrachloroethylene had a Freundlich exponent most different from unity. Using the following parameter values obtained from Curtis et al.'s (1986) sorption experiments:

$$K = 0.93 \ (cm^3/g)^{0.79}$$

$$n = 0.79$$

combined with the following hydrogeologic parameter values (Tables 5.3-5.5):

$$\rho = 1.81 \ g/cm^3$$

$$\theta = 0.33$$

$$v_o = 0.079 \ m/d$$

$$D_x' = 0.04 \ m^2/d$$

simulations were run to determine the zeroth and first spatial moments of the solute plume distribution versus sampling time. Figure 5.40 compares simulations with moments estimated from the tetrachloroethylene data. The decline in mass and deceleration simulated by the model is much less than exhibited by the data. The reason that the simulated loss in mass and deceleration is relatively insignificant is due to the assumption of equilibrium. The initial solute plume is assumed to be instantaneously equilibrated, with a fraction of the solute mass immediately sorbed. Thus, even though more and more mass goes into the sorbed phase with time, the ratio of sorbed to aqueous mass does not significantly change.

Hysteretic Sorption

Investigators have found that sorption may be hysteretic (Hornsby and Davidson, 1973; Swanson and Dutt, 1973; van Genuchten et al. 1974; Horzempa and DiToro, 1983; DiToro, 1985). Hysteretic sorption/desorption isotherms, combined with advective/dispersive transport, have been shown to simulate breakthrough responses with long tails (van Genuchten et al., 1974; van Genuchten and Cleary, 1982).

To investigate whether sorption/desorption hysteresis is an important mechanism at Borden, Curtis et al. (1986) performed a short-term (6 day) sorption/desorption experiment using Borden aquifer material and hexachloroethane. No significant sorption/desorption hysteresis was observed.

In this work, a long-term (60 day) sorption/desorption study was conducted using tetrachloroethylene and Borden aquifer material. Tetrachloroethylene was chosen, as it is the most strongly sorbing of the solutes under consideration, and would presumably exhibit the most obvious hysteresis. A long-term study was conducted based on the possibility of slow sorption due to diffusion rate limitations. Experimental details are presented in Appendix F. Figure 5.41 plots the sorption/desorption isotherm data.

The model most often used to describe hysteretic sorption/desorption isotherms, in conjunction with one-dimensional advective/dispersive solute transport (Hornsby and Davidson, 1973; van Genuchten et al., 1974; Wood and Davidson, 1975; and van Genuchten et al., 1977) is:
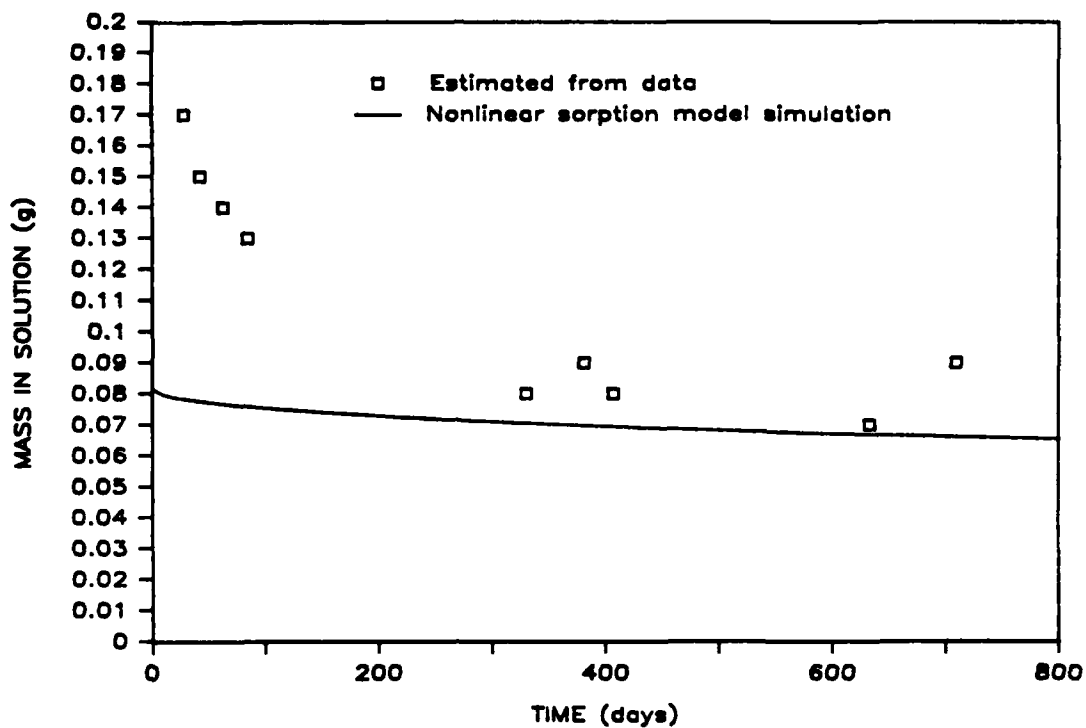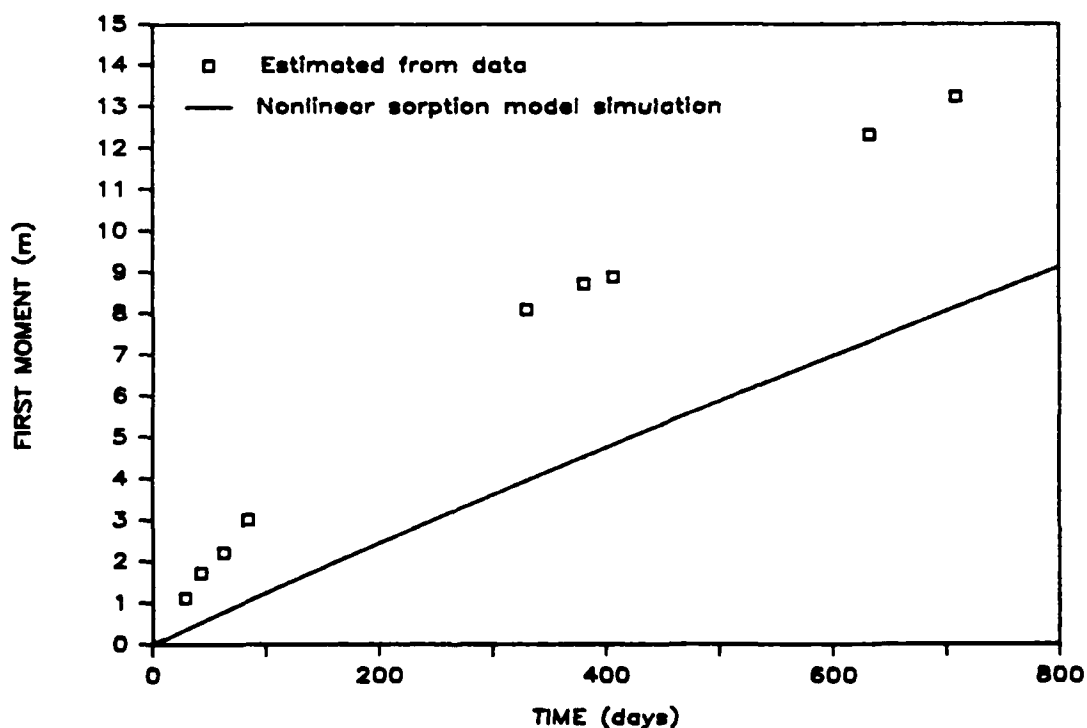
Figure 5.40. Comparison of the tetrachloroethylene plume a) mass in solution, and b) first spatial moment, estimated from the data and simulated by an equilibrium transport model assuming nonlinear sorption and using experimentally obtained sorption parameter values.

121
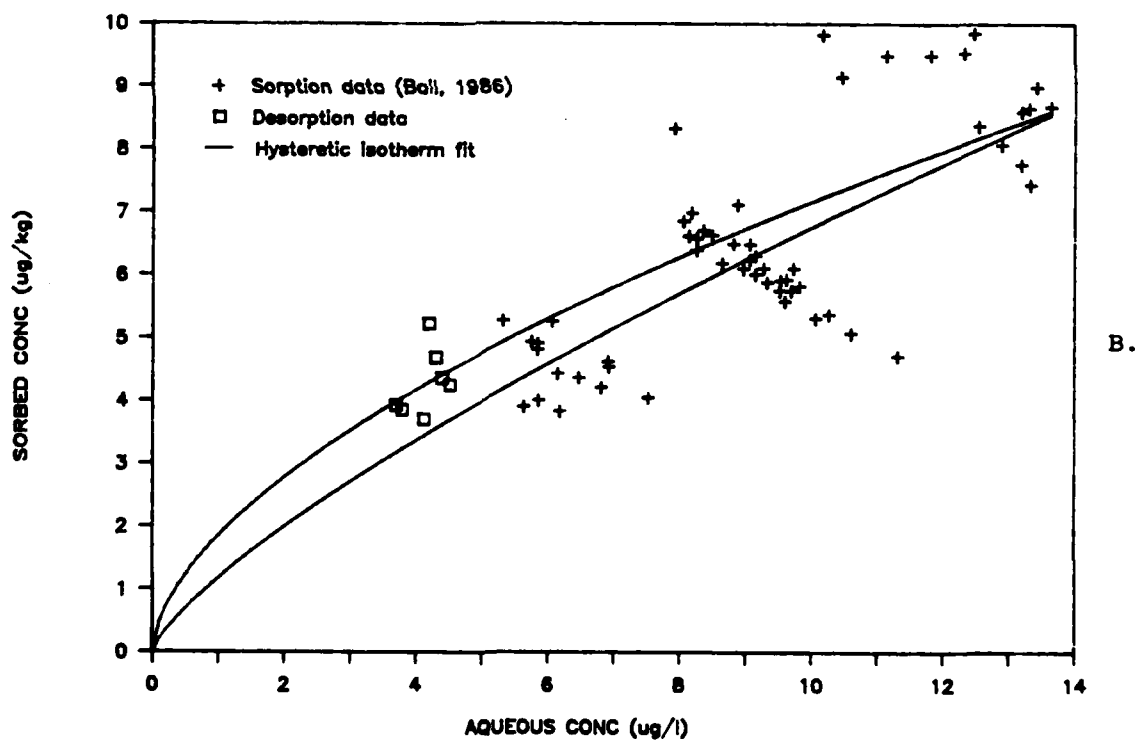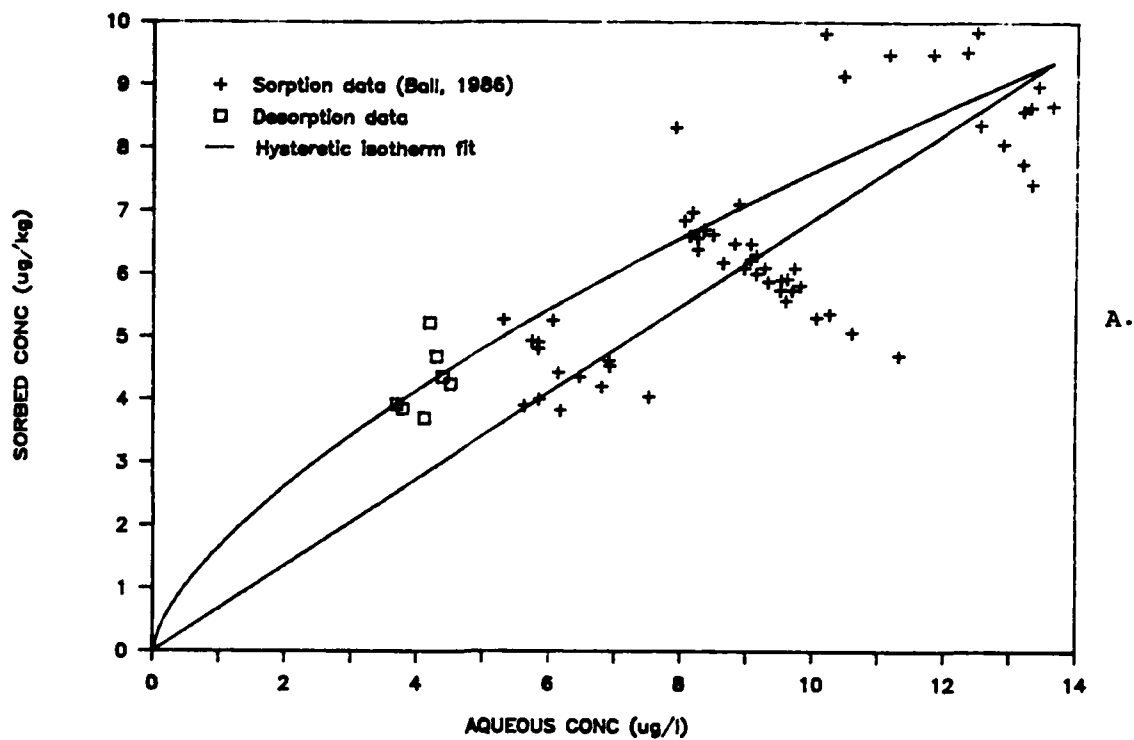
Figure 5.41. Sorption/desorption isotherm results for uptake of tetra-
chloroethylene on Borden aquifer material: a) Fit using a
linear sorption/hysteretic desorption isotherm. b) Fit
using a nonlinear sorption/hysteretic desorption isotherm.

$$\frac{\partial C}{\partial t} = D'_x \frac{\partial^2 C}{\partial x^2} - v_o \frac{\partial C}{\partial x} - \frac{\rho}{\theta} \frac{\partial S}{\partial t}$$

$$S = K_{ads} C^{n_{ads}} , \quad \frac{\partial C}{\partial t} > 0 \tag{5-5}$$

$$S = K_{des} C^{n_{des}} , \quad \frac{\partial C}{\partial t} < 0$$

where:

$$K_{des} = K_{ads} C_{max}^{n_{ads} - n_{des}}$$

This model combines the advective/dispersive solute transport equation with a sorption source/sink term descibed by a Freundlich isotherm. Depending on whether solute is sorbing or desorbing, different sets of Freundlich isotherm parameters are used.

The tetrachloroethylene sorption/desorption data shown in Figure 5.41 were used to determine Freundlich isotherm parameters for this model. In Figure 5.41a, linear sorption is assumed ($n_{ads} = 1.0$) and using least-squares regression, best fit values of K_{ads} and n_{des} were determined. In Figure 5.41b, both sorption and desorption are described by nonlinear isotherms. Least-squares regression was used to determine best fit parameter values for n_{ads}, n_{des}, and K_{ads}. In both Figures 5.41a and 5.41b, a value of $C_{max} = 13.6$ µg/l was assumed. This C_{max} value corresponds to the maximum aqueous concentration measured in the sorption half of the sorption/desorption experiments.

A Crank-Nicolson finite difference approximation of Eq. 5-5 was developed. Assuming linear sorption and hysteretic desorption (Figure 5.41a), the following set of parameter values was used in the model:

$$\rho = 1.81 \text{ g/cm}^3$$

$$\theta = 0.33$$

$$D'_x = 0.04 \text{ m}^2/\text{d}$$

$$v_o = 0.079 \text{ m/d}$$

$$K_{ads} = 0.69 \text{ cm}^3/\text{g}$$

$$n_{ads} = 1.0$$

$$n_{des} = 0.66$$

Assuming nonlinear sorption and hysteretic desorption (Figure 5.41b), the above physical and hydrodynamic parameters were used with:

$$K_{ads} = 1.18 \ (cm^3/g)^{0.76}$$

$$n_{ads} = 0.76$$

$$n_{des} = 0.59$$

Figures 5.42 and 5.43 compare model simulations of the zeroth and first spatial moments obtained using these two sets of parameter values with moments estimated from the data. The zeroth and first moment simulations obtained assuming a linear sorption isotherm with hysteretic desorption (Figure 5.42) do not exhibit the observed characteristics of the experimental data. The mass in solution exhibits a minimum with respect to time, and the first moment versus time plot is nearly linear.

The zeroth and first moment simulations obtained using the non-linear sorption isotherm with hysteretic desorption (Figure 5.43) are qualitatively comparable to the observed data, though quantitatively, the simulated loss in mass and deceleration are much less than observed. The qualitative similarity, however, indicates that it may be possible to fit such a nonlinear sorption/hysteretic desorption model to the data. Figure 5.44 compares model simulations with moments estimated from the data for the following Freundlich isotherm parameter values which were selected in an attempt to fit the data:

$$K_{ads} = 0.50 \ (cm^3/g)^{0.7}$$

$$n_{ads} = 0.70$$

$$n_{des} = 0.40$$

As Figure 5.44 shows, the nonlinear sorption/hysteretic desorption model can adequately simulate the main characteristics of the observed spatial moment data.

Chemical Nonequilibrium

Chemical nonequilibrium models that describe solute transport have been proposed (Lindstrom and Narasimhan, 1973; Nkedi-Kizza et al., 1984; Valocchi, 1985a). One such model combines the advective/dispersive transport equation with a first-order rate expression to describe a chemical reaction:
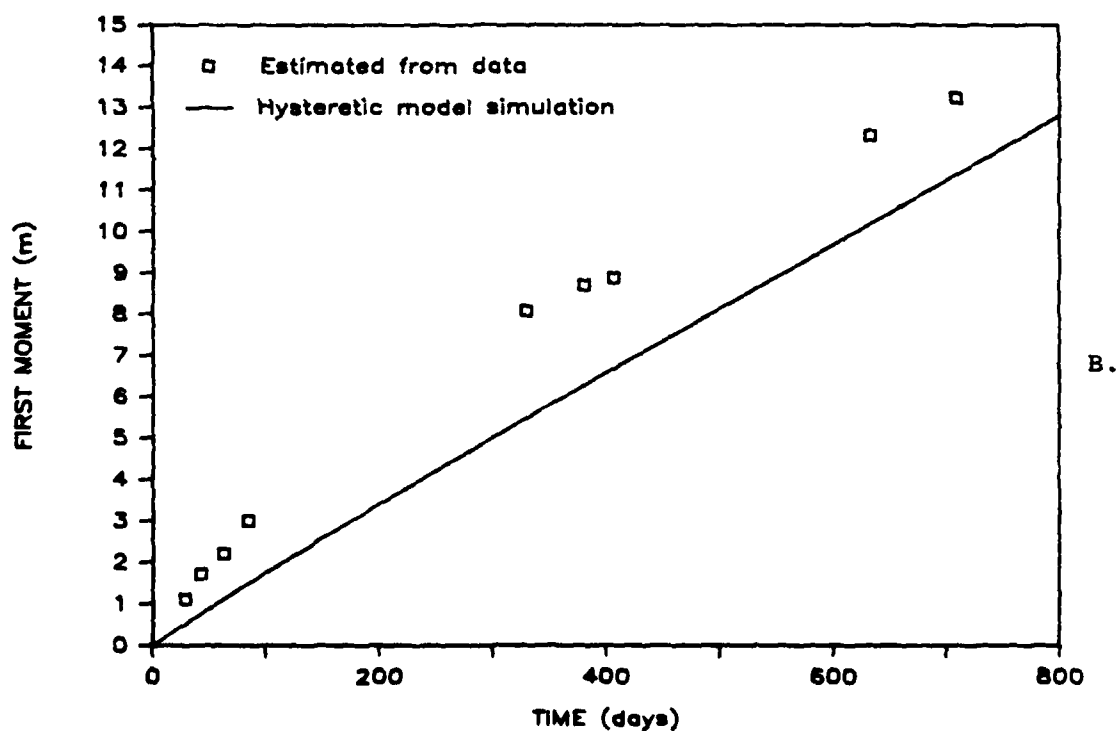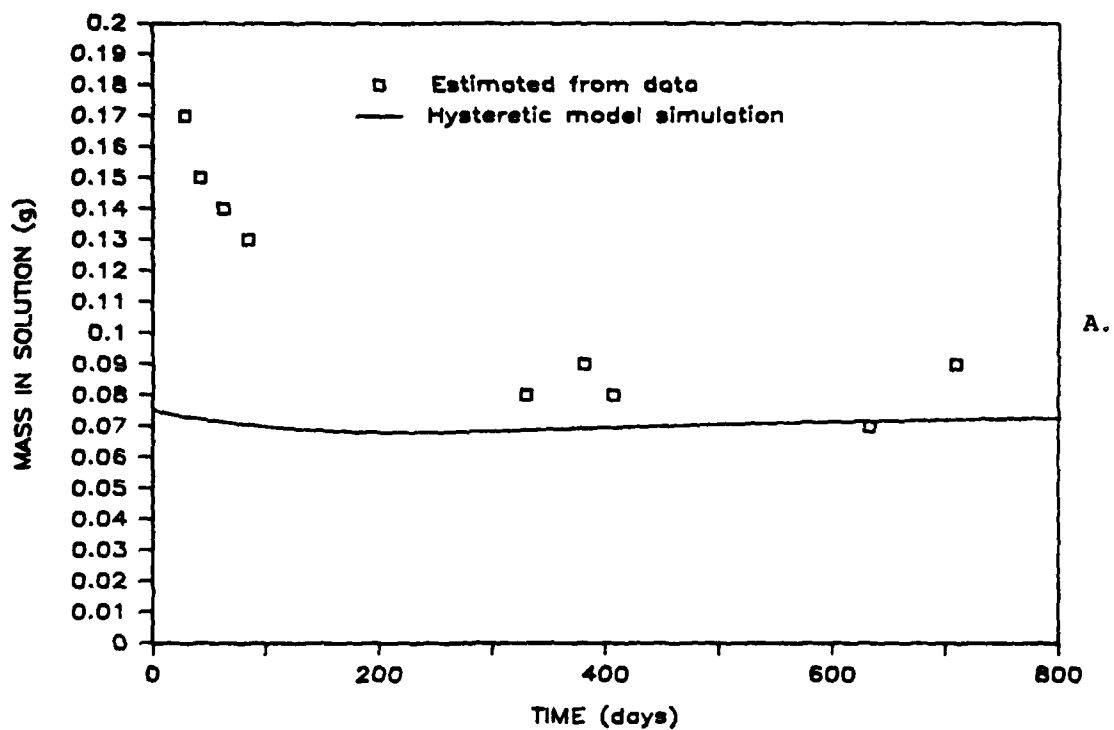
Figure 5.42. Comparison of the tetrachloroethylene plume a) mass in solution, and b) first spatial moment, estimated from the data and simulated by an equilibrium transport model assuming linear sorption/hysteretic desorption and using experimentally obtained sorption/desorption parameter values.
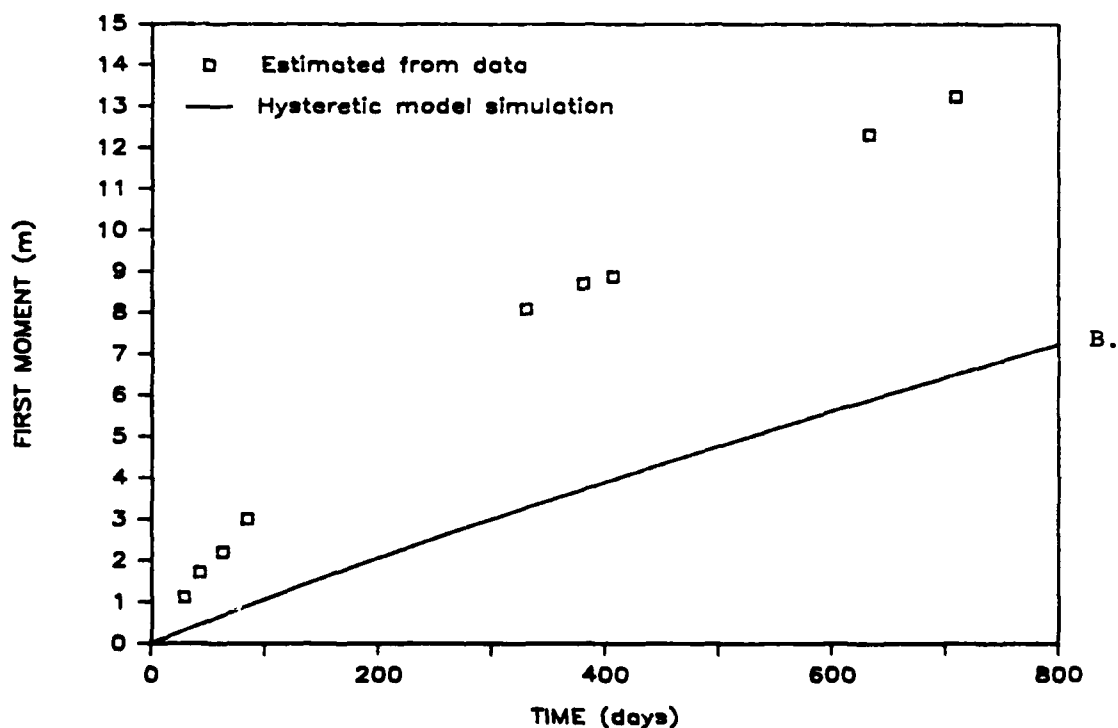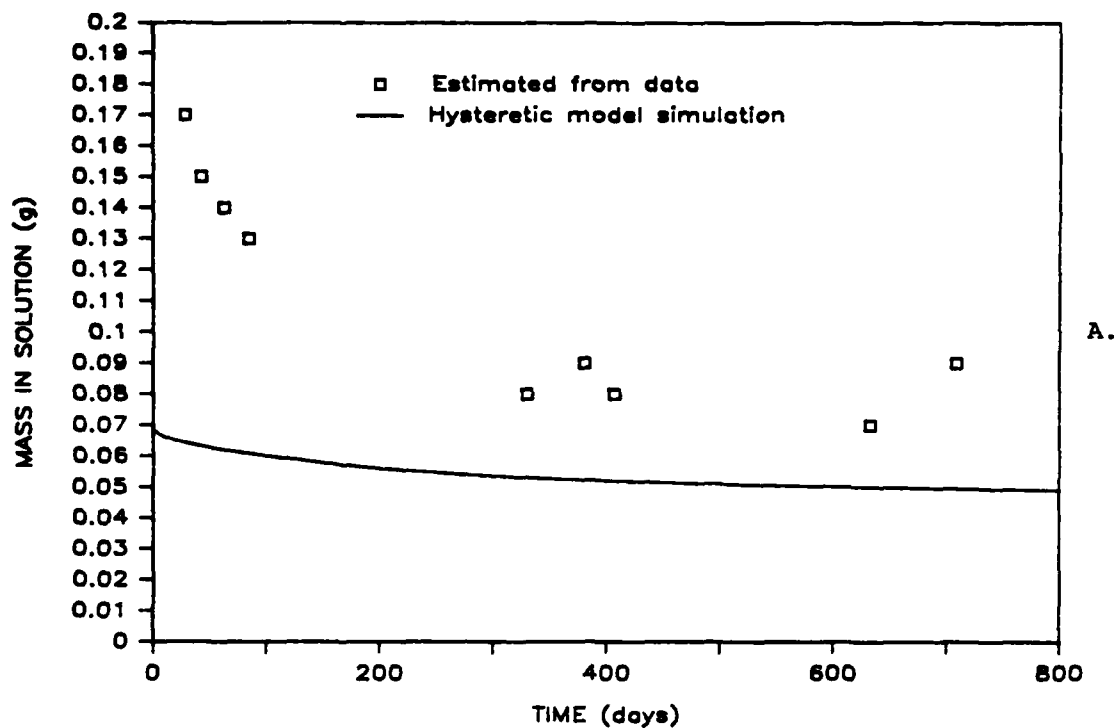
Figure 5.43. Comparison of the tetrachloroethylene plume a) mass in solution, and b) first spatial moment, estimated from the data and simulated by an equilibrium transport model assuming nonlinear sorption/hysteretic desorption and using experimentally obtained sorption/desorption parameter values.

126
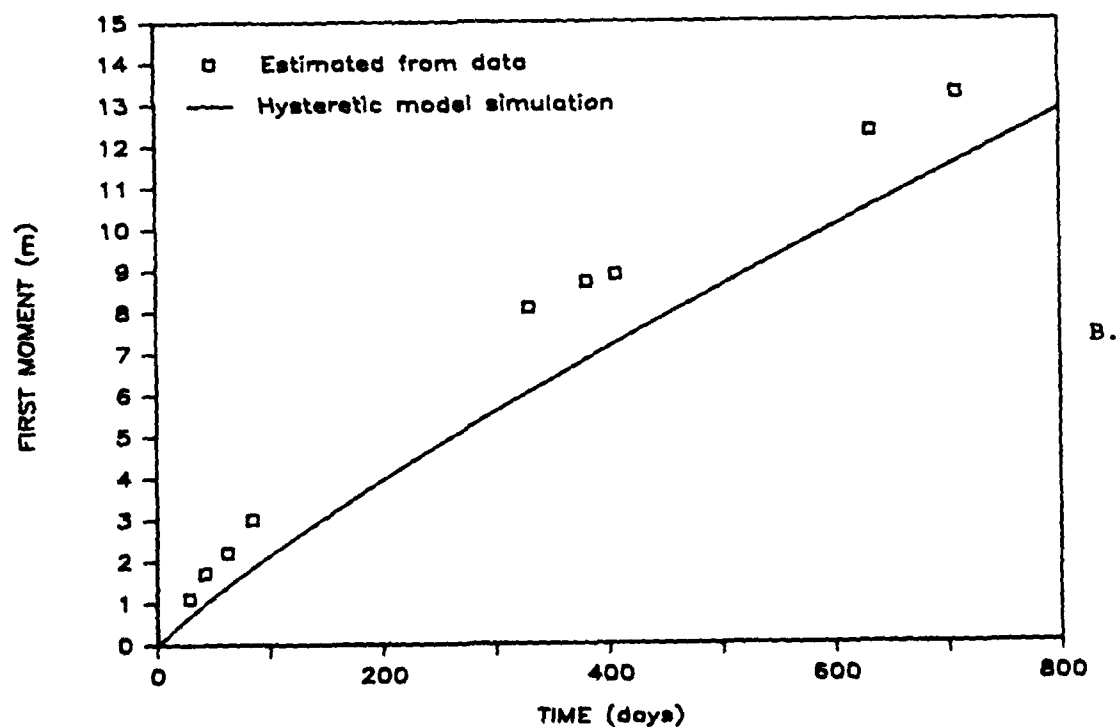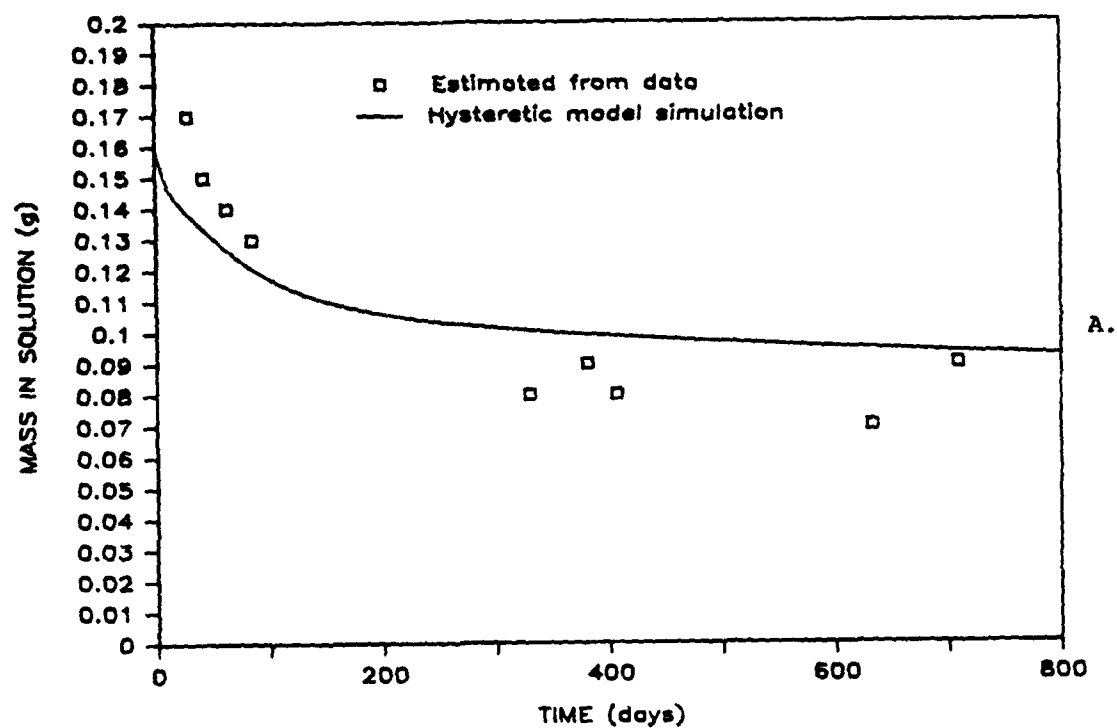
Figure 5.44. Comparison of the tetrachloroethylene plume a) mass in solution, and b) first spatial moment, estimated from the data and simulated by an equilibrium transport model assuming nonlinear sorption/hysteretic desorption and using fitted sorption/desorption parameter values.

$$\frac{\partial C}{\partial t} = D'_x \frac{\partial^2 C}{\partial x^2} - v_o \frac{\partial C}{\partial x} - \frac{\rho}{\theta} \frac{\partial S}{\partial t}$$

$$(5\text{-}6)$$

$$\frac{\partial S}{\partial t} = k_1 C - k_2 S$$

Interestingly, the mathematical form of this model is identical to the physical nonequilibrium first-order rate model (Nkedi-Kizza et al., 1984). Thus, distinguishing between the two models based on their simulated responses is impossible. In Chapter 4, it was shown that an approximate conversion of the first-order rate model to the diffusion models is possible, and that attempting to distinguish between the two types of models is difficult. On mathematical grounds, therefore, chemical nonequilibrium is as adequate an explanation of the Borden observations as is physical nonequilibrium.

However, if we consider the sorption of the organic solutes in terms of the widely held view of hydrophobic partitioning (Chiou et al., 1979; Karickhoff, 1984; Gschwend and Wu, 1985), it would seem that no chemical reaction, in the traditional sense, is occurring, and that slow sorption is really slow diffusion to a sorption "site" rather than a slow reaction at a sorption site.

Biotransformation

Roberts et al. (1986) noted that to reproduce the observed deceleration with time, biotransformation would have to occur selectively, such that solute concentrations at the leading edge of the plume would diminish more rapidly than solute concentrations at the trailing edge. Current hypotheses regarding solute transformation in groundwater suggest this pattern is unlikely, and in fact that the reverse is true: biotransformation should be greater at the trailing edges because the native microorganisms capable of transforming a particular compound have had more time to multiply or acclimate to the compound (Bouwer and McCarty, 1984). Also, the organic compounds show similar decreases in velocity, regardless of whether the loss in mass is substantial (bromoform) or not (carbon tetrachloride). For these reasons, biotransformation does not seem to explain adequately the observed spatial moment behavior.

External Mass Transfer

The physical nonequilibrium models discussed here make the assumption that external mass transfer resistance is negligible. In this section, the validity of that assumption will be assessed.

External mass transfer resistance, also called film transfer resistance, is due to a boundary layer of stagnant water surrounding the solid aquifer particles. For sorption to occur, solute molecules must first diffuse through this boundary layer. If the time required for a solute molecule to diffuse through this layer is comparable to the time required for the molecule to diffuse within the sorbing particle itself (internal diffusion), external resistance is important and should be accounted for. External mass transfer is typically described in terms of a first-order rate expression, with k_f defined as the first-order external mass transfer coefficient.

Crittenden et al. (1986) postulated criteria by which the relative effects of dispersion, internal diffusion, and external mass transfer could be assessed. According to Crittenden et al. (1986), when

$$\frac{v\ell}{D_x} = \frac{a\ell(1 + \beta)^2}{\beta v} = \frac{3(1 - \theta_m)k_f\ell(1 + \beta)^2}{\theta_m \, vb \, \beta^2}$$

(5-7)

$$\begin{array}{ccc} \text{Dispersion} & \begin{array}{c}\text{Internal}\\\text{Diffusion}\end{array} & \begin{array}{c}\text{External Mass}\\\text{Transfer}\end{array} \end{array}$$

the influence of dispersion, internal diffusion, and external mass transfer on spreading will be equal. If one or two of the three terms in Eq. 5-7 are significantly greater than the other terms, the mechanism represented by the larger term or terms can be ignored.

Table 3.8a defines an effective dispersion coefficient for the diffusion models as:

$$D_{eff} = \frac{D_x}{1 + \beta} + \frac{v^2\beta}{a(1 + \beta)^3}$$

(5-8)

The equality represented by the first two terms in Eq. 5-7 is the same as the equality obtained by setting the two terms on the right-hand side of Eq. 5-8 equal to each other. That is, the contributions of dispersion and internal diffusion to an effective dispersion coefficient are set equal to each other by the criteria of Eq. 5-7. Similarly, the last

term in Eq. 5-7 represents the contribution to spreading due to external mass transfer resistance. Since external mass transfer is described by a first-order rate expression, a first-order rate constant α may be defined as:

$$\alpha = \frac{3(1 - \theta_m)k_f}{\theta_m b \beta} \qquad (5-9)$$

Substituting this expression into Eq. 5-7 gives:

$$\frac{v\ell}{D_x} = \frac{a\ell(1 + \beta)^2}{\beta v} = \frac{\alpha\ell(1 + \beta)^2}{\beta v} \qquad (5-10)$$

In Table 3.8a an effective dispersion coefficient for the first-order rate model is defined as:

$$D_{eff} = \frac{D_x}{1 + \beta} + \frac{v^2 \beta}{\alpha(1 + \beta)^3} \qquad (5-11)$$

Setting the two terms on the right-hand side of Eq. 5-11 equal to each other gives the equality shown between the first and third terms in Eq. 5-10. Thus, the spreading criteria suggested by Crittenden et al. (1986) based on inspection of the transport equation solutions for uniform, one-dimensional flow are seen to be tantamount to equating the second moments. Examination of Table 3.8b reveals that Crittenden et al.'s (1986) criteria, derived for one-dimensional flow, are also applicable for three-dimensional flow along the path of advective transport.

Using Eq. 5-7 for a given set of parameter values allows the determination of the relative impact of dispersion, internal diffusion, and external mass transfer on spreading. Using the following parameter values for tetrachloroethylene, the compound which seems to be most affected by physical nonequilibrium mechanisms:

$\rho = 1.81$ g/cm^3 $D_e' = 6.83 \times 10^{-7}$ m^2/d

$\theta = 0.33$ $b = 0.001$ m

$D_{mx} = 0.02$ m^2/d $\ell = 0.29$ m

$K_d = 0.48$ cm^3/g $\beta = 2.71$

$\phi = 0.979$ $f = 0.0$

$v_m = 0.091$ m/d

gives the following values for the first two terms of Eq. 5-7:

$$\frac{v\ell}{D_x} = 1.32$$

$$\frac{a\ell(1 + \beta)^2}{\beta v} = 1.31$$

To evaluate the third term in Eq. 5-7, an estimate for k_f is needed. Wilson and Geankoplis (1966) developed the following correlation to determine k_f in terms of the Reynolds (Re) and Schmidt (Sc) numbers:

$$k_f = \frac{D_o}{2b} \frac{1.09}{\theta_m} (ReSc)^{1/3} \qquad (5-12)$$

where:

$$Re = \frac{2bv_m}{\nu} \quad , \quad Sc = \frac{\nu}{D_o}$$

Using the above correlation, and the value of D_o for tetrachloroethylene obtained using the Wilke and Chang (1955) correlation, gives:

$$Sc = 1265$$

$$Re = 2.11 \times 10^{-3}$$

$$k_f = 0.115 \text{ m/d}$$

Using this value of k_f in Eq. 5-7, the third term in the equation is found to be:

$$\frac{3(1 - \theta_m)k_f\ell(1 + \beta)^2}{\theta_m vb \, \beta^2} = 4.32 \times 10^3$$

From a comparison of the three terms in Eq. 5-7, it is apparent that although the impacts on spreading due to dispersion and internal diffusion are virtually equal, the effect due to external mass transfer resistance is three orders of magnitude less. Thus, it seems that for any reasonable value of k_f, the effect of external mass transfer would be negligible compared to dispersion and internal diffusion effects. This fact is illustrated in Figure 5.45. In Figure 5.45, an orthogonal collocation code developed by Crittenden et al. (1986), which combines one-dimensional advective/dispersive transport with internal diffusion into spheres and external mass transfer, is used to obtain breakthrough

131
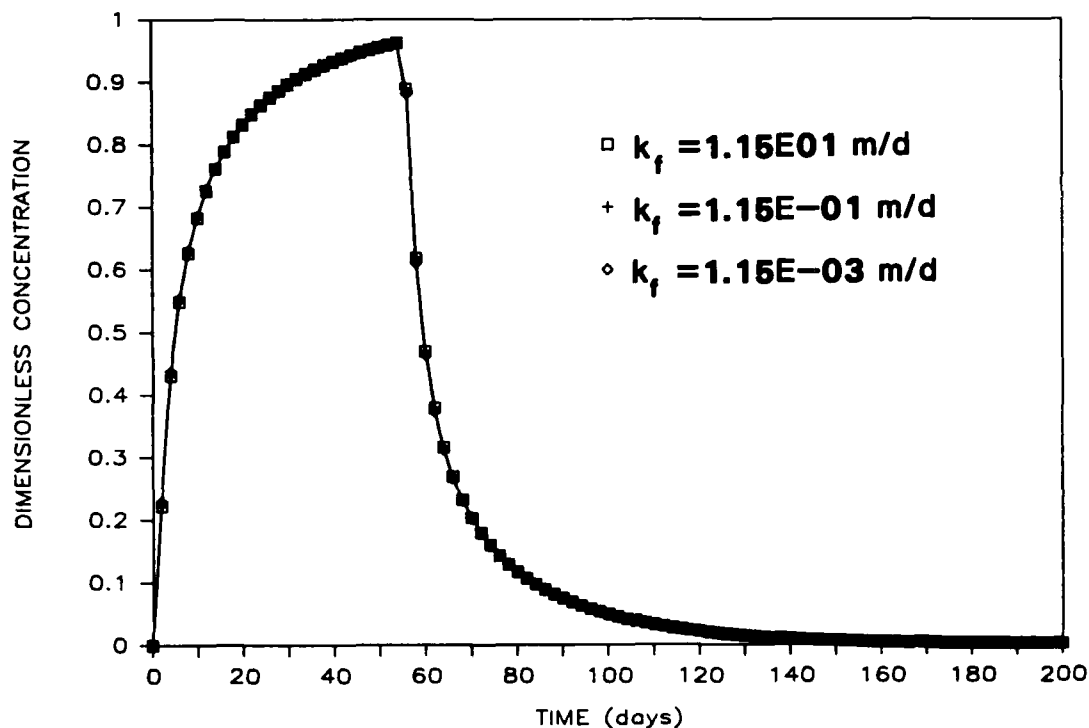
Figure 5.45. Simulations of breakthrough responses for various values of the external film transfer coefficient.

responses using the parameter values for tetrachloroethylene. The figure demonstrates that varying k_f over four orders of magnitude (i.e., increasing or decreasing by two orders of magnitude relative to the best estimate of $k_f = 0.115$ m/d) has no effect on the response. Thus, it is clear that the effect of external mass transfer resistance is negligible, for the parameter values under consideration.

Aquifer Heterogeneity

Roberts et al. (1986) postulated that a trend of increasing sorption in the direction of plume movement might lead to the observed loss of solute mass in solution and the deceleration of the solute plumes.

Durant (1986) measured the uptake of tetrachloroethylene by Borden aquifer material. The aquifer material was obtained from cores taken along the path of plume movement. A linear best fit of the measured values of tetrachloroethylene's distribution coefficient (K_d) versus plume travel distance along the path of tetrachloroethylene plume movement (i.e., cores S2-S5 of Durant, 1986) indicates an initial K_d, at the

132

area of solute injection, of 0.431 cm^3/g, with an increase of 0.016 cm^3/g per meter of plume travel distance. Assuming local equilibrium, these values of K_d can be converted to corresponding values of a retardation factor (R). Performing this conversion gives an increase in R from about 3.4 at the area of plume injection, to about 4.5 at a point 13 meters downgradient, where the center of mass of the tetrachloroethylene plume was located at the last synoptic sampling session. This increase in R is significantly less than the increase in R from 3 to 6 shown in Figure 8 of Roberts et al. (1986). The increase of 3 to 6 was estimated based on the deceleration of the tetrachloroethylene plume over the course of the experiment. A similarly large increase in R would be estimated based on the decrease in the total mass of tetrachloroethylene in solution during the experiment.

Thus, although a trend of increasing sorption in the direction of plume movement may contribute to the observed loss in mass and deceleration of the solute plumes, the extent of this contribution appears to be small when compared with the magnitude of the observed effect.

CONCLUSIONS

It has been shown that concentration distribution histories observed during a natural gradient experiment studying solute transport may be interpreted using a physical nonequilibrium model which hypothesizes advective/dispersive solute transport combined with solute diffusion into regions of immobile water. Parameter values obtained independently were shown inadequate to model spatial moment behavior. However, qualitative aspects of the spatial data were simulated by assuming hindered diffusion within spherical immobile regions, or a high sorption capacity within layered regions. The validity of these assumptions is currently under experimental investigation. Making the assumption of diffusion into layers of high sorption capacity, the model successfully simulated temporal behavior, using parameters obtained from spatial data only, thus providing an example of the complementarity of spatial and temporal behavior. This complementarity was also demonstrated by comparing results of spatial and temporal moment analyses at comparable time/distance scales. General transport behavior inferred from the spatial data could be inferred from the temporal data also.

Although a model based on the traditional assumptions of equilibrium advective/dispersive transport adequately describes many aspects of the observed behavior, several phenomena, such as the decline in organic solute mass in solution, the deceleration of the sorbing solute plumes, and the tailing of the near-field breakthrough responses, are not consistent with the equilibrium model.

Other models were also examined. In particular, numerical simulations were performed to assess the spatial moment behavior of solute concentration distributions predicted by models which assume nonlinear and/or hysteretic sorption. It was discovered that nonlinear sorption could also qualitatively explain the spatial and temporal moment behavior, though at the low concentrations under consideration, there was little experimental evidence of nonlinear sorption behavior. Nevertheless, nonlinear sorption does offer a possible explanation for the observed transport behavior as well.

CHAPTER 6

CONCLUSIONS AND RECOMMENDATIONS FOR FUTURE WORK

The focus of this work has been the development, analysis, and application of a three-dimensional solute transport model which incorporates the mechanism of diffusion into the traditional advection/dispersion transport equation. In this chapter, conclusions drawn from this study will be presented, and recommendations made for related future work.

The specific conclusions from this study can be summarized as follows:

1. Analytical solutions to various formulations of three-dimensional physical nonequilibrium solute transport models were presented. The solutions approach the well-known solution of the three-dimensional advection/dispersion equation in the limiting case where physical nonequilibrium is negligible.

2. Expressions for the spatial and temporal moments of concentration distributions simulated by the three-dimensional physical nonequilibrium models were derived, using a modified form of Aris' method of moments. Analysis of the moments showed:

   a. The zeroth spatial moment of the concentration distribution of solute in the mobile water region is a decreasing function of sampling time. Thus, the physical nonequilibrium models predict a loss of solute mass in the mobile region over time.

   b. Although the zeroth and first temporal moments are independent of the rate of solute transfer into the immobile water region, all the spatial moments are dependent on the mass transfer rate. One implication of this is that while the retardation factor obtained from temporal breakthrough response data is independent of sampling location, the retardation factor obtained from synoptic data is an increasing function of sampling time.

   c. In previous research, expressions for equilibrium model parameters which give responses equivalent to physical nonequilibrium models have been derived using temporal moment analyses. This work shows that the long time values of the

135

equivalent parameters obtained using spatial moment analyses are the same as the values obtained using temporal moments. Thus, the expressions derived previously, based on temporal distributions, are also applicable when considering spatial distributions.

3. Due to the effect of one-dimensional versus three-dimensional dispersion, the first temporal moment obtained using a one-dimensional model is greater than the first temporal moment obtained using a three-dimensional model given the same velocity. This is true for both equilibrium and nonequilibrium models.

4. At high values of Pe_m ($Pe_m > 50$), the effect of the boundary conditions on temporal simulations of the models becomes small.

5. Based on the equality of the first and second moments, equivalent parameters were defined for equilibrium, first-order rate, and diffusion models. The differences between the model simulations using these equivalent parameters are not large, and differentiating among these models based on measured breakthrough response data would be difficult, owing to parameter and measurement uncertainty. Differentiating between equilibrium and nonequilibrium models may be possible using spatial moment data, by taking advantage of qualitative differences between the spatial moment predictions of the two types of models.

6. Equilibrium and nonequilibrium models were applied to data obtained in a field experiment studying solute transport in an unconfined, sand aquifer. Although the experiment was conducted in a relatively homogeneous aquifer, and indeed, the equilibrium model adequately simulated much of what was observed, some aspects of the solute behavior could not be explained using the traditional equilibrium approach. The assumption of physical nonequilibrium offers a reasonable, simple explanation which qualitatively, and to some extent quantitatively, explains experimental observations.

The following topics are recommended for future research:

1. Development of methods to measure independently such parameter values as the diffusion rate constant and the ratio of mobile to total water content is crucial both for gaining further understanding of the diffusion mechanism and for using the models predictively.

136

2. Further improvement in the numerical method used to evaluate first and second spatial moments is needed. The method presented, though useful, is cumbersome.

3. The analytical solutions presented in this study are obviously limited in their application to real field situations, where conditions vary both spatially and temporally. The development of a three-dimensional numerical transport model which incorporates physical nonequilibrium mechanisms (using the analytical solutions presented here as developmental tools) would allow these physical nonequilibrium models to be generally applied to field transport situations.

4. The field experiment discussed in this study was conducted in a relatively homogeneous, sandy aquifer, where physical nonequilibrium effects were not expected to play an important role. Nevertheless, in this work, considerable evidence is presented indicating that physical nonequilibrium mechanisms may have impacted the solute transport. Conduct of a field experiment in an aquifer where physical nonequilibrium is expected to play a more dominant role (e.g., an aggregated or stratified medium) may shed more light on how this mechanism affects transport.

5. Based on the usefulness of the spatial data obtained from the Borden field experiment, it seems likely that further field studies will be conducted which attempt to produce corroborative data. The analysis of other transport models with respect to three-dimensional spatial concentration distributions (similar to the limited one-dimensional analysis conducted in Chapter 5 for the hysteretic and nonlinear sorption models) would assist in analyzing spatial data obtained from the field.

APPENDIX A

DERIVATION OF THE SOLUTION TO THE FIRST-ORDER RATE MODEL

FOR AN INSTANTANEOUS POINT SOURCE

Differential Equations

$$\frac{\partial C_m(x,y,z,t)}{\partial t} = D_x \frac{\partial^2 C_m}{\partial x^2} + D_y \frac{\partial^2 C_m}{\partial y^2} + D_z \frac{\partial^2 C_m}{\partial z^2} - v \frac{\partial C_m}{\partial x} - \beta \frac{\partial C_{1m}}{\partial t} \qquad (A-1)$$

$$\frac{\partial C_{1m}(x,y,z,t)}{\partial t} = \alpha(C_m - C_{1m}) \qquad (A-2)$$

Initial/Boundary Conditions

$$C_m(x,y,z,0) = M_3 \delta(x)\delta(y)\delta(z) \qquad (A-3a)$$

$$C_m(\pm\infty,y,z,t) = C_m(x,\pm\infty,z,t) = C_m(x,y,\pm\infty,t) = 0 \qquad (A-3b)$$

$$C_{1m}(x,y,z,0) = 0 \qquad (A-3c)$$

Basically following the methods of Lindstrom and Narasimhan (1973), who solved a similar set of equations, take the Laplace transform of (A-2), and then apply (A-3c) to obtain:

$$\overline{C_{1m}}(x,y,z,s) = \frac{\alpha}{s + \alpha} \overline{C_m}(x,y,z,s) \qquad (A-4)$$

where the Laplace transform, $\overline{F}(x,y,z,s)$, of a function, $F(x,y,z,t)$, is defined as:

$$\overline{F}(x,y,z,s) = \int_0^\infty e^{-st} F(x,y,z,t)dt \qquad (A-5)$$

Now, find the Laplace transform of (A-1), using (A-3a) and (A-4) to obtain the following differential equation:

$$D_x \frac{\partial^2 \overline{C_m}}{\partial x^2} + D_y \frac{\partial^2 \overline{C_m}}{\partial y^2} + D_z \frac{\partial^2 \overline{C_m}}{\partial z^2} - v \frac{\partial \overline{C_m}}{\partial x} + \left[s + \alpha\beta - \frac{\beta\alpha^2}{s + \alpha}\right] \overline{C_m}$$

$$= - M_3 \delta(x)\delta(y)\delta(z) \qquad (A-6)$$

138

with the boundary condition:

$$\overline{C_m}(\pm\infty,y,z,s) = \overline{C_m}(x,\pm\infty,z,s) = \overline{C_m}(x,y,\pm\infty,s) = 0 \qquad (A-7)$$

A solution to (A-6) and (A-7) may be found using Fourier transforms. Define $\hat{F}(p,y,z,s)$ as the Fourier transform of $\overline{F}(x,y,z,s)$ such that:

$$\hat{F}(p,y,z,s) = \int_{-\infty}^{\infty} \overline{F}(x,y,z,s)e^{-ipx}dx \qquad (A-8)$$

where p is the Fourier transform variable in the x-direction. Similarly, define q and u as the Fourier transform variables in the y- and z-directions, respectively. Taking the Fourier transform of (A-6) in the x-, y-, and z-directions, yields:

$$\hat{C}_m(p,q,u,s) = \frac{M_3}{D_x p^2 + D_y q^2 + D_z u^2 + vip + N^2} \qquad (A-9)$$

where

$$N^2 = s + \alpha\beta - \frac{\beta\alpha^2}{s + \alpha}$$

To obtain $\overline{C_m}(x,y,z,s)$, it is necessary to invert the Fourier transform. In the x-direction apply the equation:

$$\overline{F}(x,y,z,s) = \frac{1}{2\pi} \int_{-\infty}^{\infty} \hat{F}(p,y,z,s)\ e^{ipx}dp \qquad (A-10)$$

Analogous equations will be used to invert the Fourier transformed solution in the y- and z-directions.

Simplifying (A-9) to read:

$$\hat{C}_m(p,q,u,s) = \frac{A}{p^2 + ep + a^2} \qquad (A-11)$$

where

$$e = \frac{vi}{D_x}$$

$$a^2 = \frac{D_y q^2 + D_z u^2 + N^2}{D_x}$$

and

$$A = \frac{M_3}{D_x}$$

and using the definite integrals (Gradshteyn and Ryzhik, 1980):

$$\int_{-\infty}^{\infty} \frac{A \cos px \, dp}{p^2 + ep + a^2} = \frac{A \pi \exp[-x(a^2 - \frac{e^2}{4})^{1/2}] \cos \frac{ex}{2}}{(a^2 - \frac{e^2}{4})^{1/2}} \qquad \text{(A-12a)}$$

$$\int_{-\infty}^{\infty} \frac{A \sin px}{p^2 + ep + a^2} \, dp = \frac{-A \pi \exp[-x(a^2 - \frac{e^2}{4})^{1/2}] \sin \frac{ex}{2}}{(a^2 - \frac{e^2}{4})^{1/2}} \qquad \text{(A-12b)}$$

for $x > 0$, it is found that the Fourier inverse of (A-9) in the x-direction is:

$$\hat{C}_m(x,q,u,s,) = \frac{M_3 \exp(vx/2D_x - c|x|)}{2cD_x} \qquad \text{(A-13)}$$

where

$$c = (\frac{v^2}{4D_x^2} + a^2)^{1/2}$$

To obtain the inverse Fourier transform of (A-13) in the y-direction, simplify (A-13) to read:

$$\hat{C}_m(x,q,u,s) = \frac{D}{(q^2 + h^2)^{1/2}} \exp[-B(q^2 + h^2)^{1/2}] \qquad \text{(A-14)}$$

where

$$D = \frac{M_3 \exp(vx/2D_x)}{2(D_x D_y)^{1/2}}$$

$$B = |x|(\frac{D_y}{D_x})^{1/2}$$

and

140

$$h^2 = \frac{v^2}{4D_x D_y} + \frac{N^2}{D_y} + \frac{D_z u^2}{D_y}$$

Applying the y-direction analog of Eq. A-10 and using the definite integral (Gradshteyn and Ryzhik, 1980):

$$\int_0^\infty \frac{\exp[-B(q^2 + h^2)^{1/2}]}{(q^2 + h^2)^{1/2}} \cos qy \, dq = K_o[h(y^2 + B^2)^{1/2}] \tag{A-15}$$

gives

$$\hat{C}_m(x,y,u,s) = \frac{D}{\pi} K_o[h(y^2 + x^2 \frac{D_y}{D_x})^{1/2}] \tag{A-16}$$

To obtain the inverse Fourier transform of (A-16) in the z-direction, once again follow the same basic method. Simplify (A-16) to read

$$\hat{C}_m(x,y,u,s) = \frac{D}{\pi} K_o[E(D_z)^{1/2}(r^2 + k^2)^{1/2}] \tag{A-17}$$

where

$$k^2 = \frac{v^2}{4D_x D_z} + \frac{N^2}{D_z} \quad , \quad E = (\frac{x^2}{D_x} + \frac{y^2}{D_y})^{1/2}$$

Apply the z-direction analog of (A-10), using the definite integral (Gradshteyn and Ryzhik, 1980)

$$\int_0^\infty K_o[E(D_z)^{1/2}(r^2 + k^2)^{1/2}] \cos rz \, dr$$

$$= \frac{\pi}{2(E^2 D_z + z^2)^{1/2}} \exp[-k(E^2 D_z + z^2)^{1/2}] \tag{A-18}$$

to find

$$\overline{C}_m(x,y,z,s) = \frac{F}{G} \exp[-G(\frac{v^2}{4D_x} + N^2)^{1/2}] \tag{A-19}$$

where

$$F = \frac{M_3 \exp(vx/2D_x)}{4\pi(D_x D_y D_z)^{1/2}}$$

141

$$G = \left(\frac{x^2}{D_x} + \frac{y^2}{D_y} + \frac{z^2}{D_z}\right)^{1/2}$$

The inverse Laplace transform of (A-19) can be obtained using the methods of Lindstrom and Narasimhan (1973). The final result is

$$C_m(x,y,z,t) = \exp(-\alpha\beta t)G(x,y,z,t) + \alpha \int_0^t H(t,\tau)G(x,y,z,\tau)d\tau \quad (A-20)$$

where

$$H(t,\tau) = \exp\left(-\alpha(t-\tau) - \alpha\beta\tau\right)\beta\tau \frac{I_1\left[2\alpha\left(\beta(t-\tau)\tau\right)^{1/2}\right]}{\left(\beta(t-\tau)\tau\right)^{1/2}}$$

and

$$G(x,y,z,\tau) = \frac{M_3 \exp\left[-\frac{(x-vt)^2}{4D_x t} - \frac{y^2}{4D_y t} - \frac{z^2}{4D_z t}\right]}{8(\pi t)^{3/2}\left(D_x D_y D_z\right)^{1/2}}$$

$\vdots$

APPENDIX B

DERIVATION OF THE SOLUTION TO THE DIFFUSION MODEL
WITH SPHERICAL IMMOBILE ZONES

Differential Equations

$$\frac{\partial C_m(x,y,z,t)}{\partial t} = D_x \frac{\partial^2 C_m}{\partial x^2} - D_y \frac{\partial^2 C_m}{\partial y^2} - D_z \frac{\partial^2 C_m}{\partial z^2} - v \frac{\partial C_m}{\partial x} - \beta \frac{\partial C_{im}}{\partial t} \qquad (B-1)$$

$$\frac{\partial C_a(r,x,y,z,t)}{\partial t} = \frac{D_e}{r^2} \frac{\partial}{\partial r}\left(r^2 \frac{\partial C_a}{\partial r}\right) \qquad (B-2)$$

$$C_{im}(x,y,z,t) = \frac{3}{b^3} \int_0^b r^2 C_a(r,x,y,z,t)dr \qquad (B-3)$$

Initial/Boundary Conditions

$$C_m(x,y,z,0) = M_3 \delta(x)\delta(y)\delta(z) \qquad (B-4a)$$

$$C_m(\pm\infty,y,z,t) = C_m(x,\pm\infty,z,t) = C_m(x,y,\pm\infty,t) = 0 \qquad (B-4b)$$

$$C_a(r,x,y,z,0) = C_{im}(x,y,z,0) = 0 \qquad (B-4c)$$

$$C_a(0,x,y,z,t) \neq \infty \qquad (B-4d)$$

$$C_a(b,x,y,z,t) = C_m(x,y,z,t) \qquad (B-4e)$$

Following the methods of van Genuchten et al., (1984), take the Laplace transform of (B-2), applying initial condition (B-4c) to obtain the following ordinary differential equation:

$$\frac{d^2\overline{C_a}(r,x,y,z,s)}{dr^2} + \frac{2}{r} \frac{d\overline{C_a}}{dr} - \frac{s}{D_e} \overline{C_a} = 0 \qquad (B-5)$$

Transforming boundary conditions (B-4d) and (B-4e) gives

$$\overline{C_a}(0,x,y,z,s) \neq \infty \qquad (B-6a)$$

$$\overline{C_a}(b,x,y,z,s) = \overline{C_m}(x,y,z,s) \qquad (B-6b)$$

143

Solve the above ordinary differential equation with boundary conditions to find

$$\overline{C_a}(r,x,y,z,s) = \frac{\overline{C_m}(x,y,z,s)}{i_0(\omega b)} i_0(\omega r) \qquad (B-7)$$

where

$$\omega = \sqrt{\frac{s}{D_e}}$$

Now take the Laplace transform of (B-3)

$$\overline{C_{im}}(x,y,z,s) = \frac{3}{b^3} \int_0^b r^2 \overline{C_a}(r,x,y,z,s)dr \qquad (B-8)$$

and substitute (B-7) into (B-8) to obtain

$$\overline{C_{im}}(x,y,z,s) = \frac{3\overline{C_m}(x,y,z,s)i_1(\omega b)}{\omega b i_0(\omega b)} \qquad (B-9)$$

Take the Laplace transform of (B-1), using (B-9) and initial conditions (B-4a) and (B-4c) to get the following differential equation

$$D_x \frac{\partial^2 \overline{C_m}}{\partial x^2} + D_y \frac{\partial^2 \overline{C_m}}{\partial y^2} + D_z \frac{\partial^2 \overline{C_m}}{\partial z^2} - v \frac{\partial \overline{C_m}}{\partial x} - \left[\frac{3\beta s i_1(\omega b)}{\omega b i_0(\omega b)} + s\right] \overline{C_m}$$

$$= - M_3 \delta(x)\delta(y)\delta(z) \qquad (B-10)$$

Transforming boundary condition (B-4b) gives

$$\overline{C_m}(\pm\infty,y,z,s) = \overline{C_m}(x,\pm\infty,z,s) = \overline{C_m}(x,y,\pm\infty,s) = 0 \qquad (B-11)$$

A solution to (B-10) and (B-11) may be found using Fourier transforms. As in Appendix A, the Fourier transformed solution is

$$\hat{C}_m(p,q,u,s) = \frac{M_3}{D_x p^2 + D_y q^2 + D_z u^2 + vip + N^2} \qquad (B-12)$$

where

$$N^2 = \frac{3\beta s i_1(\omega b)}{\omega b i_0(\omega b)} + s$$

Note the similarity between Eq. B-12 and Eq. A-9. To obtain $\overline{C_m}(x,y,z,s)$, the methods of inverting the Fourier transform in the x-, y-, and z-directions used in Appendix A are directly applicable. The result is

$$\overline{C_m}(x,y,z,s) = \frac{F}{G} \exp[-G\Omega(s)] \tag{B-13}$$

where

$$F = \frac{M_3 \exp(vx/2D_x)}{4\pi(D_x D_y D_z)^{1/2}}$$

$$G = \left(\frac{x^2}{D_x} + \frac{y^2}{D_y} + \frac{z^2}{D_z}\right)^{1/2}$$

$$\Omega(s) = \left(\frac{v^2}{4D_x} + N^2\right)^{1/2}$$

To obtain the inverse Laplace transform of (B-13), the methods used by Rasmuson and Neretnieks (1980), and van Genuchten et al. (1984) may be followed directly. The final result, for the response to an instantaneous point source, is

$$C_m(x,y,z,t) =$$

$$\frac{M_3 D_e \exp(vx/2D_x)}{b^2 \pi^2 (D_x D_y D_z)^{1/2} G} \int_0^\infty \lambda \exp(-GZ_p) \cos\left(\frac{2D_e \lambda^2 t}{b^2} - GZ_m\right) d\lambda \tag{B-14}$$

where

$$G = \left(\frac{x^2}{D_x} + \frac{y^2}{D_y} + \frac{z^2}{D_z}\right)^{1/2}$$

$$Z_p = \left(\frac{r_p + \Omega_1}{2}\right)^{1/2} \quad , \quad Z_m = \left(\frac{r_p - \Omega_1}{2}\right)^{1/2} \quad , \quad r_p = (\Omega_1^2 + \Omega_2^2)^{1/2}$$

$$\Omega_1 = \frac{(v)^2}{4D_x} + \frac{3D_e \beta}{b^2} \psi_1 \quad , \quad \Omega_2 = \frac{2D_e \lambda^2}{b^2} + \frac{3D_e \beta}{b^2} \psi_2$$

$$\psi_1 = \frac{\lambda(\text{Sinh } 2\lambda + \text{Sin } 2\lambda)}{\text{Cosh } 2\lambda - \text{Cos } 2\lambda} - 1 \quad , \quad \psi_2 = \frac{\lambda(\text{Sinh } 2\lambda - \text{Sin } 2\lambda)}{\text{Cosh } 2\lambda - \text{Cos } 2\lambda}$$

APPENDIX C

DERIVATION OF ABSOLUTE SPATIAL MOMENTS

FOR THREE SOLUTE TRANSPORT MODELS

Local Equilibrium Model

$$\frac{\partial C}{\partial t} = D_x \frac{\partial^2 C}{\partial x^2} + D_y \frac{\partial^2 C}{\partial y^2} + D_z \frac{\partial^2 C}{\partial z^2} - v \frac{\partial C}{\partial x} \qquad (C-1)$$

$$C(x,y,z,0) = M_3 \delta(x)\delta(y)\delta(z) \qquad (C-2)$$

$$C(\pm\infty,y,z,t) = C(x,\pm\infty,z,t) = C(x,y,\pm\infty,t) = 0 \qquad (C-3)$$

Taking the Fourier transform of the equation and initial condition, where p, q, u are the Fourier transform variables in the x-, y-, z-directions, respectively, yields:

$$\frac{\partial \hat{C}(p,q,u,t)}{\partial t} = D_x i^2 p^2 \hat{C}(p,q,u,t) + D_y i^2 q^2 \hat{C}(p,q,u,t)$$

$$+ D_z i^2 u^2 \hat{C}(p,q,u,t) - vip\hat{C}(p,q,u,t) \qquad (C-4a)$$

$$\hat{C}(p,q,u,0) = M_3 \qquad (C-4b)$$

Solving for $\hat{C}(p,q,u,t)$ is straightforward:

$$\hat{C}(p,q,u,t) = M_3 e^{-(D_x p^2 + D_y q^2 + D_z u^2 + vip)t} \qquad (C-5)$$

Applying the expression

$$m_{jk\ell} = i^{j+k+\ell} \lim_{\substack{p\to 0 \\ q\to 0 \\ u\to 0}} \frac{d^j}{dp^j} \left\{ \frac{d^k}{dq^k} \left[\frac{d^\ell \hat{C}(p,q,u,t)}{du^\ell} \right] \right\} \qquad (C-6)$$

requires the differentiation of $\hat{C}(p,q,u,t)$ with respect to p, q, and u. This operation is easily done. Taking the limit as the transform variables approach 0, gives:

146

$$m_{000} = M_3$$

$$m_{100} = M_3 \, vt$$

$$m_{200} = M_3[2D_x t + v^2 t^2]$$

$$m_{010} = m_{001} = 0 \tag{C-7}$$

$$m_{110} = m_{101} = m_{011} = 0$$

$$m_{020} = M_3[2D_y t]$$

$$m_{002} = M_3[2D_z t]$$

First-Order Rate Model

$$\frac{\partial C_m}{\partial t} = D_x \frac{\partial^2 C_m}{\partial x^2} + D_y \frac{\partial^2 C_m}{\partial y^2} + D_z \frac{\partial^2 C_m}{\partial z^2} - v \frac{\partial C_m}{\partial x} - \beta \frac{\partial C_{im}}{\partial t} \tag{C-8}$$

$$\frac{\partial C_{im}}{\partial t} = \alpha(C_m - C_{im}) \tag{C-9}$$

$$C_m(x,y,z,0) = M_3 \delta(x)\delta(y)\delta(z) \tag{C-10a}$$

$$C_{im}(x,y,z,0) = 0 \tag{C-10b}$$

$$C_m(\pm\infty,y,z,t) = C_m(x,\pm\infty,z,t) = C_m(x,y,\pm\infty,t) = 0 \tag{C-10c}$$

Following Appendix A, these equations may be solved in the Laplace and Fourier domains, to obtain

$$\hat{C}_m(p,q,u,s) = \frac{M_3}{D_x p^2 + D_y q^2 + D_z u^2 + vip + s + \alpha\beta - \dfrac{\alpha^2\beta}{s + \alpha}} \tag{C-11}$$

(see Eq. A-9, Appendix A).

The inverse Laplace transform of this equation needs to be derived. Simplify, by defining

$$A = D_x p^2 + D_y q^2 + D_z u^2 + v_1 p - \alpha + \alpha\beta$$

so

$$\hat{C}_m(p,q,u,s) = \frac{M_3}{A + s + \alpha - \frac{\alpha^2 \beta}{s + \alpha}} \qquad (C-12)$$

Multiply the numerator and denominator of the right-hand side of Eq. C-12 by $s + \alpha$, to obtain

$$\hat{C}_m(p,q,u,s) = \frac{M_3(s + \alpha)}{(s + \alpha)^2 + A(s + \alpha) - \alpha^2 \beta} \qquad (C-13)$$

Defining E and F as the roots of the quadratic equation in the denominator of the right-hand side of Eq. C-13 gives:

$$\hat{C}_m(p,q,u,s) = \frac{M_3(s + \alpha)}{[(s + \alpha) - E][(s + \alpha) - F]}$$

Use the following properties of Laplace transforms

$$L^{-1}[F(s + \alpha)] = e^{-\alpha t} f(t)$$

and

$$L^{-1}\left[\frac{s}{(s - E)(s - F)}\right] = \frac{F e^{Ft} - E e^{Et}}{F - E}$$

to find

$$\hat{C}_m(p,q,u,t) = e^{-\alpha t}\left[\frac{F e^{Ft} - E e^{Et}}{F - E}\right] \qquad (C-14)$$

where E and F are functions of A, α, and β.

Differentiation of Eq. C-14 is straightforward, though tedious. Apply Eq. C-6, to find:

$$m_{000} = M_3\left[\frac{1 + \beta \, e^{-\alpha t(1+\beta)}}{1 + \beta}\right]$$

$$m_{100} = \frac{M_3 v t}{(1 + \beta)^2}\left[1 + \beta^2 \, e^{-\alpha t(1+\beta)}\right] + \frac{2M_3 v \beta}{\alpha(1 + \beta)^3}\left[1 - e^{-\alpha t(1+\beta)}\right]$$

$$m_{200} = \frac{2M_3 D_x t}{(1 + \beta)^2}\left[1 + \beta^2 \, e^{-\alpha t(1+\beta)}\right] + \frac{4M_3 D_x \beta}{\alpha(1 + \beta)^3}\left[1 - e^{-\alpha t(1+\beta)}\right]$$

$$+ \frac{v^2 t^2 M_3}{(1 + \beta)^3}\left[1 + \beta^3 \, e^{-\alpha t(1+\beta)}\right] + \frac{6v^2 \beta(\beta - 1)M_3}{\alpha^2(1 + \beta)^5}\left[1 - e^{-\alpha t(1+\beta)}\right]$$

$$+ \frac{6\beta v^2 t M_3}{\alpha(1 + \beta)^4}\left[1 - \beta \, e^{-\alpha t(1+\beta)}\right] \tag{C-15}$$

$$m_{010} = m_{001} = 0$$

$$m_{110} = m_{101} = m_{011} = 0$$

$$m_{020} = \frac{2M_3 D_y t}{(1 + \beta)^2}\left[1 + \beta^2 \, e^{-\alpha t(1+\beta)}\right] + \frac{4M_3 D_y \beta}{\alpha(1 + \beta)^3}\left[1 - e^{-\alpha t(1+\beta)}\right]$$

$$m_{002} = \frac{2M_3 D_z t}{(1 + \beta)^2}\left[1 + \beta^2 \, e^{-\alpha t(1+\beta)}\right] + \frac{4M_3 D_z \beta}{\alpha(1 + \beta)^3}\left[1 - e^{-\alpha t(1+\beta)}\right]$$

Diffusion Models

$$\frac{\partial C_m}{\partial t} = D_x \frac{\partial^2 C_m}{\partial x^2} + D_y \frac{\partial^2 C_m}{\partial y^2} + D_z \frac{\partial^2 C_m}{\partial z^2} - v \frac{\partial C_m}{\partial x} - \beta \frac{\partial C_{1m}}{\partial t} \tag{C-16}$$

$$\frac{\partial C_a}{\partial t} = \frac{D_e}{r^\nu} \frac{\partial}{\partial r}\left(r^\nu \frac{\partial C_a}{\partial r}\right) \tag{C-17}$$

$$C_{1m} = \frac{\nu + 1}{b^{\nu+1}} \int_0^b r^\nu C_a \, dr \tag{C-18}$$

$$C_m(x,y,z,0) = M_3 \delta(x)\delta(y)\delta(z) \tag{C-19a}$$

$$C_a(r,x,y,z,0) = C_{1m}(x,y,z,0) = 0 \tag{C-19b}$$

149

$$C_m(\pm\infty,y,z,t) = C_m(x,\pm\infty,z,t) = C_m(x,y,\pm\infty,t) = 0 \qquad \text{(C-19c)}$$

$$C_a(0,x,y,z,t) \neq \infty \qquad \text{(C-19d)}$$

$$C_a(b,x,y,z,t) = C_m(x,y,z,t) \qquad \text{(C-19e)}$$

Following Appendix B, these equations may be solved in the Laplace and Fourier domains, to obtain

$$\hat{C}_m(p,q,u,s) = \frac{M_3}{D_x p^2 + D_y q^2 + D_z u^2 + vip + N^2} \qquad \text{(C-20)}$$

where

$$N^2 = \frac{3\beta s \; i_1(\omega b)}{\omega b \; i_0(\omega b)} + s \qquad \text{for the spherical diffusion model}$$

$$N^2 = \frac{2\beta s \; I_1(\omega b)}{\omega b \; I_0(\omega b)} + s \qquad \text{for the cylindrical diffusion model}$$

$$N^2 = \frac{\beta s \; \text{Sinh} \; \omega b}{\omega b \; \text{Cosh} \; \omega b} + s \qquad \text{for the layered diffusion model}$$

To derive the inverse Laplace transform of Eq. C-20, it is necessary to apply Bromwich's complex inversion formula:

$$\hat{C}_m(p,q,u,t) = \frac{1}{2\pi i} \int_{\alpha-i\infty}^{\alpha+i\infty} e^{st} \; \hat{C}_m \; ds$$

Using the same technique as Rosen (1954), Rasmuson and Neretnieks (1980), and van Genuchten et al. (1984), who derived similar inversions, it can be shown that

$$\hat{C}_m(p,q,u,t) = \frac{M_3}{2\pi i} \lim_{\epsilon \to 0} \left\{ \int_{-i\infty}^{-i\epsilon} + \int_{i\epsilon}^{i\infty} + \int_{-i\epsilon}^{i\epsilon} \right\} \frac{e^{st}}{\Omega(s)} \; ds \qquad \text{(C-21)}$$

where $\Omega(s) = D_x p^2 + D_y q^2 + D_z u^2 + vip + N^2$.

Perform the above integration, basically following the methods of Rasmuson and Neretnieks (1980) and van Genuchten et al. (1984), to find:

$$\hat{C}_m(p,q,u,t) =$$

$$\lim_{\varepsilon \to 0} \left\{ \frac{M_3}{2(1+\beta)} + \frac{4M_3 D_e}{\pi b^2} \int_{b\sqrt{\frac{\varepsilon}{2D_e}}}^{\infty} \lambda \left[\frac{\Omega_1 \cos \frac{2D_e \lambda^2 t}{b^2} + \Omega_2 \sin \frac{2D_e \lambda^2 t}{b^2}}{\Omega_1^2 + \Omega_2^2} \right] d\lambda \right\}$$

where

$$\Omega_1 = D_x p^2 + D_y q^2 + D_z u^2 + \frac{3D_e \beta}{b^2} \psi_1$$

$$\Omega_2 = vp + \frac{2D_e \lambda^2}{b^2} + \frac{3D_e \beta}{b^2} \psi_2$$

and ψ_1 and ψ_2 are as defined in Chapter 2 for the different immobile region geometries. As p, q, and u approach zero, Ω_1 and Ω_2 are as defined in Appendix B (with v = 0).

Use Eq. C-6, to write

$$m_{000} = \lim_{\substack{p \to 0 \\ q \to 0 \\ u \to 0}} \hat{C}_m(p,q,u,t) = \lim_{\varepsilon \to 0} \left\{ \frac{M_3}{2(1+\beta)} \right.$$

$$\left. + \frac{4M_3 D_e}{\pi b^2} \int_{b\sqrt{\frac{\varepsilon}{2D_e}}}^{\infty} \lambda \left[\frac{\Omega_1 \cos \frac{2D_e \lambda^2 t}{b^2} + \Omega_2 \sin \frac{2D_e \lambda^2 t}{b^2}}{\Omega_1^2 + \Omega_2^2} \right] d\lambda \right\} \quad \text{(C-22)}$$

Differentiating Eq. C-22 by applying Liebnitz' rule, and then applying Eq. C-6, leads to the following expressions:

$$m_{100} = \lim_{\varepsilon \to 0} \left\{ \frac{M_3 v}{\pi \varepsilon (1+\beta)^2} + \frac{M_3 vt}{2(1+\beta)^2} + \frac{M_3 v\beta}{a(1+\beta)^3} \right.$$

$$\left. + \frac{4M_3 v D_e}{\pi b^2} \int_{b\sqrt{\frac{\varepsilon}{2D_e}}}^{\infty} \lambda \left[\frac{(\Omega_1^2 - \Omega_2^2)\cos \frac{2D_e \lambda^2 t}{b^2} + 2\Omega_1 \Omega_2 \sin \frac{2D_e \lambda^2 t}{b^2}}{(\Omega_1^2 + \Omega_2^2)^2} \right] d\lambda \right\}$$

151

$$m_{200} = \lim_{\epsilon \to 0} \left\{ \frac{2M_3 D_x}{\pi \epsilon (1+\beta)^2} + \frac{M_3 D_x t}{(1+\beta)^2} + \frac{2M_3 D_x \beta}{a(1+\beta)^3} \right.$$

$$+ \frac{8M_3 D_x D_e}{\pi b^2} \int_{b\sqrt{\frac{\epsilon}{2D_e}}}^{\infty} \lambda \left[\frac{(\Omega_1^2 - \Omega_2^2)\cos \frac{2D_e \lambda^2 t}{b^2} + 2\Omega_1 \Omega_2 \sin \frac{2D_e \lambda^2 t}{b^2}}{(\Omega_1^2 + \Omega_2^2)^2} \right] d\lambda$$

$$+ \frac{2M_3 v^2 t}{\pi \epsilon (1+\beta)^3} + \frac{M_3 v^2 t^2}{2(1+\beta)^3} + \frac{6M_3 \beta^2 v^2}{a^2(1+\beta)^5} + \frac{6M_3 v^2 \beta}{\pi \epsilon a(1+\beta)^4}$$

$$+ \frac{3M_3 v^2 t\beta}{a(1+\beta)^4} - \frac{3M_3 v^2}{c(1+\beta)^4}$$

$$\left. + \frac{8M_3 v^2 D_e}{\pi b^2} \int_{b\sqrt{\frac{\epsilon}{2D_e}}}^{\infty} \lambda \left[\frac{(\Omega_1^3 - 3\Omega_1 \Omega_2^2)\cos \frac{2D_e \lambda^2 t}{b^2} - (\Omega_1^3 - 3\Omega_1^2 \Omega_2) \sin \frac{2D_e \lambda^2 t}{b^2}}{(\Omega_1^2 + \Omega_2^2)^3} \right] d\lambda \right\}$$

where for spherical diffusion:

$$a = \frac{15D_e}{b^2} \quad , \quad c = \frac{315D_e^2}{2b^4 \beta}$$

for cylindrical diffusion:

$$a = \frac{8D_e}{b^2} \quad , \quad c = \frac{48D_e^2}{b^4 \beta}$$

for layered diffusion:

$$a = \frac{3D_e}{b^2} \quad , \quad c = \frac{15D_e^2}{2b^4 \beta}$$

$$m_{010} = m_{001} = 0$$

$$m_{110} = m_{101} = m_{011} = 0$$

$$m_{020} = \lim_{\epsilon \to 0} \left\{ \frac{2M_3 D_y}{\pi \epsilon (1+\beta)^2} + \frac{M_3 D_y t}{(1+\beta)^2} + \frac{2M_3 D_y \beta}{a(1+\beta)^3} \right.$$

$$\left. + \frac{8M_3 D_y D_e}{\pi b^2} \int_{b\sqrt{\frac{\epsilon}{2D_e}}}^{\infty} \lambda \left[\frac{(\Omega_1^2 - \Omega_2^2)\cos \frac{2D_e \lambda^2 t}{b^2} + 2\Omega_1 \Omega_2 \sin \frac{2D_e \lambda^2 t}{b^2}}{(\Omega_1^2 + \Omega_2^2)^2} \right] d\lambda \right\}$$

$$m_{002} = \lim_{\epsilon \to 0} \left\{ \frac{2M_3 D_z}{\pi \epsilon (1+\beta)^2} + \frac{M_3 D_z t}{(1+\beta)^2} + \frac{2M_3 D_z \beta}{a(1+\beta)^3} \right.$$

$$\left. + \frac{8M_3 D_z D_e}{\pi b^2} \int_{b\sqrt{\frac{\epsilon}{2D_e}}}^{\infty} \lambda \left[\frac{(\Omega_1^2 - \Omega_2^2)\cos \frac{2D_e \lambda^2 t}{b^2} + 2\Omega_1 \Omega_2 \sin \frac{2D_e \lambda^2 t}{b^2}}{(\Omega_1^2 + \Omega_2^2)^2} \right] d\lambda \right\}$$

APPENDIX D

DERIVATION OF ABSOLUTE SPATIAL MOMENTS OF THE
IMMOBILE REGION SOLUTE DISTRIBUTION

First-Order Rate Model

In Appendix A it was found

$$\overline{C_{im}}(x,y,z,s) = \frac{\alpha}{s+\alpha}\,\overline{C_m}(x,y,z,s) \tag{D-1}$$

Take the Fourier transform of (D-1):

$$\hat{C}_{im}(p,q,u,s) = \frac{\alpha}{s+\alpha}\,\hat{C}_m(p,q,u,s) \tag{D-2}$$

In Appendix C it was found

$$\hat{C}_m(p,q,u,s) = \frac{M_3(s+\alpha)}{[(s+\alpha)-E][(s+\alpha)-F]} \tag{D-3}$$

Combining (D-2) and (D-3):

$$\hat{C}_{im}(p,q,u,s) = \frac{M_3\alpha}{[(s+\alpha)-E][(s+\alpha)-F]} \tag{D-4}$$

Follow Appendix C to invert the Laplace transform, to obtain

$$\hat{C}_{im}(p,q,u,t) = \alpha\,e^{-\alpha t}\left[\frac{e^{Ft}-e^{Et}}{F-E}\right] \tag{D-5}$$

Finally, differentiate Eq. D-5 and apply Eq. 3-23 to derive the following absolute moments:

$$n_{000} = \frac{M_3\beta[1-e^{-\alpha t(1+\beta)}]}{1+\beta}$$

$$n_{100} = \frac{M_3 v t \beta[1-\beta\,e^{-\alpha t(1+\beta)}]}{(1+\beta)^2} + \frac{M_3 v \beta(\beta-1)[1-e^{-\alpha t(1+\beta)}]}{\alpha(1+\beta)^3}$$

$$n_{010} = n_{001} = 0$$

154

Diffusion Models

Follow Appendix B, to find

$$\overline{C_{1m}}(x,y,z,s) = \frac{[N^2 - s]}{s\beta} \overline{C_m}(x,y,z,s) \tag{D-6}$$

where

$$N^2 = \frac{3\beta s\ i_1(\omega b)}{\omega b\ i_0(\omega b)} + s \qquad \text{for the spherical diffusion model}$$

$$N^2 = \frac{2\beta s\ I_1(\omega b)}{\omega b\ I_0(\omega b)} + s \qquad \text{for the cylindrical diffusion model}$$

$$N^2 = \frac{\beta s\ \text{Sinh}(\omega b)}{\omega b\ \text{Cosh}(\omega b)} + s \qquad \text{for the layered diffusion model}$$

Take the Fourier transform of (D-6):

$$\hat{C}_{1m}(p,q,u,s) = \frac{[N^2 - s]}{s\beta} \hat{C}_m(p,q,u,s) \tag{D-7}$$

In Appendix B it was found

$$\hat{C}_m(p,q,u,s) = \frac{M_3}{D_x p^2 + D_y q^2 + D_z u^2 + v1p + N^2} \tag{D-8}$$

Combining (D-7) and (D-8) yields:

$$\hat{C}_{1m}(p,q,u,s) = \frac{M_3(N^2 - s)}{\beta s\left(D_x p^2 + D_y q^2 + D_z u^2 + v1p + N^2\right)} \tag{D-9}$$

Defining:

$$\Omega(s) = D_x p^2 + D_y q^2 + D_z u^2 + v1p + N^2$$

gives:

$$\hat{C}_{1m}(p,q,u,s) = \frac{M_3\left[\Omega(s) - D_x p^2 - D_y q^2 - D_z u^2 - v1p - s\right]}{\beta s\ \Omega(s)} \tag{D-10}$$

Follow Appendix C to obtain the inverse Laplace transform of $\hat{C}_{1m}(p,q,u,s)$, using Bromwich's complex inversion formula, to find:

$$\hat{C}_{im}(p,q,u,t) = \lim_{\varepsilon \to 0} \left\{ \frac{M_3}{\beta} - \frac{M_3 At}{2\beta(1+\beta)} - \frac{M_3 A}{\beta(1+\beta)\pi\varepsilon} \right.$$

$$- \frac{M_3 A}{2a(1+\beta)^2} + \frac{2M_3 A}{\pi\beta} \int_{b\sqrt{\frac{\varepsilon}{2D_e}}}^{\infty} \left[\frac{\Omega_2 \, \text{Cos} \, \frac{2D_e \lambda^2 t}{b^2} - \Omega_1 \, \text{Sin} \, \frac{2D_e \lambda^2 t}{b^2}}{\lambda(\Omega_1^2 + \Omega_2^2)} \right] d\lambda$$

$$\left. - \frac{M_3}{2\beta(1+\beta)} - \frac{4M_3 D_e}{\pi \, b^2 \beta} \int_{b\sqrt{\frac{\varepsilon}{2D_e}}}^{\infty} \lambda \left[\frac{\Omega_1 \, \text{Cos} \, \frac{2D_e \lambda^2 t}{b^2} + \Omega_2 \, \text{Sin} \, \frac{2D_e \lambda^2 t}{b^2}}{\Omega_1^2 + \Omega_2^2} \right] d\lambda \right\} \qquad \text{(D-11)}$$

where $A = D_x p^2 + D_y q^2 + D_z u^2 + vip$

$$a = \frac{\nu(\nu + 2)D_e}{b^2} \qquad \text{where} \quad \begin{array}{l} \nu = 3 \quad \text{for spherical diffusion} \\ \nu = 2 \quad \text{for cylindrical diffusion} \\ \nu = 1 \quad \text{for layered diffusion} \end{array}$$

and Ω_1 and Ω_2 are defined in Appendix C. Differentiating and applying Eq. 3-23 leads to:

$$n_{000} = \lim_{\varepsilon \to 0} \left\{ M_3 - \frac{M_3}{2(1+\beta)} - \frac{4M_3 D_e}{\pi \, b^2} \int_{b\sqrt{\frac{\varepsilon}{2D_e}}}^{\infty} \lambda \left[\frac{\Omega_1 \, \text{Cos} \, \frac{2D_e \lambda^2 t}{b^2} + \Omega_2 \, \text{Sin} \, \frac{2D_e \lambda^2 t}{b^2}}{\Omega_1^2 + \Omega_2^2} \right] d\lambda \right\}$$

$$n_{100} = \lim_{\varepsilon \to 0} \left\{ \frac{M_3 v t \beta}{2(1+\beta)^2} + \frac{M_3 v \beta}{\pi\varepsilon(1+\beta)^2} + \frac{M_3 v \beta(\beta-1)}{2a(1+\beta)^3} \right.$$

$$- \frac{2vM_3}{\pi} \int_{b\sqrt{\frac{\varepsilon}{2D_e}}}^{\infty} \left[\frac{\Omega_2 \, \text{Cos} \, \frac{2D_e \lambda^2 t}{b^2} - \Omega_1 \, \text{Sin} \, \frac{2D_e \lambda^2 t}{b^2}}{\lambda(\Omega_1^2 + \Omega_2^2)} \right] d\lambda \qquad \text{(D-12)}$$

$$\left. - \frac{4vM_3 D_e}{\pi \, b^2} \int_{b\sqrt{\frac{\varepsilon}{2D_e}}}^{\infty} \lambda \left[\frac{(\Omega_1^2 - \Omega_2^2) \, \text{Cos} \, \frac{2D_e \lambda^2 t}{b^2} + 2\Omega_1 \Omega_2 \, \text{Sin} \, \frac{2D_e \lambda^2 t}{b^2}}{(\Omega_1^2 + \Omega_2^2)^2} \right] d\lambda \right\}$$

$$n_{010} = n_{001} = 0$$

APPENDIX E

BREAKTHROUGH RESPONSE DATA

Figure E.1.   Breakthrough response at well location x = 2.50 m,
y = 0.00 m, and z = -3.20 m.
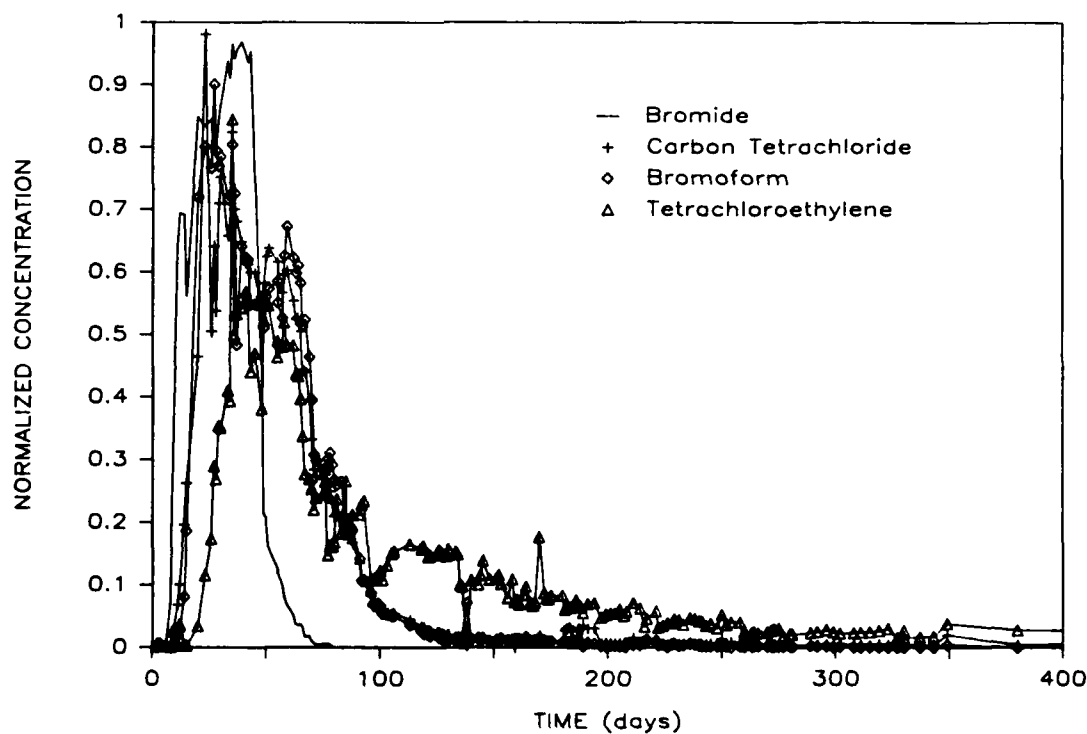
Figure E.2.   Breakthrough response at well location x = 2.50 m,
y = 1.25 m, and z = -3.62 m.

158
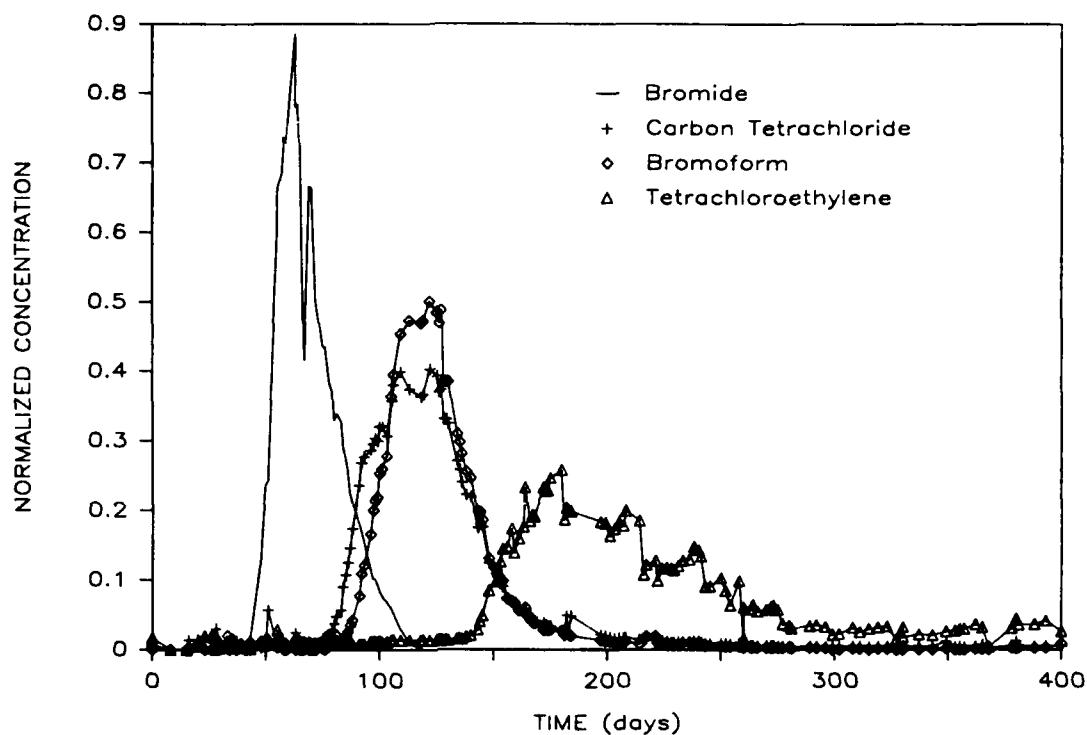
Figure E.3. Breakthrough response at well location x = 5.00 m, y = 0.00 m, and z = -3.26 m.
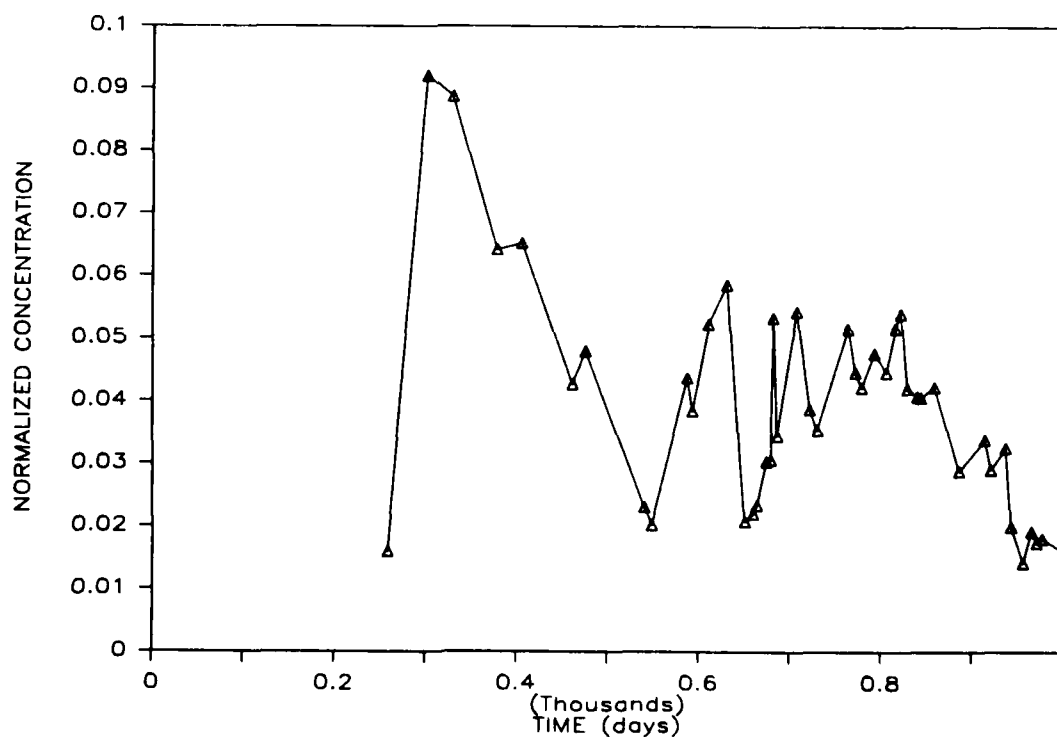
Figure E.4. Tetrachloroethylene breakthrough response at well location x = 10.00 m, y = 4.60 m, and z = -3.88 m.

159
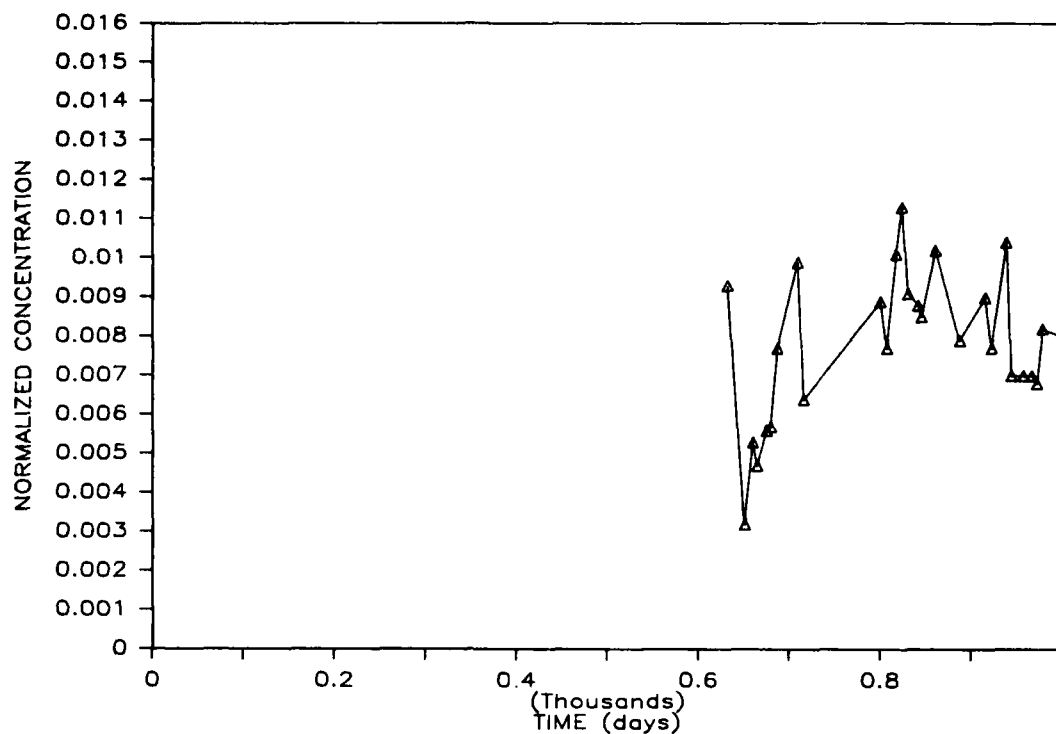
Figure E.5. Tetrachloroethylene breakthrough response at well
location x = 10.00 m, y = 4.60 m, and w: = -4.48 m.
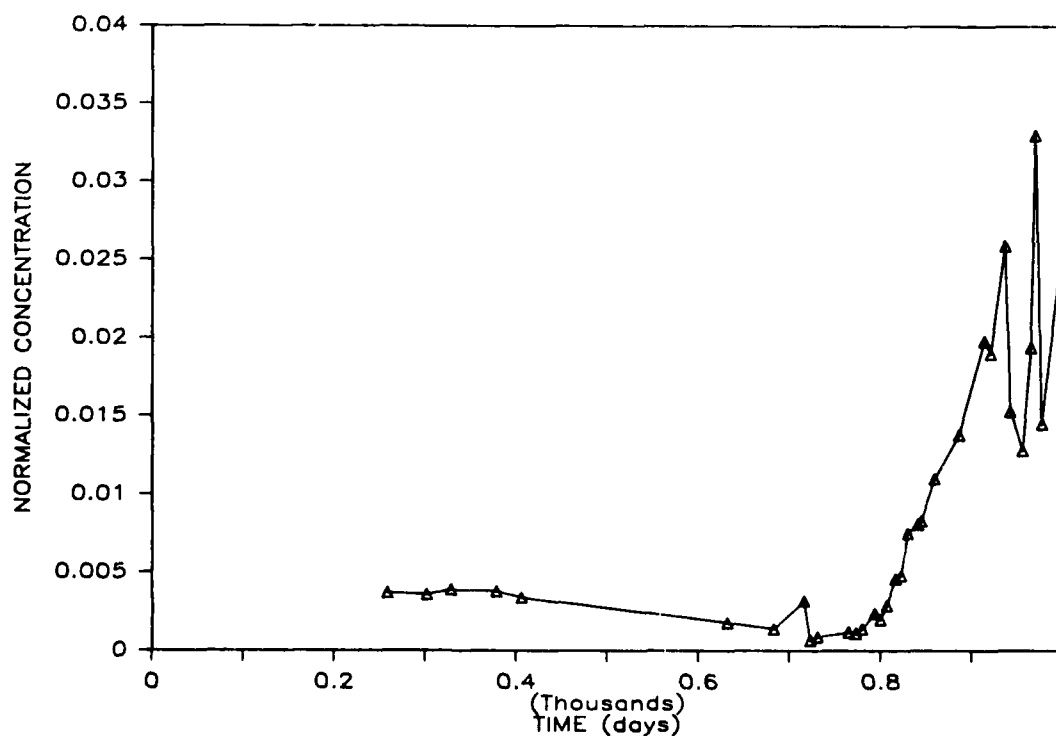
Figure E.6. Tetrachloroethylene breakthrough response at well
location x = 13.10 m, y = 4.05 m, and z = -3.42 m.
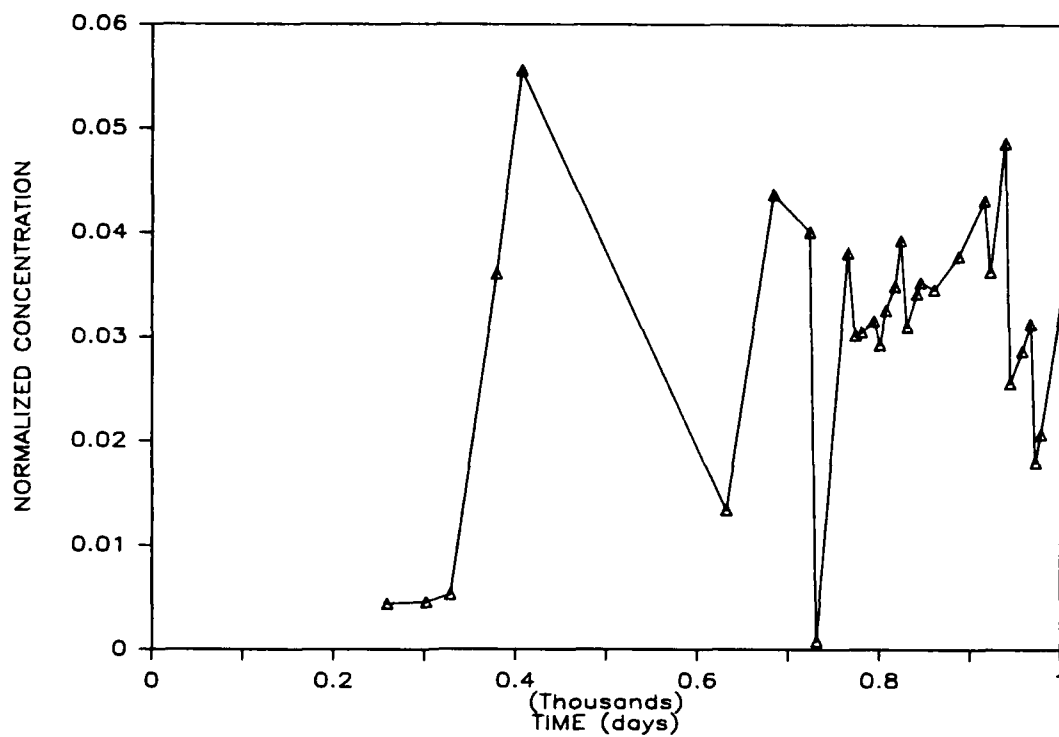
Figure E.7. Tetrachloroethylene breakthrough response at well
location x = 13.10 m, y = 4.05 m, and z = -3.72 m.

Figure E.8. Breakthrough response at well location x = 18.00 m,
y = 9.00 m, and z = -4.13 m.

161
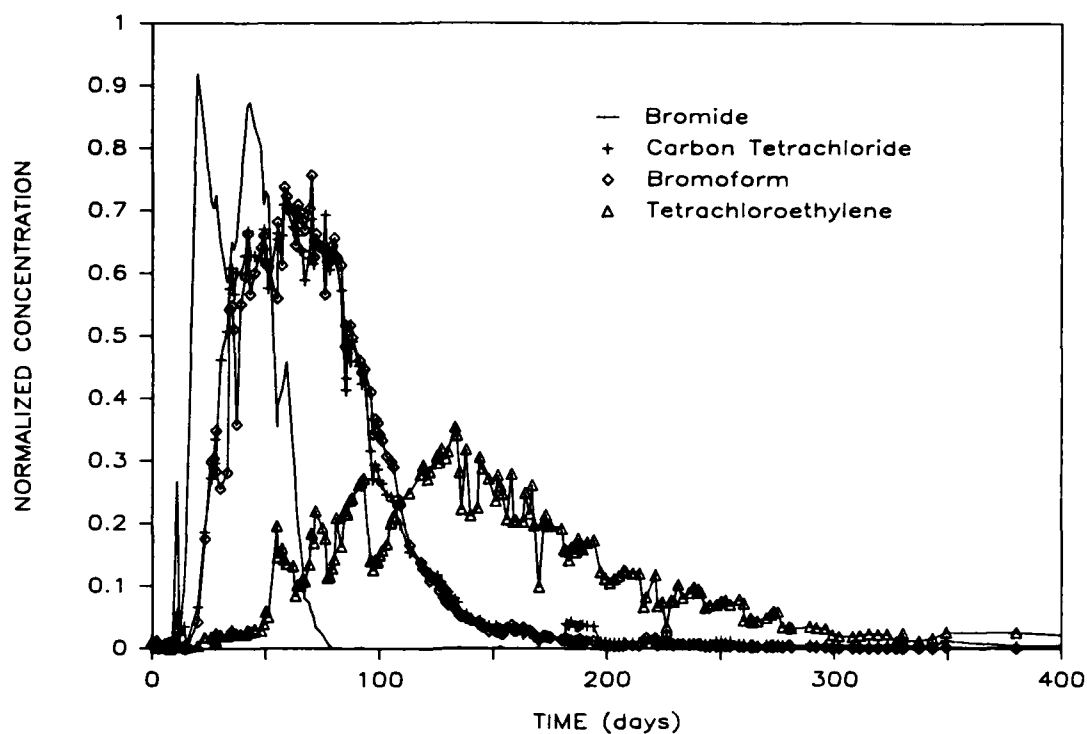
Figure E.9.   Breakthrough response at well location x = 18.00 m,
   y = 9.00 m, and z = -4.73 m.

Figure E.10.   Breakthrough response at well location x = 21.00 m,
               y = 9.00 m, and z = -4.17 m.

162

Figure E.11. Breakthrough response at well location x = 21.00 m, y = 9.00 m, and z = -4.77 m.

Figure E.12. Bromide breakthrough response at well location x = 24.00 m, y = 9.00 m, and z = -4.76 m.

163

APPENDIX F
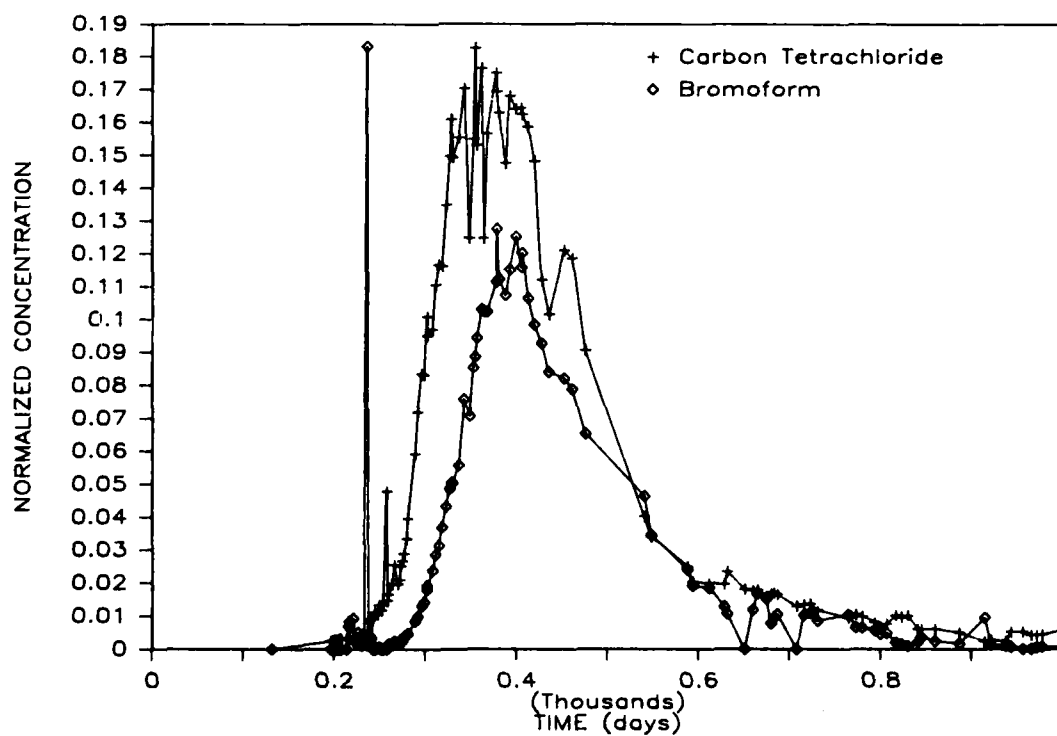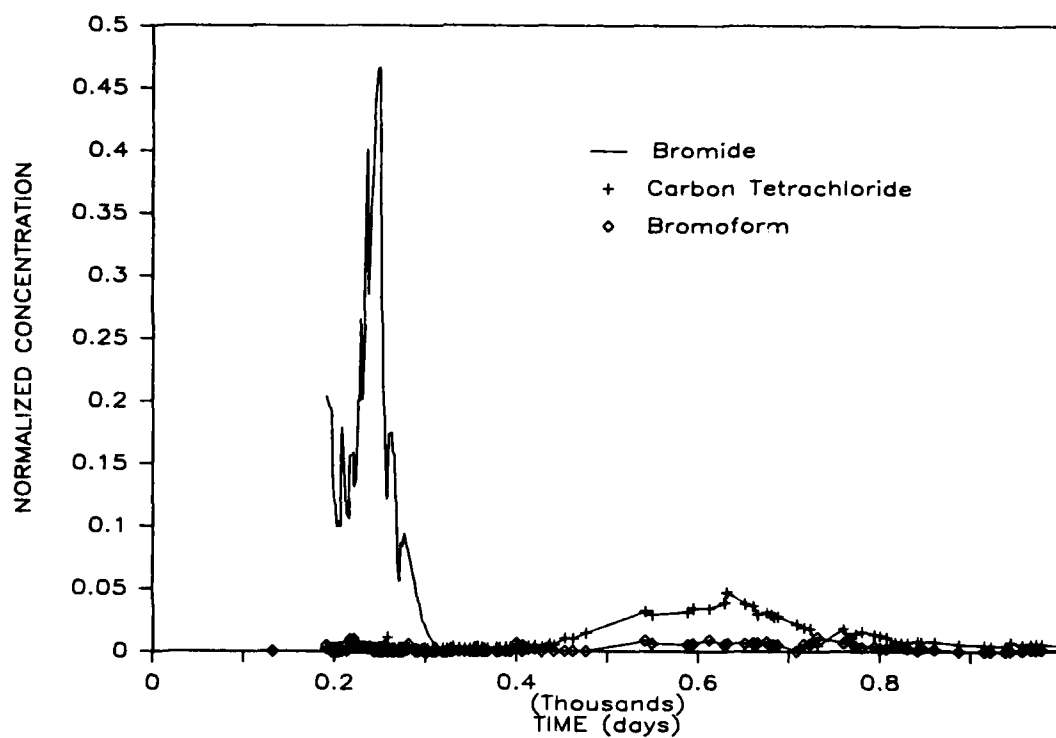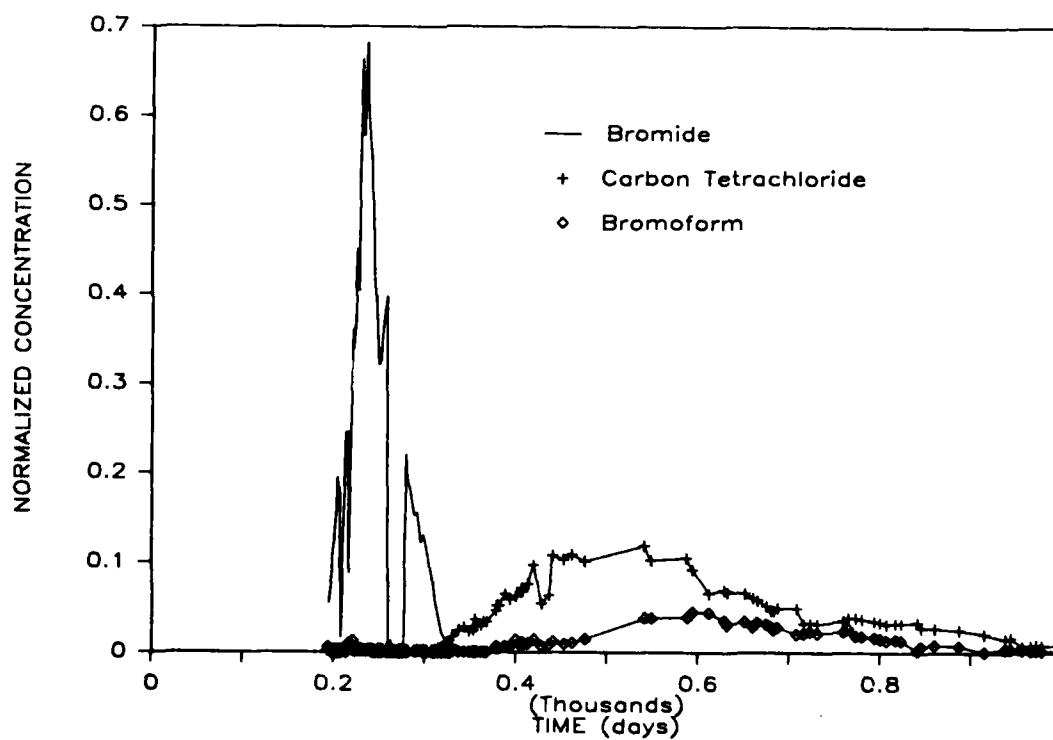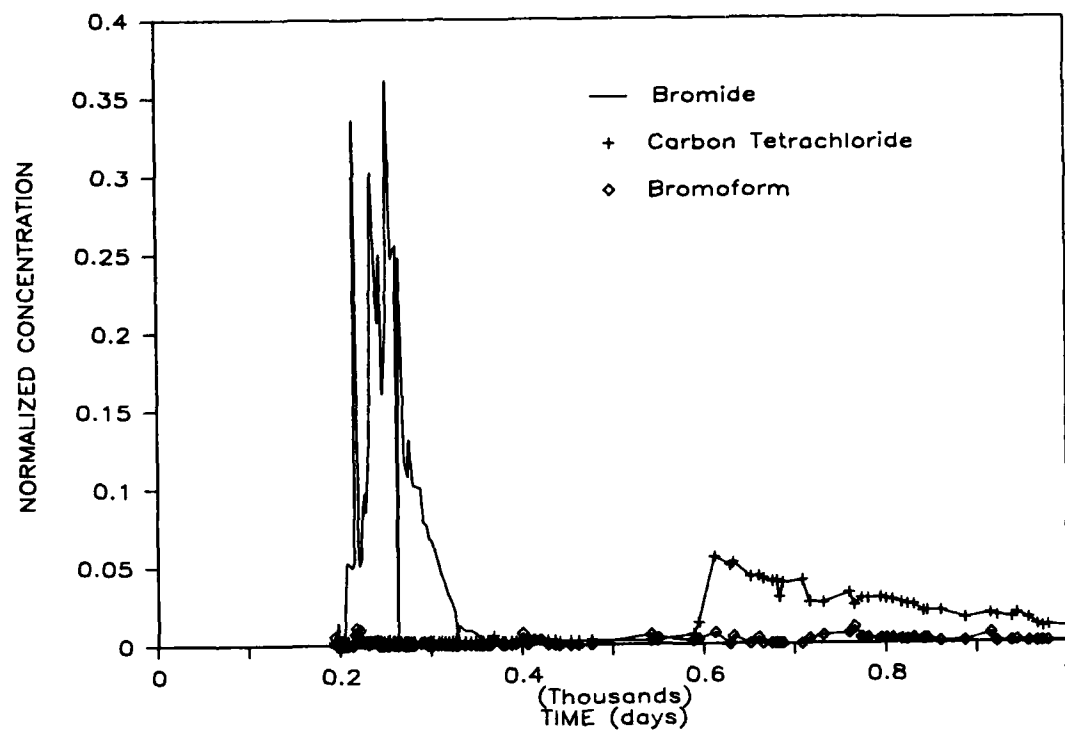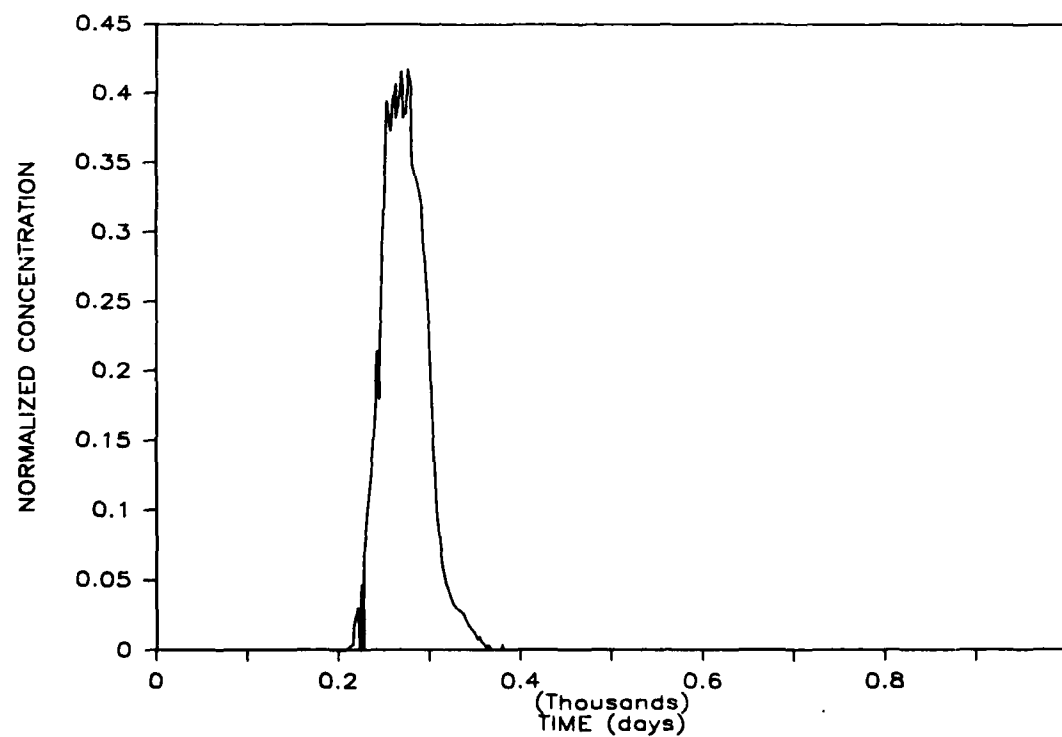
HYSTERESIS EXPERIMENT METHODOLOGY

A bottle-point partitioning technique to measure long-term sorption (Ball and Roberts, 1985) was combined with a technique to measure long-term desorption, in order to assess whether sorption/desorption of tetrachloroethylene onto Borden aquifer material was hysteretic.

Sorption Experiments

Sorption experiments were conducted using the bottle-point partitioning technique of Ball and Roberts (1985) to measure long-term sorption while carefully controlling losses. Using this technique, a known mass of groundwater synthesized to approximate aquifer conditions (Curtis et al., 1986) and a known mass of sorbent, consisting of homogenized Borden aquifer material, were added to glass ampules and the sorbent allowed to come to complete water saturation. A known amount of carbon-14 labeled solute was then injected into the glass ampule, and the ampule immediately flame-sealed. After sealing, the sample was allowed to equilibrate over a 30-day period. After the 30 days, half the samples were centrifuged (2000 rpm for 30 min), cracked open, and supernatant immediately transferred to scintillation cocktail for counting on a Packard Tricarb Model 4530 Scintillation Counter. This count provided an accurate measure of the solute concentration in the aqueous phase. By difference, the sorbed-phase concentration was determined, thus determining a point on the sorption isotherm. Losses due to partitioning to the glass ampule and to the small volume of air in the ampule were accurately and reproducibly quantified using blanks without soil.

Desorption Experiments

Desorption experiments were then conducted upon those samples not opened in the sorption experiments. These samples were placed into specially fabricated stainless steel vessels. To minimize losses, the vessels were constructed to be airtight and to have only stainless steel in contact with the sample. Synthetic groundwater, which had been pre-equilibrated with the aquifer material, was added to the vessel, the cap to the vessel closed, and the vessel shaken vigorously and centrifuged

164

for 30 min. The shaking and centrifugation broke the glass ampule in the steel vessel, causing the aquifer material and solute within the ampule to be diluted by the synthetic groundwater in the vessel. The sample was then allowed to equilibrate for 30 days. After the 30 days, the steel vessel was centrifuged, opened, and the supernatant transferred to scintillation cocktail for counting. As in the sorption experiment, aqueous-phase concentration was thus directly measured, and the sorbed-phase concentration determined by difference. Blanks showed that losses over the course of the 60-day sorption/desorption experiment amounted to less than 15%.

REFERENCES

Aris, R., 1958. On the dispersion of linear kinematic waves, Proc. R. Soc. London, Ser. A, 245, 268-277.

Baker, L. E., 1977. Effects of dispersion and dead-end pore volume in miscible flooding, Soc. Pet. Eng. J., 17, 219-227.

Ball, W.P., 1986. Unpublished data.

Ball, W. P., and P. V. Roberts, 1985. Rate limited sorption of halogenated aliphatics onto sandy aquifer material--experimental results and implications for solute transport, EOS, 66(46), 894.

Bear, J., 1972. Dynamics of Fluids in Porous Media, American Elsevier Publishing Co., Inc., New York.

Bear, J., 1979. Hydraulics of Groundwater, McGraw-Hill, Inc., New York.

Bibby, R., 1979. A Numerical Model of Contamination by Mine Drainage Water of the Chalk Aquifer, Tilmanstone, Kent, Water Research Centre Report LR 1005, Medmenham Laboratory, Medmenham, Marlow, Bucks., Great Britain.

Bouwer, E. J., and P. L. McCarty, 1984. Modeling of trace organics biotransformation in the subsurface, Ground Water, 22(4), 433-440.

Bracewell, R. N., 1978. The Fourier Transform and Its Applications, 2nd ed., McGraw-Hill Book Company, New York, pp. 141, 251.

Bremermann, H., 1963. Distributions, Complex Variables and Fourier Transforms, Addison-Wesley, Inc., Reading, MA, p. 143.

Carnahan, C. L., and J. S. Remer, 1984. Nonequilibrium and equilibrium sorption with a linear sorption isotherm during mass transport through an infinite porous medium: some analytical solutions, Journal of Hydrology, 73, 227-258.

Carslaw, H. S., and J. C. Jaeger, 1959. Conduction of Heat in Solids, Oxford University Press.

Chiou, C. T., L. J. Peters, and V. H. Freed, 1979. A physical concept of soil-water equilibria for nonionic organic compounds, Science, 206, 831-832.

Christodoulou, G. C., 1986. Dispersion response of two-layer flows, J. Env. Eng. Div., ASCE, 112(2), 433-438.

Coats, K. H., and B. D. Smith, 1964. Dead-end pore volume and dispersion in porous media, Soc. Pet. Eng. J., 4, 73-84.

Crank, J., 1975. The Mathematics of Diffusion, 2nd ed., Oxford University Press, Oxford.

Crittenden, J. C., N. J. Hutzler, D. G. Geyer, J. L. Oravitz, and G. Friedman, 1986. Transport of organic compounds with saturated groundwater flow: model development and parameter sensitivity, Water Resources Research, 22(3), 271-284.

Curtis, G. P., P. V. Roberts, and M. Reinhard, 1986. A natural gradient experiment on solute transport in a sand aquifer. IV. Sorption of organic solutes and its influence on mobility. Accepted for publication, Water Resources Research.

Cussler, E. L., 1984. Diffusion Mass Transfer in Fluid Systems, Cambridge University Press, Cambridge.

Dance, J. T., 1980. Evaluation of reactive solute transport in a shallow unconfined sandy aquifer, M.S. Thesis, University of Waterloo, Waterloo, Ontario, 93pp.

Deisler, P. F., Jr., and R. H. Wilhelm, 1953. Diffusion in beds of porous solids: measurement by frequency response techniques, Industrial and Engineering Chemistry Journal, 45, 1219.

Demond, A. H., 1984. Unpublished data.

De Smedt, F., and P. J. Wierenga, 1979a. Mass transfer in porous media with immobile water, Journal of Hydrology, 41, 59-67.

De Smedt, F., and P. J. Wierenga, 1979b. A generalized solution for solute flow in soils with mobile and immobile water, Water Resources Research, 15(5), 1137-1141.

De Smedt, F., and P. J. Wierenga, 1984. Solute transfer through columns of glass beads, Water Resources Research, 20(2), 225-232.

DiToro, D. M., 1985. A particle interaction model of reversible organic chemical sorption, Chemosphere, 14(10), 1503-1538.

Durant, M. G., 1986. Sorption of halogenated organic solutes in the Borden aquifer: evidence of spatial variability, Engineer Thesis, Dept. of Civil Engineering, Stanford University, Stanford, CA.

Freyberg, D. L., 1985. Personal communication.

Freyberg, D. L., 1986. A natural gradient experiment on solute transport in a sand aquifer: II. Spatial moments and the advection and dispersion of nonreactive tracers. Accepted for publication, Water Resources Research.

Gelhar, L. W., and C. L. Axness, 1983. Three-dimensional stochastic analysis of macrodispersion in aquifers, Water Resources Research, 19(1), 161-180.

Gelhar, L. W., A. L. Gutjahr, and R. L. Naff, 1979. Stochastic analysis of macrodispersion in a stratified aquifer, Water Resources Research, 15(6), 1387-1397.

Gillham, R. W., E. A. Sudicky, J. A. Cherry, and E. O. Frind, 1984. An advection-diffusion concept for solute transport in heterogeneous unconsolidated geological deposits, Water Resources Research, 20(3), 369-378.

Goltz, M. N., and P. V. Roberts, 1984. Mass transfer effects on groundwater transport of organic solutes. Presented at ASCE Annual Convention, San Francisco, 1-5 October, 1984.

Goltz, M. N., and P. V. Roberts, 1986. Interpreting organic solute transport data from a field experiment using physical nonequilibrium models, Journal of Contaminant Hydrology, 1, 77-93.

Gradshteyn, I. S., and I. M. Ryzhik, 1980. Table of Integrals, Series, and Products, Academic Press, New York.

Gschwend, P. M., and S. C. Wu, 1985. On the constancy of sediment-water partition coefficients of hydrophobic organic pollutants, Environ. Sci. Technol., 19(1), 90-96.

Güven, O., F. J. Molz, and J. G. Melville, 1984. An analysis of dispersion in a stratified aquifer, Water Resources Research, 20(10), 1337-1354.

Hornsby, A. G., and J. M. Davidson, 1973. Solution and adsorbed fluometuron concentration distribution in a water-saturated soil: experimental and predicted evaluation, Soil Sci. Soc. Am. Proc., 37, 823-828.

Horzempa, L. M., and D. M. DiToro, 1983. The extent of reversibility of polychlorinated biphenyl adsorption, Water Research, 17(8), 851-859.

Hunt, B., 1978. Dispersive sources in uniform groundwater flow, J. Hydraulics Div., ASCE, 104(HY1), 75-85.

Hutzler, N. J., J. C. Crittenden, J. S. Gierke, and A. S. Johnson, 1986. Transport of organic compounds with saturated groundwater flow: experimental results, Water Resources Research, 22(3), 285-295.

IMSL Library Reference Manual, 1982. The IMSL Library, 9th ed., IMSL, Houston, TX.

Karickhoff, S. W., 1984. Organic pollutant sorption in aquatic systems, J. Hydraulics Div., ASCE, 110(6), 707-735.

Koch, D. L., and J. F. Brady, 1986. Nonlocal dispersion in porous media: nonmechanical effects. Submitted to Chem. Eng. Sci.

Kucera, E., 1965. Contribution to the theory of chromatography. Linear non-equilibrium elution chromatography, J. Chromatog., 19, 237-248.

Leland, D. F., and D. Hillel, 1982. A field study of solute dispersion in a shallow, unconfined aquifer, Soil Sci. Soc. Am. J., 46, 905-912.

Lindstrom, F. T., and M. N. L. Narasimhan, 1973. Mathematical theory of a kinetic model for dispersion of previously distributed chemicals in a sorbing porous medium, SIAM J. Appl. Math., 24, 496-510.

MacFarlane, D. S., J. A. Cherry, R. W. Gillham, and E. A. Sudicky, 1983. Migration of contaminants in groundwater at a landfill: a case study, Journal of Hydrology, 63, 1-29.

Mackay, D. M., D. L. Freyberg, P. V. Roberts, and J. A. Cherry, 1986. A natural gradient experiment on solute transport in a sand aquifer: I. Approach and overview of plume movement. Accepted for publication, Water Resources Research.

Matheron, G., and G. de Marsily, 1980. Is transport in porous media always diffusive? A counterexample, Water Resources Research, 16(5), 901-917.

Mercado, A., 1967. The spreading pattern of injected water in a permeable stratified aquifer, Symposium of Haifa, Artificial Recharge and Management of Aquifers, Publ. 72, pp. 23-36, Int. Assoc. Hydrol. Sci., Gentbrugge, Belgium.

Miller, C. T., and W. J. Weber, Jr., 1986. Sorption of hydrophobic organic pollutants in saturated soil systems, Journal of Contaminant Hydrology, 1(1/2), 243-261.

Nkedi-Kizza, P., P. S. C. Rao, R. E. Jessup, and J. M. Davidson, 1982. Ion exchange and diffusive mass transfer during miscible displacement through an aggregated oxisol, Soil Sci. Soc. Am. J., 46, 471-476.

Nkedi-Kizza, P., J. W. Biggar, H. M. Selim, M. Th. van Genuchten, P. J. Wierenga, J. M. Davidson, and D. R. Nielsen, 1984. On the equivalence of two conceptual models for describing ion exchange during transport through an aggregated oxisol, Water Resources Research, 20(8), 1123-1130.

National Research Council (NRC), 1984. Groundwater Contamination, Panel on Groundwater Contamination, National Research Council, National Academy Press, Washington, D.C., 179pp.

O'Hannesin, S. F., 1981. Spatial variability of grain-size parameters and hydraulic conductivity at a dispersion test site, Bachelor of Environmental Studies Honours Report, University of Waterloo, Waterloo, Ontario, 46pp.

Parker, J. C., and A. J. Valocchi, 1986. Constraints on the validity of equilibrium and first-order kinetic transport models in structured soils, Water Resources Research, 22(3), 399-407.

Passioura, J. B., 1971. Hydrodynamic dispersion in aggregated media. 1. Theory, Soil Science, 111(6), 339-344.

169

Pellett, G. L., 1966. Longitudinal dispersion, intraparticle diffusion, and liquid-phase mass transfer during flow through multiparticle systems, Tappi, 49, 75-82.

Prasher, B. D., and Y. H. Ma, 1977. Liquid diffusion in microporous alumina pellets, AIChE J., 23(3), 303-311.

Rao, P. S. C., J. M. Davidson, R. E. Jessup, and H. M. Selim, 1979. Evaluation of conceptual models for describing nonequilibrium adsorption-desorption of pesticides during steady-flow in soils, Soil Sci. Soc. Am. J., 43, 22-28.

Rao, P. S. C., D. E. Rolston, R. E. Jessup, and J. M. Davidson, 1980. Solute transport in aggregated porous media: theoretical and experimental evaluation, Soil Sci. Soc. Am. J., 44, 1139-1146.

Rasmuson, A., and I. Neretnieks, 1980. Exact solution of a model for diffusion in particles and longitudinal dispersion in packed beds, AIChE J., 26, 686-690.

Rasmuson, A., and I. Neretnieks, 1981. Migration of radionuclides in fissured rock: The influence of micropore diffusion and longitudinal dispersion, J. Geophys. Res., 86(B5), 3749-3758.

Reynolds, W. D., R. W. Gillham, and J. A. Cherry, 1982. Evaluation of distribution coefficients for the prediction of strontium and cesium migration in a uniform sand, Can. Geotech. J., 19, 92-103.

Roberts, P. V., 1966. The adsorption of normal paraffins from binary liquid solutions by molecular sieve 5A adsorbent, Ph.D. Thesis, Cornell University. University Microfilms, Inc., Ann Arbor, MI.

Roberts, P. V., J. Schreiner, and G. D. Hopkins, 1982. Field study of organic water quality changes during groundwater recharge in the Palo Alto Baylands, Water Research, 16, 1025-1035.

Roberts, P. V., M. N. Goltz, and D. M. Mackay, 1986. A natural gradient experiment on solute transport in a sand aquifer: III. Retardation estimates and mass balances for organic solutes. Accepted for publication, Water Resources Research.

Rosen, J. B., 1954. General numerical solution for solid diffusion in fixed-beds, Ind. Eng. Chem. Journal, 46, 1590.

Satterfield, C. N., C. K. Colton, and W. H. Pitcher, Jr., 1973. Restricted diffusion in liquids within fine pores, AIChE J., 19(3), 628-635.

Schneider, P., and J. M. Smith, 1968. Adsorption rate constants from chromatography, AIChE J., 14(5), 762-771.

Schwartz, F. W., 1977. Macroscopic dispersion in porous media: the controlling factors, Water Resources Research, 13(4), 743-752.

Spiegel, M. R., 1968. Mathematical Handbook of Formulas and Tables, McGraw-Hill Book Company, Inc., New York.

Smith, L., and F. W. Schwartz, 1980. Mass transport. 1. A stochastic analysis of macroscopic dispersion, Water Resources Research, 16(2), 303-313.

Sudicky, E. A., 1983. An advection-diffusion theory of contaminant transport for stratified porous media, Ph.D. Thesis, 203pp., University of Waterloo, Waterloo, Ontario.

Sudicky, E. A., 1986. A natural gradient experiment on solute transport in a sand aquifer: V. Spatial variability of hydraulic conductivity. Accepted for publication, Water Resources Research.

Sudicky, E. A. and E. O. Frind, 1982. Contaminant transport in fractured porous media: Analytical solutions for a system of parallel fractures, Water Resources Research, 18(6), 1634-1642.

Sudicky, E. A., J. A. Cherry, and E. O. Frind, 1983. Migration of contaminants in groundwater at a landfill: a case study. 4. A natural-gradient dispersion test, Journal of Hydrology, 63, 81-108.

Swanson, R. A., and G. R. Dutt, 1973. Chemical and physical processes that affect atrazine movement and distribution in soil systems, Soil Sci. Soc. Am. Proc., 37, 872-876.

U.S. Environmental Protection Agency (EPA), 1980. Groundwater Protection, Washington, D.C., 36pp.

Valocchi, A. J., 1985a. Validity of the local equilibrium assumption for modeling sorbing solute transport through homogeneous soils, Water Resources Research, 21(6), 808-820.

Valocchi, A. J., 1985b. Personal communication.

van Genuchten, M. Th., 1985. A general approach for modeling solute transport in structured soils. In Hydrogeology of Rocks of Low Permeability, Proc. 17th Int. Congress, Int. Assoc. of Hydrogeologists, Tucson, AZ, January 1985, pp. 513-526.

van Genuchten, M. Th., and P. J. Wierenga, 1976. Mass transfer studies in sorbing porous media: I. Analytical Solutions, Soil Sci. Soc. Am. J., 40, 473-480.

van Genuchten, M. Th., and P. J. Wierenga, 1977. Mass transfer studies in sorbing porous media: II. Experimental evaluation with tritium (^3H_2O), Soil Sci. Soc. Am. J., 41, 272-278.

van Genuchten, M. Th., and R. W. Cleary, 1982. Movement of solute in soil: computer-simulated and laboratory results. In Soil Chemistry. B. Physico-Chemical Models, G. H. Bolt (Ed.), Elsevier Scientific Publishing Co., pp. 349-386.

van Genuchten, M. Th., J. M. Davidson, and P. J. Wierenga, 1974. An evaluation of kinetic and equilibrium equations for the prediction of pesticide movement through porous media, Soil Sci. Soc. Am. Proc., 38, 29-35.

van Genuchten, M. Th., P. J. Wierenga, and G. A. O'Connor, 1977. Mass transfer studies in sorbing porous media: III. Experimental evaluation with 2,4,5-T, Soil Sci. Soc. Am. J., 41, 278-285.

van Genuchten, M. Th., D. H. Tang, and R. Guennelon, 1984. Some exact solutions for solute transport through soils containing large cylindrical macropores, Water Resources Research, 20(3), 335-346.

Vermuelen, T., 1953. Theory for irreversible and constant pattern solid diffusion, Ind. Eng. Chem. Journal, 45, 1664.

Wakao, N., and S. Kaguei, 1982. Heat and Mass Transfer in Packed Beds, Gordon and Breach Science Publishers, New York.

Wakao, N., and J. M. Smith, 1962. Diffusion in catalyst pellets, Chem. Eng. Sci., 17, 825-834.

Warren, J. E., and F. F. Skiba, 1964. Macroscopic dispersion, Soc. Pet. Eng. J., 4, 215-230.

Wilke, C. R., and P. Chang, 1955. Correlation of diffusion coefficients in dilute solutions, AIChE J., 1(2), 264-270.

Wilson, E. J., and C. J. Geankopolis, 1966. Liquid mass transfer at very low Reynolds numbers in packed beds, Ind. Eng. Chem. Fundamentals, 5(1), 9-14.

Wood, A. L., and J. M. Davidson, 1975. Fluometuron and water content distributions during infiltration: measured and calculated, Soil Sci. Soc. Am. Proc., 39, 820-825.

END

DTIC

9-86